# PLACENTAL ABNORMALITIES AND HYPERTENSION IN PREGNANCY

**GABRIELE BOBEK**

**A thesis submitted in fulfilment of the requirements for the award of the degree of**

**Doctor of Philosophy, University of Western Sydney**

**November 2014**

**(Amended Aug 2015)**

# Abstract

Preeclampsia is a significant and common complication of pregnancy, with characteristic signs of hypertension and proteinuria. Current theories postulate a role for altered placental perfusion as a consequence of abnormal placental development in the aetiology of preeclampsia. Animal models of human preeclampsia have shown that an imbalance of the inflammatory cytokine TNF-α leads to a similar maternal phenotype as seen with a surgical reduction of placental perfusion pressure. This suggests a role for the inflammatory response in generating the maternal signs of hypertension and proteinuria. Currently, there is no direct link showing that a cytokine imbalance (specifically increased TNF-α) affects placental development in such a way as to result in altered blood flow. The ability to detect morphological changes and alterations in blood flow in experimental models of preeclampsia would provide a significant boost in our understanding of the syndrome.

The aim of this study was to develop an "imbalance in pro-inflammatory cytokine (TNF-α)" experimental mouse model of preeclampsia and to utilize magnetic resonance imaging (MRI) for visualization of placental anatomy and for the analysis of changes in tissue morphology and function including blood flow and perfusion. Secondly, this study aimed to examine the relationship between; an imbalance in inflammatory cytokines; changes in placental markers involved in inflammation, hypoxia and pH homeostasis; and changes in blood flow in the aetiology of the maternal hypertensive response.

Pregnant C57BL/6JArc mice were subject to either reduced utero-placental perfusion (RUPP), subcutaneous infusion of the inflammatory cytokine TNF-α, or control procedures. Blood pressure was measured by either tail cuff sphygmomanometry or by telemetry. Urine was collected to measure proteinuria and blood was collected to measure levels of

the anti-angiogenic molecule soluble fms-like tyrosine kinase 1 (sFlt-1), a biomarker of the human disease.

MRI images were acquired on anaesthetised mice on day 17 of gestation using a Bruker Avance 11.7 Tesla wide-bore spectrometer. Quantitative analysis of changes in $T_2$ relaxation measurements were carried out by using Matlab™ to generate $R_2$ (i.e., $1/T_2$) maps from the acquired $T_2$ measurement data, with the $T_2$ values being calculated from selected regions of interest. Additional high resolution MRI images were acquired on formalin fixed, Magnevist™ contrast agent infused placenta.

Placentas were harvested on day 17 of pregnancy, either formalin fixed and paraffin embedded for histology or snap frozen for proteomics and genomics. Histology was performed on sections using either Haematoxylin and Eosin (H&E) or Periodic acid-Schiff (PAS) stains. Immunohistochemistry using secondary anti rabbit horse radish peroxidise linked polymer and visualising with DAB, or quantitative immunofluorescent histochemistry using Alexa 488 goat anti-rabbit IgG was performed using primary antibodies to Cytokeratin (trophoblast marker), HIF-1a (Hypoxia inducible transcription factor 1), CLIC-3 (chloride intracellular channel 3; $Cl^-/H^+$ co-transporter) and TLR-3 and TLR-4 (Toll-like receptor 3 and 4). Quantitative PCR (qPCR) was used to measure mRNA expression of *mFlt-1*, *sFlt-1*, *hif-1*, *tlr-3, tlr-4, clic-3* and *clic-4* in placental tissue.

This thesis demonstrates that infusion of the inflammatory cytokine (TNF-α) is an experimental model for hypertension and proteinuria in murine pregnancy. Hypertension in the RUPP model was not definitively confirmed despite the proteinuria. No increase in sFlt-1 above the constitutively high levels of normal pregnancy was detected in the maternal serum of either model, suggesting sFlt-1 is not a reliable marker for disease in the mouse model.

This thesis demonstrates that that morphologically distinct regions of the mouse placenta can be detected and quantified by MRI. Mapping of $T_2$ relaxation times ,which are attenuated by both hypoxia (increased levels of deoxyhaemoglobin) and acidosis (increase in free protons), indicate contrast between regions which is is lost when blood flow ceases. Similar decrease in contrast is detected upon $T_2$ mapping in the placentas of both the artificially reduced perfusion (RUPP) and imbalance of inflammatory cytokines (TNF-α) experimental models.

Immunohistochemistry and qPCR detected increases in the presence of molecules involved in response to both inflammation (TLR-3 and TLR-4) and changes in oxygen (HIF-1α) and pH (CLIC-3) levels in placentas from animals subject to either TNF-α infusion or RUPP.

These results demonstrate for the first time that morphological differences or abnormalities related to blood flow can be detected by $T_2$ mapping in the placenta of mice subject to experimental models of preeclampsia and may be used to analyse changes quantitatively. This technology has the potential to be used when studying the dynamic changes in the placenta of pregnancies complicated by preeclampsia. Analysis of the MRI images suggests changes involve both increases in deoxyhaemoglobin (hypoxia) and decreases in intracellular pH (acidosis) and suggests that pH dependent mechanisms may be as equally important as hypoxia in the perturbed placenta.

The results also indicate that the metabolic changes in the placenta in response to both decreased blood flow and TNF-α infusion involve upregulation of both TLR-3 and TLR-4 protein expression and upregulation of HIF-1α mRNA and protein. Alterations in expression and localisation of the $H^+/Cl^-$ co transporter CLIC-3 was demonstrated in the placenta after TNF-α infusion, consistent with the metabolic change observed by MRI. Inflammation-driven changes in both oxygen and pH-dependent signalling pathways are thus implicated

in alterations of the complex metabolic pathways of homeostasis and angiogenesis in the placenta that lead to the subsequent maternal hypertensive response.

# Table of Contents

# Acknowledgements

No man is an island, and least so in research. This body of work would not have been possible without the contributions and encouragement of many including the support of the School of Medicine, UWS; the National Imaging Facility (NIF) and grants from the National Health and Medical Research Council.

I would like to sincerely thank my prime supervisors Annemarie Hennessy and Bill Price for the opportunity to undertake this study and the wonderful support and encouragement throughout the work. Secondly, I would like generously thank Tim Stait-Gardner (NIF) whose expertise and able operation of the Magnetic Resonance Spectrometer enabled the MRI components of this study to be completed. A tremendous thank you is given to Laura Surmon, not only for her assistance with PCR and other aspects of the work, but for her good friendship in and out of the lab. I would like to gratefully acknowledge the assistance of Katrina Mirabito of the Blood Pressure Research group, Monash Uni with the surgical implantation of the telemeters. I would like to acknowledge Perry Abbineni for his assistance with the 2D gels, David Harman for his assistance with Mass spectrometry and Joanne Lind for her help with statistics. A big thank you goes to the animal house staff and to my young friend Karen who has provided welcoming cheer in the office. Lastly I would like to thank my children Liam and Samuel and my good friend Nick for keeping me focussed on the important things…

# Statement of Authentication

The work presented in this thesis is, to the best of my knowledge and belief, original except as acknowledged in the text. I hereby declare that I have not submitted this material, either in full or in part, for a degree at this or any other institution.

……

Gabriele Bobek

November 2014

# List of Abbreviations

| | |
|---|---|
| 2ME | 2-methoxyestradiol |
| A1M | alpha-1 microglobin |
| ADC | apparent diffusion coefficient |
| Ang II | angiotensin II |
| Ang-1 | angiopoetin-1 |
| Arnt | arylhdrocarbon receptor nuclear translocator (HIF-1β) |
| ASL | arterial spin labelling |
| $AT_1$-AA | $AT_1$ receptor agonistic autoantibody |
| $AT_1R$ | angiotensin 1 receptor |
| ATP | adenosine triphosphate |
| ATP5b | ATP synthase subunit beta |
| Bact | beta actin |
| Bcl-2 | B-cell lymphoma 2 regulatory protein |
| BOLD | blood oxygen level dependent |
| BP | blood pressure |
| CA IX | carbonic anhydrase IX |
| CF6 | coupling factor 6 |
| CLIC | chloride intracellular channel protein |
| COMT | catechol-O-methyltransferase |
| c-Src | proto-oncogene tyrosine-protein kinase Src |
| Ct | cycle threshold |
| CTAD | sodium citrate, theophylline, adenosine and dipyridamole |
| C-TAD | COOH-terminal transcriptional domain |
| DAB | diaminobenzidine |
| DAMP | damage-associated molecular pattern |
| DAP | diastolic arterial pressure |

| | |
|---|---|
| DCE | dynamic contrast-enhanced |
| dHb | deoxygenated haemoglobin |
| DWI | diffusion-weighted imaging |
| EDTA | ethylene diamine tetra acetic acid |
| ELISA | enzyme linked immunosorbent assay |
| E-PE | early onset preeclampsia |
| EPI | echo planar imaging |
| EPU | embryo placental unit |
| ER | endoplasmic reticulum |
| ERK7 | mitogen activated protein kinase ERK7 |
| FGF-1 | acidic fibroblast growth factor |
| FGF-2 | basic fibroblast growth factor |
| FGR | fetal growth restricted |
| FID | free induction decay |
| FIH | factor inhibiting HIF-1 |
| FLASH | fast low angle shot |
| fMRI | functional magnetic resonance imaging |
| FOV | field of view |
| gd | gestational day |
| GEFI | gradient echo east image |
| Glut-1 | glucose transporter-1 |
| GPR91 | a G protein coupled receptor 91 |
| Grp78 | 78 kDa glucose regulated protein |
| GSH | glutathione |
| GST | glutathione-S-transferase |
| H&E | haemotoxylin and eosin |
| Hb | haemoglobin |

| | |
|---|---|
| HbF | free fetal haemoglobin |
| HIF-1α | hypoxia inducible factor 1-α |
| HIF-1β | hypoxia inducible factor 1-α (Arnt) |
| HMGB1 | high mobility group box protein 1 |
| HO-1 | heme oxygenase 1 |
| HR | heart rate |
| HSP | heat shock protein |
| I/R injury | ischaemia/reperfusion injury |
| IDO | indoleamine 2,3-dioxygenase |
| IFN | interferon |
| IgG | immunoglobulin |
| IHC | immunohistochemistry |
| ISH | *in situ* hybridisation |
| IL-1β | interleukin 1β |
| IRES | internal ribosome entry site |
| IRF-3 | IFN regulatory factor |
| IUGF | intrauterine growth restriction |
| IVIM | intravoxel incoherent motion |
| KCIP-1 | protein kinase C inhibitor protein 1 |
| LC-MS/MS | tandem liquid chromatography mass spectrometry |
| L-PE | late onset preeclampsia |
| LPS | lipopolysaccharide |
| mAb | monoclonal antibody |
| MAP | mean arterial pressure |
| MAPK | mitogen activated protein kinase |
| MCT-4 | lactate/H+ symporter monocarboxylate transporter |
| miRNA | microRNA |

| | |
|---|---|
| MMP | matrix metalloprotease |
| MRI | magnetic resonance imaging |
| MSME | multi slice multi echo |
| MSD | mean square displacement |
| MyD88 | myeloid differentiation primary response gene 88 |
| NF-κB | nuclear factor kappa beta |
| NK | natural killer |
| NP | normal pregnant |
| N-TAD | N-terminal transcriptional domain |
| pAb | polyclonal antibody |
| PAI-1 | plasminogen activator inhibitor 1 |
| PAMP | pathogen-associated molecular pattern |
| PAPP-A | pregnancy associated protein |
| PAS | periodic acid-Schiff |
| PBMC | peripheral blood mononuclear cell |
| PBS | phosphate buffered saline |
| PDGF | platelet derived growth factor |
| PDIA1 | protein disulphide isomerise |
| PE | preeclampsia |
| PHD | HIF prolyl hydroxylase |
| pHe | extracellular pH |
| pHi | intracellular pH |
| pI | isoelectric point |
| PI3K | phosphatidylinositol 3-kinase |
| PlGF | placental growth factor |
| Poly I:C | polyinosinic-polycytdidylic acid |
| PP | pulse pressure |

| | |
|---|---|
| PP13 | placental protein 13 |
| PRR | pattern recognition receptors |
| pVHL | von Hippel-Lindau tumour suppressor |
| qPCR | quantitative PCR |
| RAS | renin angiotensin system |
| RF | radio frequency |
| RAS | renin-angiotensin system |
| ROS | reactive oxygen species |
| RUPP | reduced uterine perfusion pressure |
| SAP | systolic arterial pressure |
| SEM | standard error of the mean |
| sEng | soluble endoglin |
| sFlt-1 | soluble fms-like tyrosine kinase 1 |
| SIAHs | E3 ligases seven in absentia homologues |
| $T_1$ | spin-lattice or longitudinal relaxation time |
| $T_2$ | spin-spin or transverse relaxation time |
| TCA | tricarboxylic acid |
| TGF-β | transforming growth factor β |
| Th1 | T helper 1 cells |
| TIE-1 | angiopoetin receptor 1 |
| TIMP | tissue inhibitor of matrix metalloproteinase |
| TLR | toll like receptor |
| TNF-α | tumour necrosis factor α |
| Treg | regulatory T cells |
| TRIF | toll/IL-1 receptor domain containing adaptor inducing IFN-β |
| TrueFISP | true fast imaging with steady state precession |
| U-II | urotensin II |

| | |
|---|---|
| uPA | urokinase plasminigen activator |
| vATPase | vacuolar proton ATPase |
| VEGF | vascular endothelial growth factor |
| VEGFR-1 | vascular endothelial growth factor receptor 1 (Flt-1) |
| VEGFR-2 | vascular endothelial growth factor receptor 2 (Flk-1/KDR) |

# List of Figures

# List of Tables

# Chapter 1 Introduction

## 1.1 The Aetiology of Preeclampsia

### 1.1.1 Pre-eclampsia: Diagnosis, Rates and Risk factors

Preeclampsia (PE) is a condition affecting women during pregnancy resulting in hypertension (high blood pressure) and proteinuria (protein in urine). Without treatment it can progress to dangerous conditions such as eclampsia (convulsions), stroke, kidney injury and maternal and foetal death (Karumanchi et al., 2005). It is the most significant and common complication of pregnancy, affecting 5% of all pregnancies (Kanasaki and Kalluri, 2009). Currently the only treatment is administration of hypertensive medications, seizure prophylaxis or delivery of the baby even if this is premature (Sibai, 2003, Duley, 2009, Tranquilli et al., 2014). Epidemiologically, preeclampsia is found in increased ratio in patients with risk factors such as diabetes, obesity, chronic heart or renal disease and urinary tract infections (Ness and Roberts, 1996, Duckitt and Harrington, 2005, Conde-Agudelo et al., 2008, Minassian et al., 2013). Preeclampsia has been linked with a risk for cardiovascular diseases in later life for both the mother (Agatisa et al., 2004, Charlton et al., 2014) and her offspring (Davis et al., 2012).

### 1.1.2 Role of the Placenta

The placenta is the interface between the maternal and the foetal environments and is vital for the exchange of gases, nutrients and wastes between mother and baby. In addition, the placenta produces hormones that alter maternal physiology during pregnancy and forms a barrier against the maternal immune system (Rossant and Cross, 2001). The placenta is

essential for survival and growth of the foetus and defects in its function can result in foetal growth restriction or even death and is central in the aetiology of preeclampsia.

A two stage model of preeclampsia proposes that reduced placental perfusion as a result of abnormal placental implantation (stage 1) produces factors that lead to the clinical maternal manifestations (stage 2) (Redman, 1991, Redman and Sargent, 2009). Later modifications to this model (Figure 1.1.1) propose that whatever the cause of this abnormal placentation, the maternal syndrome is a result of interaction of the aberrant physiological changes in the placenta with maternal constitutional factors such as genetics, diabetes, obesity, diet (Roberts and Hubel, 2009). The same maternal factors that predispose placental abnormalities may exacerbate the maternal effects of placental abnormalities leading to a vicious cycle that magnifies the pregnancy complications.

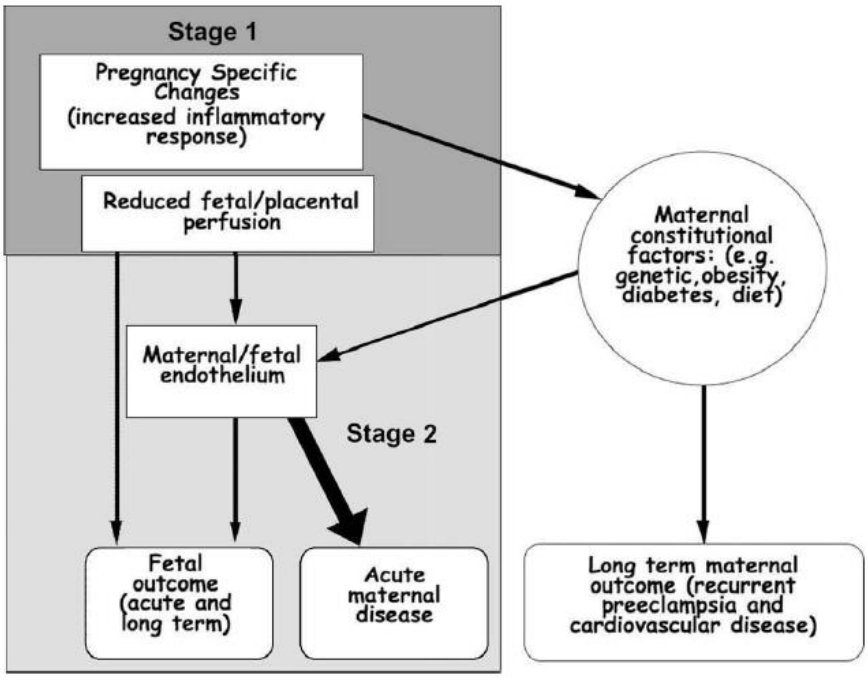


**Figure 1.1.1: Role of the placenta in the aetiology of preeclampsia. This version of the Two Stage Model emphasizes that reduced placental perfusion (Stage 1) is not sufficient to cause preeclampsia but requires interaction with maternal constitutional factors that may be genetic, behavioural or environmental. These are modified by the maternal patho-physiological changes of preeclampsia. Taken (Roberts and Hubel, 2009)**.

### 1.1.3 Human Placental Anatomy and Development

The placenta (Figure 1.1.2) is the site of interactions between the mother and the foetus and can be divided into layers: (Georgiades et al., 2002)

- An outer maternal layer including the decidual cells of the uterus as well as maternal vasculature that provides blood flow to and from the implantation site.
- A middle region which attaches the foetal placenta to the uterus and contains fetoplacental (trophoblast) cells that invade the uterine walls and maternal vessels. In humans this is termed the basal plate or implantation site.
- An inner layer composed of highly branched villi designed for efficient nutrient exchange between the maternal and foetal circulations, termed the foetal placenta.
- The chorionic plate indicates the innermost membrane containing larger placental (foetal) vessels and amniotic membrane cover.

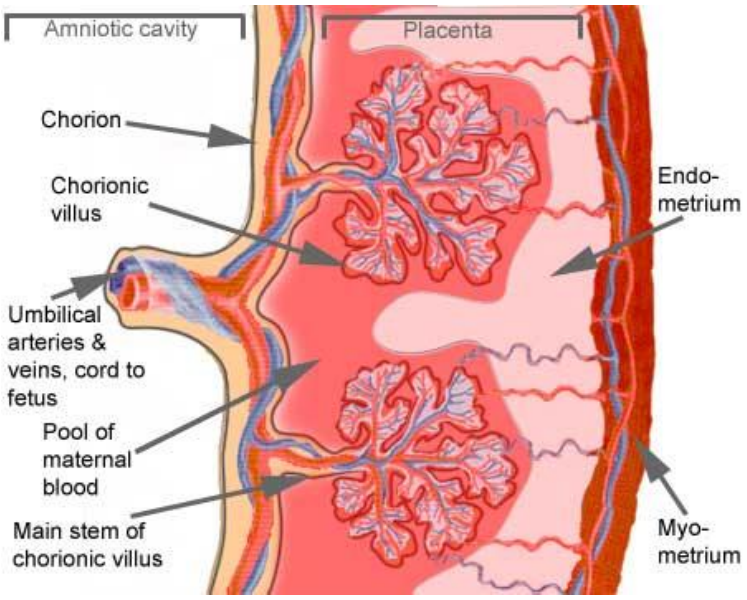


**Figure 1.1.2: Structure of the Human Placenta. Taken from the McGill Physiology Virtual Lab** http://www.medicine.mcgill.ca/physio/vlab/other_exps/endo/reprod_horm.htm

The formation of the placenta begins in the human about 6-7 days post conception when the blastocyte, consisting of an inner cell mass surrounded by a layer of trophoblast, attaches to the uterine epithelium. The polar trophoblast (those cells overlying the inner cell mass) begin to differentiate and fuse to form oligonucleated syncytiotrophoblast. They have an invasive phenotype and are able to penetrate the uterine epithelium allowing the early embryo to embed itself into the decidual stroma. The remaining mononucleated trophoblasts (cytotrophoblast) which are not in contact with maternal tissue rapidly divide and fuse with the syncytiotrophoblast resulting in continual expansion of the latter.

Eight days after conception, fluid filled spaces occur within the syncytiotrophoblast and coalesce to form larger lacunae surrounded by syncytiotrophoblastic masses termed trabeculae. The lacunae and the trabeculae develop into the intervillous space and the villous trees. Extraembryonic mesodermal cells and the inner layer of cytotrophoblast are termed the chorion, and from day 12 post conception cytotrophoblasts from the chorionic plate penetrate into the trabeculae and reach the maternal tissue to differentiate into extravillous cytotrophoblasts (Huppertz, 2008). A subset of these cells will invade the walls of the spiral arteries to transform them into highly dilated vessels that have lost the smooth muscle layer and have an invasion of foetal cytotrophoblasts into the endothelium layer. Both the spiral shape of the arteries and the transformations that occur during placentation result in a steady and low pressure flow into the intervillous space of the placenta (Pijnenborg et al., 2006). Cytotrophoblast plugs of the spiral arteries prevent maternal blood flow into the placenta until the end of the first trimester (around weeks 10-12) (Kaufmann et al., 2003). Initial nutrient requirements for survival and growth of the embryo are dependent on perfusion of the vitelline circulation to the yolk sac (Mu and Adamson, 2006). At about day 13 post conception the trabeculae begin to develop side branches and these cytotrophoblastic structures are termed primary villi. Extraembryonic

mesodermal cells of the chorionic plate begin to penetrate into the trabeculae and the primary villi giving them a mesenchymal core and transforming them into secondary villi. Haematopoietic progenitor cells develop within the mesoderm of the secondary villi and start to differentiate into the first placental blood cells and endothelial cells forming the foetal placental vascular system. Thus the foetal vasculature forms within the chorionic villus completing the transformation into tertiary villi (Huppertz, 2008). In a full term placenta, 60-70 villous trees (or foetal lobules) arise from the chorionic plate, with 1-4 foetal lobules corresponding to a visible maternal lobule on the maternal surface of the placenta. (Huppertz, 2008).

### 1.1.4 Comparison with Murine Placental Development

The mouse is often used as an experimental model to investigate pregnancy pathologies as the anatomy of the human and mouse placenta are similar in that maternal blood directly bathes the foetal villi and substances are exchanged across a haemochorial barrier between the maternal blood and the foetal capillaries (Figure 1.1.3). They have similar placental cell types and similar genes controlling placental development but differences include the mode of implantation, fewer placental hormones in mice, prominence of yolk sac, and length of gestation (18-19 days in mice) (Carter, 2007), with the most crucial difference being that trophoblast invasion into the decidua is very limited in the mouse and transformation of uterine arteries depends more on natural killer cells than trophoblast cells than in human placentation (Georgiades et al., 2002).

The development of the murine placenta as outlined in Table 1.1 follows a similar line of development to human with some structural and developmental differences. In humans organogenesis is largely completed by end of the $12^{th}$ week and effective maternal circulation of blood in the placenta does not begin until the end of the first trimester. In

mice maternal circulation begins at gestational day (gd) 10.5 suggesting that mid-gestation in mice is temporally equivalent to end of the first trimester in humans. In the human, the villi develop as branched trees into the intervillous space into which maternal blood enters from the maternal spiral arteries. In the mouse, the villi form a labyrinth structure and the maternal blood supply passes through to the foetal side of the placenta via 1 or 2 central canals before entering the small winding sinusoid spaces of the labyrinth where it directly bathes the foetal trophoblastic villi (Adamson et al., 2002).

In the human placenta, the vascularisation of the chorionic villi occurs after chorionic villus formation, whereas in the mouse the vascularisation of the labyrinth is coincidental with trophoblast branching morphogenesis of the chorionic plate, and the trophoblast have a role in directing the development of the underlying vasculature (Rossant and Cross, 2001). For example, mice with a mutant *Esx1* gene which encodes for a homeobox transcription factor that is expressed solely in the trophoblast cells of the labyrinth, have shown normal chorioallantoic branching morphogenesis but deficiencies in foetal blood vessel growth in the labyrinth villi (Watson and Cross, 2005). Mice have a layer of giant trophoblast cells next to the spongiotrophoblast at the junctional zone between the labyrinth and the outer decidual layer which are not apparent in the human placenta (Georgiades et al., 2002). While these differences need to be considered when extrapolating from experimental mice models of placentation or diseases of pregnancy, mouse models can be of benefit in unravelling the aetiologies of human placental pathologies and diseases as they allow us to easily test hypotheses about mechanisms and pathways which in turn will refine hypotheses that can be tested in humans.

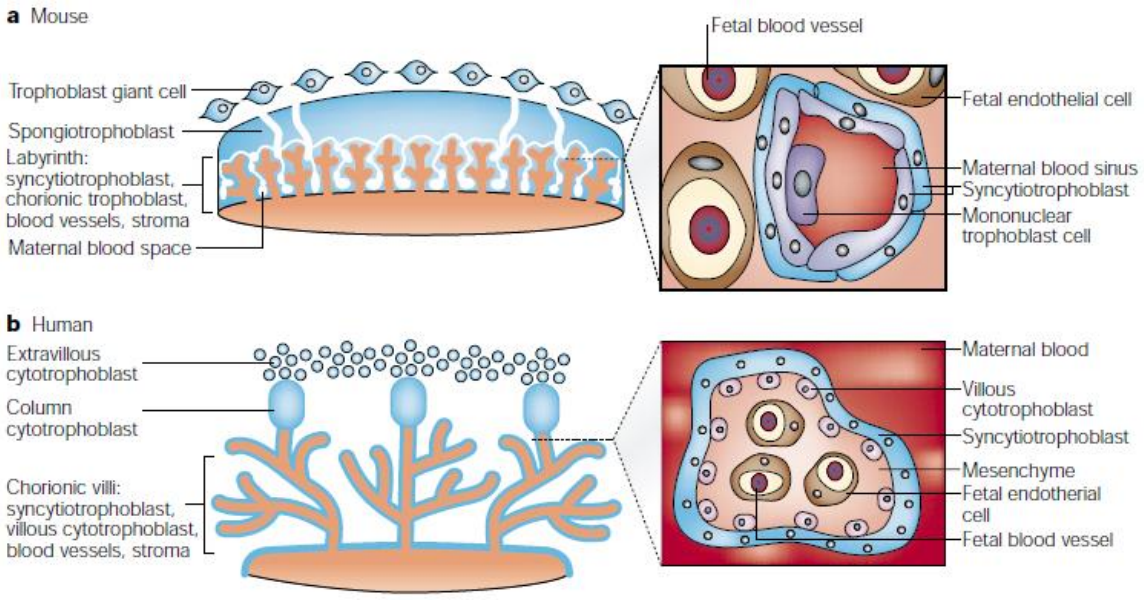


**Figure 1.1.3: Comparative anatomy of the mouse and human placenta. a) Structure of the mouse placenta. The inset details the foetal-maternal interface in the labyrinth. b) Structure of the human placenta. The inset image shows a cross-section through the chorionic villus; trophoblast derived structures (blue) and mesoderm derived structures (orange). The inset images illustrate the number and type of cell layers between the maternal and foetal blood. Taken from Rossant and Cross, 2001**

**Table 1.1: Time course of mouse placental development** *(sources are indicated)*

| Develop-mental Stage | Feature |
|---|---|
| **gd3.5** | Blastocyte consisting of trophectoderm layer and inner cell mass that gives rise to the embryo (Watson and Cross, 2005) |
| **gd4.5** | Implantation<br>Mural trophectoderm cells become trophoblast giant cells (analogous to human extravillous cytotrophoblast cells). Polar trophectoderm (adjacent to inner cell mass) become either extraembryonic ectoderm (develop into trophoblast cells of chorion layer and later, the labyrinth) or ectoplacental cone (develop into spongiotrophoblast, a compact layer of cells between labyrinth and outer giant cell layer, analogous to human column cytotrophoblast; later glycogen trophoblast cells differentiate from this layer and invade uterine wall) (Watson and Cross, 2005) |
| **gd8.5** | Extraembryonic mesoderm (allantois) at posterior end of embryo and chorion join together (chorioallantoic attachment). (Watson and Cross, 2005) |
| **gd9.0** | Chorion begins to fold to form the villi, creating a space into which the foetal blood vessels grow from the allantois (foetal endothelium). Chorionic trophoblast cells differentiate into 2 cell types; multinucleated syncytiotrophoblast cell formed from fusion of trophoblast cell which surround the foetal endothelium of the capillaries or mononuclear trophoblast cell which lines the maternal blood sinuses. (Watson and Cross, 2005) |
| **gd8.5-gd10.5** | Extensive branching morphogenesis of labyrinth to form dense villi (comparable human chorionic villi). Villi become larger and more extensively branched until birth.(Watson and Cross, 2005) |
| **gd10.5** | Maternal blood is first evident in labyrinth (Muntener and Hsu, 1977). Placenta has a mature structure, consisting of a layer of trophoblast giant cells in contact with the decidua basalis, an underlying cell dense region called the spongiotrophoblast, and the inner labyrinth. The trophoblast giant cells and spongiotrophoblast together have been termed the junctional layer (Coan et al., 2004).<br>Extensive growth and expansion of labyrinth layer until term with trophoblast sinusoids becoming smaller and more intricate. |
| **gd12.5** | Glycogen trophoblast cells (cytokeratin and PAS positive) appear in the decidua outside the trophoblast giant layer. They have diffuse interstitial invasive pattern and do not preferentially localize to vessels (Adamson et al., 2002) |
| **gd16.5** | Maximal placental volume reached though the labyrinth volume fraction increases till term at the expense of the spongiotrophoblast and trophoblast glycogen cells (junctional zone) and the decidua. Most of expansion in maternal blood spaces in the labyrinth occur between E14.5 and E16.5 while foetal capillary volumes increase linearly from E14.5 to E18.5 (Coan et al., 2004). |
| **gd18.5-19 (Term)** | The maternal blood supply to the placenta consists of radial arteries that enter the uterus through the myometrium and branch into several spiral-shaped arteries (5-10). After traversing the decidua basalis the spiral arteries converge at the trophoblast giant cell layer to form a small number (1-4) of centrally located arterial canals. The arterial canals and flow to the base (embryonic side) of the placenta before opening into the small tortuous sinusoid spaces of the labyrinth. The central canals and the maternal blood space within the labyrinth are lined with cytokeratin-positive trophoblast cells. Maternal and foetal blood flows in countercurrent manner. (Adamson et al., 2002). |

gd (gestational day)

### 1.1.5 Molecular Determinants of Placental Development

A large number of factors have been determined as necessary for normal placental development including cell cycle markers, markers of invasion and adhesion, metabolic, hypoxic and inflammation markers, nuclear factors and factors that control vasculogenesis and angiogenesis (Cross et al., 1994). Much of the data has been derived from experimental mouse models. The trophoblast expressed Glial cells missing-1 (*Gcm1*) gene and the Frizzled5 (*Fzd5*) genes are key genes that direct chorionic branching morphogenesis in a positive feedback loop, with a likely similar signalling role in trophoblast syncytialisation conserved from mouse to human (Lu et al., 2013). Aberrant regulation of these genes has also been associated with preeclampsia (Lu et al., 2013). Recently the *Fzd5* gene has shown to be essential for *Vegf* expression in the chorionic plate (Lu et al., 2013). Vascular endothelial growth factor (VEGF) is a key growth factor involved in vasculogenesis and angiogenesis, (Ahmed et al., 2000, Demir et al., 2007). Arylhdrocarbon receptor nuclear translocator (Arnt), also known as hypoxia inducible factor 1β (HIF-1β) heterodimerizes with HIF-1α to mediate transcription of specific genes, including VEGF, in response to oxygen deprivation (Wiener et al., 1996, Semenza, 2002). Arnt knockout mice have a defect in labyrinth formation, but as Arnt is expressed in the trophoblast, it appears that the vascularization defect is secondary to the trophoblast defect (Watson and Cross, 2005). Mutants that exhibit defects early in labyrinth development will die between gd10.5 and gd12.5 (Watson and Cross, 2005), which is at the point where embryonic /foetal growth becomes dependent on umbilical blood flow via the placenta rather than vitelline circulation to the yolk sac for nutrients (Mu and Adamson, 2006).

Thus it appear that adequate labyrinth development in mice involves a complex interplay between chorionic trophoblast cells and the foetal endothelial cells of the allantois and

alterations in a number of genes or signalling pathways can perturb villi formation and vascularisation , and thus the normal development and functioning of the placenta. In humans, an analogous interplay of genes and signalling pathways would control normal development and perturbations even in timing would have detrimental impacts on function, and thus foetal and maternal health.

### 1.1.6 Reduced Placental Perfusion in Preeclampsia

During placental development there is extensive invasion of the foetal cells into the uterine wall and a remodelling of the maternal uterine spiral arteries that deliver blood from the maternal system into the intervillous space. In preeclampsia it has been noted that the changes in maternal remodelling of the spiral arteries are defective (Brosens et al., 1972) and that there is impaired maternal placental perfusion in hypertensive pregnancies (Browne and Veall, 1953). In preeclampsia invading cytotrophoblasts fail to switch expression of adhesion receptors to those that are expressed by vascular cells and it has been suggested that the defective remodelling of the spiral arteries is due to a failure of the cells to mimic a vascular adhesion phenotype (Zhou et al., 1997).

The reduced placental perfusion seen in preeclamptic pregnancies is thought to be the outcome of the abnormal cytotrophoblast invasion and remodelling of the maternal spiral arteries and is postulated to be the initiating event that leads to the widespread dysfunction of the maternal vascular endothelium (Redman and Sargent, 2005).

The importance of reduced placental perfusion as an underlying feature of preeclampsia has been supported by evidence that demonstrates that experimental hypertension in monkeys, dogs, rabbits and rats can be induced by a reduction in placental perfusion (Abitbol et al., 1976, Abitbol et al., 1977, Abitbol, 1981, Abitbol, 1982).

Reduced placental perfusion is thought to result in placental hypoxia and to lead to placental oxidative stress and inflammation (Redman and Sargent, 2009) with a release of toxic compounds including anti-angiogenic compounds such as soluble fms-like tyrosine kinase 1 (sFlt-1) and soluble endoglin (sEng) into the maternal circulation. The hypertension characteristic of preeclampsia is currently thought to be a result of endothelial dysfunction in response to an excess of circulating anti-angiogenic compounds (Maynard et al., 2003b, Makris et al., 2007).

It has been suggested that rather than reduced placental perfusion *per se* and a subsequent hypoxia, the major contributor of oxidative stress in the preeclamptic placenta is ischaemia-reperfusion (I/R) injury (Burton et al., 2009). A comparison of the blood flow in normal and preeclamptic placentas by mathematical modelling has shown that in the absence of maternal spiral artery conversion, blood flow, as it enters the intervillous space, would be more turbulent and that the high momentum may damage villous architecture and increase the risk of ischaemia-reperfusion injury and oxidative stress (Burton et al., 2009).

Systemic hypoxia may also reduce placental perfusion. Using dynamic contrast enhanced magnetic resonance imaging, (Tomlinson et al., 2010) have shown that exposure to hypoxia near the end of mouse pregnancy reduces placental perfusion and clearance of contrast agent. Pregnant mice exposed to hypoxia experience preeclampsia like signs with elevated anti-angiogenic compounds sFlt-1 and soluble sEng, with the response particularly severe in IL-10 null mutant mouse compared to wild type (Sharma et al., 2010).

### 1.1.7 Hypoxia and the Developing Placenta

Hypoxia is a key feature of the developing placenta, with oxygen levels varying both temporally and spatially during development (Jauniaux et al., 2000). Development of the early placenta and embryo takes place in a low oxygen environment (Rodesch et al., 1992, Jauniaux et al., 2000). During the first trimester there is a steep gradient in the oxygen concentration from the decidua to the placenta, resulting in a mean $pO_2$ in the placenta of less than 20 mm Hg (Jauniaux et al., 2000). Oxygen is considered one of the key regulators of trophoblast differentiation and it is thought that a low oxygen environment is in fact necessary for successful development of placenta and embryo (Genbacev et al., 1997).

Hypoxia has been shown to directly affect the differentiation of different types of trophoblast cells from trophoblast stem cell lines (Adelman et al., 2000) and to affect the differentiation of invasive human trophoblasts in vitro (Genbacev et al., 1997, Caniggia and Winter, 2002). One study using cultured cytotrophoblasts showed that when cultured under low oxygen (2%) conditions mimicking the environment near the uterine surface before 10 weeks of gestation, the cells continued proliferating and differentiated poorly. When cultured in 20% oxygen, mimicking the environment near uterine arterioles, the cells stopped proliferating and differentiated normally. Thus, oxygen tension determines whether cytotrophoblasts proliferate or invade, thereby regulating placental growth and cellular architecture (Genbacev et al., 1997). One rodent study using *in vivo* hypobaric hypoxia to delineate hypoxia-sensitive events during placentation showed that hypoxia-activated endovascular trophoblast invasion required exposure to hypoxia in a short window of sensitivity from gd 8.5 to gd 9.5 (Rosario et al., 2008).

It has been shown that a premature supply of maternal blood to the placenta, and thus a premature increase in oxygen, accounts for a loss in placental mass or even spontaneous

abortion (Jauniaux et al., 2000). After maternal arterial blood starts to reach the intervillous space at the end of the first trimester (10-12 weeks in humans) the oxygen tension rises threefold (Rodesch et al., 1992, Jauniaux et al., 2000). Blood flow is first seen in the periphery of the placenta and only later extends to the centre; therefore the oxygen gradient is maintained for some time. This promotes vascular regression of the peripheral villous capillaries and the generation of stem vessels in the centre of the villi. Thus the development of the villi are directed by the oxygen tension and it has been proposed that the alteration of the organisation and shape of the villous tree in different placental pathologies may be a consequence of different placental oxygenations (Huppertz and Peeters, 2005, Huppertz et al., 2009). In mature intermediate villi, lower oxygen promotes endothelial cell growth and induces villous sprouting and the resultant villous crowding may increase resistance to flow and have a negative impact on the rheological properties of the blood travelling across the villous space (Huppertz and Peeters, 2005). The temporal and spatial changes in oxygenation may therefore be crucial to adequate placental development.

Premature oxygenation of the decidua has been proposed to lead to abnormal placental development (Tranquilli and Landi, 2010). It is argued that as trophoblast invasion depends on low oxygen tension in the decidual environment at the time of adhesion and implantation, premature oxygenation would lead to a defect in the hypoxia induced angiogenesis and defective trophoblast invasion. The 'hypoxic' placenta described in preeclampsia would then only be a late result of the defective trophoblast tissue which initially failed to progress having no need to seek oxygen at the very beginning of implantation. While it seems more likely that this circumstance would lead to completely inadequate placental development and thus early miscarriage, the concept that

trophoblast invasion and vasculogenesis and neogenesis of the placenta is dependent on the correct and timely hypoxic cues is an increasingly popular one.

Altered oxygen supply to the placenta could be due to high altitude (hypobaric hypoxia), maternal anaemia or uteroplacental factors such as defective spiral artery transformation. Controversies over the role of spiral artery transformation and its role in adequate perfusion and/or hypoxia in the placenta have arisen. Defective transformation of the spiral arteries (Brosens et al., 1972) has been considered as a cause of the inadequate perfusion (Pijnenborg et al., 2006), and hence hypoxia, in the placenta, however others have argued that failure of the spiral arteries to transform results in an increase in blood flow velocity toward the placenta (Burton et al., 2009) and at the same time to an increase in placental oxygen levels (Huppertz et al., 2013).

A key difference between the human and murine placentas highlights the discrepancy. In the human the spiral arteries are transformed by invasion of cytotrophoblasts into dilated vessels that open out from the decidua to deliver low pressure diffuse flow of blood into the intervillous space. In the murine placenta spiral arteries converge onto 1-4 central canals that deliver blood to the foetal side of the placenta, therefore defective transformation of the spiral arteries is unlikely to have the same impact on the developing placenta in the mouse as in the human. In fact studies using Rag2 $^{-/-}$Il2rg$^{-/-}$ immune-deficient mice that do not undergo spiral artery transformation, have shown normal placental growth, no placental hypoxia and no maternal hypertension (Burke et al., 2010, Leno-Duran et al., 2010).

The current evidence thus suggests that in humans it is not necessarily the lack of transformation of the spiral arteries that is the problem *per se* in pregnancy complications such as preeclampsia, but rather that altered blood flow to the developing placenta and

altered timing of developmental changes in oxygenation to the placenta, which may or may not be a result of the inadequate spiral arteries, leads to alterations in the development of the villi, abnormal placentas and the oxidative stress and inflammation that is thought to lead to a release of toxic compounds, including anti-angiogenic compounds, into the maternal circulation and the ensuing hypertensive response seen in preeclamptic pregnancies.

### 1.1.8 Vasculogenesis and Angiogenesis in the Developing Placenta

Foetal vasculogenesis and angiogenesis are a major component of the development of the placenta (Charnock-Jones et al., 2004, Demir et al., 2007). Much of the recent work on angiogenesis has come from oncological research and many of the findings are equally relevant to the developing placenta, given that both tumours and the placenta have requirements to incorporate into foreign tissues, become vascularised and evade the maternal immune system. During tumour expansion and embryonic and placental development, growing cells will rapidly outstrip their supply of nutrients unless angiogenesis takes place (Charnock-Jones et al., 2004). Vasculogenesis involves the *de novo* formation of blood vessels from mesodermally derived precursor cells which are stimulated to differentiate into endothelial cells and to form tube structures. Angiogenesis involves the creation of new vessels from pre-existing vessels. The regulation of the migration and organisation of the cells into tubes is complex and involves a number of angiogenic factors including vascular endothelial growth factors (VEGF-A to VEGF-D), Angiopoetin-1 and 2 (Ang-1, Ang-2) and their receptors (TIE-1 and TIE-2), acidic and basic fibroblast growth factor (FGF-1, FGF-2) and placental growth factor (PlGF)(Charnock-Jones et al., 2004).

VEGF is known to act via its receptors VEGFR-1 (Flt-1) and VEGFR-2 (Flk-1/KDR), which are both type III receptor kinases. A soluble form of Flt-1 that lacks the transmembrane and

cytoplasmic domains is generated by alternative splicing and can bind to VEGF and PlGF, acting as a competitive antagonist to the transmembrane VEGF receptors (Kendall et al., 1996, Clark et al., 1998, He et al., 1999), and thus providing an anti-angiogenic effect. Migration and organisation into vessels will also involve activation of proteases such as matrix metalloproteinases (MMPs) (van Hinsbergh et al., 2006) leading to degradation of basement membranes, and protease inhibitors such as plasminogen activator inhibitor (PAI-1 and PAI-2) and tissue inhibitors of matrix metalloproteinases (TIMPS) (Van Hinsbergh and Koolwijk, 2008). Integrins and cadherins are also involved in the migration and chemotaxis of endothelial cells (Eliceiri, 2001).

The steps involved in human placental angiogenesis have been investigated and outlined as a three stage process (Demir et al., 2007). The first stage involving vasculogenesis in the primitive villi is under control of VEGF which is mainly expressed by the cytotrophoblastic layer of the villi and differentiating angiogenic cell precursor, suggesting a trophoblast dependent paracrine induction of vasculogenesis and angiogenesis. The following two stages of angiogenesis are controlled by combined mechanisms of the microenvironment regulating lineage-specific gene transcription and it has been suggested that a distinct gene program at each developmental stage is essential for the establishment of the vascular network in the placental villi tree (Demir et al., 2007). This multistep process with the involvement of a number of different factors over a time course of development is clearly complex and aberrant expression of any molecules involved in the regulation of this process could clearly have considerable consequences for the developing placenta.

The anti-angiogenic compound sFlt-1, an antagonist to the action of VEGF and PlGF, has been shown to be secreted from cytotrophoblasts (Kendall et al., 1996, Nagamatsu et al., 2004, Ahmad and Ahmed, 2004) and to inhibit angiogenesis (Ahmad and Ahmed, 2004) by directly inhibiting endothelial cell migration and tube formation (Zhou et al., 2007). It has

been proposed that the increased sFlt-1 release during pregnancy (Levine et al., 2004, Hirashima et al., 2005) functions to regulate placental vascular development (Zhou et al., 2007, Shibuya, 2011), making sFlt-1 one of the key molecules whose aberrant expression or release can have considerable impacts on normal placental development.

Given that angiogenesis is a response to enable increased blood flow and oxygen delivery to hypoxic tissues, oxygen sensing has emerged as a central control mechanism of vasculogenesis (Pugh and Ratcliffe, 2003), with hypoxia-inducible factor (HIF) a key element of the hypoxia signalling pathway.

### 1.1.9 Hypoxia Inducible Factor-1 (HIF-1) in Normal Placental Development

The transcription factor hypoxia inducible factor (HIF-1) has emerged as a key molecule in placental development, regulating angiogenesis and trophoblast differentiation (Genbacev et al., 1997). HIF-1 activates the transcription of a vast array of genes that code for proteins that are involved in angiogenesis, glucose metabolism, intracellular pH (pHi) regulation, cell proliferation/survival and invasion (Semenza, 2002, Semenza, 2003) . It controls the expression of two key angiogenic factors: VEGF-A (Ikeda et al., 1995) and angiopoietin-2 (Ang-2) (Mandriota and Pepper, 1998) and of the anti-angiogenic factor sFlt-1 (Nevo et al., 2006). Other target genes include erythropoetin, heme oxygenase, endothelin-1, the glucose transporter-1 (Glut-1) (Semenza, 2003) placing *hif* as a master gene controlling nutritional stress, angiogenesis, tumour metabolism, invasion and autophagy/cell death (Pouysségur et al., 2006).

While HIFs are involved in the regulation a number of genes in response to chronic or acute low oxygen environments they are also activated by non-hypoxic stimuli such as growth factors, the renin-angiotensin system (RAS), reactive oxygen species (ROS) and by

inflammatory stimuli under normoxic conditions (Semenza, 2002, Patel et al., 2010, Imtiyaz and Simon, 2010).

HIF-1 consists of the HIF-1α subunit, whose expression levels are sensitive to oxygen concentrations, and the constitutively expressed HIF-1β subunit (also known as Arnt). HIF-1 activation involves stabilisation of the HIF-1α subunit, translocation to the nucleus, heterodimerization with the HIF-1β subunit and binding to Hypoxia Response Elements (HRE) leading to the transcription of a wide set of HIF-1 target genes (Figure 1.1.4) (Patel et al., 2010). In well oxygenated cells HIF-1α is targeted for ubiquitin-proteasome degradation by the $O_2$ dependent hydroxylation of two proline residue. In hypoxic conditions, the proline residues are not hydroxylated and the HIF-1 unit is stabilised and able to be translocated to the nucleus. Upon hydroxylation, by a family of HIF prolyl hydroxylases (PHDs), HIF-1α binds to pVHL, the product of the von Hippel-Lindau tumour suppressor gene and is targeted for degradation (Maxwell et al., 1999). The PHDs are the real oxygen sensors, with their hydroxylase activity tightly regulated by a range of $O_2$ concentrations from normoxia (21% $O_2$) to <0.1% $O_2$. (Hirsila et al., 2003). Prolonged hypoxia can however enhance PHD activity, thus limiting HIF-1 activity in a feedback mechanism that may protect cells against necrotic cell death (Ginouvès et al., 2008).

A number of other factors besides oxygen regulate PHDs including reactive oxygen species (ROS), oncogenes, second messengers and protein interactions (Berra et al., 2006). In addition HIF-1α is regulated by the oxygen dependent hydroxylation of an asparagine residue by factor inhibiting HIF-1 (FIH) which inactivates the COOH-terminal transcriptional domain (C-TAD) by inhibiting the interaction of HIF-1 with the transcriptional coactivators p300/CBP (Lando et al., 2002). HIF-1 has a second TAD (N-TAD) which is not inhibited by FIH, and the two TADs regulate different sets of genes (Dayan et al., 2006). A third molecule, p300/CPB interacting transactivator with ED-rich tail 2 (CITED2,) that binds

competitively with p300/CBP also is involved in the regulation of HIF activity. Given that FIH and the PHDs have different affinities for $O_2$, and that C-TAD and N-TAD regulate different sets of genes, there is the ability of different sets of HIF activated genes to be expressed in response to varying oxygen concentrations (Dayan et al., 2009). This would have clear implications for the developing placenta with its changing oxygen concentrations. Normal development would be highly dependent on both gradient and temporal changes in gene activation dependent on fine control of the hypoxia signalling pathway. Premature oxygenation or prolonged hypoxia would both have repercussions on the sets of genes activated and the structural and functional development of the placenta.

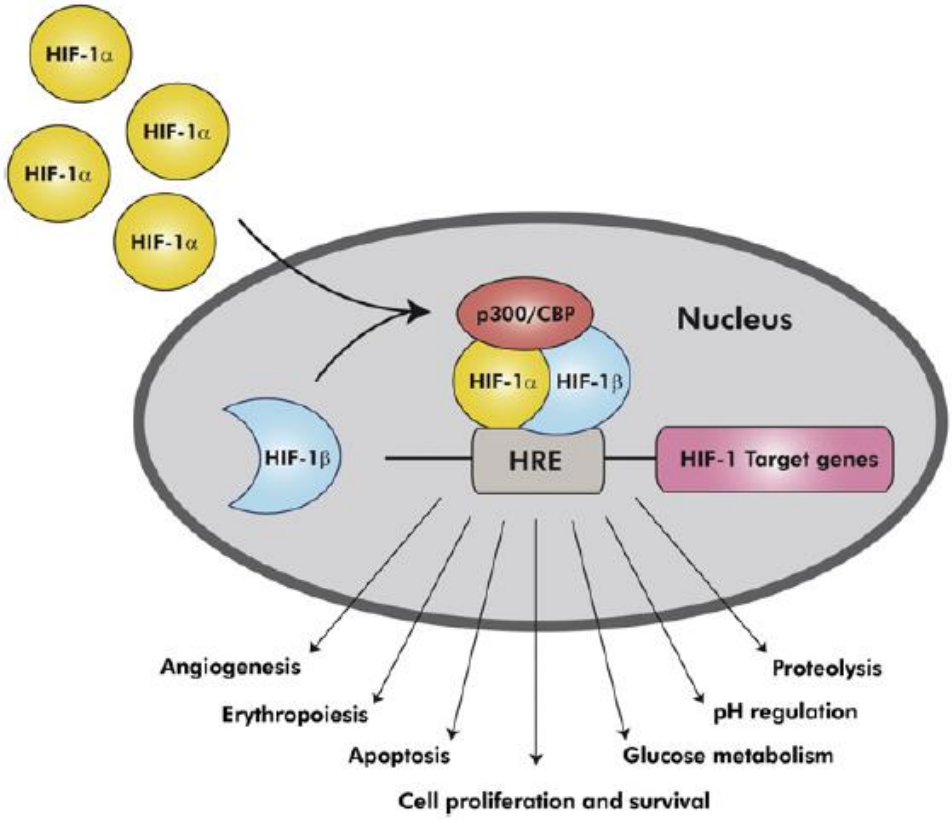


**Figure 1.1.4: Activation of HIF-1α leads to transcription of a wide set of target genes. During hypoxia, HIF-1α translocates into the nucleus dimerising with HIF-1β (Arnt) to form a complex. This complex will bind to associated Hypoxia Response Elements (HRE's) leading to transcription of HIF-1 target genes. Taken from(Patel et al., 2010) .**

While oxygen levels regulate HIF-1α activity by either affecting its stability or its transcriptional activity, expression levels of HIF-1α mRNA in cells are reported to be unchanged or only modestly increased following induced hypoxia (Wiener et al., 1996, Wenger et al., 1997, Olmos et al., 2007). Transcription and translation of *de novo* HIF-1α is largely dependent upon non-hypoxic mechanisms such as growth factors and inflammatory stimuli.

Activation of the innate immune system regulates the expression of HIF-1 α at the mRNA level through an NF-κβ dependent process (Frede et al., 2006). The increase in HIF-1 expression in response to lipopolysaccharide (LPS), a bacterial product that binds to Toll-like receptor 4 (TLR-4), was further shown to upregulate expression of the pro-inflammatory cytokine TNF-α (Kim et al., 2007). HIF-1α mRNA has more recently been shown to be upregulated by TNF-α in airway smooth muscle cells through an NF-κβ sensitive pathway (Tsapournioti et al., 2013). TNF-α has also been found to increase protein expression of HIF-1α via activation of NF-κβ, Pl3k and MAPK, downstream expression of Bcl-2 and Bcl-2 mediated internal ribosome entry site (IRES) translation (Zhou et al., 2004). Given the TNF-α induced upregulation of TLR-4 (Muzio et al., 2000, Faure et al., 2001) it is reasonable to envision a positive feedback regulation of inflammatory induced HIF-1 α expression.

TNF-α has also been shown to regulate HIF-1 translocation and activation in a non-hypoxic, ROS-sensitive manner in primary foetal alveolar cells (Haddad and Land, 2001). Angiotensin II (Ang II) has also been reported to upregulate the expression of HIF-1 α mRNA and protein in 1$^{st}$ trimester placental explants (Araki-Taguchi et al., 2008). Cytokines and growth factors such as IL-1β and TGF-β have also been shown to affect HIF-1 protein stabilisation (Sartori-Cintra et al., 2012).

### 1.1.10 Aberrant Expression of HIF-1α in Preeclampsia

Hypoxia Inducible Factor-1 (HIF-1) is crucial for placental development and therefore either aberrant expression, stabilisation or activation of HIF-1α during the developmental pathway of the placenta would lead to aberrant expression or aberrant timing of expression of key molecules involved in trophoblast invasion and angiogenesis and thus in structural abnormalities that could affect the adequate blood flow in the placenta and the normal functioning of nutrient exchange between mother and foetus.

Elevated levels of HIF-1α have been found in preeclamptic placentas (Caniggia and Winter, 2002, Rajakumar et al., 2004) and pregnant mice overexpressing HIF-1α have significantly elevated blood pressure and proteinuria compared with pregnant controls. These animals also exhibited decreased placental weights and histopathological placental abnormalities. Glomerular endotheliosis in the kidneys, a typical lesion in preeclampsia, was also observed in these animals (Tal et al., 2010). HIF-1 targets such as VEGF and sFlt-1 are overexpressed in preeclampsia (Maynard et al., 2003b, Ahmad and Ahmed, 2004, Nevo et al., 2006). Angiotensin ($AT_1$) receptor activation via AngII has been associated with reduced trophoblast invasion and angiogenesis (Xia et al., 2002), likely through the up regulation of HIF-1α (Araki-Taguchi et al., 2008). Overstimulation of $AT\text{-}_1$ receptor increases the expression and production of the anti-angiogenic molecule sFlt-1 (Lamarca et al., 2012). Women with preeclampsia produce autoantibodies known as $AT_1$ receptor agonistic autoantibody ($AT_1$-AA) (Wallukat et al., 1999) and activation of the $AT_1$ receptor by $AT_1$-AA have been shown to induce hypertension in a rodent model of preeclampsia (LaMarca et al., 2009). ). Matrix metalloproteases (MMP2 and MMP-9) and urokinase plasminogen activator (uPA), proteins involved in the degradation of extracellular matrix necessary for trophoblast invasion (Bischof, 2001, Knöfler and Pollheimer, 2012, Pollheimer et al., 2014)

are also HIF-1 targets (Semenza, 2002) and have been shown to be aberrantly regulated in preeclampsia (Bauer et al., 2004, Shokry et al., 2009, Onogi et al., 2011, Plaks et al., 2013).

A recent study investigating the control of HIF-1α stability in preeclampsia by the $O_2$-sensing enzymes PHDs, FIH, and E3 ligases Seven In Absentia Homologues (SIAHs) found that expression of PHD2, FIH and SIAHs were significantly downregulated in early onset preeclampsia(E-PE) compared to control or late onset preeclampsia (L-PE) while HIF-1α levels were increased (Rolfo et al., 2010). Expression of HIF-1α remained high in human villous explants from E-PE cultured at 20% $O_2$ compared to L-PE explants or pre-term matched control explants. Thus there appears to be a dysregulation of oxygen sensing in early onset preeclampsia but not late onset preeclampsia and thus differences in the regulation of HIF-1α levels and the regulation of transcription of the HIF-1 target genes. This study implies that other, non-hypoxic, mechanisms are responsible for changes in the preeclamptic placenta that are upstream of the transcriptional response of HIF-1 to oxygen levels. These changes may include factors that regulate expression of PHDs, FIDs and SIAHs and non-hypoxic mechanisms that regulate HIF-1 mRNA expression and protein synthesis including inflammatory stimuli.

### 1.1.11 Linkage of Hypoxia and Acidosis

One of the consequences of limited oxygen supply is the switching to anaerobic glycolysis rather than mitochondrial oxidative phosphorylation in order to supply the cell's energy requirements in the form of ATP molecules. In a decreased oxygen environment, the increased formation of ATP by anaerobic glycolysis results in a net increase in $H_3O^+$ ions and intracellular pH (pHi) declines. (Dennis et al., 1991, Robergs et al., 2004). In order to survive and proliferate, cells must extrude both these protons and the $CO_2$ from residual mitochondrial respiration in order to maintain a balance between intracellular and

extracellular pH. The role of pHi regulating pumps, transporters and exchangers would therefore seem crucial in maintaining homeostasis in tissues undergoing hypoxia. With a change in intracellular pH the activity of enzymes are altered and metabolic pathways are regulated. There is a suggestion for a universal signalling role of intracellular pH that is dynamic and can affect multiple regulatory levels simultaneously (Orij et al., 2011) and that plays a fundamental role in many tissues (Vaughan-Jones et al., 2009) including the possible regulation of apoptosis (Lagadic-Gossmann et al., 2004). Recent studies have investigated the impact of acidification on gene expression in cultured mesothelioma cells and found a dramatic change in the expression of receptors, signal proteins and cytokines at pH 6.7 compared to 7.5, with 379 genes increased by more than twofold and 412 genes decreased by more than twofold, suggesting that signal pathways in acidic diseased areas such as cancer nests, inflammation loci and infarction areas are different from normal (Fukamachi et al., 2013).

Hypoxia thus is accompanied by a switch to anaerobic glycolysis and by cellular pH changes. Hypoxia upregulates the expression of a number of stress proteins mediated by HIF-1α, including glycolytic enzymes and glucose transporters (Semenza, 2003, Pouysségur et al., 2006). HIF-1α also upregulates the expression of molecules involved in pH homeostasis such as lactate/H+ symporter monocarboxylate transporter (MCT-4) and carbonic anhydrase IX and XII (Pouysségur et al., 2006).

Hypoxic tumour cells counteract local acidosis, which is a major constraint of protein synthesis and cell growth, by inducing pH regulating molecules and extruding protons from the cell. Tumours therefore have low extracellular pH which benefits tumour cells by promoting extracellular matrix degradation, migration and invasiveness (Stubbs et al., 2000). Similarly, the early developing placenta with its low oxygen environment would also

have a need to counteract low intracellular pH as a result of reliance on anaerobic glycolysis before the onset of the maternal blood flow and higher $O_2$ levels.

### 1.1.12 pH Homeostasis and CLIC $Cl/H^+$ Transporters

Ion transporters including $Na^+/H^+$ exchanger, the $Na^+/HC0_3^-$ cotransporter and the vacuolar proton ATPase play an important role in pH homeostasis, regulating the balance of transport of protons or base between the cell and extracellular medium and within the different vesicles of the endosomal pathway . The translocation of $H^+$ across the membranes by the vATPase pump generates an electrochemical potential gradient difference that is normally dissipated by a parallel and passive movement of $Cl^-$ ions (Stauber and Jentsch, 2013). While the identity of the all the $Cl^-$ transporters are not as yet fully elucidated, the Chloride intracellular channel proteins (CLIC) family of chloride transporters are emerging as key molecules. Many members of this family function as $H^+/Cl^-$ co transporters and may have other roles as well (Littler et al., 2010, Stauber and Jentsch, 2013).

High levels of expression of CLIC3 relative to other tissues have been found in the placenta (Qian et al., 1999) and CLIC3 is associated with the mitogen activated protein kinase ERK7, suggesting that CLIC3 may play a role in regulation of cell growth (Qian et al., 1999). Recently high levels of CLIC1 and CLIC 4, and lower levels of CLIC 5 have been identified in the placenta and localised to both first trimester and term trophoblast cells and term placental endothelial cells (Money et al., 2007). This same study identified CLIC3 only in syncytiotrophoblast and villous cytotrophoblast cells in human placenta from first trimester and term pregnancies, with relative abundance of mRNA and CLIC3 staining intensity in tissue sections similar at both gestational ages indicating that CLIC3 expression may remain relatively constant throughout pregnancy. More recently highly levels of CLIC-3 mRNA and

protein have been found in placentas from pregnancies affected by preeclampsia, foetal growth restriction and PE/FGR combined (Murthi et al., 2012).

The impact of hypoxia induced acidosis in the normal developing placenta and in pathologic situations, and the role of intracellular pH in signalling in placental development remains unexamined.

### 1.1.13 Inflammatory Stimuli and Preeclampsia

The cause of the poor placental development is an area of major interest. The possibility of a breakdown of 'immunological tolerance' towards the foetal cells and an alteration in the cytokine balance towards an inflammatory T helper cell (Th1) response involving increases in inflammatory cytokines such as IFNγ and TNF-α and a reduction in anti-inflammatory (Th2) cytokines such as IL-10 has been discussed (Sargent et al., 2006). Women with preeclampsia have a deficiency in IL-10 (Hennessy et al., 1999) and TNF-α is upregulated in the blood and placenta of preeclamptic women (Schiff et al., 1994, Wang and Walsh, 1996). Adoptive transfer of activated Th1 cells leads to preeclampsia-like signs in mice (Hayakawa et al., 2000, Zenclussen et al., 2004) and treatment with an IL-10 blocking antibody leads to hypertension in pregnant baboons which is abrogated with the co-administration of anti TNF-α antibodies.(Orange et al., 2005), suggesting that the balance of anti-inflammatory versus pro-inflammatory cytokines is important. The role of regulatory T cells (Treg) in regulating immune responses towards a tolerogenic environment, with secretion of immunosuppressive cytokines such as IL-10 and TGF-β in normal pregnancies, is under investigation (Leber et al., 2010, Hsu and Nanan, 2014) as is the role of decidual NK cells in both regulating feto-maternal tolerance (Saito et al., 2007) and trophoblast invasion (Goldman-Wohl and Yagel, 2008, Chakraborty et al., 2012). The involvement of the innate immune system in successful placentation has been speculated upon with the hypothesis

that the success of the pregnancy depends on how well the trophoblast can successfully orchestrate their inflammatory environment and regulate immune cells differentiation and activation (Koga et al., 2009, Riley and Nelson, 2010). Additionally it has been proposed that “danger signals” at the feto-maternal interface, which are recognized by trophoblasts through innate immune processes such as toll-like receptor pathways, may play a key role in the creation of a local abnormal cytokine milieu in preeclampsia (Kim et al., 2005).

### 1.1.14 Role of Toll-like Receptors in Inflammation and Angiogenesis

Toll-like receptors are a family of transmembrane proteins with an extracellular domain of leucine-rich repeat motifs that are part of the innate immune system that provides the first line of defence against invading pathogens. They are pattern recognition receptors that detect foreign microbes by evolutionarily conserved pathogen-associated molecular patterns or PAMPS. (Kawai and Akira, 2009). Activation of TLRs yields an inflammatory response either signalling through NF-kβ or MAPK via MyD88 or Toll/IL-1 receptor domain containing adaptor inducing IFN-β (TRIF) to enhance transcription and secretion of pro-inflammatory cytokines (all TLRs except TLR3) or signalling through IRF-3 to induce expression of type I interferons (IFN) and IFN-inducible proteins such as TLR3 and TLR4 (Koga et al., 2009) (Figure 1.1.5).

Increasingly it has become apparent that TLRs can also recognise endogenous ligands such as heat shock proteins, breakdown products of hyalurons, reactive oxygen species (ROS) and exposed DNA/RNA that are released by distressed or damaged tissues (Koga et al., 2009). The concept of danger-associated molecular patterns or DAMPS, which may be of either foreign (PAMPS) or endogenous alarm signals to which the innate immune system responds, was proposed (Seong and Matzinger, 2004) and aligns with the “Danger model” which suggests that the immune system is more concerned with damage rather than with

foreignness, and is called into action by alarm signals from injured tissues, rather than by the recognition of non self (Matzinger, 2002). DAMPS are either inaccessible to the immune system under physiologic conditions or undergo changes in response to injury, leading to recognition by pattern recognition receptors (PRRs) such as TLRs. After tissue injury, these patterns are unmasked or released from damaged cells, and subsequently trigger inflammation via TLRs and other PRRs.

A new paradigm with TLRs as sentinels for tissue damage, regardless of whether due to infection or sterile injury has been proposed (Mollen et al., 2006), along with the notion that maladaptive responses may be triggered if damaging stimulus is not eliminated (Huebener and Schwabe, 2013). Their role in oxidative stress driven inflammation (Gill et al., 2010) and ischaemia-reperfusion injury (Arumugam et al., 2009) clearly shows their role in responding to cellular danger. More recent developments show a role for TLRs in wound healing (Huebener and Schwabe, 2013) and liver regeneration (Seki et al., 2005) suggesting a function in tissue remodelling reminiscent of the original identified function of toll as a regulator of embryogenesis in the fruit fly *Drosophila melanogaster* (Nusslein-Volhard and Wieschaus, 1980, Anderson et al., 1985, Lemaitre, 2004). Recently it has been speculated TLRs may exhibit roles in tissue homeostasis and physiology which are crucial to the integrity of tissues even in the absence of danger (Huebener and Schwabe, 2013).

Recent evidence has shown that TLR activation promotes angiogenesis in various inflammatory settings in response to both exogenous and endogenous ligands (Grote et al., 2011). Angiogenesis involves a number of cell types including endothelial cells and inflammatory cells which are a major source of growth factors such as VEGF, TGF-β bFGF and PDGF, cytokines such as TNF-α, IL6 and IL8. The angiopoietins, Ang-1 and Ang-2, have also been shown to be key molecules regulating and linking inflammation and angiogenesis (Imhof and Aurrand-Lions, 2006). While the involvement of TLRs in postnatal angiogenesis

is becoming elucidated, the precise role of TLRs in angiogenesis during embryonic development has not yet been addressed.

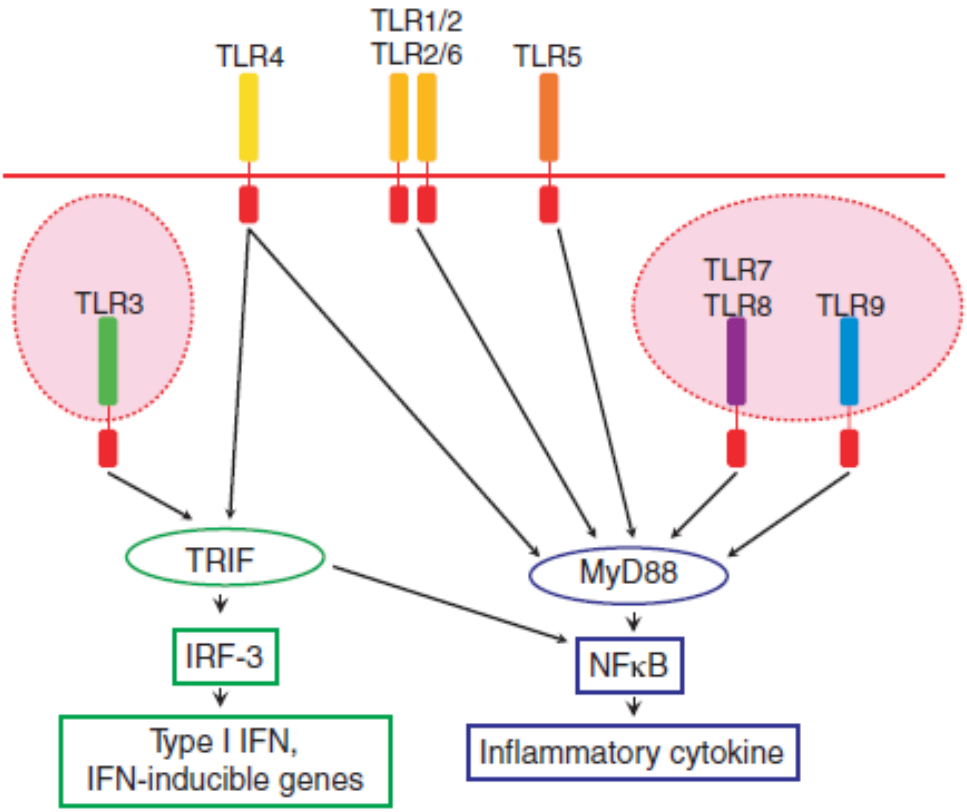


**Figure 1.1.5: Toll-like receptor (TLR) signals. Membranal TLRs; TLR1, 2, 4, 5, 6, can recognize external signals, while cytoplasmic TLRs; TLR3, 7, 8, 9 will recognize intracellular signals. Following ligation, the majority of TLRs induce activation of NF-κB and cytokine production in MyD88-dependent manner. TLR4, like TLR3, can also signal in a MyD88-independent manner, which induces the expression of type I interferons (IFN) and IFN-inducible proteins. IFN, TRIF (Toll /IL-1 receptor domain containing adaptor inducing IFN-β), IRF3 (IFN regulatory factor). Taken from Koga et al., 2009.**

### 1.1.15 Role of TLRs in Placental Development

It has been recently argued that TLRs play a key role in the success of pregnancy, with the early stage of pregnancy described an inflammatory state (Koga et al., 2009). The trophoblast must adhere and invade into the uterine epithelium, as well as replace vascular smooth muscle of the uterine arteries. These activities involve invading, dying and repairing cells with the release of many DAMPS by the distressed maternal tissue. Natural killer (NK) cells, macrophages and dendritic cells infiltrate the decidua and accumulate around invading trophoblast cells and it has been proposed that these immune cells, rather than inducing immunological tolerance of the foetus, are critical for decidual and trophoblast development (Koga et al., 2009). The human placenta expresses all ten TLR, predominantly on trophoblast cells, but they are also found on endothelial cells and macrophages (Koga et al., 2009, Riley and Nelson, 2010). The trophoblast cells thus can sense the surrounding environment and recognize the presence of bacteria, viruses, dying cells and damaged tissue. In response they will secrete a specific set of cytokines that in turn will act upon the immune cells within the decidua (i.e. macrophages, NK cells, T regulatory cells) "educating" them to work together in support of the growing foetus (Fest et al., 2007).

The placenta holds an immunologically unique position at the interface between mother and 'foreign' foetus and it seems plausible that the inflammatory response and TLR pathways play a key role in not only implantation, but in the inflammation driven angiogenesis of early development of the placenta. It has been hypothesised that stimulation of specific TLRs may induce a specific pattern of proangiogenic growth factors that regulate sufficient tissue regeneration (Grote et al., 2011) and it could be further hypothesised that TLR activation at the immunologically unique position of the placenta could be a key gatekeeper, regulating normal or 'sufficient' placental angiogenesis in contrast to abnormal or 'pathological' placental angiogenesis.

Indeed embryogenesis must be a highly inflammatory process (Van Mourik et al., 2009), with constant tissue remodelling involving the breakdown of existing cells and extracellular matrix. TLR as a highly conserved molecule sensing the environment and responding to danger at the same time as directing angiogenesis, would seem to be a prime component of embryonic development.

### 1.1.16 Altered Expression of TLRs in Preeclampsia and Experimental Preeclampsia

The expression pattern of TLR on trophoblast cells varies by gestational age as well as by the stage of trophoblast differentiation (Riley and Nelson, 2010, Koga and Mor, 2010). This suggests a temporal regulation of TLRs may be involved in placental development and that dysregulation of this pattern might have implications for the normal development of the placenta. TLR4 protein expression has been shown to be increased in the interstitial trophoblasts of patients with preeclampsia (Kim et al., 2005) and TLR3 activation during pregnancy causes preeclampsia like features such as hypertension and proteinuria in rats (Tinsley et al., 2009) and mice (Chatterjee et al., 2011). TLR3 stimulation has been found to upregulate sFlt-1 production from trophoblast cells (Nakada et al., 2009) and injection of the TLR3 agonist polyinosinic-polycytidylic acid (poly I:C) into CBA x DBA/2 mice was shown to upregulate TLR3 expression in the decidua basalis and induce impairment of spiral artery modification and result in foetal losses (Zhang et al., 2007). TLR-4 deficient mice have increased expression of pulmonary HIF-1α in normoxic conditions compared to wild type, yet when exposed to sustained hypoxia (16 weeks), they markedly downregulate HIF-1 in contrast to upregulation by wild type animals (Young et al., 2010). TLR4 activation may therefore be an important component of the non-oxygen dependent regulation of HIF-1α, an important regulator itself of placental development. TLR4 deficient mice also exhibit decreased activity of the metalloproteinase MMP-9 during hypoxia, whereas the normoxic

TLR-4 deficient mice had 4-fold higher activity as compared to normoxic wildtype (Young et al., 2010).

Metalloproteinases are one group of proteins that are involved in matrix degradation, a key requirement of capillary morphogenesis, tissue remodelling and development (Ghajar et al., 2008). TLR4 defective mice showed decreased TNF-α and decreased MMP-2 and MMP-9 in response to myocardial infarct release of the TLR-4 ligand, alternatively spliced extra domain A of fibronectin (EDA) (Timmers et al., 2008). Less left ventricular maladaptive remodelling was observed in the TLR-4 defective mice, indicating a possible role of TLR-4 in matrix turnover. Matrix turnover is a key aspect in placental development. Matrix metalloproteinases and their inhibitors have been shown to play a major role in vascular remodelling, angiogenesis, and the uterine and systemic vasodilation during normal pregnancy (Raffetto and Khalil, 2008). Additionally, deficiency of MMP-9 in human trophoblasts has been associated with preeclampsia (Shokry et al., 2009), and MMP-9 deficiency in mice causes physiological and placental abnormalities which mimic "preeclampsia" (Plaks et al., 2013).

### 1.1.17 Imbalance in Regulatory Control and Positive Feedback Cycles

It has been pointed out that the immunology of the maternal foetal interface faces a diverse set of demands that may not always be compatible. Interactions between the trophoblast and the maternal immune cells that populate the decidua must foster placental development, minimize the chance that the placenta is attacked as a foreign organ transplant and combat infection simultaneously (Erlebacher, 2013). TLRs considered from the viewpoint as key molecules for detecting changes in cellular environments may be fundamental molecules in keeping the balance between these diverse roles of immunological protection and tolerance and provide a crucial link between

development/angiogenesis and inflammation/immunity. They may provide a link between infections and/or incomplete maternal tolerance to allogeneic trophoblast, abnormal placental development and subsequent preeclampsia.

TLR activation leads to pathways that activate pro-inflammatory cytokines, but they are themselves upregulated by inflammatory cytokines in a positive feedback process (Kim et al., 2005). Inflammatory stress due to infection or due to breakdown of immunological tolerance towards feto-paternal alloantigens (Redman and Sargent, 2010) and cellular stresses such as hypoxia, oxidative stress or I/R injury caused by poor placentation are both situations that would involve the release of danger signals into the cellular environment. This would result in continued activation of TLRs and the release of pro-inflammatory cytokines. A positive feedback cycle would act to exacerbate the damage and continue the pathological response.

Dysregulation of the normal temporal expression of TLRs or chronic stimulation of TLRs either through exogenous infection or endogenous damage may thus trigger maladaptive responses and be a prime mechanism behind abnormal placental development and the syndrome of preeclampsia.

A dysregulation of TLR pathways that trigger maladaptive inflammatory responses is also consistent with the view that preeclampsia is not an intrinsically different state from normal pregnancy but the extreme end of a continuous spectrum of inflammatory responses that are a feature of pregnancy itself (Redman and Sargent, 2010, Redman et al., 2014).

### 1.1.18 Timing of Ischaemia and Angiogenic balance

It has recently been suggested that all women may be destined to get preeclampsia if their pregnancy continued long enough (Redman et al., 2014). It is argued that there is a spectrum of syncytiotrophoblast (STB) cellular stress within both normal and pathological pregnancies, leading to secretion of biomarkers such as sFlt-1 that can perturb maternal angiogenic balance. STB stress may present early in pregnancy due to dysregulated perfusion due to poor placentation, or may present later in pregnancy due to the size of the placenta restricting intervillous perfusion, precipitating early-onset or late onset preeclampsia respectively. Either of these may present on a spectrum or manifest in combination, resulting in the array of pathologies that account for preeclampsia.

In studies in rats using a RUPP experimental model of preeclampsia it was found that the timing during which placental insufficiency occurred played a role in determining both the severity of hypertension and the presence of an angiogenic imbalance (as determined by endothelial tube formation assay and an increase in serum sFlT ), leading to the proposal that the amount of relative ischemia may be important to the determination of angiogenic balance in late gestation and that the placental response to a reduced uterine perfusion pressure may be dependent upon the balance between supply and demand of nutrients (Banek et al., 2012).

Others have also suggested that the timing and amount of ischaemia is central to the foetal response and to the timing of presentation of preeclampsia, leading to the proposal for sub-classification of preeclampsia according to whether there is evidence of absolute or relative uteroplacental ischaemia (Espinoza, 2012). It is argued that early onset preeclampsia may be the result of “absolute” uteroplacental ischaemia due abnormalities in placental development limiting blood flow to the placenta whereas late onset

preeclampsia might have more to do with “relative” uteroplacental ischemia due to a mismatch between a limited uteroplacental blood flow and increased foetal demand for nutrients. Support for this argument includes observations that 50% of patients with late onset preeclampsia do not have placental lesions consistent with ‘maternal underperfusion’ and that their angiogenic imbalances are less severe than women with placental lesions (Soto et al., 2012). Other data demonstrates that high impedance to blood flow in both uterine arteries in the second trimester is associated with a higher risk for preeclampsia at ≤ 34 weeks than at > 34 weeks of gestation (Papageorghiou et al., 2002). Late onset preeclampsia is frequently associated with foetuses that are large or adequate for gestational age and it is proposed that in these cases an increased foetal demand for substrates that surpass the placental ability to sustain foetal growth may induce foetal signalling for placental overproduction of anti-angiogenic factors and lead to a subsequent “compensatory” maternal hypertension (Espinoza, 2012).

The unifying feature in all these hypotheses is that placental ‘stress’ leads to a secretion of anti-angiogenic factors with the ensuing maternal pathological response. The absolute cause of the placental stress, the timing of onset, and the relation of these to each other, to molecular and structural changes in the placenta, to changes in blood flow, and to the severity of the maternal syndrome remain to be fully elucidated.

This thesis aims to examine further the relationship between inflammatory cytokine effects, TLR and HIF-1 α expression, placental structural changes, placental blood flow, secretion of anti angiogenic factors and subsequent elevated maternal blood pressure in order to better understand the complex of events occurring in pre-clinical preeclampsia.

## 1.2 Animal models of human preeclampsia

A number of animal models of preeclampsia have been established in order to elucidate the physiological mechanisms in the development of this syndrome.

Some of these models focus on creating a state of placental ischaemia (Abitbol, 1981, Abitbol, 1982, Alexander et al., 2000, Makris et al., 2007), in order to mimic the placental hypoxia thought to occur in preeclampsia. Other models involve perturbations downstream in the aetiology of preeclampsia, namely overexpression of soluble fms-like tyrosine kinase 1 (sFlt-1) using injection of adenovirus carrying sFlt-1 (Maynard et al., 2003b, Lu et al., 2007, Suzuki et al., 2009, Bytautiene et al., 2010, Bergmann et al., 2010). While the sFlt-1 model has demonstrated the role of increased secretion of the anti-angiogenic molecule sFlt-1 in preeclamptic pregnancies on the development of maternal hypertension and blocking studies with antagonists vascular endothelial growth factor (VEGF-A) or placental growth factor (PlGF) indicate a role for sFlt-1 antagonists in ameliorating hypertension in pregnancy (Suzuki et al., 2009), this model is not pregnancy specific as non-pregnant mice administered the adenoviral-sFlt-1 construct also develop hypertension and proteinuria (Maynard et al., 2003a). Therefore this model, while useful for examining effects of anti-angiogenic molecules on the maternal vasculature is not useful as a tool for examining the development or role of placental abnormalities in the aetiology of preeclampsia or the specific contribution of placental production of sFlt-1 to disease states.

Alternatively, an immunological approach has been employed in the development of a number of models. Pregnant rats receiving an ultralow dose of endotoxin present with hypertension and proteinuria (Faas et al., 1994). Adoptive transfer of activated T helper-1 (Th1) cells into allogeneically pregnant BALB/c mice leads to hypertension,

glomerulonephritis and proteinuria (Hayakawa et al., 2000, Zenclussen et al., 2004), implicating Th1 cytokines in initiating preeclampsia like features.

Infusion of the inflammatory cytokine TNF-α results in hypertension in pregnant rats (Alexander et al., 2002) and in pregnant baboons with a concomitant increase in circulating sFlt-1 and proteinuria (Sunderland et al., 2009). Injection of angiotensin II type I receptor agonistic autoantibodies ($AT_1$-AA) into pregnant mice also provokes key preeclamptic features (Zhou et al., 2008). Activation of toll-like receptor 3 during pregnancy with polyinosinic: polyctyidylic acid (poly I:C) has also been used to elicit preeclampsia-like features in rats (Tinsley et al., 2009). Mice treated with an inhibitor of placental indoleamine 2,3-dioxygenase (IDO), which degrades L-tryptophan and blocks the proliferation of T cells elicited hypertension and proteinuria in addition to local circulation impairment in the placenta (Nishizawa et al., 2008). Most recently, sera from mild or severe preeclampsia patients injected into $IL10^{-/-}$ mice have elicited hypertension, proteinuria and release of sFlt-1, with similar features being observed in wild type mice using severe preeclampsia sera only, however without the sFlt-1 release (Kalkunte et al., 2010).

These immunological models are pregnancy specific and have the advantage in that they allow an exploration of the role of the immune system and inflammatory cytokines on the development of placental abnormalities that precede the maternal features. While the Th1 adoptive transfer model in mice implicates Th1 cytokines in initiating preeclampsia like features, it is interesting to note that in further experiments this group did not get the same degree of hypertensive response and they suggest that the environmental conditions of housing may modulate the immunological response (Schmid et al., 2007).

Other models of preeclampsia include administration of saline and the mineral-corticoid deoxycorticosterone acetate (DOCA) to pregnant mice (Ianosi-Irimie et al., 2005); intravenous injection of phosphatidylserine/phosphatidylcholine (PS/PC) microvesicles into pregnant mice (Zhang et al., 2009) and treatment of pregnant rats with the angiogenesis inhibitor Suramin (Carlstrom et al., 2009). Other models using transgenic mice have been used to provide molecular insights into pregnancy associated hypertension in humans. Transgenic female mice or rats expressing human angiotensinogen mated with transgenic males expressing human renin display an elevation of blood pressure in late pregnancy, due to secretion of human renin into the maternal circulation (Takimoto et al., 1996, Bohlender et al., 2000). Pregnant mice deficient in catechol-O-methyltransferase (Comt-/-) show a pre-eclampsia-like phenotype resulting from an absence of 2-methoxyoestradiol (2-ME), a natural metabolite of oestradiol that is elevated during the third trimester of normal human pregnancy (Kanasaki et al., 2008). These models may be useful in answering specific questions in the pathology of preeclampsia however they offer little value in understanding the aetiology of the syndrome. More valuable in this respect are two mouse models of spontaneous preeclampsia ; BPH/5 mice (Davisson et al., 2002) and CBA/J x DBA/2 mice (Ahmed et al., 2010) These models may be helpful in clarifying sequence of changes and underlying mechanisms in preeclampsia. The BPH/5 mice are mildly hypertensive before pregnancy so may be useful for teasing out links between predisposition for hypertension and impaired placentation, while the CBA/J x DBA/2 mice is valuable for investigation of immunologically mediated origins of preeclampsia . A recent model of superimposed preeclampsia on chronic hypertension involving pregnant double transgenic mice overexpressing both human renin and angiotensinogen (Falcao et al., 2009), may also prove valuable for investigating mechanisms behind the higher risk for development of preeclampsia in chronically hypertensive women.

### 1.2.1 Ischaemia model: Reduced Uterine Perfusion Pressure (RUPP)

Uterine perfusion pressure is reduced in the pregnant mouse by approximately 40% by placing a sterile tie around the aorta below the renal arteries. A tie is also placed on both the right and left uterine arcade at the ovarian end just before the first segmental artery to counteract the adaptive increase in uterine blood flow via the ovarian artery. This model results in significant and consistent elevations in arterial pressure of 20-30 mmHg as compared to control pregnant rodents at day 19 of gestation in rats (Alexander et al., 2000). It was found that the RUPP-induced hypertension is associated with proteinuria, reductions in renal plasma flow and glomerular filtration rate, a hypertensive shift in the pressure natriuresis relationship, and IUGR in the pups from RUPP hypertensive rats (Alexander et al., 2000). Thus, RUPP-induced hypertension in the pregnant rodent is seen to have features of preeclampsia in women and as such, makes it possible to investigate the functional changes in placental blood flow and correlate these with changes in placental vascular anatomy as they specifically relate to increases in blood pressure and proteinuria.

### 1.2.2 Cytokine imbalance model: TNF-α infusion

TNF-α is infused into the rodent via a subcutaneous implantation of a mini-osmotic pumps designed to deliver a constant release of TNF-α over a period of the pregnancy. This model results in significant and consistent elevations in arterial pressure of 20 mmHg, as compared to control pregnant rodents receiving a saline infusion, at day 19 of gestation in rats (Alexander et al., 2002). In pregnant baboons TNF-α infusion was also shown to lead to an increase in circulating sFlt-1 and proteinuria (Sunderland et al., 2009).

### 1.2.3 Links between cytokine imbalance and ischaemia

Some of these models have elucidated links between TNF-α, ischaemia and even autoimmunity. Serum levels of TNF-α have been shown to increase in response to reduced uterine perfusion pressure (RUPP) in pregnant rats and the administration of a TNF-α antagonist has resulted in both a reduction in TNF-α levels and in hypertension (LaMarca et al., 2005, LaMarca et al., 2008a). Injection of Injection of angiotensin II type I receptor agonistic autoantibodies ($AT_1$-AA) in pregnant mice also leads to an increase in circulating TNF-α and administration of TNF-α neutralizing antibodies results in a decrease of the preeclampsia like features seen in the $AT_1$-AA injected pregnant mice (Irani et al., 2010). Further, both TNF-α induced hypertension and reduced uterine perfusion pressure (RUPP) induced hypertension were associated with the increased production of $AT_1$-autoantibodies (LaMarca et al., 2008b).

While it is has been determined that RUPP and the resultant placental ischaemia leads to an increase in TNF-α (LaMarca et al., 2005), it remains to be determined whether an overproduction of the pro-inflammatory cytokine results in altered placental blood flow and whether this is due to effects on trophoblast invasion and placentation. Outstanding questions to be addressed include whether an imbalance in inflammatory cytokines such as TNF-α affect placental metabolism and lead to changes in placental development, and what the source of an increased inflammatory response in the placenta is in the pre-clinical syndrome in women. Does activation of the innate immune system via toll-like receptors (TLR) stimulate the release of pro-inflammatory cytokines? Does activation of TLR via 'danger' signals released from an abnormal or damaged placenta lead to a positive feedback system where further inflammatory cytokines are released leading to further activation of TLR? The TNF-α infusion model may prove to be a valuable model for investigation of some of these questions.

This thesis will establish a TNF-α infusion experimental mouse model of preeclampsia in order to determine whether an imbalance in pro-inflammatory cytokines alters placental metabolism and development in such a way that placental blood flow is affected. It will investigate whether there is a relationship between; an imbalance in inflammatory cytokines; changes in placental markers involved in inflammation, hypoxia and pH homeostasis; and changes in blood flow in the aetiology of the maternal hypertensive response. Magnetic resonance imaging (MRI) will be utilised for visualization of placental anatomy and for the analysis of changes in tissue morphology and function including blood flow and perfusion. The RUPP model will be established as a perturbed blood flow control model.

## 1.3 Visualization of Placental Structure and Function by MRI

Magnetic resonance imaging (MRI) offers visualization of anatomy and analysis of changes in tissue morphology and function including blood flow and perfusion. Magnetic Resonance Imaging (MRI) studies of placental anatomy and perfusion have been conducted in humans (Damodaram et al., 2010, Moore et al., 2000a, Moore et al., 2000g), mice (Salomon et al., 2006, Tomlinson et al., 2010, Plaks et al., 2011) and rats (Girsh et al., 2007). While dynamic contrast-enhanced MRI, using injected contrast agents, has yielded estimates of mean blood flow in the placenta of animals (Taillieu et al., 2006) non-invasive techniques such as arterial spin labelling (ASL), diffusion weighted imaging (DWI)and measurements of $T_1$ (spin-lattice or longitudinal) and $T_2$ (spin-spin or transverse) relaxation times have been investigated to provide alternative safe techniques for assessing human placental structure and function (Chalouhi et al., 2011). The BOLD (blood oxygen level dependent) effect which relies on the fact that oxygenated and deoxygenated haemoglobin have different magnetic properties, may have the potential to give a functional evaluation of placental oxygenation (Ghugre and Wright, 2012).

### 1.3.1 MRI Imaging Principles

MRI is a technique that relies on the fundamental magnetic properties of atomic nuclei, most commonly that of hydrogen (i.e.,$^1$H; with a nucleus consisting of a proton). As such, MRI can be carried out in a non-invasive manner, with image contrast an inherent property of the differences in type of molecules, motion, position and environment within the tissue.

The hydrogen nuclei possess “spin”, an inherent angular momentum and a magnetic moment. In the absence of an external magnetic field, these spins are randomly oriented and their magnetic moments cancel, however when placed in an external static magnetic field ($B^0$; taken to be oriented along the z-direction), the spins align, in a statistical sense,

with $B^0$ (Figure 1.3.1). A real sample contains an enormous number of such spins. If a sample is then subjected to a pulse sequence; a specific set of short radio frequency (rf) pulses of an oscillating electromagnetic field, delays and, in the case of imaging sequences, magnetic field gradient pulses, the nuclear spins are nutated into the xy plane and it is these coherent transverse components that provide the signal (an oscillating voltage) that is detected and ultimately transformed to produce the image (Figure 1.3.2).

After an rf pulse the system returns to equilibrium through a process known as spin relaxation (Levitt, 2008, Keeler, 2010). There are two types of spin relaxation: longitudinal relaxation which is characterised by a time constant $T_1$, and transverse relaxation which is characterised by a time constant $T_2$. Longitudinal or spin-lattice relaxation involves the loss of energy to the lattice (the surroundings) and determines the time taken for the spins to realign with the magnetic field. Transverse or spin-spin relaxation involves a loss of phase coherence between the individual spins and determines how quickly the signal is lost.

Relaxation is dependent on local fluctuations of the magnetic field around a nucleus due to the presence of other nuclei and their interactions (NB. a spin is itself a small magnet) and mainly results from the reorientational motion of the molecules containing the spins and to a lesser extent translational motion (Reisse, 1983) (Figure 1.3.3). Translational motion or translational self diffusion (herafter referred to as 'diffusion') is the random thermal motion (or Brownian) motion of molecules and is distinct from mutual diffusion (molecular motion due to a concentration gradient). Since molecular motion depends on factors such as the type of molecule, solution viscosity and binding, relaxation times are tissue specific (Price, 2009).

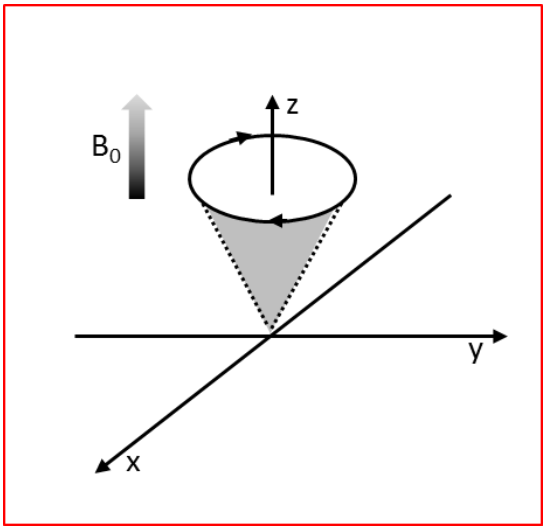


**Figure 1.3.1: Alignment of proton 'spins' in an external magnetic field. Nuclear 'spin' is an inherent angular momentum and magnetic moment and when hydrogen nuclei (protons) are placed in a homogeneous external magnetic field, $B_0$, they will precess around the direction of magnetic field (z-axis).**

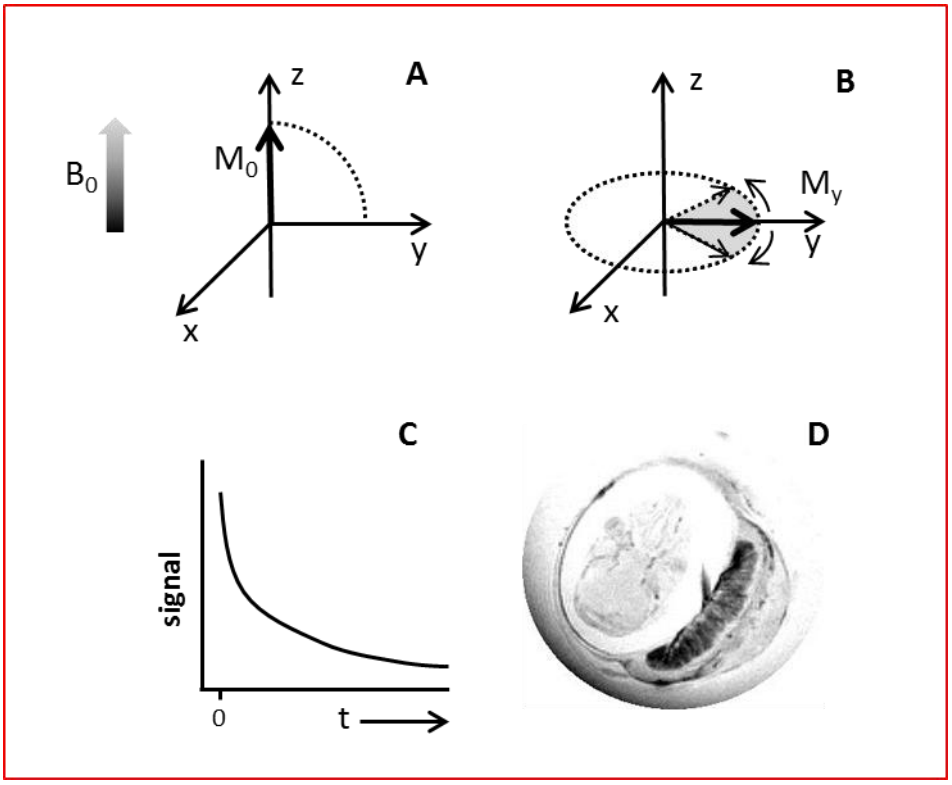


**Figure 1.3.2: Typical NMR experiment. A) In an external magnetic field $B_0$, the nuclear spins are aligned with the z-axis (magnetisation, $M_0$). B) A radiofrequency (rf) pulse rf nutates the nuclear spins into the xy plane and this transverse magnetization is detected. C) The time taken for the spins to lose the magnetisation component in the transverse plane is the spin-spin relaxation time, $T_2$. D) Ultimately the signal is transformed to produce an image.**

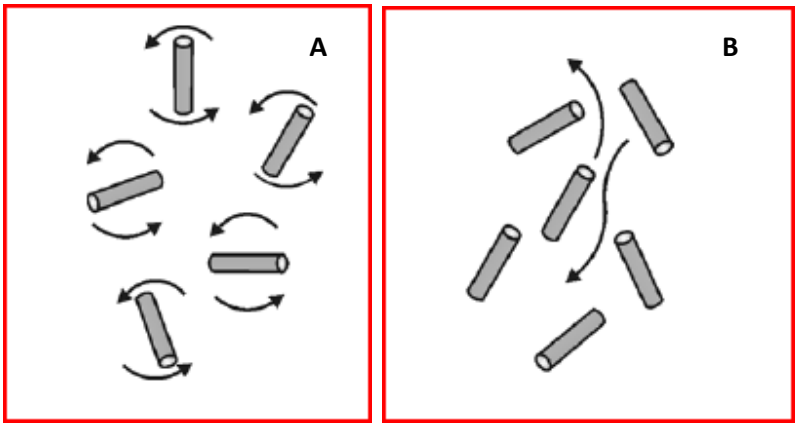


**Figure 1.3.3: Diagrammatic of molecular motion. A) shows reorientational motion and B) shows translational motion or diffusion.**

### 1.3.2 $T_2$ Mapping for Morphology and Function

$T_2$ mapping is a non-invasive technique that has been used extensively to examine tissue morphology. A major source of image contrast in MRI studies performed without the use of contrast agents comes from the inherent variation in relaxation times between tissues, as well as contributions from proton density, diffusion and flow. $T_1$ and $T_2$ relaxation are tissue specific with $T_1$ relaxation tending to be longest when the protons are "bound" to macromolecules, shorter when they are "free" in solution and shortest when they are in intermediate "structured" states. $T_2$ relaxation tends to be longest where protons are "free" in solution and shortest when "bound" to macromolecules (Bottomley et al., 1984). Hence, for instance, highly vascularised tissue will have longer $T_2$ values than cellularly dense tissue, reflecting differences in the amount of freely moving protons in the form of free water within these regions. The presence of paramagnetic ions (*e.g.,* deoxyhaemoglobin) give rise to a short $T_2$ (Ogawa et al., 1990, Meyer et al., 1995, Thulborn et al., 1982) therefore $T_2$ can be sensitive to $O_2$ levels in tissue. Lower intracellular pH has been shown to increase $T_2$ in muscle tissue (Jehenson et al., 1993, Louie et al., 2009).reflecting an increase in free protons in the form of $H_30^+$ ions. Rapidly flowing

protons (e.g., flow of arterial blood) will result in loss of signal as the protons move out of the field of view.

The paramagnetic property of deoxyhaemoglobin (dHB) has been exploited in the blood oxygen level dependent (BOLD) effect, which relies on levels of oxygen saturation of haemoglobin to attenuate the ability of dHb to act as an endogenous contrast agent within tissue (Ogawa et al., 1990, Le Bihan, 2007). Deoxyhaemoglobin causes local magnetic field inhomogeneities leading to dephasing of nearby water protons and resulting in decreased $T_2$ and signal loss in the time constant $T_2^*$ (a parameter that reflects both molecular interactions and local magnetic field inhomogeneities). An increase in oxygen saturation, and thus a decrease in deoxyhaemoglobin (dHb) increases the $T_2$*weighted signal (Ghugre and Wright, 2012). BOLD functional MRI (fMRI) using changes in $T_2$* was first developed for functional brain studies where changes in blood flow and blood oxygenation are closely linked to neural activity (Chen and Li, 2012). The BOLD effect using quantitative $T_2$ relaxation has been used determine the in vivo tissue oxygenation state in myocardial tissue, and has been considered to be potentially more specific than signal intensity measures (traditional BOLD fMRI), allowing regional, longitudinal and cross-subject comparison (Ghugre and Wright, 2012). A recent study has used the quantitative $T_2$ BOLD effect to distinguish between ischaemic, non-ischaemic and normal myocardial segments in a clinical patient population exhibiting coronary artery disease (Manka et al., 2010). The BOLD effect may thus be utilized as an indirect measure of tissue blood flow.

In previous studies of $T_1$ and $T_2$ relaxation times, human placenta has been reported as appearing homogeneous, with no internal morphology apparent (Gowland et al., 1998, Gowland, 2005, Wright et al., 2011). These studies involved static magnetic field strengths of 0.5 or 1.5 Tesla and have shown a correlation of $T_1$ and $T_2$ relaxation times with gestational age and a trend for shorter $T_1$ and $T_2$ times in pregnancies complicated by

preeclampsia and foetal growth restriction (Gowland et al., 1998). No studies correlating placental blood flow or levels of tissue oxygenation with $T_1$ and $T_2$ have been previously reported.

Human MRI scanners have field strengths below 3.0 Tesla, with the majority at 1.5 Tesla. Research spectrometers typically have higher field strengths offering greater signal-to-noise ratios allowing either a reduction in scan times or an increase in spatial resolution which permits much better visualization of anatomical detail. The Bio-Medical Magnetic Resonance Facility at University of Western Sydney offers an 11.7 Tesla wide-bore spectrometer that can accommodate a small mouse, enabling live placental studies at a much higher resolution than previously reported. Issues of animal safety due to the presence of higher magnetic fields and rf electromagnetic waves require consideration (Crook and Robinson, 2009, Smith, 2010); however the facility offers the potential for powerful analysis of tissue morphology and function.

### 1.3.3 MRI Protocols for Measurement of Tissue Perfusion

Perfusion, the process of nutritive delivery of arterial blood to a capillary bed in biological tissue, has been measured by MRI in three different ways. The first, dynamic contrast-enhanced (DCE) MRI is based on the use of contrast agents and the analysis of time-resolved images as the bolus of contrast agent moves through the tissue attenuating the MRI signal. It is useful when blood volume information is required (Petersen et al., 2006) The second, arterial spin labelling (ASL), involves magnetically tagging water protons before they move into the area being imaged, and MRI signals obtained before and after tagging. The advantage of this method is that it is completely non-invasive without the need for injection of any contrast agent and has high spatial and temporal resolution; however it relies on being able to locate and tag an artery perfusing the target tissue. The third

method is Intravoxel Incoherent Motion (IVIM) diffusion-weighted imaging (DWI) and differs from the other two in that it is not a direct measurement of the blood flow to the tissue, but instead measures quasi random blood movement within a single imaging voxel (volume element). (Le Bihan et al., 1988).

### 1.3.4 Diffusion Weighted Imaging

DWI is based on the differential diffusion of water protons in biological tissue. Free diffusion is described by random Brownian motion of the water molecules; however in biological tissue diffusion is restricted by contact with macromolecules, membranes and other cellular or tissue architecture. The extent of movement of water protons is reflected in an attenuation of the signal intensity acquired in a series of images using different diffusion sensitizing gradients. The degree of signal attenuation is proportional to both the movement of water protons and the strength of the gradient pulse (Stejskal and Tanner, 1965, Price, 2009).

To obtain diffusion weighted images a pair of gradient pulses are added to the MRI pulse sequence (Figure 1.3.4). The effect of the first gradient pulse is to create a magnetization helix and the second pulse unwinds the helix thereby refocussing the nuclear spins into coherent transverse magnetisation (i.e., an ‘echo’). In the absence of diffusion the nuclear spins are completely refocussed and a maximum signal will be obtained. In the presence of diffusion, the nuclear spins will have moved and will not be subject to exactly the same magnetic gradient field during the two gradient pulses, and hence the unwinding of the magnetisation helix by the second gradient pulse will be incomplete. As a result not all spins will be in phase leading to an attenuation of the signal intensity. (Stejskal and Tanner, 1965, Price, 2009).

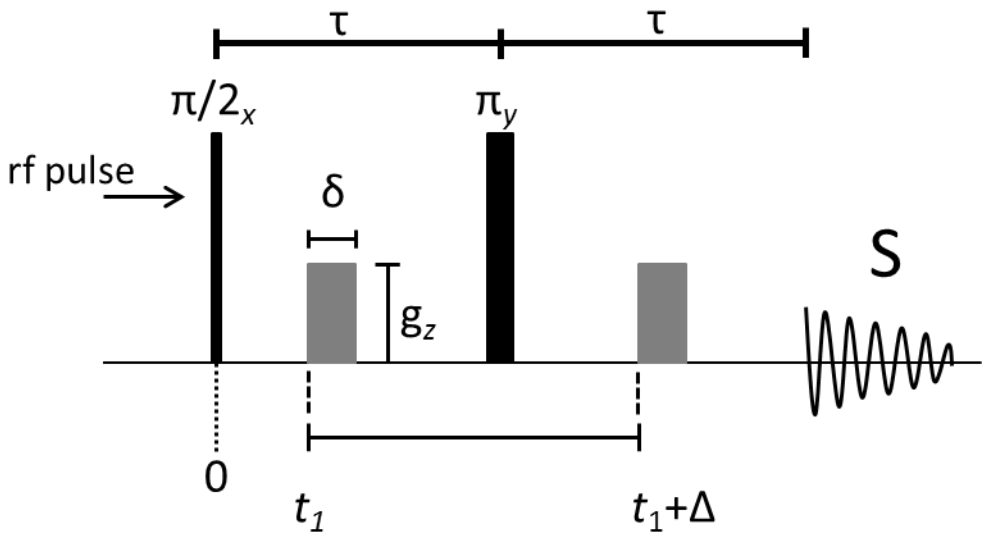


**Figure 1.3.4: The pulsed gradient spin-echo sequence used for measuring diffusion. This sequence (or some variation) is incorporated into the MRI sequences to produce diffusion weighting of the image. The rf pulse prepares coherent transverse magnetisation. The first gradient pulse of length δ and strength g is applied at time $t_1$ and winds the magnetisation into a helix. After a delay Δ, which defines the timescale of the measurement, an identical gradient pulse but of opposite magnitude refocusses the transverse magnetisation which is then detected at $t_{echo}$ =2τ. (adapted from (Price, 2009).**

The signal attenuation is given by; (Stejskal, 1965, Price, 1997, Price, 2009) );

$$E = \frac{S}{S_0} = \exp\left(-\gamma^2 g^2 D\delta^2 \left(\Delta - \delta/3\right)\right) = \exp\left(-bD\right) \quad (1)$$

where *S* is the signal intensity and $S_0$ is the signal intensity when *b*= 0, *γ* is the gyromagnetic ratio, g is the strength of the magnetic gradient pulse, *D* is the diffusion coefficient, *δ* is the length of the gradient pulse and Δ is time between leading edges of the gradient pulses and defines the timescale of the diffusion measurement. All the experimental variables can be grouped into the gradient or diffusion weighting factor, *b*

The signal intensity decays exponentially with increasing *b* values. The decay is sensitive to the mean square displacement (MSD) of the diffusing species. Thus, increased solution

viscosity or physical restrictions (e.g., cell membranes) will reduce MSD over a time dependent on how free or restricted the water movement is in the tissue being imaged. Data analysis proceeds by regressing Eq. (1) onto the signal attenuation data to recover *D*, the only unknown. If the water movement is within a restricted geometry, as is the case for biological tissue, an apparent diffusion coefficient (ADC) rather than the true diffusion coefficient is obtained since the derivation of Eq. (1) does not account for the effects of restriction (Le Bihan et al., 1986)(Figure 1.3.5). The ADC for each voxel of the acquired image can be plotted as a map reflecting differences in tissue diffusivity.

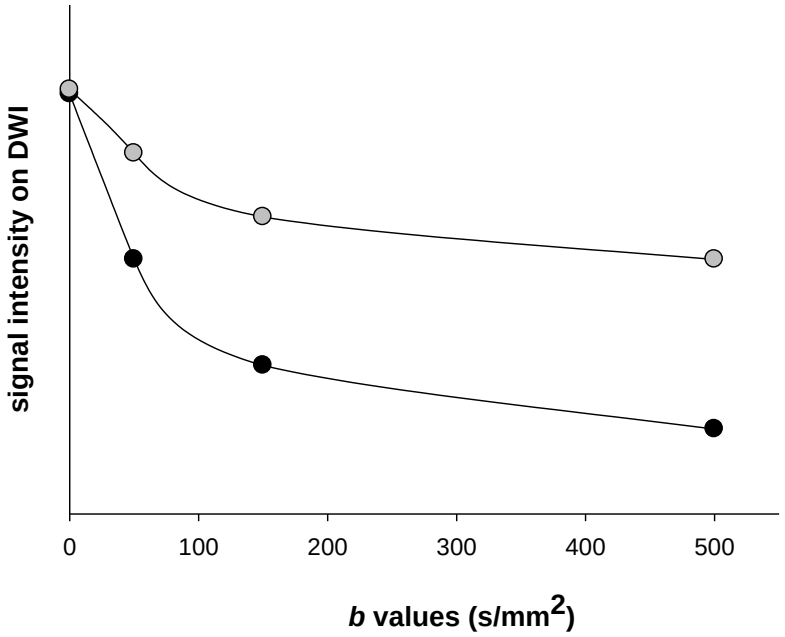


**Figure 1.3.5: Diffusion-weighted imaging signal of tissue with normal or restricted diffusion of water molecules. The attenuation of signal intensity at different *b* values is shown for the case of normal or unrestricted diffusion (black circles) and for restricted diffusion (grey circles). The units for *b* are the inverse of diffusion. In the case of restriction, such as due to tissue cellularity, the apparent diffusion coefficient (mm/2) is less than the true diffusion coefficient. Taken from (Qayyum, 2009).**

### 1.3.5 Measuring Perfusion with Intravoxel Incoherent Motion DWI

Intravoxel Incoherent Motion (IVIM) DWI as first developed by Le Bihan, shows that pure molecular diffusion can be distinguished from perfusion provided that multiple *b* values encompassing both low and high *b* values are used. Signal decay was shown to be bi-exponential with blood flow or perfusion the predominant reason for loss of signal intensity at low *b* values and pure diffusion accounted for at higher *b* values (Le Bihan et al., 1988).IVIM has been used previously for analysis of human placenta (Moore et al., 2000a, Moore et al., 2000g) and for human liver (Luciani et al., 2008).

When the measured signal comes from two populations with different diffusion coefficients the signal attenuation can be expressed by (Le Bihan et al., 1988).

$$E_{voxel} = \left(\frac{S}{S_0}\right)_{voxel} = exp(-bD_S)(1-f) + f\ exp\ (-bD_F) \qquad (2)$$

where $D_S$ is the diffusion coefficient representing pure diffusion (slow component) and $D_F$ is the pseudo-diffusion coefficient associated with perfusion (fast component) and $f$ is the fraction of diffusion linked to perfusion in the voxel.

By plotting the logarithm of the signal intensity against the *b* value, it is possible to differentiate diffusion $D_S$ from perfusion or pseudo-diffusion $D_F$ and then to calculate *f*, the fraction of blood flowing in the voxel compared to the total voxel volume (Figure 1.3.6). In the placenta, $D_F$ can be related to the movement of blood in the intervillous spaces and the flow of blood in the foetal capillaries of the villi.

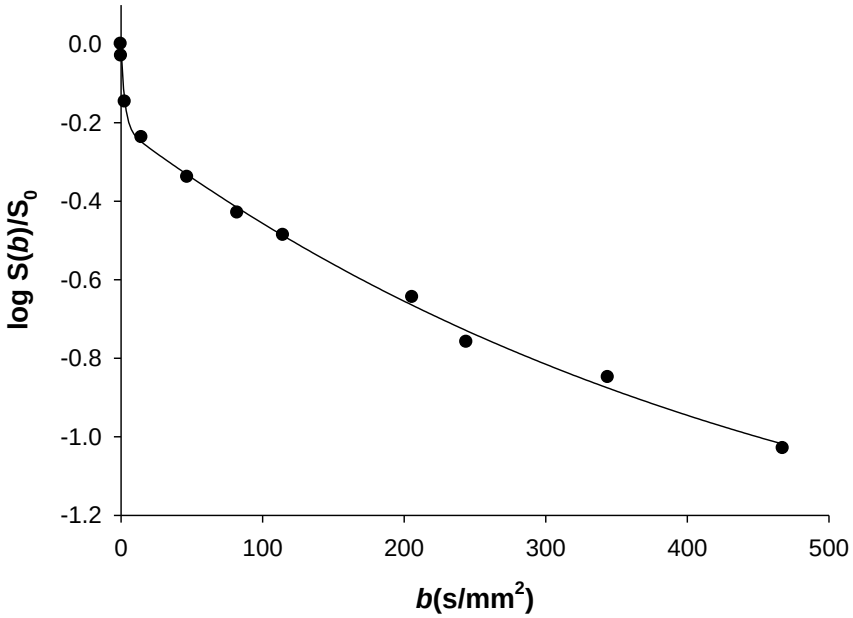


**Figure 1.3.6: A typical IVIM-DWI plot of signal attenuation versus *b* value. The bi-exponential nature of the data on this log/lin plot is obvious and reflects a combination of perfusion and diffusion. At low *b* values loss of signal intensity is due to blood flow, and at higher *b* values loss of signal intensity reflects pure diffusion. Taken from (Moore et al., 2000a)**

## 1.4 Analysis of Placental Structural and Molecular Change

### 1.4.1 Placental Structural change

The structural anatomy of the normal mouse placenta and its blood flow is well documented (Adamson et al., 2002) while others have provided extensive quantitative data describing the structural development of the mouse placenta using stereological techniques (Coan et al., 2004). These techniques enable the analysis of the 3-D structure of tissue whereby features such as volumes, surface areas, lengths and number within tissues can be quantified from images of 2D histological sections using estimation tools and unbiased sampling of randomly generated thin sections (Mouton, 2002, Howard and Reed, 2005). Mayhew has reviewed ways in which stereology has been used to interpret the functional morphology of human and murine placentas including the process of villous growth, trophoblast differentiation, vascular morphogenesis and diffusive transport (Mayhew, 2009), and recent work has used image analyses to determine volume densities and volumes of trophoblast, foetal capillaries, maternal blood space, surface density and surface area of trophoblast and collate those with gene expression and protein changes (McArdle et al., 2009).

Reviewing the studies on human placentas using stereological techniques a number of investigators concluded that in cases of preeclampsia (PE) no significant changes in morphology compared to uncomplicated pregnancies are shown in terms of surface area of capillaries, volume of trophoblast, surface area of trophoblasts, number of cytotrophoblast or syncytiotrophoblast nuclei, thickness of basal lamina or of villous membrane (Teasdale, 1985, Mayhew, 2003, Mayhew et al., 2004, Egbor et al., 2006, Mayhew et al., 2007). However in a study comparing the effect of preeclampsia and foetal growth restriction, found that compared to normal control placentas there were significant reductions in the

intervillous space and terminal villi volumes in preeclampsia alone, while only foetal growth restriction with or without preeclampsia resulted in significant reductions in volumetric and surface area of terminal villous and vascular features, as well as reductions in lengths and diameters of villi and vasculature (Egbor et al., 2006). Smaller surface areas and lengths of villi and capillaries as well as larger diameter capillaries in PE were demonstrated in one study (Burton et al., 1996), and another showed reductions in placental volumes and surfaces (Boyd and Scott, 1985). The classification systems used for PE and IUGR and the time of onset PE may explain the conflicting findings and complicate the interpretations of these results.

While the structural development of the mouse placenta has been described using stereological techniques (Coan et al., 2004), no stereological analysis of the placenta in mouse models of preeclampsia has been undertaken. This thesis aims to investigate the feasibility of measuring and comparing structural features of the placenta by creating complete 3D reconstructions using high resolution MRI images of fixed whole placenta. Conventional stereology uses unbiased sampling and estimation tools to estimate parameters of 3D structures from 2D histological sections. MRI enables imaging of the complete placenta, with visualization software such as Amira™ (Visualization Sciences Group; Mérignac Cedex, France) enabling accurate reconstruction of 3D volumes, and potentially allowing powerful and accurate comparisons of placental morphology.

### 1.4.2 Placental molecular change

Molecular change in tissues can be assessed by examining changes in both protein and mRNA expression and localisation. Some of the most common methods for protein expression include immunohistochemistry (IHC) of tissue sections, and gel electrophoresis of isolated protein fractions followed by immunoblotting. Common methods for examining gene transcription include quantitative polymerase chain reaction (qPCR), and *in situ* hybridisation (ISH) using complimentary RNA. These methods either target known proteins using labelled antibodies or target known genes of interest using complementary sequences. IHC is widely used in basic research for the localisation, distribution and differential expression of proteins in biological tissue. Similarly ISH allows localisation of gene transcription. To screen for and identify changes in unknown proteins, a powerful tool can be found in the combination of two dimensional (2D) gels, followed by excision of protein spots of interest and tandem liquid chromatography and mass spectroscopy (LC-MS/MS) .

The techniques used in this study were IHC for localisation and expression of target molecules and qPCR for quantification of target gene transcripts. A pilot study using 2D gels and LC-MS was carried out and is reported in Appendix 1.

# Chapter 2 Research Hypothesis and Aims

## 2.1 Hypotheses

This project addresses three related hypotheses:

***Hypothesis 1:***

The pro-inflammatory cytokine TNF-α induces hypertension during pregnancy in mice. The induced hypertension correlates with alterations in; placental morphology, molecular markers of hypoxia, molecular markers of inflammation, pH homeostasis, and results in an increase in the release of the toxic compound sFlt-1 into the maternal circulation.

***Hypothesis 2:***

An imbalance in pro-inflammatory cytokine (increased TNF-α) leads to altered placental blood flow as measured by MRI techniques and that this change in blood flow mimics that seen after surgical reduction of the uteroplacental blood flow (RUPP).

***Hypothesis 3:***

Changes in blood flow correlate with the observed changes in morphology and molecular markers of hypoxia, inflammation and pH homeostasis.

## 2.2 Aims

The aims of this project are:

***A.*** To establish two mouse models of preeclampsia; reduced uterine perfusion pressure (RUPP) model and TNF-α Infusion model.

***B.*** To determine the effect of exogenous TNF-α infusion in the pregnant mouse on maternal hypertension, proteinuria and release of sFlt-1 into the maternal serum.

**C.** To measure placental blood flow by MRI, and to determine the effect of exogenous TNF-α infusion in the pregnant mouse on placental blood flow and to compare these changes with those induced by surgical reduction in uterine perfusion pressure (RUPP).

**D.** To investigate the use of high field strength (11.74 Tesla) MRI to assess placental morphology and to determine the effect of exogenous TNF-α infusion and RUPP in the pregnant mouse on changes in placental morphology.

**E.** To determine the effect of exogenous TNF-α infusion and RUPP in the pregnant mouse on changes in molecules involved in response to hypoxia (HIF-1α), inflammation (TLR-3 and 4) and pH homeostasis (CLIC-3).

***F.*** To correlate changes in placental blood flow with changes in placental molecular markers.

# Chapter 3 Methodology

## 3.1 General Outline

C57BL/6JArc mice were timed mated and allocated to one of the treatment groups. Comparisons were made between animals receiving reduced placental blood flow through surgical treatment (RUPP Model), those receiving TNF-α infusions (TNF-α Model), and appropriate controls (sham RUPP or saline infusion). A pilot study was carried out to determine the appropriate dose of TNF-α and the appropriate timing of the interventions to enable successful establishment of the mouse model of preeclampsia.

Animals were allocated to three sets; the pilot study, Set A or Set B (Figure 3.1.1).

Animals in **Set A** had their blood pressure monitored throughout the experiment by tail cuff monitoring equipment (IITC$^{TM}$) to give baseline and post intervention measurements. Baseline and post intervention blood and urine samples were taken in order to test for sFlt-1 (blood) and proteinuria (urine). Animals were euthanized at gestational day (gd) 17, pups counted and weighed and placentas collected for histological analysis of structure and for genomic and proteomic studies. Additionally some animals (Subset A1) underwent post intervention Magnetic Resonance Imaging (MRI) at gd 17 while under anaesthetic in order to measure and quantify placental blood flow. MRI studies were done with the assistance of the Department of Nanotechnology at UWS.

Animals in **Set B** had radiotelemetry devices implanted prior to mating and were subject to continuous blood pressure monitoring until euthanasia 2 days post-delivery. These animals were unable to undergo MRI as the telemeters interfere with the MRI signal. Litters were examined for the number of pups and combined weight and these parameters were

compared. The study outline is shown in Table 3.1 and the sequence of events are shown in Table 3.2

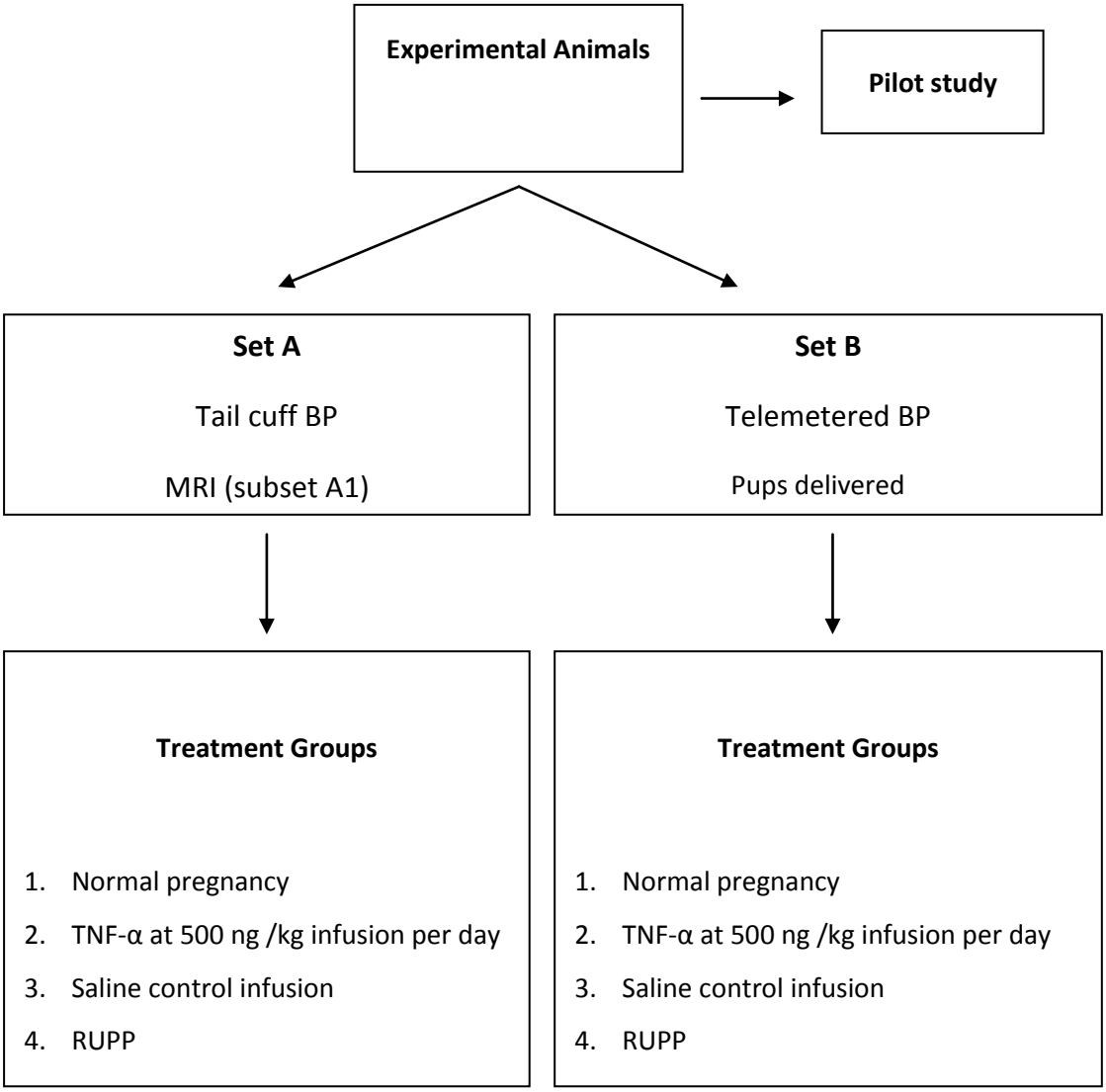


**Figure 3.1.1: Schematic of study**

**Table 3.1: Study outline**

**Pilot study**

| | **Early intervention** | **Late intervention** |
|---|---|---|
| Group 1 Normal pregnancy (n=4)<br>Group 2 TNF-α at 500 ng/kg/day d11 (n=3)<br>Group 3 TNF-α at 500 ng/kg/day d13 (n=3)<br>Group 4 TNF-α at 170 ng/kg/day d13 (n=1)<br>Group 5 RUPP early (d11)<br>Group 6 RUPP late (d14) | **Gestation Day 9-10**<br>confirm pregnancy<br>**Gestation Day 11**<br>RUPP or begin TNF-α or saline infusion<br>**Gestation Day 17**<br>collect placentas | **Gestation Day 9-10**<br>confirm pregnancy<br>**Gestation Day 13/14**<br>RUPP or begin TNF-α or saline infusion<br>**Gestation Day 17**<br>collect placentas |
| Mice euthanized at day 18 for tissue collection<br>BP measured by tail cuff | | |

**Set A: Placental morphology and magnetic resonance imaging (MRI) (subset A1) arm**

| | |
|---|---|
| Group 1 Normal pregnancy (n=11)<br>Group 2 TNF-α at 500 ng/kg/day (n=7)<br>Group 3 Saline control infusion (n=4)<br>Group 4 Sham RUPP (n=5)<br>Group 5 RUPP (n=9) | **Gestation Day 9-10** confirm pregnancy<br>**Gestation Day 13**<br>RUPP or begin TNF-α or saline infusion<br>**Gestation Day 17** MRI (Subset A1)<br>placental collection |
| Subset A1: 3 mice each group with MRI at day 17<br>mice euthanized at day 17 for tissue collection<br>BP measured by tail cuff | |

**Set B: Pregnancy outcomes arm**

| | |
|---|---|
| Group 1 Normal pregnancy<br>Group 2 TNF-α at 500 ng/kg/day<br>Group 3 Saline control infusion<br>Group 4 Sham RUPP<br>Group 5 RUPP | **Gestation Day 9-10** confirm pregnancy<br>**Gestation Day 13**<br>RUPP or begin TNF-α or saline infusion<br>**Postpartum Day 0**<br>pups weighed |
| Total = 5 x 3 pregnant mice (30 total)<br>mice delivered and pups weighed<br>BP measured by telemetry completed for groups 2 and 3 only | |

**Table 3.2: Sequence of events**

| Gestation Day | Set A (Tail cuff and MRI) | Set B (Telemetered) |
|---|---|---|
| Non-pregnant | Acclimatisation to tail cuff restrainer and baseline blood pressure (BP) readings | Telemetric device implanted for continuous blood pressure measurement. 10 days for recovery of diurnal blood pressure pattern. |
| -3 | Oestrus stimulated with male bedding | Oestrus stimulated with male bedding |
| 0 | Time-mated | Time-mated |
| 0.5 | Checked for vaginal plug to confirm mating | |
| 1-9 | Tail cuff BP measured | |
| 10 | Weighed and palpated to confirm pregnancy.<br>Non-pregnant mice returned to a repeat cycle of oestrus and time-mating. | Weighed and palpated to confirm pregnancy.<br>Non-pregnant mice returned to a repeat cycle of oestrus and time-mating. |
| 11-12 | Tail cuff BP | |
| 13 | Tail cuff BP, blood and urine collection (baseline)<br>Interventions according to treatment group | Blood, urine collection (baseline)<br>Interventions according to treatment group |
| | Subcutaneous insertion of TNF-$\alpha$ or saline mini-osmotic pump or RUPP or sham RUPP surgery | Subcutaneous insertion of TNF-$\alpha$ or saline mini-osmotic pump or RUPP or sham RUPP surgery |
| 14-16 | Tail cuff BP | |
| 17 | Tail cuff BP, MRI, blood and urine | Blood and urine collection |
| | *Animals euthanized, pups weighed and placentas collected for histology and genomics and proteomics* | |
| 18-19 | | Pups delivered. Litters examined for number of pups and combined weight<br>Animals euthanized 1-2 days post delivery |

## 3.2 Animals

Experiments were performed on C57BL/6JArc mice. The animals were housed in individually ventilated cages (IVC) (up to 5 per cage), maintained in a 12:12-h light-dark cycle and had *ad libitum* access to water and standard rodent chow. All procedures were approved by the University of Western Sydney Animal Care and Ethics Committee (ACEC) (Approval no A6668, A6908, A10059) and follow the "Guidelines to Promote the Wellbeing of Animals used for Scientific Purposes" as laid out by the National Health and Medical Research Council of Australia (NH&MRC).

Animals subject to blood pressure measurements by telemetry had a blood pressure transducer implanted at 10-12 weeks of age and were then housed individually with the cage placed on a radio receiver. Two weeks after implantation the animals were brought into oestrus by exposure to male bedding in their cage and mated with a stud male 72 hours later at a ratio of 1 male to 1 female. The females were removed from the males the next morning and checked for presence of a vaginal plug. A positive plug was marked as gd 0.5 and pregnancy was confirmed by weight gain and palpation at gd 10.5.

Animals subject to blood pressure measurements by tail cuff had baseline measurements taken for a week prior to bringing into oestrus and mating. Animals were time mated as above. After mating females were housed together until confirmed pregnant and interventions began on gd 11.5 or gd 13.5, where after they were housed individually until the termination of the experiment.

## 3.3 Surgical techniques

### 3.3.1 Radiotelemetry Device Insertion

Surgical anaesthesia was induced with an intra-peritoneal injection of ketamine (100 mg/kg) and xylazine (10 mg/kg). Typically a 20 g mouse received 0.2 ml of a 10 mg/ml ketamine and 1mg/ml xylazine dilution. Alternatively, anaesthesia was performed using isoflurane inhalation, with induction at 4% and maintenance at 2%. This method of anaesthesia allowed better control of depth of anaesthesia, quicker recovery times and no losses due to anaesthetic complications. Analgaesia was administered pre-operatively via subcutaneous injection (buprenorphine 0.1 mg/kg; 0.1 ml/10g of 0.01 mg/ml dilution). The mouse was shaved on the ventral neck and chest area and wiped clean with alcohol. It was gently placed on its back on a heating mat set at 37 °C and covered with a surgical drape. The tail and fore limbs were taped down and the head secured by hooking a thread around the upper incisors and taping to the table. The depth of anaesthesia was monitored by decrease in respiratory rate and pedal reflex. Eyes were coated with ophthalmic lubricant or saline. The surgical procedure was carried out under a stereomicroscope (Nikon, SMZ 1500).

A 1 cm incision was made midline at the neck to expose the salivary glands. A subcutaneous channel was made from the neck site to the right abdomen by blunt dissection to make a pocket to insert the telemetric device. The salivary glands were separated by blunt dissection and the left carotid artery was located deep to the trachea. Using blunt dissection techniques the artery was separated from the connective tissue and the vagus nerve and a silk ligature (5.0) tied at the bifurcation. Two other ligatures were placed loosely around the artery. Haemostats were used to hold and raise the ligature proximal to the heart to occlude blood flow and to raise and hold the distal ligature. The

raised and stabilised artery was then subject to an arteriotomy adjacent to the bifurcation using the bent tip of a 25 gauge needle allowing cannulation of the catheter towards the heart. The proximal traction was loosened to allow entry of the catheter into the artery as far as the aortic arch (Figure 3.3.1). A pulsing radio signal on a portable radio set at 500 kHz confirmed a functional implant in the correct position. The proximal and middle ligature was tied to secure the catheter and the initial ligature was also tied around the catheter to anchor the loose end to the artery. Sterile warmed saline (0.3 ml) was injected into the subcutaneous pocket and the transducer was pushed gently into the pocket. The salivary glands were moved back into position and the skin closed with three to four 5.0 silk sutures (Look, Vitalmed, Dural, Australia).

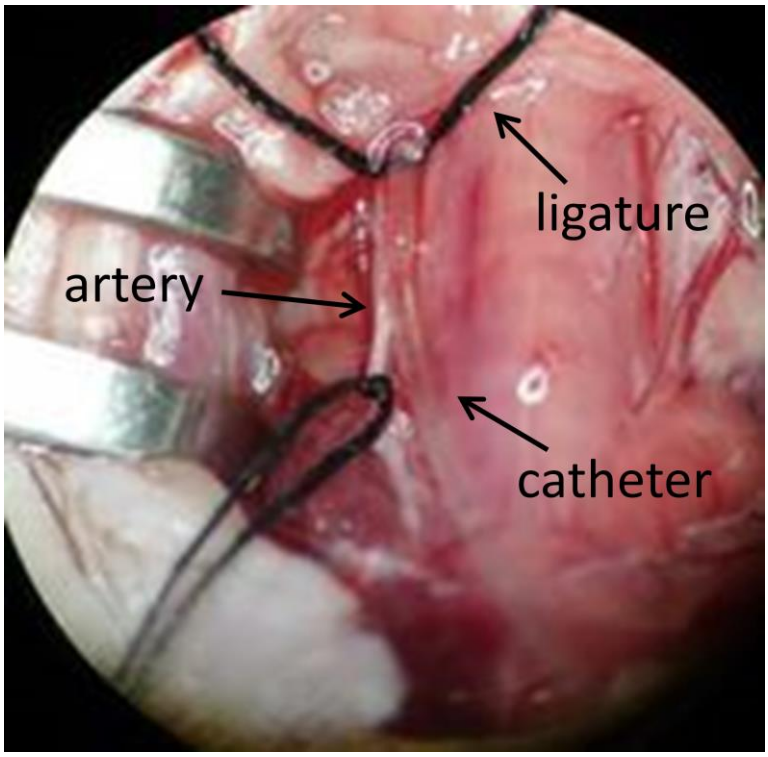


**Figure 3.3.1: Placement of the pressure transducing catheter of the radiotelemetric device. Position of the catheter in the right carotid artery is shown.**

Animals were kept in a warmed environment post-operatively until recovered from the anaesthetic and moving around actively. They were monitored for the presence of pain and additional analgaesia was provided by self-medication using jelly squares containing oral buprenorphine (0.1mg/5ml squares).

In total 34 Telemeter insertions were initiated, the latter number done with the assistance of Kate Mirabato, Monash University, resulting in usable data from 6 animals as detailed below.

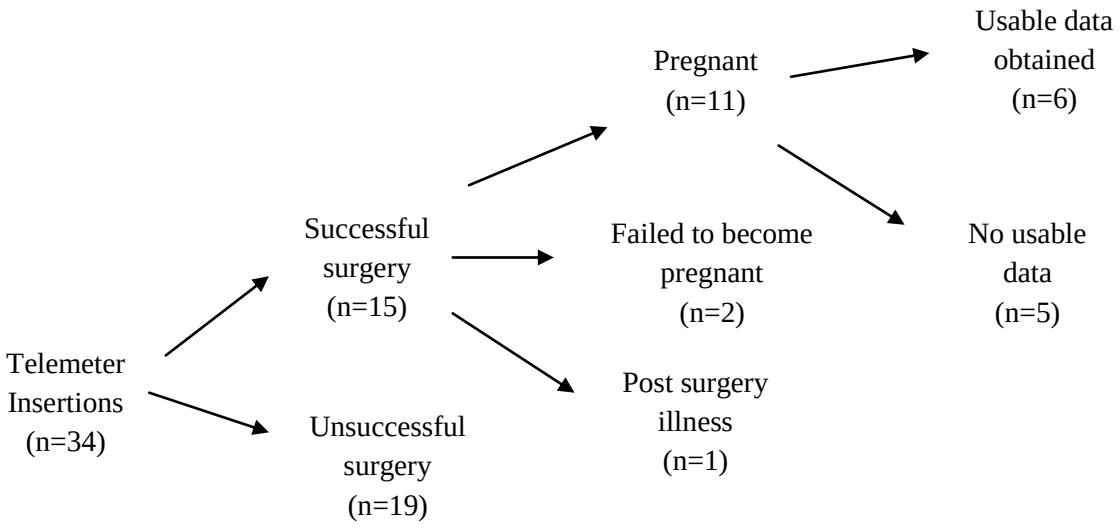


The low overall success rate is due to both the technicality of the surgery and to various issues that arise in obtaining good quality data from the implanted device, including problems with signal interference, difficulties with blood clots in the catheter and variability due to sub-optimal positioning of the catheter. A successful outcome required that the telemetered animals become pregnant and then be subject to further surgical interventions, all within the battery life of the device.

### 3.3.2 Reduced Uterine Perfusion Pressure (RUPP) Surgery

Anaesthesia, analgaesia and mouse preparation was as above except that the abdominal area was shaved. A 1.5 cm incision was made through the skin and muscle of the lower abdominal wall and the bowel was retracted with a swab soaked in warm sterile isotonic saline (0.9% NaCl). After location and isolation from the inferior vena cava, the lower descending aorta was partially ligated with a 5.0 silk suture. Pulsation distal to the ligature was observed and palpable femoral pulses were ensured. The right and left uterine arcade at the ovarian end just before the first segmental artery were located and completely ligated with 5.0 silk sutures. The abdominal wall was closed in layers using 5.0 silk sutures. Animals were kept in a warmed environment post-operatively until recovered from the anaesthetic and moving around actively. They were monitored for the presence of pain and additional analgaesia was provided by self-medication using jelly squares containing oral buprenorphine (0.1 mg/5ml squares) or sub-cutaneous injection of buprenorphine 0.05-0.10 mg/kg every 6-8 hours for 24 hours.

The procedure was designed to make the animal's blood pressure rise by a moderate amount (20 mm Hg) and not to make them sick; however animals which became unwell as a result of this procedure were immediately euthanized. Animal wellbeing was monitored by activity levels (feeding, eating drinking, moving). The first few animals did not appear to tolerate this procedure well. Three of the first 8 animals became ill and required euthanasia, and a further two animals aborted/resorbed all the pups; therefore the subsequent procedure was modified to involve only unilateral ligation of the right uterine artery. The overall success rate was approximately 50% of animals as detailed below.

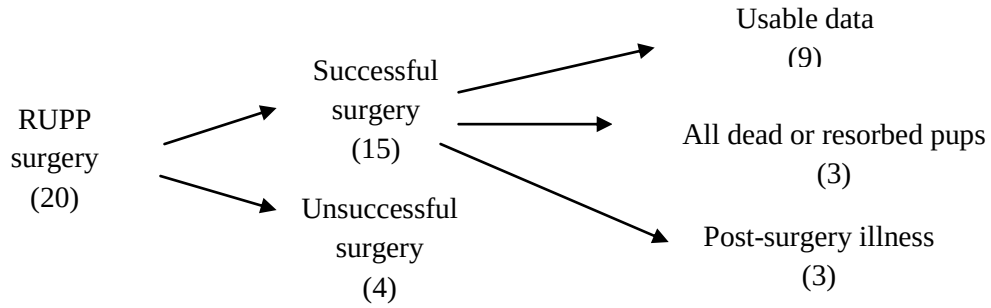


### 3.3.3 TNF-α or Saline Mini-osmotic pump insertion

Anaesthesia, analgaesia and mouse preparation was as above except that the mouse was shaved on the dorsal area below the scapulae and wiped clean with alcohol and was placed on its stomach on a heating mat. A 1 cm incision was made through the skin on the right hand side just below the scapulae. Using a haemostat a subcutaneous pocket was formed by spreading the subcutaneous tissues apart. Warmed saline (0.3 ml) was injected into the pocket. A mini-osmotic pump (Model 1007D, Alzet, Cupertino, CA), primed with either TNF-α or saline, was inserted into the pocket with the flow moderator pointing away from the incision. The mini-osmotic pumps were primed to deliver 500 ng/kg/day of TNF-α for up to 7 days. The skin incision was closed with 5.0 silk sutures.

Animals were kept in a warmed environment post-operatively until recovered from the anaesthetic and moving around actively. They were monitored for the presence of pain but no further pain relief was generally required. The success rate for this surgical procedure was 100% and no animals became ill as a result of this procedure.

## 3.4 Measurement of Mouse Systolic Blood Pressure by Tail-cuff or Radiotelemetry

### 3.4.1 Tail-cuff Sphygmomanometry

Tail-cuff measurements are non-invasive and simple to perform however they have the disadvantage in that the animal requires handling and restraint in order to record a measurement. This process is liable to stress the animals and affect their blood pressure. In order to minimise this effect the animals require acclimatisation to the restrainer and warming cabinet. Additionally, the animals must remain still during the measurement otherwise movement artefacts are encountered. Measurements represent only a single time point and may not accurately reflect the animal's average blood pressure. Tail cuff measurements are the only method available to determine the blood pressure of the animals undergoing MRI as telemetry is incompatible with the scanning equipment.

The procedure for taking blood pressure measurements by tail-cuff involves restraining the mice in a Perspex cylindrical restrainer (Model 84, IITC) and threading the tail through a latex cuff and sensor (Model B60-1/4, IITC Life Sciences, Woodland Hills, CA) (Figure 3.4.1). The restrainer was placed in a warming cabinet (Model 312, IITC Life Sciences) set at 34 °C to warm the mice and to allow blood flow to the tail. The sensor-cuff attached to an amplifier/pump (Model 229, IITC) was inflated to occlude pulsations and the systolic blood pressure was determined at the pressure where tail pulses start to be detected by a photoelectric sensor upon release of occlusion of the blood flow. Mean blood pressure was calculated by the data acquisition software (Model 31, IITC) at the pressure where the highest pulse is detected and diastolic blood pressure was calculated by the software from the systolic and mean blood pressure.

The blood pressure data acquisition software was set for a maximum cuff pressure of 200 mm Hg, deflation rate of 6 units, filter of 250-680 bpm, pulse gain of 9, trigger level 0.26 V, trigger reset 0.25 sec and mean update window of 2.00 sec. After 5-10 min stabilisation in the chamber the inflation/deflation cycle was repeated until 5 acceptable readings were obtained (free of gross movement artefacts and with detectable pulses). The maximum time in the chamber was 30 minutes.

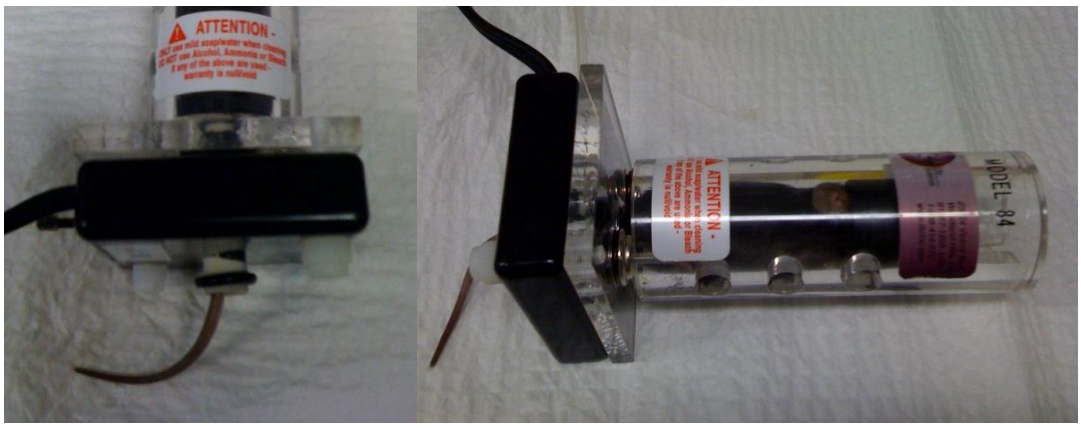


**Figure 3.4.1: Mouse in the Perspex restrainer showing tail cuff and sensor**

Mice were conditioned to the restraint and the warming cabinet for 10-20 min a day for at least three days before measurements were recorded. The mice were handled gently and were not forced into the restraint. The mice will readily move through a cardboard roll into a restraint impregnated with the scent of their bedding, further enticed by a peanut butter treat located in the darkened nose cone of the restraint. Fans in the warming cabinet gently blowing warm air over the noses of the mouse help to calm them and after a few days mice will typically remain still and unperturbed during measurements.

After acclimatisation to the restraint and the procedure, tail cuff measurements were taken for a week prior to mating to gain basal blood pressure readings. Measurements were made during the middle of the daytime resting period of these nocturnal animals. Measurements were repeated until five acceptable pulse envelopes free of gross

movement artefacts and with detectable pulses were obtained and the average systolic blood pressure was recorded. A typical ideal pulse envelope is shown in Figure 3.4.2.

Difficulties in obtaining a good pulse envelope often made it problematic to reliably determine systolic blood pressure. If the mouse did not settle the resultant movement artefacts could preclude an accurate determination of the beginning of the pulse envelope. Sometimes the mouse would restrict blood flow to the tail, resulting in no detectable pulse envelope. Furthermore there were often ambiguous pulse envelopes where it was difficult to determine either the beginning of the pulse and/or the maximum pulse, and indeed the software allows that the “rules” used to determine the beginning of the pulse envelope may be inferior to human judgement, and as such allows manual relocation of the green and red lines which it uses to calculate the systolic and mean blood pressures respectively (Figure 3.4.3). Repeated recordings were not very reproducible, with variations of 30 mmHg not uncommon, often indicating a transient hypertensive response. Readings that were 20 mmHg above the average for the animal for that day were excluded from the data. The overall reliability of the data was very dependent on having well acclimatised animals that remained calm within the restrainer during measurement.

Mean blood pressure is calculated by the software from the pressure where the maximum pulse was detected. This often appeared arbitrary by the software “rules”, and manual determination of maximum pulse was even more so, therefore mean blood pressure and diastolic blood pressure, whose calculation is dependent upon the mean blood pressure calculation, were not reported as they were considered unreliable.

Therefore only systolic blood pressure was recorded for the animals used for the MRI experiments in order to provide BP data in combination with the blood flow analysis.

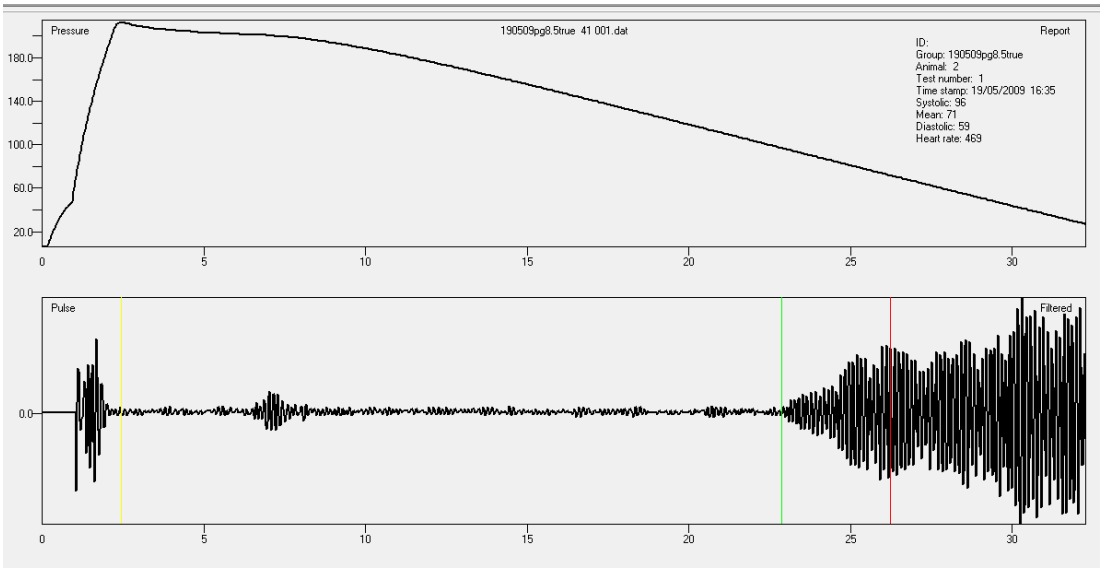


**Figure 3.4.2: Ideal tail cuff blood pressure recording. The top panel shows cuff pressure (mmHg), with the yellow line indicating maximum cuff pressure. The bottom panel shows the tail pulse envelope upon release of occlusion of the blood flow. Systolic blood pressure was determined at the pressure where tail pulses started to be detected upon release of occlusion of the blood flow (green line). Mean blood pressure was taken as the pressure where the highest pulse was detected (red line) and diastolic blood pressure is calculated by the software from the systolic and mean blood pressure.**

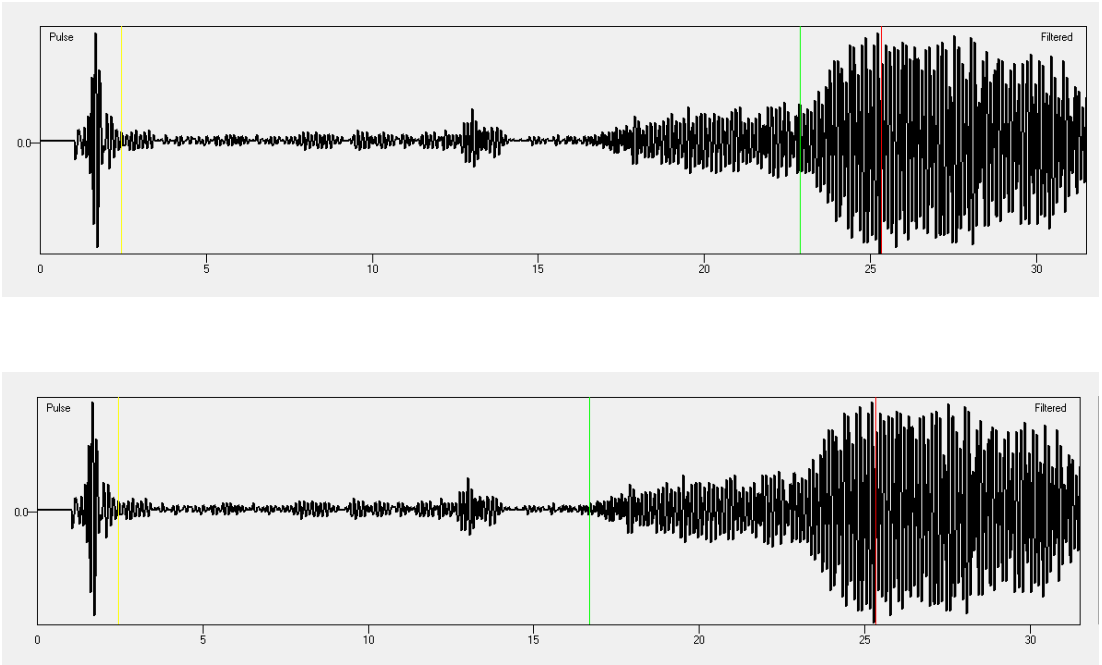


**Figure 3.4.3: Problematic tail cuff blood pressure recording. Typical recordings which show ambiguity in accurately determining the beginning of the pulse envelope (green line), and hence the calculated systolic blood pressure.**

### 3.4.2 Radiotelemetry

Radiotelemetry blood pressure measurement is a direct method of measuring blood pressure whereby a catheter is inserted into either the left carotid artery of the mouse. The catheter is fluid filled and attached to a pressure transducer that transmits signals to a radio receiver. The device (TA11PA-C10, Data Sciences International, St Paul, MN) was implanted into a subcutaneous pocket on the right hand side of the abdomen and after the initial implantation blood pressure was monitored constantly without disturbing the animal. Telemetry enables a more accurate and reliable measurement of blood pressure and can record circadian patterns and dynamic changes after experimental interventions. The device measures mean pressure, systolic blood pressure, diastolic blood pressure, heart rate and animal activity (determined by a relative score dependent on movement of the transmitter in relation to the receiver). Data was recorded for 10 sec every 10 minutes and analysed for average resting (daytime) and active (night time) systolic, diastolic and mean arterial blood pressure (MAP) as well as heart rate and activity. Calculations of average resting (daytime) haemodynamic parameters excluded data corresponding to activity scores above 10, for reasons as will be discussed in Section 4.2.1

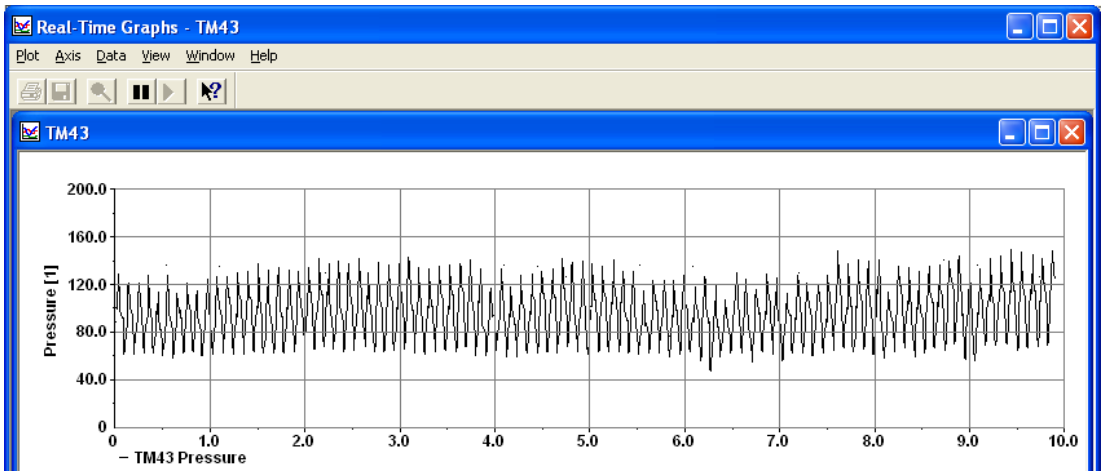


**Figure 3.4.4: Typical waveform of recorded telemetric pressure data. Graph shows 10 seconds of continuous reading.**

## 3.5 Magnetic Resonance Imaging (MRI)

MRI offers a non-invasive technique to conduct dynamic studies on changes in placental structure and blood flow in animal models of preeclampsia. $^{1}H$ MRI images were taken of anaesthetised mice placed in a vertical animal probe using a Bruker Avance 11.74 Tesla wide-bore spectrometer with micro-imaging probe capable of generating magnetic gradients of 0.45 T/m. A number of different imaging protocols were used including FLASH (Fast Low Angle SHot) method, GEFI (Gradient Echo Fast Image) protocol, Multi Slice Multi Echo (MSME) protocol, TrueFISP sequence in FID mode, and Diffusion Weighted Imaging (DWI). Sequence acquisition was gated on respiration in order to reduce motion artefacts.

### 3.5.1 Preparation of Live Animals for MRI

Mice were strapped into the animal probe and the probe inserted vertically into the centre of the magnet from underneath. Preliminary studies used freshly euthanized mice. For studies using live mice anaesthesia was initially by injection of ketamine/xylazine, as this did not require a set up for continuous delivery of gases into the MRI probe, however it did not allow the longer period of anaesthesia that is necessary for all the imaging scans, nor the ability to vary the depth of anaesthesia to standardize the respiration rate used while imaging is undertaken. The final procedure involved induction of anaesthesia with 4% isofluorane in a chamber before the animals were transferred supine to the animal imaging probe. Isofluorane (lowered to 2%) was continuously delivered via a nose cone at an air flow of 150 ml/min. A small collar was used to maintain their head in a vertical position during scanning. A pressure sensitive pillow was taped to their abdomen to monitor respiration, the mice were wrapped for insulation and the animal chamber of the imaging probe was maintained at around 28 °C. The probe was inserted vertically into the scanner and the isofluorane concentration reduced to 1.5-1.7% and titrated to a respiration rate of

approximately 50-60 breaths per minute. Sequence acquisition was gated on respiration (Model 1025 Small Animal Monitoring and Gating System, SA Instruments Inc, Stony Brook, NY, USA) in order to reduce motion artefacts. Initially an anal temperature probe was utilised to monitor body temperature, however as the animal was in a vertical position in the MRI chamber, the probe had a tendency to slip out and as it was observed that the animal did retain its body temperature doing the scanning procedure, the anal temperature probe was not regularly required.

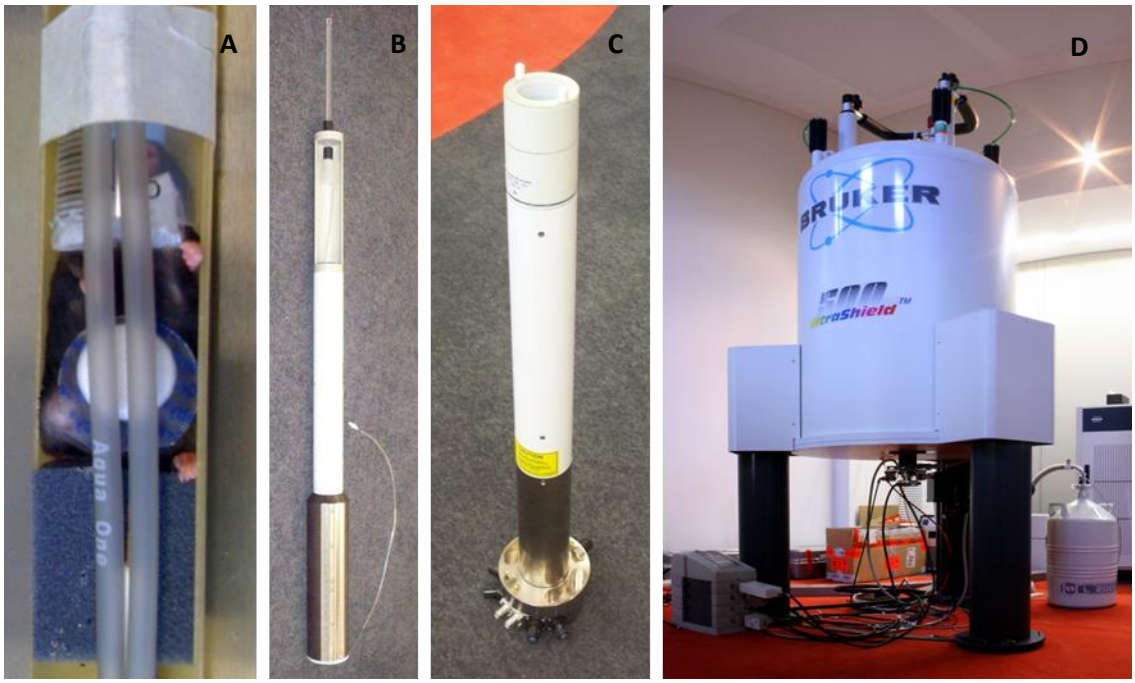


**Figure 3.5.1: Mouse probe and MRI spectrometer. A) shows mouse placed in animal probe bed. B) Animal probe insert, showing animal probe bed at the top which is inserted into C) probe chamber, which is inserted from underneath into D) the 11.7 T magnet of the MRI spectrometer.**

### 3.5.2 Imaging Sequences

A number of parameters including proton density, $T_1$ relaxation and $T_2$ relaxation (among others) contribute to an MRI image. A $T_2$ weighted image is one where the scanning parameters are set up to have a larger contribution from $T_2$ relaxation, but still entail components from the others.

$T_2$ weighted GEFI or FLASH sequences using Paravision 4 Software (Bruker Biospin GmbH, Karlsruhe, Germany) were used to obtain images with enough contrast to identify anatomical structures within the abdomen. Routinely, the GEFI sequence was used to localise the placenta and selected slices were subject to Diffusion Weighted Imaging (DWI), $T_2$ measurements or $T_1$ measurements.

#### *3.5.2.1 Fast Low Angle Shot*

A FLASH sequence using a slice thickness of 1 mm, a repetition time of 100 ms and an echo time of 6 ms was used to obtain high resolution images (in plane resolution of 0.12 mm) in initial studies in order to identify anatomical features of the placenta.

#### *3.5.2.2 Gradient Echo Fast Imaging*

A GEFI sequence was used to obtain a series of localising images across the abdominal region. Images in either the axial or coronal plane were taken from thirty contiguous 1 mm "slices", with a repetition time of 1600 ms and echo time of 2.6 ms, with an in plane resolution of 0.25 mm. High resolution images; repetition time 60ms, echo time 2.6 ms and in plane resolution of 0.12 mm, were taken of selected slices where clear images of multiple placentas could be obtained.

### *3.5.2.3 Diffusion Weighted Imaging*

Slices containing placentas were selected and then subjected to a DWI stimulated echo sequence. After initial trials the following parameters were determined for the acquisition sequence; slice thickness 1 mm, diffusion gradient duration 2 ms, diffusion gradient separation 12.8 ms, echo time 20 ms, repetition time 500 ms, 4 averages, a single $b_0$ image, one direction and 6 different gradient pulses per experiment corresponding to diffusion gradient *(b)* values of 2, 4, 8, 16, 32, 64 s/mm$^2$. As we were interested in the apparent diffusion coefficient (ADC) that correlates to perfusion rather than diffusion, only low *b* values were used. Less b values also made the scan acquisitions faster, reducing the amount of time the animal remained in the scanner. Images were obtained with an in-plane resolution of 0.2 mm.

### *3.5.2.4 Multi Slice Multi Echo*

$T_2$ measurements using the same geometry as the selected GEFI images were also acquired using a MSME sequence (Bruker MSME-$T_2$-map) with a 10 ms echo time and an in-plane resolution of 0.1-0.2 mm. Additional $T_2$ measurements were acquired on the same slices of one normal pregnant mouse immediately after blood flow was reduced to zero by terminal anaesthesia. A MSME sequence keeps all the parameters $T_1$, proton density etc. the same but changes echo time (TE) in order to get a series of images with contrast affected only by $T_2$ relaxation.

### *3.5.2.5 TrueFISP*

$T_1$ measurements using the same geometry as the selected GEFI images were also acquired on some slices of individual placenta using the TrueFISP sequence in FID mode (Scheffler and Hennig, 2001) with a flip angle of 5 degrees, 16 frames and a repetition time of 5 ms.

#### *3.5.2.6 Echo Planar Imaging (EPI)*

Slices containing placentas were selected and then subjected to a EPI-Diffusion weighted sequence with the following parameters; slice thickness 1 mm, diffusion gradient duration 3 ms, diffusion gradient separation 7.5 ms, echo time 20 ms, repetition time 3800 ms, 4 averages, five $b_0$ images, 1 direction and 10 different gradient pulses per experiment corresponding to *b* values of 1, 2, 4, 8, 16, 32, 64, 100, 200, 300 s/mm$^2$.

### 3.5.3 Analysis of DWI and $T_2$ images

MATLAB (The Mathworks, Natick, MA, USA) was used to construct an ADC map of the image by plotting the signal attenuation per voxel against the *b* value of the different gradient pulses used in the sequence. The equation E=A exp(-*bD*) was regressed onto the data using non-linear least squares regression using the Levenberg-Marquardt-Fletcher algorithm in order to recover *D*. A visual image of the relative ADC value per voxel was created. Alternatively, the average signal intensity of groups of 4 voxels in 3 selected regions within individual placenta was plotted against the diffusion sensitive parameter *b* and data fitted to the curve as above.

MATLAB was used to generate $1/T_2$ ($R_2$) maps. The equation A exp ($-t/T_2$) (where *t* is the echo image times) was regressed onto the acquired data using non-linear least squares regression using the Levenberg-Marquardt-Fletcher algorithm.

When calculating $T_2$ a mask was applied that defined the signal intensity threshold. Pixels below this threshold were of low signal intensity and are coloured black and no attempt is made to fit $1/T_2$ to them. Pixels very near the threshold can give erroneous $1/T_2$ values and end up with a white colour. When averaged across the region, the noise affecting the

individual pixels is smoothed out and $1/T_2$ values are obtainable from the sum over a number of the pixels.

For quantification, $T_2$ values were calculated from three groups of 4 voxels in each selected region of interest within 2-5 individual placentas. The ratio of the $T_2$ values of the labyrinth and junctional zone regions ($T_2$lab/$T_2$junc) for each individual placenta was also calculated.

$T_1$ maps were produced for some placentas using MATLAB from data acquired using the TrueFISP sequence in FID mode using non-linear least squares regression using the Levenberg-Marquardt-Fletcher algorithm.

### 3.5.4 Preparation of Fixed Placenta for High Resolution Images

Intact embryo placental units still surrounded by the uterine wall were rinsed in ice cold PBS and fixed in 10% formalin (Sigma-Aldrich, Sydney, Australia) at 4 °C for 14 days, rinsed briefly with Phosphate buffered saline pH 7.4, then equilibrated with 2 mM dimeglumine gadopentetate (Magnevist™) (Bayer Healthcare, Pymble, NSW, Australia) for a further 10 days. Magnevist is a contrast medium for magnetic resonance imaging, acting by decreasing the $T_1$ and $T_2$ relaxation time in tissues where it accumulates.

The placenta, along with the uterine wall, was dissected away from the foetus and embedded in 1% agarose gel containing 2 mM Magnevist in a 10 mm thin wall 500 MHz NMR sample tube (Wilmad Lab Glass, NJ, USA).

### 3.5.5 High Resolution Imaging of Fixed Placenta

A Gradient Echo (GEFI) sequence was used to obtain a series of contiguous images across the complete fixed placenta using the following parameters; echo time 8 ms, repetition time 40 ms, excitation pulse angle 58.4 degrees, 16 averages with 3D 50 µm isotropic voxels, a field of view (FOV) of 11 mm x 11 mm x 20 mm and an MTX of 220 x 220 x 400. Scans typically took 16 h.

### 3.5.6 Creation and Analyses of Placental Maps

Analyses of the placental images were performed with Amira 3D Analysis software (FEI Visualization Sciences Group, Mérignac Cedex, France). MRI image sets from each placenta were imported into the software, segmented into regions on the basis of areas of image contrast and the known anatomy of mice placenta, and volume reconstruction and volume analysis performed.

## 3.6 Tissue collection

Blood was collected from the saphenous vein at times of surgical intervention (20-40 µl) and by cardiopuncture (500 µl) at euthanasia. Blood was collected into a micro EDTA tube (Sarstedt Aust, Technology Park, South Australia), and spun at 3000 rpm for 10 min at 22 °C within 30-60 min of collection. The serum was collected and stored at -80 °C until used for testing.

Urine was collected by free voiding of the mice. A mouse was placed in a clean Perspex cage and allowed to move freely until it had voided. The urine was immediately collected and stored in a microfuge tube at -20 °C until required for testing.

Upon euthanasia of the animal by cervical dislocation, the uterus was dissected from the mouse, weighed, and the placentas and pups removed. The number and individual weights of pups was recorded. Any abnormalities or resorbed foetuses were also recorded. Placentas were dissected with the uterine wall still attached for histology and without uterine wall for proteomics and genomics. Kidney, liver, heart and brain were also collected for future use. For histology, tissues were rinsed in PBS and fixed for 24 hrs in 10% formalin before further processing. For genomics and proteomics, tissues were rinsed in ice-cold PBS, minced and snap frozen in liquid nitrogen before being stored at -80 °C until required.

## 3.7 Measurement of Proteinuria

The urinary spot protein/creatine ratio was initially determined (pilot study) using an IDEXX Urine:PC Ratio Kit (IDEXX, Westbrook, ME, USA), but due to frequent difficulties in collecting enough urine for the kit requirements, protein was determined in the main study using the more sensitive Bradford method (Bradford, 1976) using the commercially available Bradford Reagent (Sigma Aldrich, Sydney, Australia). The assay is based on the

formation of a protein-dye complex which causes a shift in the absorption maximum of the dye from 465 to 595 nm. The amount of absorption is proportional to the protein present. The assay was performed in a 96 well plate with a linear concentration range of 0.1-1.4 mg/ml protein using bovine serum albumin (BSA) as a standard. The intra-assay variability using a single sample was determined to have a CV of 7.9%.

## 3.8 Measurement of sFlt-1

Quantification of levels of sFlt-1 in the pregnant mouse serum was carried out using a commercially available Enzyme linked immunosorbent assay ELISA kit (R&D Systems, Minneapolis, MN, USA). This assay employs the quantitative sandwich enzyme immunoassay technique. A polyclonal antibody specific for mouse VEGF R1 (Flt-1) is pre-coated onto a microplate. Standards, Control, and samples are pipetted into the wells and any mouse sFlt-1 present is bound by the immobilized antibody. After washing away any unbound substances, an enzyme-linked polyclonal antibody specific for mouse sFlt-1 is added to the wells. Following a wash to remove any unbound antibody-enzyme reagent, a substrate solution is added to the wells. The enzyme reaction yields a blue product that turns yellow when the Stop Solution is added. The intensity of the colour measured is in proportion to the amount of mouse soluble sFlt-1 bound in the initial step. The sample values are then read off the standard curve. The specificity of the assay is natural and recombinant mouse sFlt-1 with <0.5% cross-reactivity observed with available related molecules. The sensitivity of the assay is 15.2 pg/ml and the assay range is 125-8,000 pg/ml. The pregnant mouse serum samples were diluted 1/25 immediately prior to assay in order to fall within the assay range. Intra assay reliability was determined using two individual samples, with coefficients of variation (CV) of 6.9% and 8.6% respectively.

## 3.9 Placental Histology and Immunohistochemistry

### 3.9.1 Histology

Fixed tissues were rinsed in 50% ethanol and processed to paraffin overnight through 50%, 70%, 80%, 95%, 100% alcohol and xylene using a Microm STP120 spin tissue processor (Microm International, Walldorf, Germany). Tissues were embedded in paraffin blocks prior to sectioning using a microtome, (Model HM 325, Microm International, Walldorf, Germany). Sections (5-20 µm) were cut and floated on silanised glass slides and examined by Haematoxylin and Eosin (H&E) staining (Grale HDS, Wetherill Park, Australia). For some placenta, serial sections were cut through the whole placenta in order to create a placental map. Periodic acid-Schiff (PAS) stain (Grale HDS, Wetherill Park, Australia) was used to identify glycogen trophoblast cells and uNK cells.

### 3.9.2 Immunohistochemistry

Immunohistochemistry for mouse cytokeratin (trophoblast cells), TLR3 and TLR4, HIF-1, CLIC-3 as well as sFlt-1 and mFlt-1 was undertaken using standard protocols. Antigen retrieval was performed using proteinase K (Dako Aust Campbellfield, Vic, Aus) for 7 min or heat treatment (60min at 98 °C in target retrieval solution pH 6 (Dako Aust, Campbellfield, Vic, Aus) and sections were blocked for 1 hr at 22 °C using blocking buffer (Dako, Aust) and incubated overnight at 4 °C with primary rabbit anti-mouse antibodies as listed in Table 3.3. Visualization was performed by incubating with secondary anti rabbit horse radish peroxidise linked polymer followed by reaction with the chromogenic peroxidise substrate diaminobenzidine (DAB) (Envision kit, Dako Aust) and counterstaining with haematoxylin. Alternatively, immunofluorescent visualization was carried out by secondary staining with Alexa 488 goat antirabbit IgG (Life Technologies, Mulgrave, Vic, Australia). Nonspecific background staining was determined by staining with normal rabbit serum IgG fraction.

**Table 3.3: Antibodies used for immunostaining placental sections**

| Target protein | Abbreviation | Antibody | Supplier | Dilution factor | Antigen retrieval |
|---|---|---|---|---|---|
| Cytokeratin | cyto | pAb Z0622 rabbit pAb | Dako | 1/1000 | Proteinase K 7 min |
| Hypoxia inducible factor 1 | HIF-1α | EP12154 rabbit mAb | Millipore | 1/50 | pH6 heat denature 98 °C 60 min |
| Chloride intracellular channel 3; $Cl^-/H^+$ co transporter | CLIC-3 | Ab128941 rabbit mAb | Abcam | 1/50 | pH6 heat denature 98 °C 60 min |
| Toll-like receptor 3 | TLR-3 | Ab53424 rabbit pAb | Abcam | 1/50 | Proteinase K 7 min |
| Toll-like receptor 4 | TLR-4 | Ab47093 rabbit pAb | Abcam | 1/50 | Proteinase K 7 min |
| Non-specific background | IgG | normal rabbit serum IgG fraction | Dako | 1/2000 | Proteinase K 7 min |

A Zeiss LSM 510 confocal microscope was used to collect images in native lsm format (512 x 512 or 1024 x 1024 pixels). In order to visualize the complete placental section, tile scans using a 10x objective (total magnification 100x) were performed. A region in the centre of the section encompassing approximately $1/5^{th}$ of the placental cross section was selected for a 40 x tile scan (total magnification 400 x) as shown in Figure 3.9.1. This region was selected to be in the central area of the placenta and to encompass all zones of the placenta: the labyrinth, the junctional zone and the decidua. For immunofluorescent studies, this representative 40x tile region (1125 x1125 μm) was used for quantification of fluorescent intensity of target molecules.

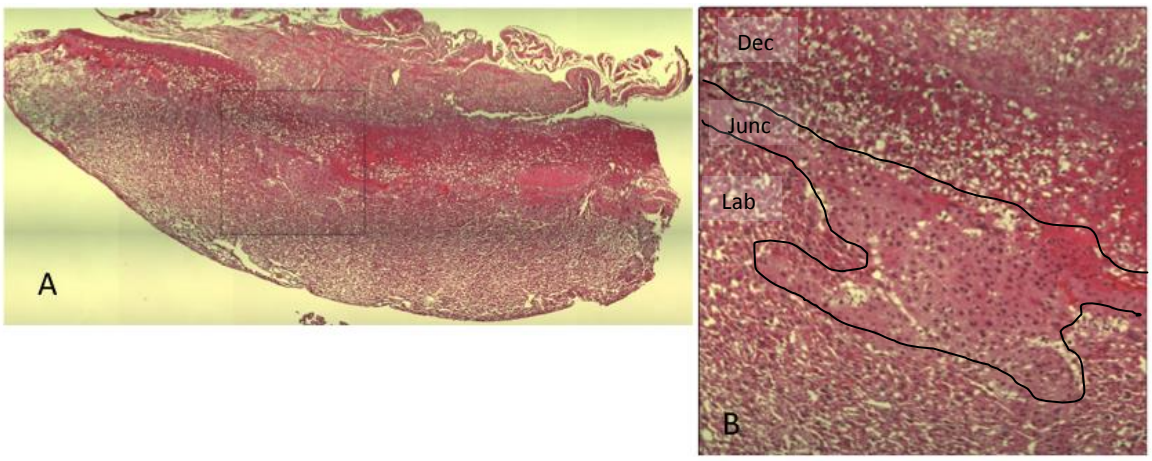


**Figure 3.9.1: Selection of area for immunofluorescent quantification studies. A) 10x tile scan of whole placental cross section with box showing B) region selected for 40x magnification tile scan. Labyrinth (Lab), Junctional zone (Junc) and Decidua (Dec) are indicated.**

### 3.9.3 Quantification of Fluorescent Intensity

Quantification of fluorescent intensity was performed using Image J software (National Institute of Health, Bethesda, Maryland, USA). Each image was analysed and boundaries drawn around the three different placental regions. Two different protocols were employed for fluorescence analysis depending on whether a polyclonal or monoclonal antibody was used.

In the case of the monoclonal antibodies against HIF-1α and CLIC-3, there was little non-specific background staining and staining was predominantly nuclear. The images were thresholded according to the 'moments' algorithm in the Auto-threshold plug-in in Image J software, and both the fluorescent intensity above the threshold and the percent area above the threshold were recorded. The integrated fluorescent density was calculated according to the formula below and used for comparisons between treatment groups.

*Integrated fluorescent density = mean fluorescent intensity above threshold x percent area above threshold.*

In the case of the polyclonal antibodies against cytokeratin, TLR-3 and TLR-4, significant background staining was detected and correction was required. Additionally as the staining pattern was cytoplasmic and widespread, segmenting the data by threshold algorithms was not appropriate. In this case mean fluorescent intensity of each placental region was recorded and corrected for the background fluorescence as determined by control staining with normal rabbit serum IgG fraction. Corrected mean fluorescence was used for comparisons between treatment groups.

## 3.10 PCR

### 3.10.1 Tissue homogenisation, RNA extraction and cDNA synthesis

For tissue studies, 2-4 placentas from each litter were homogenised in the deep frozen state using the Mikro Dismembrator [Sartorius BBI, Bethleham PA, USA]. Total RNA was extracted from 25 mg of powderised tissue using the RNeasy Plus Mini Kit [Qiagen, Hilden, Germany] as per the manufacturer's protocol. RNA was quantified using the NanoPhotometer [Implen, Germany] and cDNA was synthesised from 1000 ng RNA using the Affinity Script qPCR cDNA Synthesis kit [Stratagene, La Jolla, CA, USA] according to the manufacturer's protocol.

### 3.10.2 Quantitative PCR

Quantitative PCR (qPCR) was used to measure mRNA expression of *mFlt-1*, *sFlt-1*, *Hif-1α*, *Tlr-3, Tlr-4, Clic-3* and *Clic-4* in placental tissue. Beta actin *(bAct*) was used as a normaliser gene. Primer sequences are shown in Table 3.4. Primers for *Tlr-3, Tlr-4, Clic-3* and *Clic-4* were designed using Primer3Plus web based software (Untergasser et al., 2007) (see Table 3.5). Published primer sequences for *mFlt-1* and *sFlt-1* (Huckle and Roche, 2004), *Hif-1α* (Chiu et al., 2013) and *bAct* (Surmon et al., 2014) were used. Individual reactions (10 µl) contained GoTaq® Flexi Buffer, 2.5 mM $MgCl_2$ and 1.25 U GoTaq® DNA Polymerase [Promega, Madison, WI, USA], 0.4 mM dNTPs [Bioline, Boston, MA, USA], Sybr® Green I [Sigma Aldrich], 3% v/v dimethylsulphoxide [Sigma Aldrich], forward and reverse primers (0.5 µM), and 4 µl of cDNA (or 4 µl water for no template controls). A pooled sample of cDNA from all placentas was serially diluted to generate a standard curve for each primer set, and the efficiency of the reaction was calculated. Reactions were carried out in a MxPro3005P Real Time PCR System (Stratagene, Agilent Technologies, USA) under the following conditions: 95 °C for 3min; then 40 cycles of 95 °C for 30 sec, 60 °C for 1min,

followed by a dissociation curve. All samples were run in triplicate. Cycle threshold (Ct) values for each sample were calculated using the MxPro QPCR software. Triplicate Ct values were averaged and the fold change of each sample was calculated using the delta-delta Ct method, normalised to *bAct* expression (Livak and Schmittgen, 2001). Normalised fold changes were then log transformed prior to statistical analysis.

**Table 3.4: Primer sequences used for quantitative PCR**

| gene | Forward primer sequence (5'→3') | Reverse primer sequence (5'→3') |
|---|---|---|
| *mFlt-1* | TTCGGAAGACAGAAGTTCTCGTT | GACCTCGTAGTCACTGAGGTTTTG |
| *sFlt-1* | GGGAAGACATCCTTCGGAAGA | TCCGAGAGAAAATGGCCTTTT |
| *tlr-3* | TTGTCTTCTGCACGAACCTG | CGCAACGCAAGGATTTTATT |
| *tlr-4* | ATGGAAAAGCCTCGAATCCT | CTCTCGGTCCATAGCAGAGC |
| *clic-3* | CAGGAGCCACATCTTCGTGA | TGCAACGCACTGTCCAAGTA |
| *clic-4* | AGCGAAGTCAAGACGGATGT | CGCTTCATTAGCCTCTGGTC |
| *hif-1α* | GCTTCTGTTATGAGGCTCACC | TCAAACTGAGTTAACCCCATGT |
| *bAct* | GCTGTATTCCCCTCCATCGTG | CACGGTTGGCCTTAGGGTTCAG |

**Table 3.5: Primers designed using Primer3Plus**

| Primer name | Sequence (5'→3') | Product size | Tm | % GC |
|---|---|---|---|---|
| mouse CLIC3 forward | CAGGAGCCACATCTTCGTGA | 179 | 62.4 | 55 |
| mouse CLIC3 reverse | TGCAACGCACTGTCCAAGTA | | 61.5 | 50 |
| mouse CLIC4 forward | AGCGAAGTCAAGACGGATGT | 174 | 59.9 | 50 |
| mouse CLIC4 reverse | CGCTTCATTAGCCTCTGGTC | | 60.0 | 55 |
| mouse TLR3 forward | TTGTCTTCTGCACGAACCTG | 205 | 60.0 | 50 |
| mouse TLR3 reverse | CGCAACGCAAGGATTTTATT | | 60.1 | 40 |
| mouse TLR4 forward | ATGGAAAAGCCTCGAATCCT | 164 | 60.0 | 45 |
| mouse TLR4 reverse | CTCTCGGTCCATAGCAGAGC | | 59.8 | 50 |

## 3.11 Statistics

Statistical analysis was carried out using Statistical Packages for the Social Sciences (SPSS) software version 21 (SPSS, Inc., Chicago, IL, USA).

### 3.11.1 BP Analysis

Generalized linear modelling using linear regression was used to evaluate the differences between treatment groups in the change in the haemodynamic parameters measured in the telemetered animals between gd 0 and gd 17. A p-value < 0.05 was considered statistically significant.

Generalized linear modelling using linear regression was used to evaluate the differences in systolic BP changes measured by tail cuff between treatment groups. A p-value < 0.05 was considered statistically significant.

### 3.11.2 Maternal and Foetal Outcome Analysis

Generalized linear modelling using linear regression was used to evaluate the differences in a number of parameters between treatment groups. Parameters included concentration of serum sFlt-1, concentrations of protein in urine, number of pups, number of dead/resorbed pups and pup weight. A p-value < 0.05 was considered statistically significant.

### 3.11.3 $T_2$ Analysis

Generalized linear modelling using linear regression was used to evaluate the differences in $T_2$ values between regions in 5 placentas before and after blood flow. Generalized Estimating Equation Modelling clustering placenta within animals and animals within treatment groups was used to evaluate the differences in $T_2$ values and the $T_2$lab/$T_2$junc

ratios. Data are expressed as means ± SE with the level of significance being $p<0.05$. A logarithmic transformation was carried out on ratios prior to statistical analysis.

### 3.11.4 Histochemistry Analysis

Generalized linear modelling using linear regression was used to evaluate the differences in mean fluorescent intensity (Cytokeratin, TLR-3 and TLR-4), or mean integrated fluorescent intensity above the threshold (HIF-1, CLIC-3), of each placental region between treatment groups. A p-value < 0.05 was considered statistically significant.

### 3.11.5 PCR Analysis

Generalized linear modelling using linear regression was used to evaluate the differences in transcript expression between the treatment groups. A p-value < 0.05 was considered statistically significant.

# Chapter 4 Blood Pressure Measurements

## 4.1 Measurement of Mouse BP by Tail-Cuff Sphygmomanometry

### 4.1.1 Tail Cuff Measurements

Measurement of blood pressure (bp) by tail cuff sphygmomanometry was required for the animals undergoing MRI as it is not possible to perform an MRI on animals that have a radiotelemetric device implanted due to both reasons of animal safety should the device move because of torque placed on it by the magnet (Smith, 2010), and because of interference with the image quality (Nolte et al., 2011).

After acclimatisation to the restraint and the procedure, tail cuff measurements were taken for a week prior to mating to gain basal blood pressure readings. Measurements were made during the middle of the daytime resting period of these nocturnal animals. Measurements were repeated until five acceptable pulse envelopes free of gross movement artefacts were obtained and the average systolic blood pressure was recorded.

### 4.1.2 Variation in Normal Systolic Blood Pressure during Pregnancy

Basal blood pressure measurements were taken during the week prior to mating and displayed a wide intra and inter animal variance (Figure 4.1.1). This wide variance was displayed over the course of normal pregnancy and confounded the observation of temporal patterns in blood pressure during the course of gestation. In order to make the trends clearer, alterations in systolic blood pressure during gestation were expressed as the change in blood pressure in relation to basal measurements for each individual animal (Figure 4.1.2). A three phase pattern in gestational change in systolic blood pressure was observed. This temporal trend showed a slow decrease of blood pressure until mid-gestation at gestational day (gd) 10-11, followed by a rise until gd 14, and then a decrease

until gd 17. However, as both the basal measurements and the measurements at each time point had wide intra animal variance, a wide inter animal variance on the group data was obtained. Initial studies with normal pregnant mice saw a rise of blood pressure again at gd 18, presumably due to the onset of labour. As it was considered unwarranted to complicate the data with parturition related blood pressure changes, further experiments beyond the pilot set were terminated at gd 17, and blood and placental tissue were collected before parturition related changes commenced.

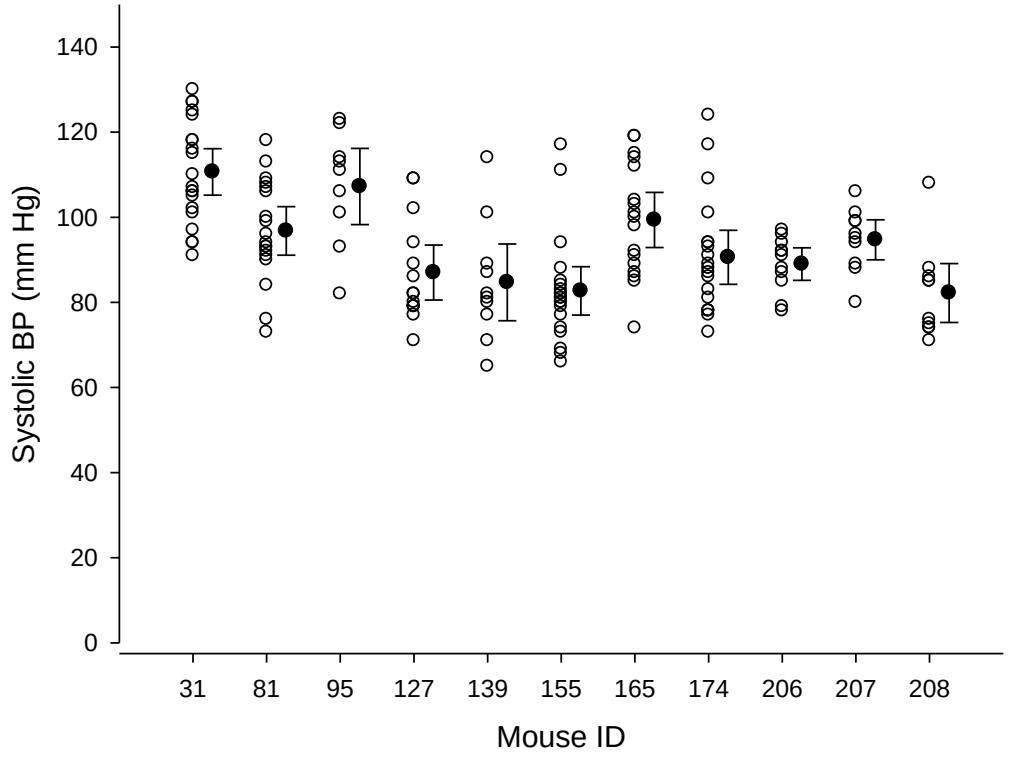


**Figure 4.1.1: Intra and Inter animal variance in systolic blood pressure as measured by tailcuff in individual non-pregnant mice. Plot represents replicate basal BP measurements for individual animals recorded over 3-4 days prior to mating (open circles) or the mean ± 2 SEM (closed circles)**

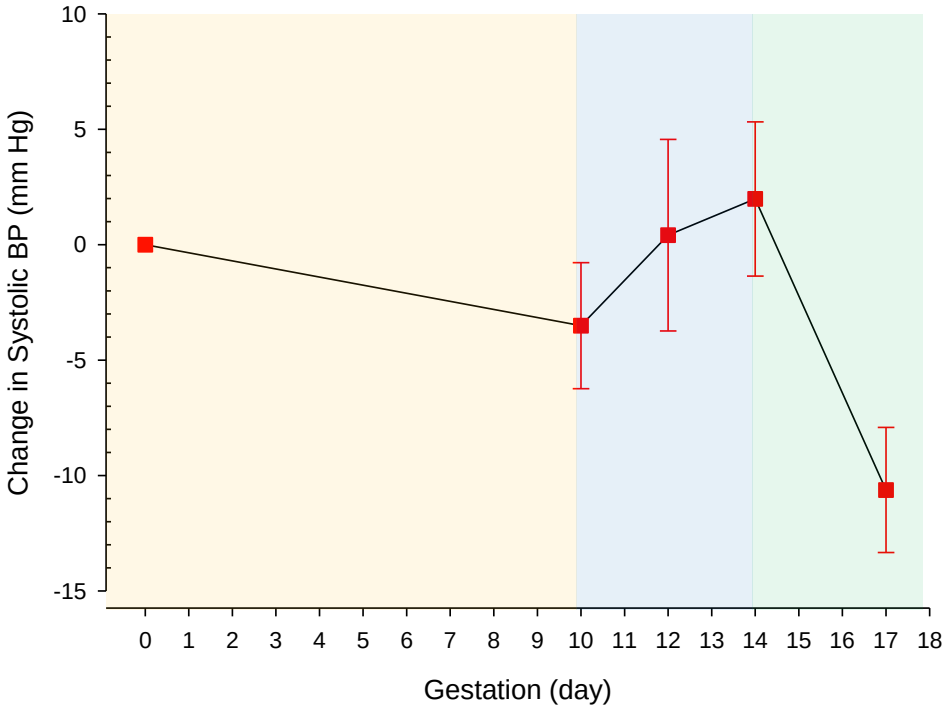


**Figure 4.1.2: Temporal change in systolic blood pressure during gestation. Change in systolic BP compared to basal measurements for each individual animal. (Mean ± SEM, n=11). Shading represents the three biological phases of BP change during gestation; yellow depicts decrease of BP until nadir; blue depicts period of BP rise during mid gestation; and green depicts period until parturition.**

### 4.1.3 Effects of Time of Intervention in the RUPP and TNF-α Models

Initial studies were undertaken to determine an appropriate time for intervention in the two models of preeclampsia; reduced uterine perfusion pressure (RUPP) and TNF-α infusion. RUPP was carried out at gd 11 or gd 14 (Figure 4.1.3). The temporal pattern of gestational changes in blood pressure that were observed in the normal pregnant animals was also observed in the animal in which RUPP was carried out on gd 14. The increase in blood pressure seen after mid gestation (gd 10-11) was not observed in the animal where RUPP was carried out at gd 11. Further experiments with the RUPP model were therefore carried out using a later time point. Gestational day 13 rather than gd 14 was chosen in

order to allow sufficient time for the intervention to have a physiological effect before termination at gd 17.

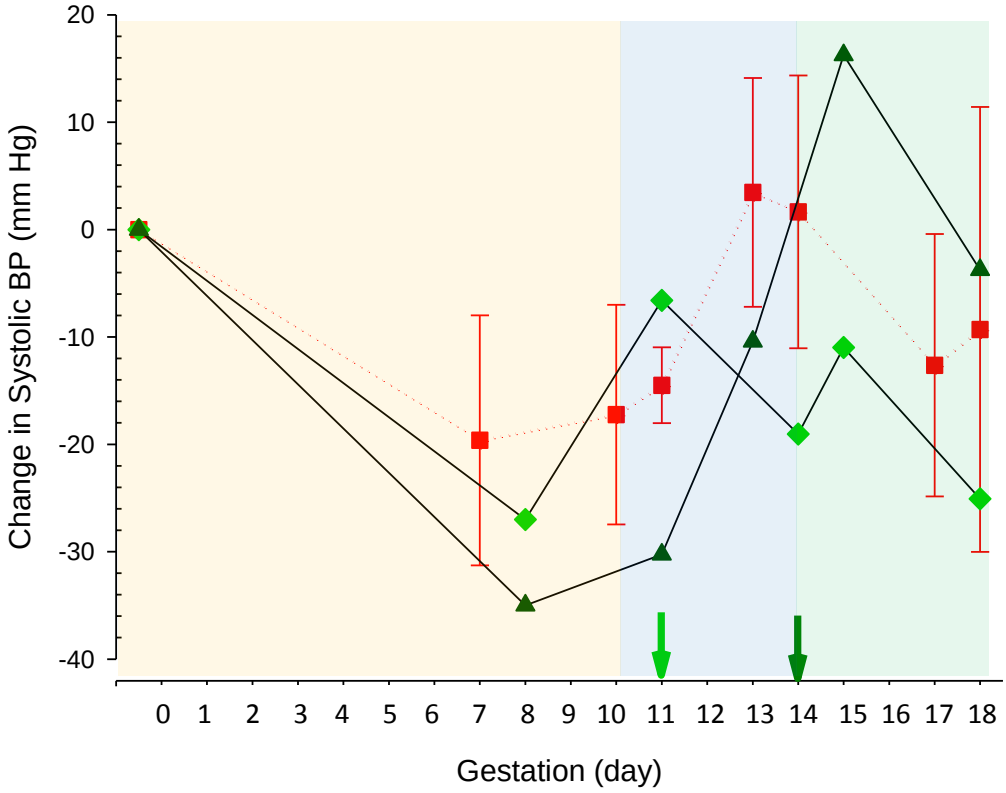


**Figure 4.1.3: Changes in systolic blood pressure during gestation in individual mice subject to RUPP. Control (red, n=4), Early RUPP (light green diamonds, n=1), Late RUPP (dark green triangles, n=1). Shading represents the three biological phases of BP change as outlined in Figure 4.1.2.**

Preliminary experiments with TNF-α infusion of 500 ng/kg/ml was carried out with subcutaneous implantation of the mini-osmotic pump at gd 11 or gd 13, with active treatment period being gd 11-18 or gd 13-18 respectively. In both cases a decrease in systolic blood pressure was observed post intervention, followed by the increase seen after mid gestation in normal pregnant animals (Figure 4.1.4). It appeared that intervention caused a shift in the normal temporal pattern of gestation. An experiment with TNF-α infusion of 170ng/kg/ml from gd 13-18 did not show as pronounced a response (data not shown).

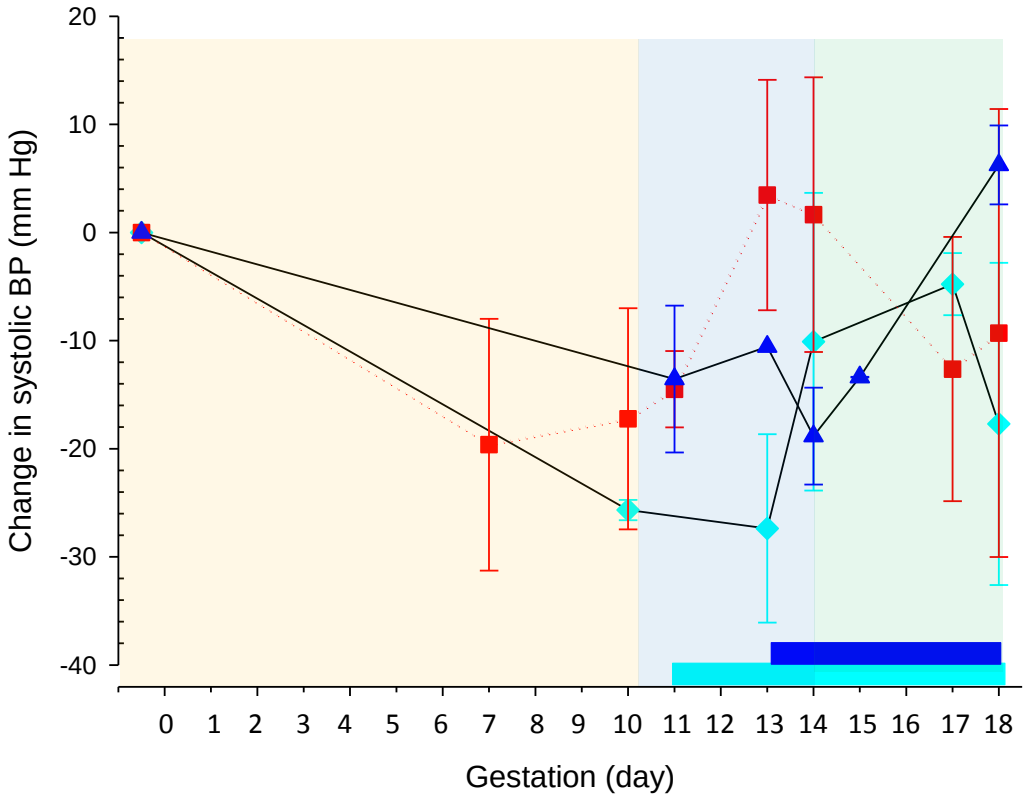


**Figure 4.1.4: Changes in systolic blood pressure during gestation in TNF-α infused mice. Mice were either given early (light blue diamonds, n=3) or late (dark blue triangles, n=3) TNF-α infusion. Control animals (red, n=4) and Active treatment phase (light and dark blue bars) are shown. Shading represents the three biological phases of BP change as outlined in Figure 4.1.2.**

Further experiments with this model were thus performed with infusion of 500 ng/kg/ml from gd 13 as the physiological response was more pronounced with the later timing of intervention, and was consistent with the RUPP intervention time point. Further experiments were also terminated at gd 17 before parturition related changes commenced.

### 4.1.4 Tail Cuff BP Measurements in the RUPP and TNF-α Models

After establishment of the intervention time point, the remaining animals in the experimental groups had tail cuff blood pressure measurements carried out prior to pregnancy (basal) and at gd 12 prior to intervention at gd 13, and at gd 14 and gd 17 only. The within and between animal variation of tail cuff blood pressure measurements created difficulties in identifying significant changes in the RUPP and TNF- α experimental model animals. Patterns and trends could be discerned and are documented below, but they are not significant due to the large standard error in the data. The RUPP animals displayed a similar pattern to normal pregnant animals, with a slight rise in systolic blood pressure at gd 14 followed by a decrease at gd 17 (Figure 4.1.5). Sham animals showed a similar decrease in systolic blood pressure at gd 17. The TNF- α infused animals however exhibited a different pattern, with a decrease in systolic blood pressure at gd 14 following implant of the mini-osmotic pump, and then an increase by gd17 (Figure 4.1.6). This same pattern was observed in the saline infused animals. This trend for a decrease in systolic blood pressure at gd14 may be related to the surgery at gd 13 as it was seen in the TNF- α, saline and sham operated controls, but not the RUPP animals. The RUPP animals showed a trend for an increase in blood pressure the day after surgery possibly as a compensation mechanism for the reduced flow into the uterus, however by gd 17 this effect was no longer observed. While the other treatment groups had recovered from the early pregnancy dip in blood pressure by the gd 12 time point prior to intervention, the TNF-α infused group had not. The TNF-α infused animals are the only group that shows a trend at gd 17 for a rise in systolic blood pressure compared to the gd 12 pre-intervention measurements (Figure 4.1.7).

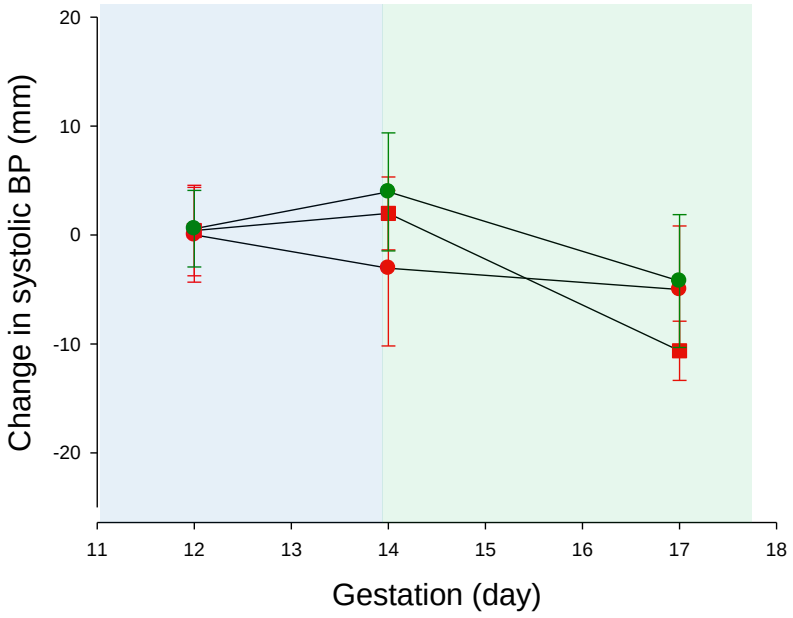


**Figure 4.1.5: Change in systolic blood pressure of RUPP animals as measured by tailcuff. Change in systolic BP compared to basal (non pregnant) at day 12, 14, and 17 of gestation in normal pregnant (red squares, n=11), RUPP (green=9) and sham operated (red circles, n=5) animals. Mean ± 2 SEM (p=N.S) Shading represents the biological phases of BP change as outlined in Figure 4.1.2.**

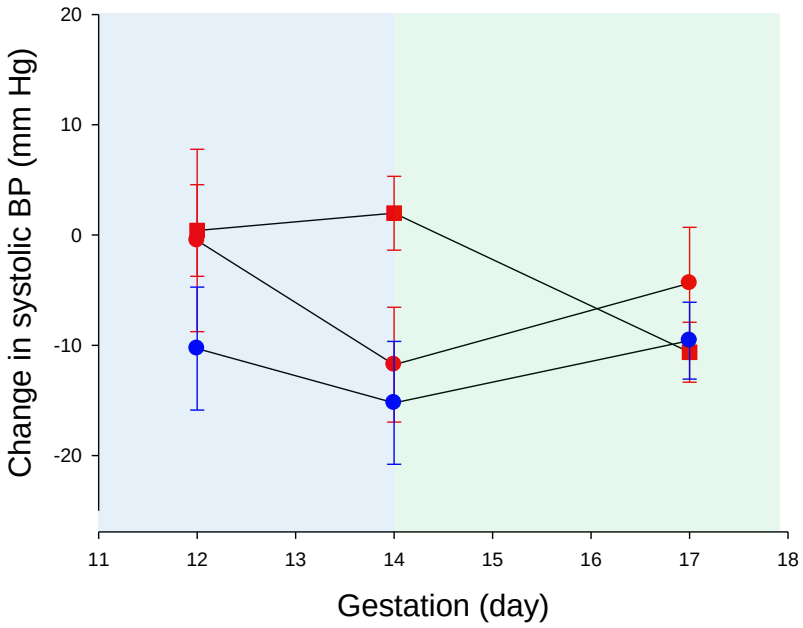


**Figure 4.1.6: Change in systolic blood pressure of TNF-α animals as measured by tailcuff. Change in systolic blood pressure compared to basal (non pregnant) at day 12, 14, and 17 of gestation in TNF-α (blue, n=7), saline (red circles, n=4) infused animals. Mean ± 2 SEM (p=N.S). Shading represents the biological phases of BP change as outlined in Figure 4.1.2.**

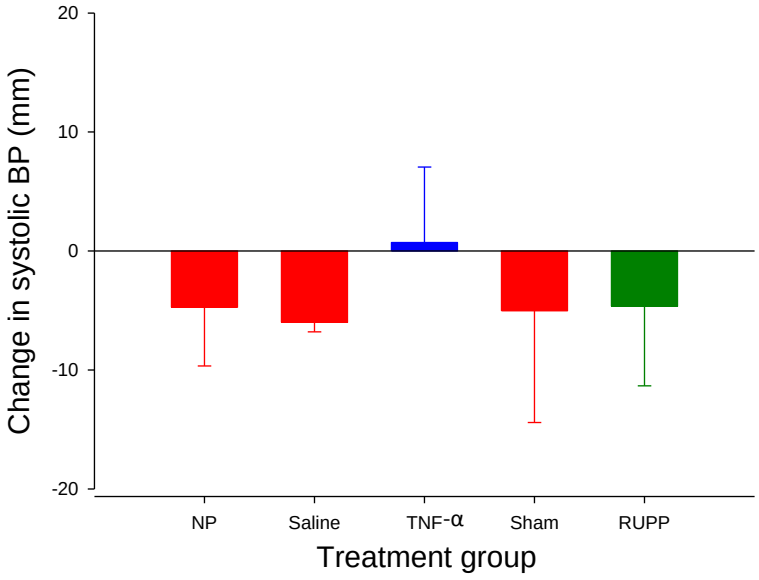


**Figure 4.1.7: Change in systolic blood pressure of RUPP and TNF-α animals as measured by tail cuff. Change in systolic BP compared to day 12 gestation (pre-intervention) at day 17 of gestation in normal pregnant (NP, n=11), saline (n=4) and TNF-α (n=7) infused animals, and sham operated (n=5) and RUPP (n=9) animals. Mean ± 2 SEM (p=N.S)**

### 4.1.5 Summary

Tail-cuff measurements are non-invasive and simple to perform however they have the disadvantage in that the animal requires handling and restraint in order to record a measurement. This process is liable to stress the animals and affect their blood pressure. Additionally, the animals must remain still during the measurement otherwise movement artefacts are encountered. Measurements represent only a single time point and may not accurately reflect the animal's average blood pressure. Large intra animal variance in the replicate basal and gestational measurements created difficulties in detecting whether there were any significant differences in systolic blood pressure across the treatment groups. While the data enabled the determination of the time point of intervention for the study, it was unable to validate the models as experimental models of hypertension in pregnancy. Data from telemetered animals was relied upon for this purpose.

## 4.2 Measurement of Mouse Blood Pressure by Radiotelemetry

### 4.2.1 Telemetric measurements

Radiotelemetry blood pressure measurement is a direct method of measuring blood pressure allowing continuous measurements to be recorded, without any animal handling post surgical implantation. It enables a more accurate and reliable measurement of blood pressure and can record circadian patterns and dynamic changes after experimental interventions. This method of blood pressure measurement was only available for animals not undergoing MRI due to interference of the implanted radiotelemetric devices with the image acquisition and the possibility of damage to the animal should the device move in the magnetic field. Telemetered animals were monitored until parturition in order to collect birth data.

Upon recording the first set of data from a telemetered mouse, the dynamic variations in blood pressure within an animal became evident. Figure 4.2.1 shows basal systolic recordings over four days in a non-pregnant animal. The diurnal variation in blood pressure can be clearly seen in these nocturnal animals. Night time (active) blood pressure was higher than daytime (resting) blood pressure. Within the three hour block around the midday nadir there was a variation up to 30 mmHg in the moment to moment readings. This corresponds to the period in which the tail cuff blood pressure readings were taken and highlights the fact that single measurements are not necessarily representative of the average resting blood pressure. The collection of more data points over greater representative time periods in both the active (night) and resting (day) in the telemetered animals as compared to the tail cuff animals allows for more reliable calculation of mean blood pressure.

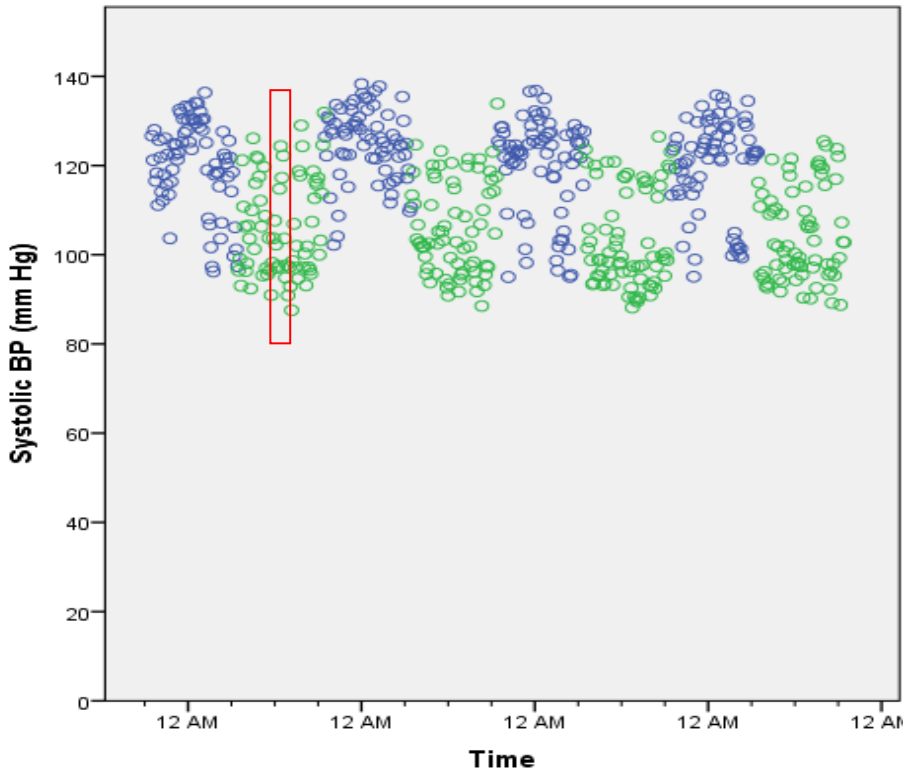


**Figure 4.2.1: Basal systolic blood pressure measurements over four days in a non-pregnant animal. Circles represent the 10sec average recorded every 10 min. Active (night) period is shown in blue and resting (daytime) period is shown in green. The red rectangle indicates the 3 h block around the midday nadir.**

The relationship of locomotor activity to blood pressure was examined in order to determine whether the wide range in daytime measurements was due to changes in levels of activity. Higher levels of locomotor activity clearly correspond to increased blood pressure. However, when activity is recorded as zero or close to zero there is still a wide variation in the recorded blood pressure measurements (Figure 4.2.2). A greater proportion of time spent active during the night (active) period results in a higher mean blood pressure than the daytime (resting) period. Daytime disturbances such as a cage change or other room disturbance can increase the locomotor activity of an animal resulting in a shift in the mean blood pressure (Figure 4.2.3). If data points during active periods are included in the calculation of the resting mean, then the mean will be elevated and not a true indication of

resting mean. Therefore, in order not to confound the resting (daytime) data with the effect of incidental activity, resting blood pressure measurements corresponding to an activity level above 10 were excluded from the mean blood pressure calculations. The effect of exclusion of these data points on the calculation of mean daytime BP over a basal period of eight days are illustrated (Figure 4.2.4) and clearly indicates the need to take into consideration the effect of locomotor activity on blood pressure in mice (Van Vliet et al., 2006). Night time (active) data was not filtered. A number of mice used in the study had diastolic pressures that dropped below 40 mmHg. As this does not fall within the physiological normal range these mice were excluded from the study.

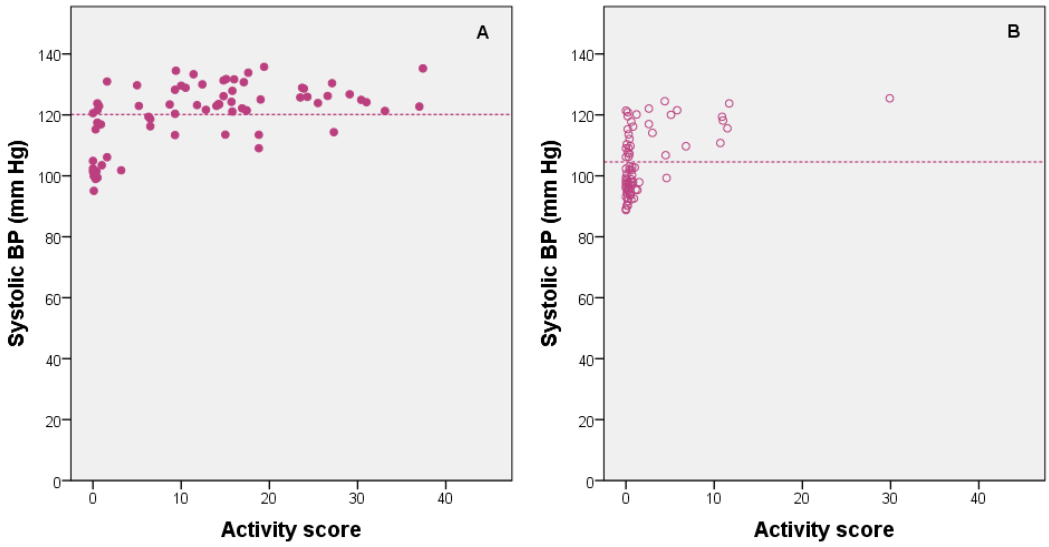


**Figure 4.2.2: Effect of locomotor activity on systolic blood pressure. A) Systolic BP measurements correlating with the activity score of a typical animal during A) the active (night) period and B) the resting (day) period. Dotted line shows the calculated mean for active (113.5 mm Hg) and resting (104.6 mm Hg) periods.**

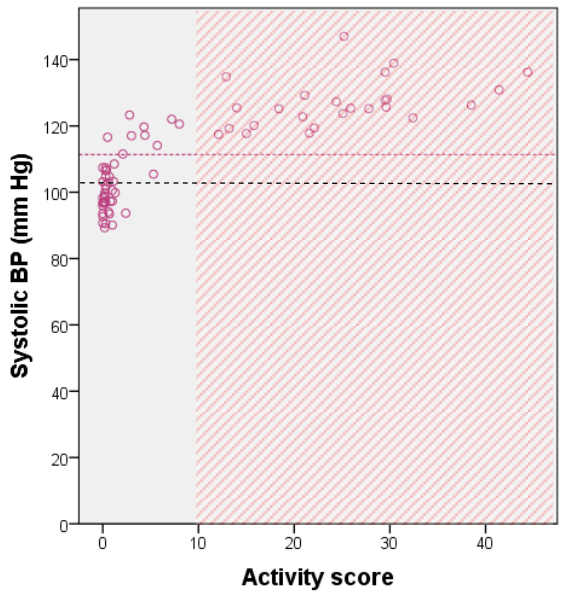


**Figure 4.2.3: Effect of disturbances during the resting period on the calculated mean systolic blood pressure. Systolic BP measurements correlating with the activity score of an animal during the resting (day) period on a day when the animal was disturbed by cage changes. The purple dotted line shows the mean calculated with all data points (mean 111.3 mm Hg) and the black dotted line shows the mean when data points corresponding to an activity > 10 are excluded (mean 103.8 mm Hg). Shading shows excluded data points.**

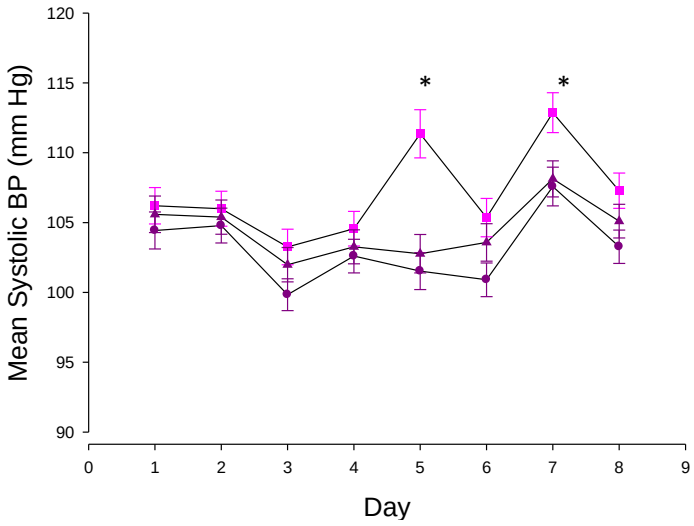


**Figure 4.2.4: Effect of activity filters on mean resting systolic BP of basal (non-pregnant) mice. Activity filters were applied to exclude BP measurements corresponding to high activity caused by incidental disturbances during the animal's resting period from calculation of the daily mean resting BP. Mean BP calculated with all data points included (pink squares). Mean BP calculated with data points corresponding to activity >10 excluded (purple triangles); Mean calculated with data points corresponding to activity >5 excluded (purple circles). Asterisks indicate outliers that are significantly different from the group mean over the 8 days (104.3±0.43, p<0.001)**

### 4.2.2 Blood pressure phenotype of TNF-α Model mice

Pre pregnancy baseline haemodynamic data for the C57BL/6 mice strain used in this study are shown in Table 4.1. The animals were randomised to receive either TNF-α infusion or saline infusion from gd 13 till parturition. Haemodynamic changes during gestation are shown in Figures 4.2.5 to 4.2.10. Daytime (resting) and night time (active) measurements are illustrated separately. The three phase changes in systolic BP that were observed in the control animals by tail cuff measurements were also observed in the telemetered animals. In both the resting and active periods, the control animals exhibited a slow decrease of systolic arterial pressure (SAP) until a nadir at gd 9, and then an increase back towards baseline by gd 12-13 followed by a plateau until parturition at gd 18 or 19. Diastolic arterial pressure (DAP) and mean arterial pressure (MAP) exhibited a similar pattern, except the rise after the nadir at gd 9 was not as pronounced as for SAP. The TNF-α infused animals followed the same pattern as controls until the intervention at gd 13, however from this point on the SAP, DAP and MAP continued to rise significantly until parturition.

A difference in the temporal pattern of pulse pressure (PP) was observed between the resting and active periods. During the active period the PP of the TNF-α infused animals exhibited the same significant hypertension observed in the SAP, DAP and MAP measurements, compared to the control animals, however during the resting period there was no difference between control and TNF-α infused animals. Heart rate (HR) increased until gd 8, then decreased until gd 12-13, then increased slightly or plateaued until parturition, with no significant difference between control and TNF-α infused animals. The pattern was more pronounced during the active period. There was no gestational change in activity during the resting period for either group, while during the active period there is an marked increase in activity till gd 6-7 followed by a decrease until parturition for both

control and TNF-α infused animals, with no significant differences between the two groups observed.

The differences in changes in pulse pressure between treatment groups that were seen during the active period, but not the resting period, may be a consequence of a differential response to the decrease in night time (active) activity in the latter stages of gestation. Pulse pressure is determined by an interaction of stroke volume and properties of the arterial circulation (Dart and Kingwell, 2001) and is known to increase during exercise due to an increase in stroke volume (Higginbotham et al., 1986). During gestation, the night time activity of the mice decreases, and the slight decrease in night time pulse pressure observed in control animals would be consistent with the decrease in activity. However, despite the decrease in activity, the pulse pressure of the TNF- α animals remains high during the night time (active) period, indicating a hypertensive response.

These results confirm that TNF- α infusion is an experimental model for induced hypertension in pregnancy.

**Table 4.1: Baseline haemodynamic parameters of saline infused (n=3) and TNF-α infused (n=3) C57BL/6 mice.**

| Parameter | Saline | | | TNF-α | | |
|---|---|---|---|---|---|---|
| | **Night (active)** | **Day (resting)** | **24 hr** | **Night (active)** | **Day (resting)** | **24 hr** |
| **SAP (mm Hg)** | 136.1 (3.1) | 123.9 (2.2) | 130.3 (2.8) | 126.2 (5.9) | 118.4 (5.8) | 122.3 (5.9) |
| **DAP (mm Hg)** | 97.4 (4.4) | 88.0 (2.9) | 92.9 (3.5) | 93.2 (3.1) | 86.3 (4.1) | 89.7 (3.6) |
| **MAP (mm Hg)** | 116.5 (1.0) | 106.7 (0.7) | 111.9(0.4) | 109.4 (3.8) | 102.2 (4.7) | 105.8 (4.2) |
| **PP (mm Hg)** | 38.4 (7.4) | 35.9 (5.1) | 37.2 (6.3) | 33.0 (4.9) | 32.0 (3.8) | 32.5 (4.3) |
| **HR (bpm)** | 568.6 (3.3) | 563.0 (16.8) | 566.0 (9.7) | 544.0 (13.9) | 559.8 (13.6) | 552.0 (12.8) |
| **Activity (au)** | 15.4 (1.5) | 3.4 (0.8) | 9.4 (0.4) | 11.5 (1.7) | 5.4 (1.1) | 8.4 (1.0) |

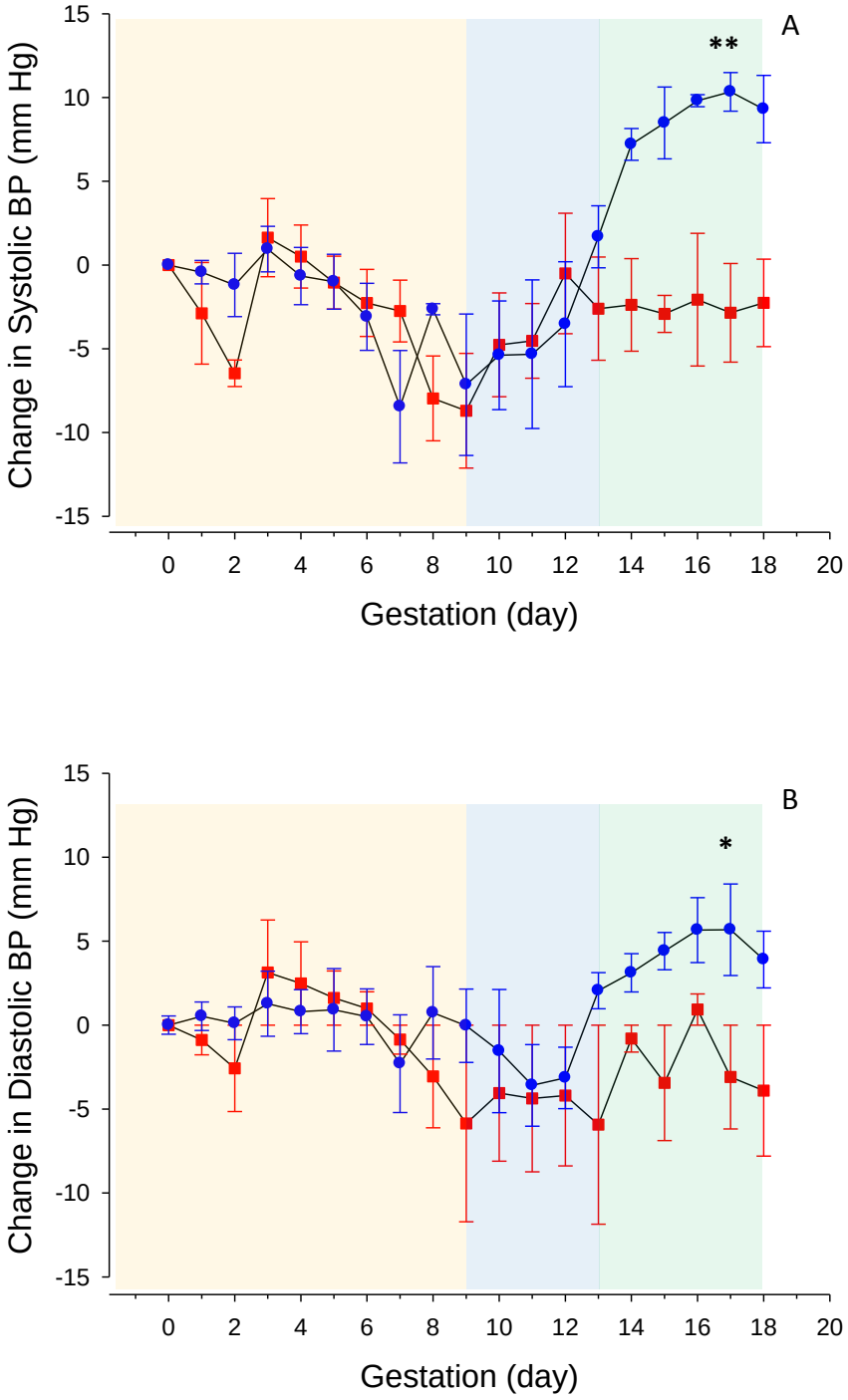


**Figure 4.2.4: Change in resting (daytime) systolic (A) and diastolic (B) blood pressure. Plot shows TNF-α infused animals (blue dots, n=3) and saline infused control animals (red squares, n=3). Data is averaged over the 12 hr light (resting) period, normalised to gestational day 0 baseline for each animal and presented as mean ± SEM (*p<0.05, **p<0.01). Data points coinciding with Activity >10 have been excluded. Shading represents the three biological phases of BP change as outlined in Figure 4.1.2.**

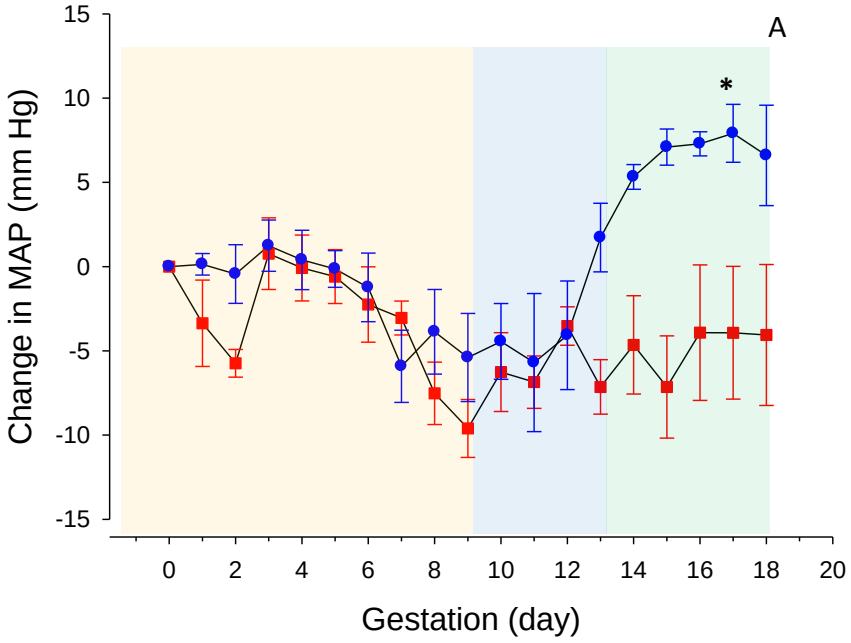


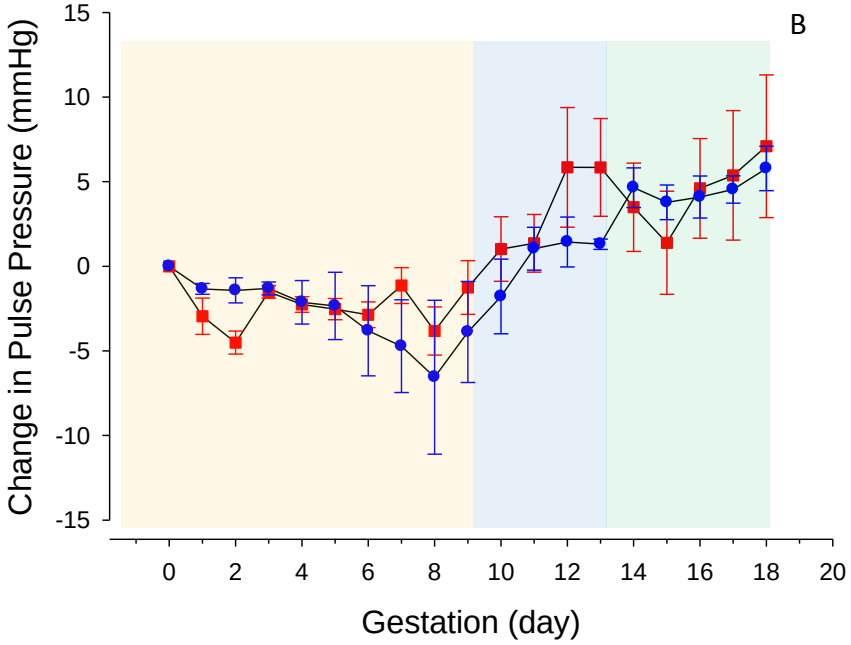


**Figure 4.2.5: Change in resting (daytime) mean arterial pressure (A) and pulse pressure (B). Plot shows TNF-α infused animals (blue dots, n=3) and saline infused control animals (red squares, n=3). Data is averaged over the 12 hr light (resting) period, normalised to gestational day 0 baseline for each animal and presented as mean ± SEM. (*p<0.05) Data points coinciding with Activity >10 have been excluded. Shading represents the three biological phases of BP change as outlined in Figure 4.1.2.**

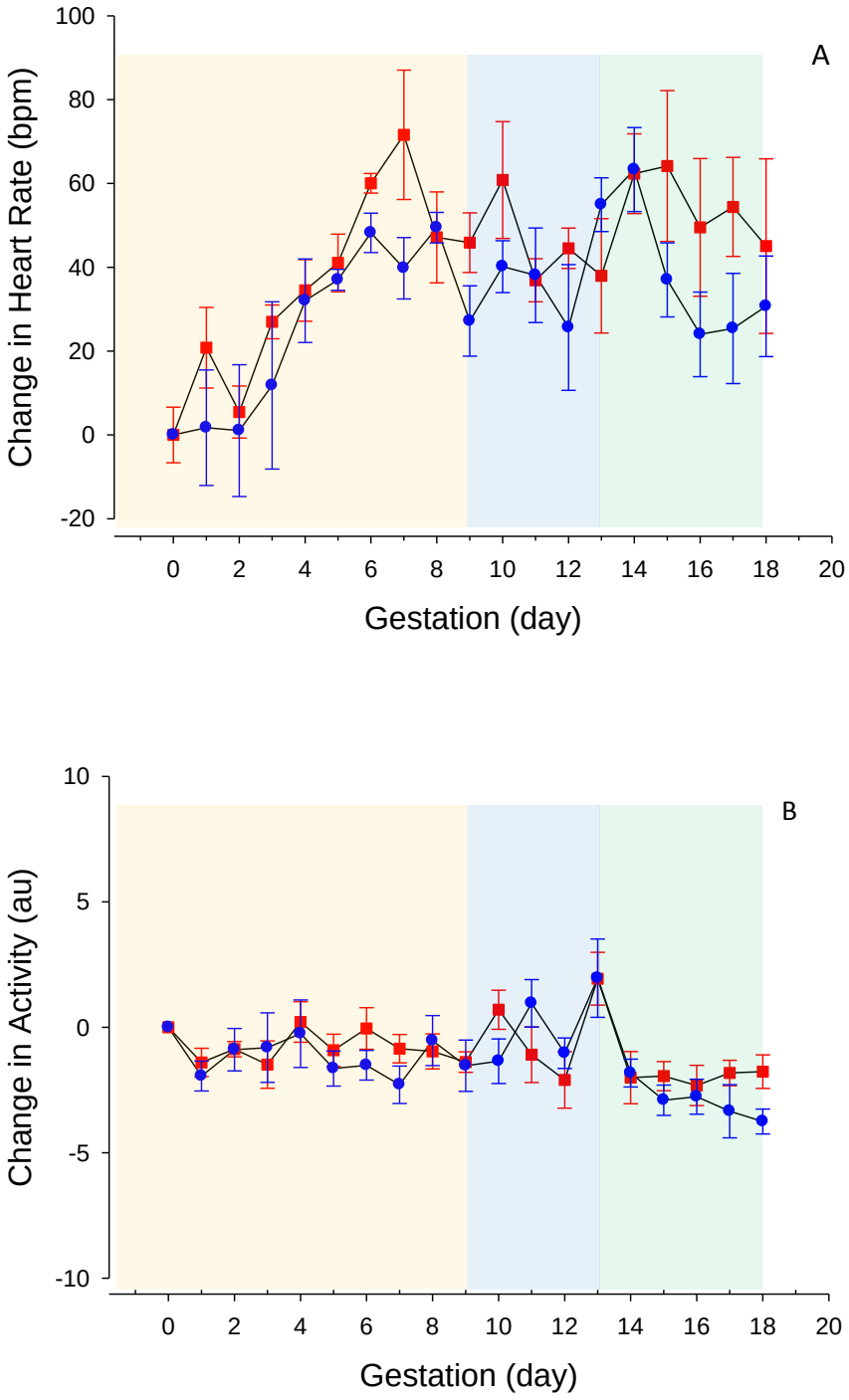


**Figure 4.2.6: Change in resting (daytime) heart rate (A) and activity (B). Plot shows TNF-α infused animals (blue dots, n=3) and saline infused control animals (red squares, n=3). Data is averaged over the 12 hr light (resting) period, normalised to gestational day 0 baseline for each animal and presented as mean ± SEM. Except for the Activity curve, data points coinciding with Activity >10 have been excluded. Shading represents the three biological phases of BP change as outlined in Figure 4.1.2.**

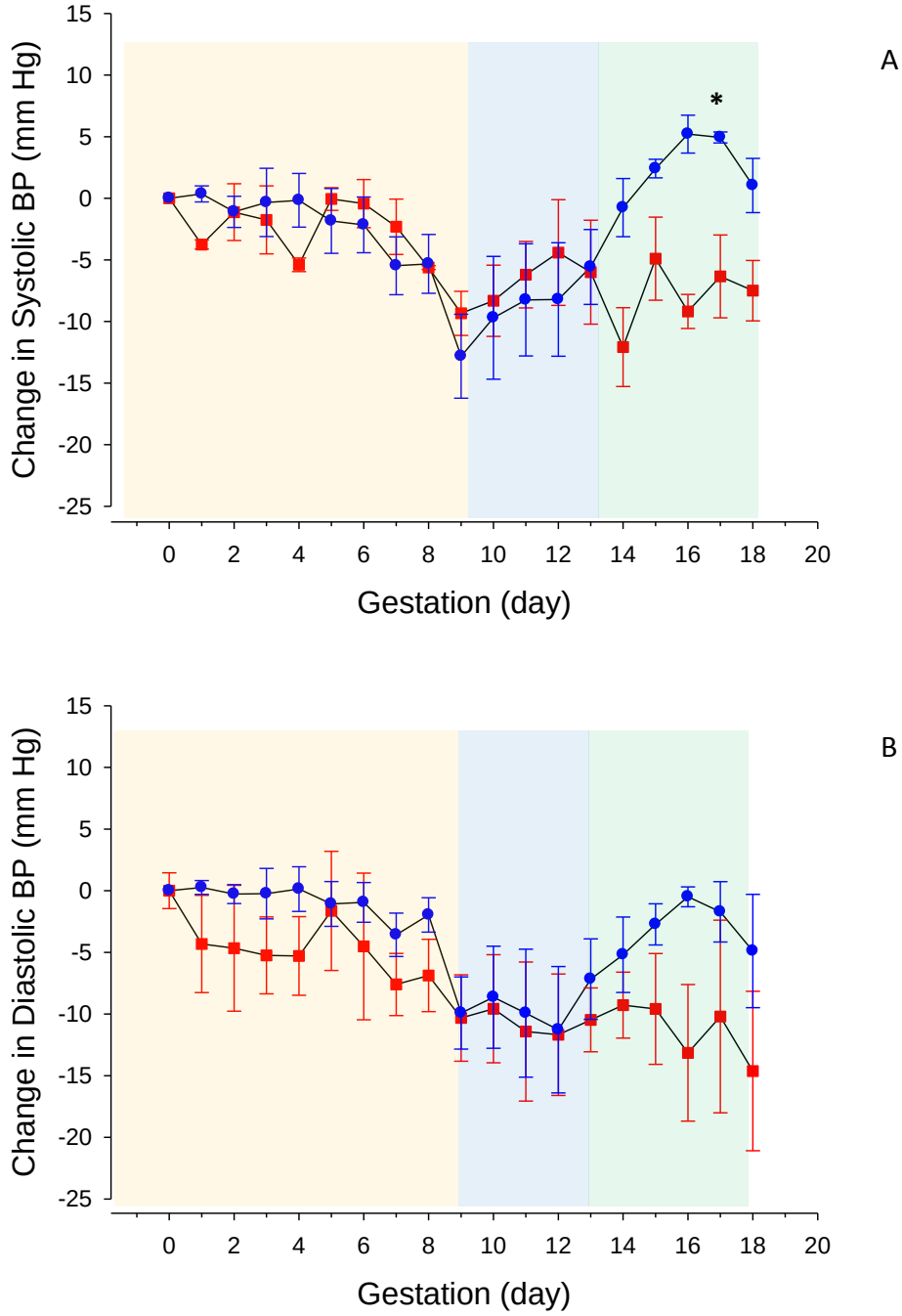


**Figure 4.2.7: Change in active (night time) systolic (A) and diastolic (B) blood pressure. Plot shows TNF-α infused animals (blue dots, n=3)) and saline infused control animals (red squares, n=3). Data is averaged over the 12 hr dark (active) period, normalised to gestational day 0 baseline for each animal and presented as mean ± SEM. (*p<0.05) Shading represents the three biological phases of BP change as outlined in Figure 4.1.2.**

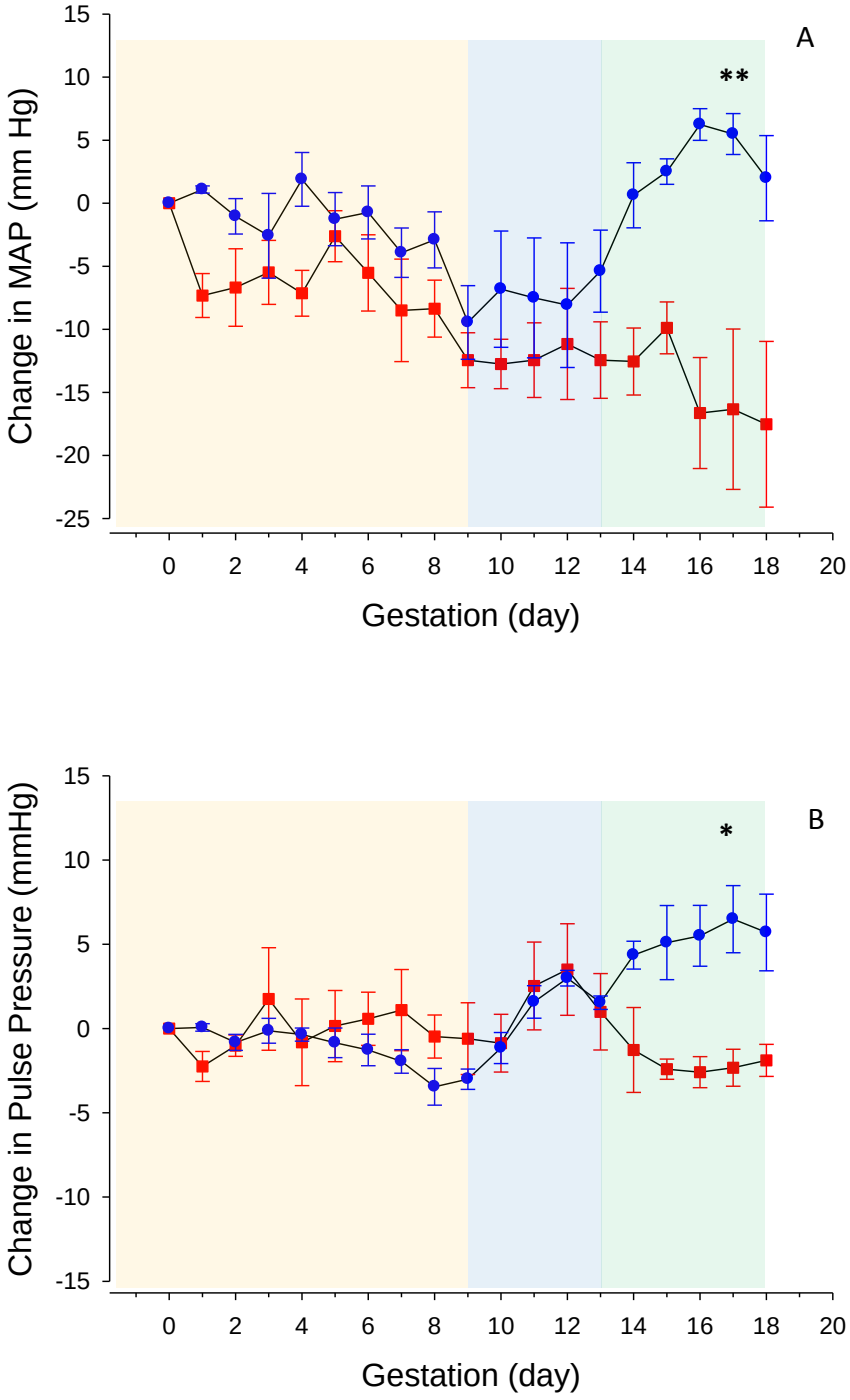


**Figure 4.2.8: Change in active (night time) mean arterial pressure (A) and pulse pressure (B). Plot shows TNF-α infused animals (blue dots, n=3)) and saline infused control animals (red squares, n=3). Data is averaged over the 12 hr dark (active) period, normalised to gestational day 0 baseline for each animal and presented as mean ± SEM. (*p<0.05, **p<0.01) Shading represents the three biological phases of BP change as outlined in Figure 4.1.2.**

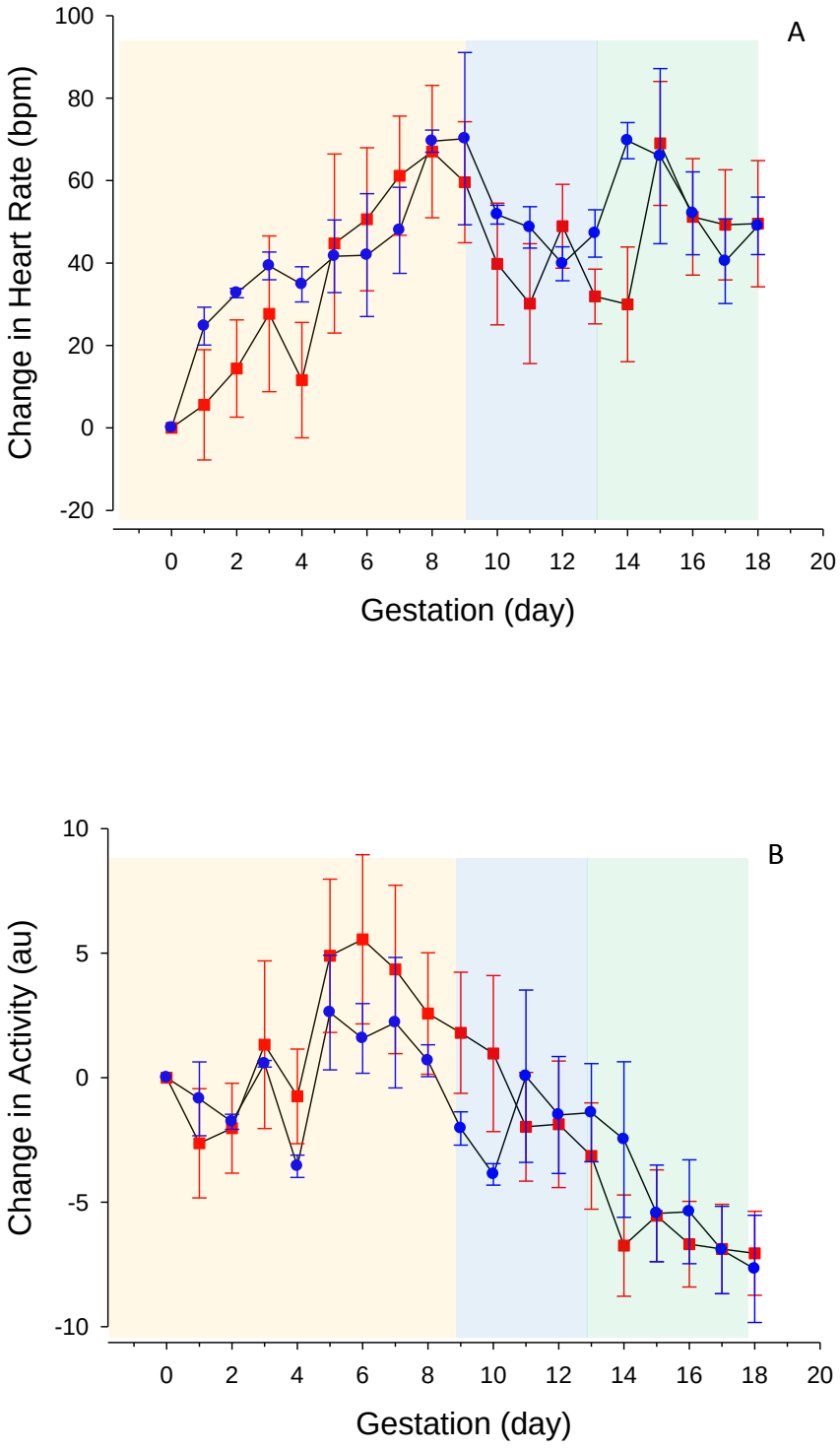


**Figure 4.2.9: Change in active (night time) heart rate (A) and activity (B). Plot shows TNF-α infused animals (blue dots, n=3) and saline infused control animals (red squares, n=3). Data is averaged over the 12 hr dark (active) period, normalised to gestational day 0 baseline for each animal and presented as mean ± SEM. Shading represents the three biological phases of BP change as outlined in Figure 4.1.2.**

### 4.2.3 Blood pressure phenotype of RUPP Model mice

Difficulties in carrying out the RUPP procedure on the telemetered mice due to technical constraints resulted in the inability to collect data from these animals post RUPP. As this model was primarily a control against which to gauge any perfusion related effects of cytokine treatment in the MRI analysis, it is felt that the omission of this data does not substantially impair the remaining results and conclusions.

### 4.2.4 Summary

These results show that subcutaneous infusion of the inflammatory cytokine TNF-α (500 ng/kg/day from gd 13) results in hypertension in pregnancy in mice and can act as an experimental model for induced hypertension in pregnancy.

# Chapter 5 Maternal and Foetal Outcomes and Measures of Experimental Preeclampsia

## 5.1 Maternal Outcomes

All of the animals included in the study had healthy pregnancies and displayed no visual or behavioural signs of illness as a result of the interventions. Preliminary experiments with the RUPP procedure that involved bilateral uterine artery ligation and partial ligation of the lower descending aorta resulted in animals becoming unwell or complete abortion of the pups. The RUPP procedure was subsequently modified to involve only unilateral ligation of the right uterine artery. Only modified RUPP animals were included in the study.

## 5.2 Foetal Outcomes

Pup weights and litter numbers were recorded. There were no significant differences between saline and TNF-α treated animals in either litter numbers (Figure 5.2.1) or numbers of resorbed or dead pups (Figure 5.2.2). A significant reduction in number of pups in the RUPP animals compared to the sham operated was observed (Figure 5.2.1). There was a trend for both sham and RUPP animals to have an increase in the number of resorbed or dead pups; however this was not significantly different to normal pregnant animals (Figure 5.2.2).

There was no significant difference in pup weights between these saline and TNF-α treated animals, or between sham and RUPP animals (Figure 5.2.3), however there was a significant decrease in pup weights in the RUPP animals compared to normal pregnant animals.

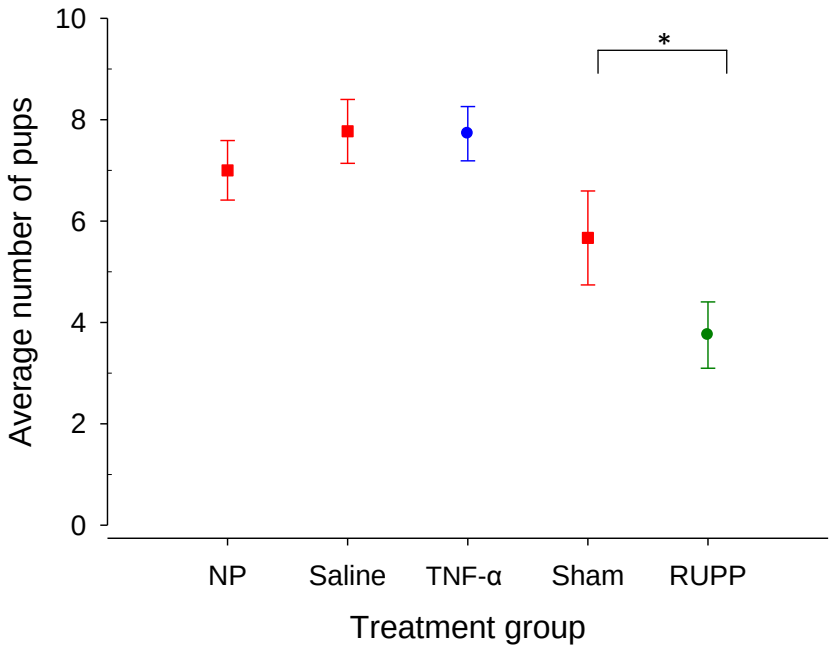


**Figure 5.2.1: Average litter number in normal pregnant (NP, n=12), saline (n=9), TNF-α (n=9) sham operated (n=4) and RUPP (n=7) animals. Data shown is mean ± SEM and represents both pups born live at gd 19 and pups harvested at gd 17 (*p<0.05)**

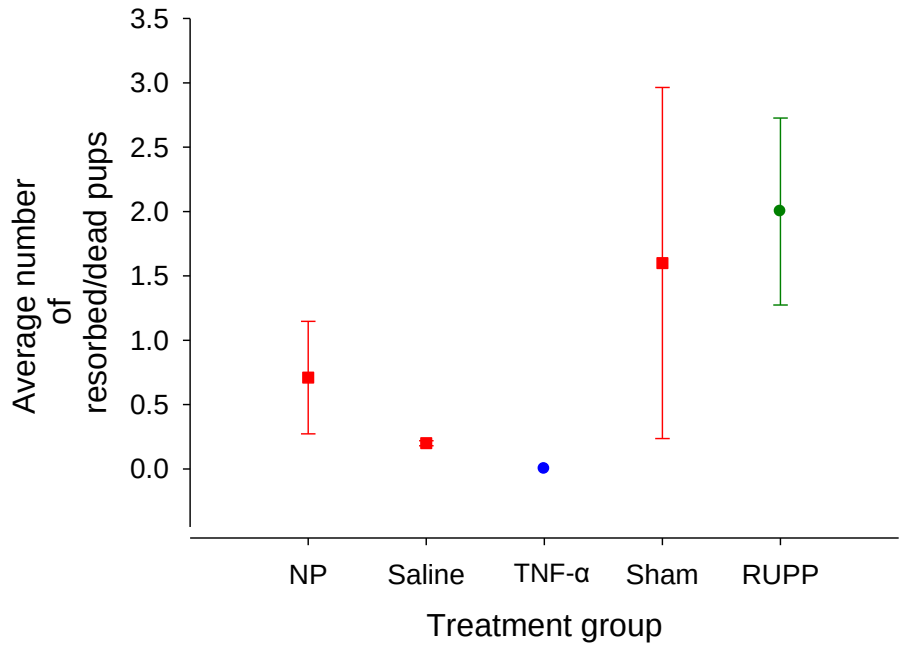


**Figure 5.2.2: Average number of resorbed/dead pups at gd 17 in normal pregnant (NP, n=12), saline (n=5), TNF-α (n=9) sham operated (n=4) and RUPP (n=7) animals. Data shown is mean ± SEM**

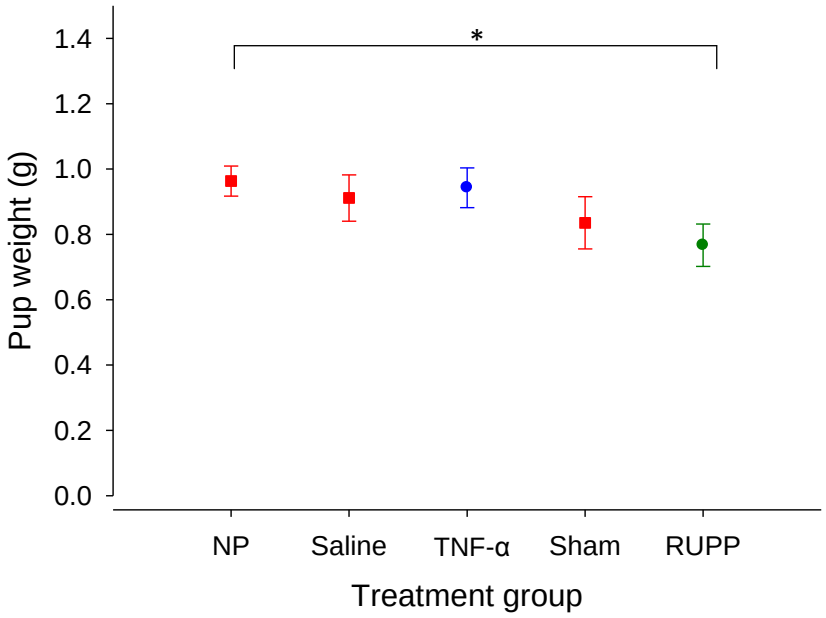


**Figure 5.2.3: Average pup weight at gd 17 in normal pregnant (NP, n=12), saline (n=5), TNF-α (n=7) sham operated (n=4) and RUPP (n=6) animals. Data shown is mean ± SEM (*p<0.05)**

## 5.3 Proteinuria

Urine was collected at gd 17 and analysed for presence of protein. Initially, during the pilot study, an IDEXX Urine:PC Ratio Kit was used to determine the urinary spot protein/creatine ratio, but due to difficulties in often collecting enough urine for the kit requirements, in the main study protein was determined using the more sensitive Bradford method (Bradford, 1976). TNF-α treated animals and RUPP animals showed significant levels of proteinuria as compared to their saline and sham controls (Figure 5.3.1). This data shows that the experimental model animals exhibit this feature of proteinuria in common with preeclampsia.

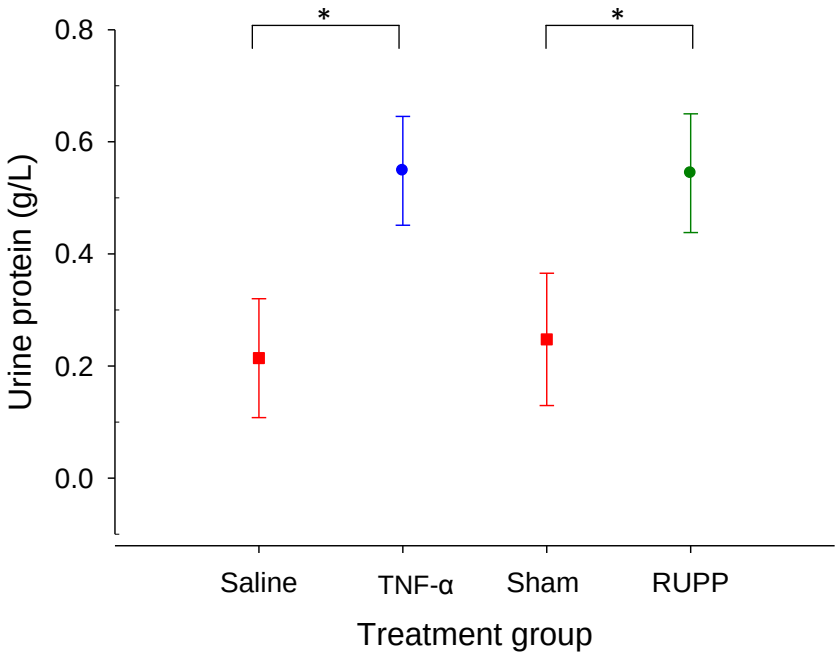


**Figure 5.3.1: Spot urine protein concentration at gd 17 in saline (n=5), TNF-α (n=6), sham operated (n=3) and RUPP (n=5) animals. Data shown is mean ± SEM (*p<0.05)**

## 5.4 Anti-angiogenic molecules in maternal serum: sFlt-1

Maternal plasma was collected at time of intervention on gd 13 (immediately after surgery) and on gd 17. At gd 17, 4 days after intervention, there was no statistical difference in the concentrations of sFlt-1 between saline and TNF-α treated animals or between sham and RUPP animals or between normal pregnant animals and experimental animals (Figure 5.4.1). It was observed however that animals that underwent subcutaneous surgery (saline and TNF-α mini-osmotic pump insertions) had significantly higher concentrations of sFlt-1 at gd 17 than the animals that underwent abdominal surgery (sham and RUPP) (Figure 5.4.1).

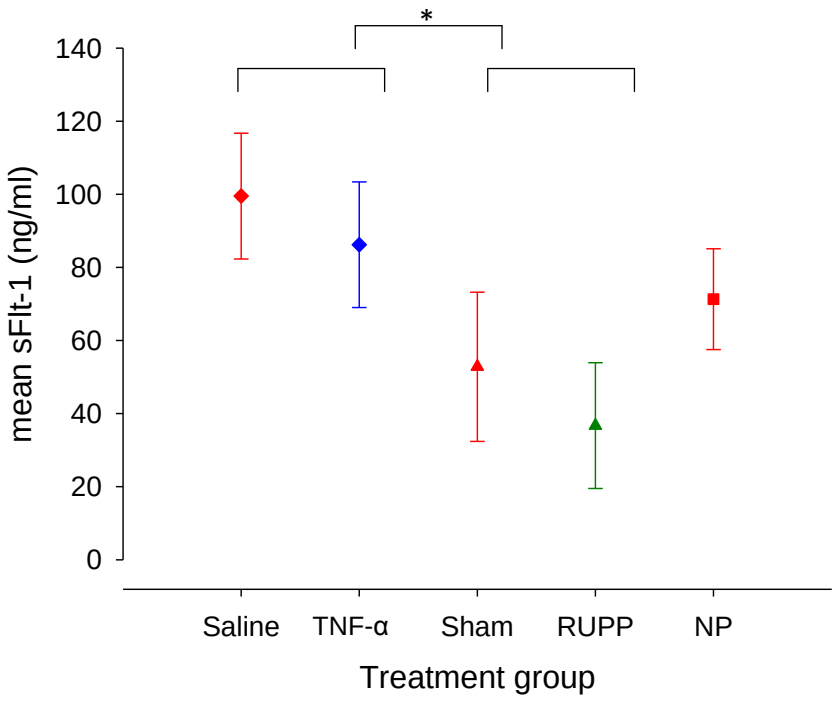


**Figure 5.4.1: Concentrations of sFlt-1 in pregnant mouse serum at gd 17 in saline (n=7) or TNF-α (n=7) infused animals and in sham operated (n=5) or RUPP (n=7) or normal pregnant (NP, n=11) animals. Data shown is the mean ± SE. There is no statistical difference between saline and TNF-$\alpha$ treated animals or between sham and RUPP animals or between normal pregnant animals and experimental animals. There is a statistical difference between animals undergoing subcutaneous surgery (diamonds) and abdominal surgery (triangles) ($p<0.005$)**

Plasma was also analysed at gd 13 from blood collected immediately after surgery prior to recovery from the anaesthesia. The rationale for the blood collection at this time point was to follow changes in maternal sFlt-1 in individual animals. However the surprising finding was made that concentrations of sFlt-1 were significantly higher in animals immediately post abdominal surgery (RUPP and sham surgery) than in the animals immediately post subcutaneous mini-osmotic pump insertions (TNF-α and saline) (Figure 5.4.2).

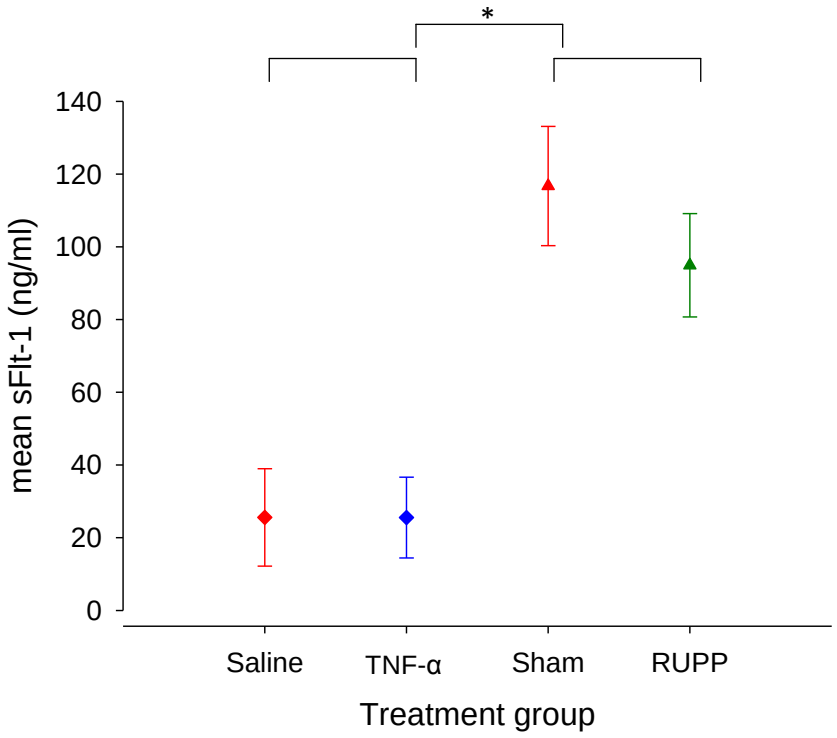


**Figure 5.4.2: Concentrations of sFlt-1 in pregnant mouse serum immediately after surgical intervention at gd 13 in saline (n=7) or TNF-α (n=7) infused animals and in sham operated (n=5) or RUPP (n=7). Data shown is the mean ± SE. There is no statistical difference between saline and TNF-$\alpha$ treated animals or between sham and RUPP animals. There is a statistical difference between animals undergoing subcutaneous surgery (diamonds) and abdominal surgery (triangles) ($p<0.005$)**

## 5.5 Discussion

The experimental models presented here indicate proteinuria as a key feature, in common with preeclampsia (Roberts and Gammill, 2005). Severe preeclampsia has also been associated with small for gestational age babies (Karumanchi et al., 2005). The experimental models presented here show no significant differences in pup weight between the treated animals and their respective controls, although there was a small but significant difference between normal pregnant animals and RUPP animals. A decrease in average number of pups was also observed for the RUPP animals. These results indicate that foetal outcomes are affected in the experimental ischaemia model, but not in the imbalance in inflammatory cytokines, perhaps reflecting the severity of the intervention.

An increase in sFlt-1 in maternal serum has been widely accepted as a marker for preeclampsia (Levine et al., 2004, Maynard et al., 2005, Tjoa et al., 2007), and has also been shown to be associated with hypertension in animal models of preeclampsia (Makris et al., 2007, Lu et al., 2007, Zhou et al., 2007). The lack of significant difference between the control and experimental model animals observed here may be partly due to the wide variation in measured values combined with a lack of power in the experimental numbers. This wide variation in sFlt-1 concentrations between individuals is also displayed in data from other groups who show an eight fold range in values from control mice alone (Suzuki et al., 2009). Levels of sFlt-1 in serum from pregnant mice reported here and by others (Zhou et al., 2007, Suzuki et al., 2009) are up to an order of magnitude higher than that reported in humans (Maynard et al., 2003b, Levine et al., 2004), baboons (Makris et al., 2007) and rats (Gilbert et al., 2007, Murphy et al., 2010) and it is possible that the combination of high basal levels and wide individual variation within groups masks any

increases in sFlt-1 release in the experimental animals. It has not been reported whether the commercial Eliza kit used (R&D) detects both, or discriminates between, free sFlt-1 and sFlt-1 complexed to VEGF and these considerations may complicate the interpretation of the results.

A more likely explanation for the lack of difference in elevation of sFlt-1 concentrations in the intervention groups is that there may be insufficient time between intervention (gd 13) and the time point of measurement (gd 17) to be able to discern any differences in the release of placental sFlt-1 into the maternal circulation. In a recent study that investigated the effect of timing of ischaemia in rats it was demonstrated that there was no increase in sFlT-1 compared to controls after 5 days chronic RUPP when the ligation of uterine arteries was performed at gd 12 rather than gd 14 (Banek et al., 2012).

Another possible explanation may arise from the fact that concentrations of sFlt-1 in maternal serum do not exclusively source from placental origins. sFlt-1 is expressed in placental trophoblasts, vascular endothelial cells, monocyte-macrophage lineage cells and hypoxia stressed smooth muscle cells (Shibuya, 2011) and a recent study has suggested that peripheral blood mononuclear cells (PBMC's) may be a significant extraplacental source of measured sFlt-1 in maternal blood samples (Zamudio et al., 2013). This may help to explain the variability in sFlt-1 values reported here and in the literature as it has been shown that concentrations of sFlt-1 measured in samples where blood is collected into sodium citrate, theophylline, adenosine and dipyridamole (CTAD), a combination designed to inhibit platelet activation and release of growth factors, are reduced by a range of 1-69% (Zamudio et al., 2013). Other studies have shown that complement activation can trigger release of sFlt-1 by monocytes and macrophages (Girardi et al., 2006). This suggests that PBMC's may be activated to release sFlt-1 and that measured concentrations in maternal serum may not necessarily be a true reflection of placental release. Blood samples

collected for this thesis were not always able to be processed with precise timing, and collection of the blood by cardiopuncture at euthanasia by needle and syringe into an EDTA tube may have resulted in variable activation of PBMC's and thus contributed to the variability in measured sFlt-1 values.

Surprisingly however, despite the wide range in sFlt-1 values, it was observed that animals that underwent subcutaneous surgery (saline and TNF-α mini-osmotic pump insertions) had significantly higher concentrations of sFlt-1 at gd 17 (four days after intervention) than the animals that underwent abdominal surgery (sham and RUPP). This may indicate that the implant of the mini-osmotic pump alone may cause an extraplacental inflammation reaction that may affect sFlt-1 release into the maternal circulation. Neither group, however, were significantly different to normal pregnant animals that underwent no surgical intervention.

Immediately post-surgery however the pattern was completely opposite, with significantly higher levels of sFlt-1 in animals undergoing abdominal surgery. The abdominal surgery required for the RUPP and sham procedures is more invasive than the simple subcutaneous insertion of the saline or TNF-α mini-pumps and may have precipitated an activation of PBMC's or vascular endothelial cells leading to release of sFlt-1.

Other studies have shown that during coronary bypass graft surgery with extracorporeal circulation, sFlt-1 concentrations increase 75 fold and return to pre-operative levels by 6 hours post, with kinetics pointing to either a release from a pre-existing pool or proteolysis from the membrane form (Denizot et al., 2007). The soluble form of vascular endothelial growth factor receptor 1 (sVEGFR-1/sFlt-1) is generated by alternative splicing of the Flt-1 gene (He et al., 1999, Whitehead et al., 2011). sFlt-1 protein expression and mRNA is known to be upregulated by hypoxia (Ahmad and Ahmed, 2005), via a HIF-1α dependent

pathway (Nevo et al., 2006, Rajakumar et al., 2007, Tal, 2012), by angiotensin II via the calcineurin signalling pathway (Zhou et al., 2007) and by TNF-α (Sunderland et al., 2011, Murphy et al., 2013). However the immediate release of sFlt-1 after surgery cannot be related to increased transcription or translation in the placenta, and some other mechanism must be involved that allows rapid release of sFlt-1 into the maternal circulation. Recently a number of regulatory proteins have been identified to be involved in the trafficking and secretion mechanisms of sFlt-1 (Jung et al., 2012) and storage depots for sFlt-1 such as blood vessel walls (Sela et al., 2011) or extracellular matrix (Searle et al., 2011) have been identified. Heparin induced release of stored sFlt-1 (Rosenberg et al., 2011, Sela et al., 2011, Searle et al., 2011, Yagel, 2011, Tal, 2012) or even shedding of the extracellular domain of Flt-1 receptor (Rosenberg et al., 2011) have been shown to result in increased release of sFlt-1. Thus a number of mechanisms may be involved in the release of sFlt-1, and modulation anywhere along the secretory/storage pathway may account for the increased concentrations seen in maternal serum at gd 13 in the sham and RUPP animals (abdominal surgery groups). This data indicates that some circumspection is warranted when attributing cause of release of sFlt-1 into the maternal circulation.

## 5.6 Summary

This data shows that while animals from both RUPP and TNF-α experimental models exhibited proteinuria, foetal outcomes were affected only in the experimental ischaemia model.

No increase in maternal serum sFlt-1 concentrations above control levels were observed in either the RUPP or inflammatory cytokine models of preeclampsia. This may be a consequence of insufficient time span between intervention at gd 13 and plasma collection at gd 17 or due to high basal levels in pregnant animals masking small changes. Alternatively the data is consistent with the concept that concentrations of sFlt-1 measured in maternal serum may not necessarily be a true reflection of placental release, and that other factors act to affect concentrations of sFlt-1 in maternal plasma.

The data indicates that the TNF-α experimental model animals shows signs of proteinuria and hypertension (Section 4.2.2) in common with the human syndrome of preeclampsia, however maternal serum sFlt-1 is not a reliable marker of disease in this mouse model. Other more suitable markers would need to be determined.

# Chapter 6 Dynamic MRI studies on the placenta

MRI offers a non-invasive technique to conduct dynamic studies on changes in placental structure and blood flow in animal models of preeclampsia. A number of different imaging protocols were used to visualize the placenta including FLASH, GEFI, TrueFISP sequence in FID mode, MSME and DWI. FLASH and GEFI sequences were primarily used for localising images. DWI measures quasi random blood movement within a single imaging voxel and was utilized in an attempt to obtain an indirect measurement of blood flow. The MSME sequence was utilized to provide a $1/T_2$ map of the placenta that is sensitive to the blood oxygenation level and thus was also employed as an indirect measure of blood flow.

$^1$H MRI images were taken of live anaesthetised mice placed in a vertical animal probe. Although the vertical position is not normal for mice, horizontal scanning was not possible with the available equipment. While the effect on their normal haemodynamics is unknown, all the animals in the study were subject to this same limitation with the relevant comparison being between animals in different treatment groups. Contrast agents could not be used with these animals as the experimental set up did not allow for injection of the animals while they were in the scanner. Initial studies to determine sequence parameters for scanning were performed on a euthanized mouse at day 14.5 of gestation.

## 6.1 Localising images

GEFI or FLASH sequences were used to obtain images with enough contrast to identify anatomical structures within the abdomen (see Figure 6.1.1). The placenta can be easily discerned within the embryo placental units (EPUs) (see Figure 6.1.2). For routine scans, GEFI sequences were preferentially utilised as they were a faster protocol. Using a series of 1 mm thick contiguous axial slices across the whole viewing region, a map of all the EPUs

with their placentas could be acquired (see Figure 6.1.3). It was determined that a single 5 min scan of a series of 20 non-contiguous 1 mm thick slices with an interslice distance of 2 mm over the 5 cm field of view was sufficient to locate all the placentas.

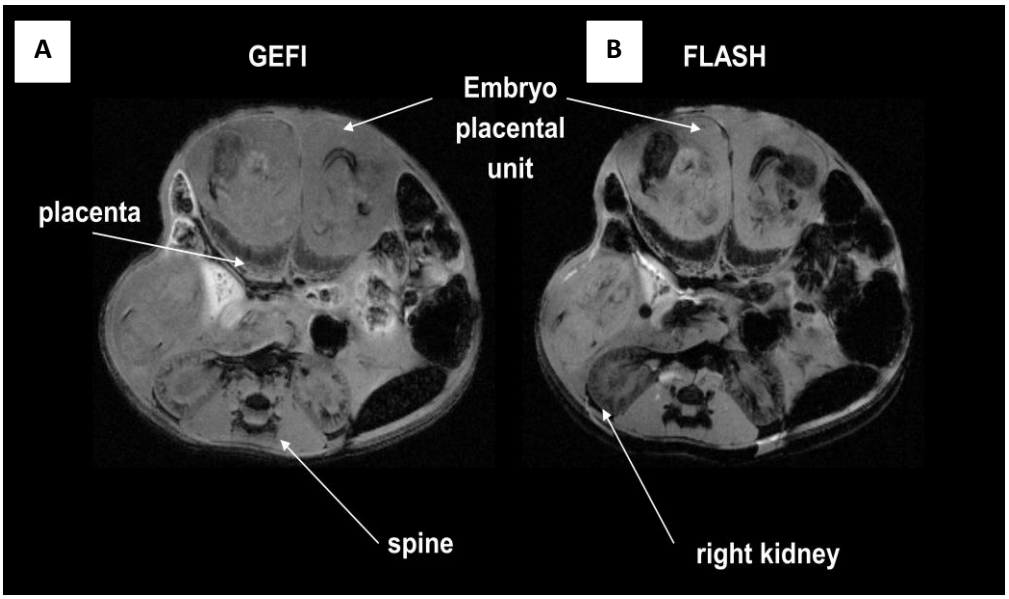


**Figure 6.1.1: Comparison of images obtained using different imaging protocols. A) a Gradient Echo Fast Image (GEFI) and B) a Fast Low Angle Shot (FLASH) Image of an axial slice of a C57BL/6JArc euthanized mouse at day 14.5 of gestation. Arrows indicate the embryo placental unit, the placenta, the spine and the right kidney.**

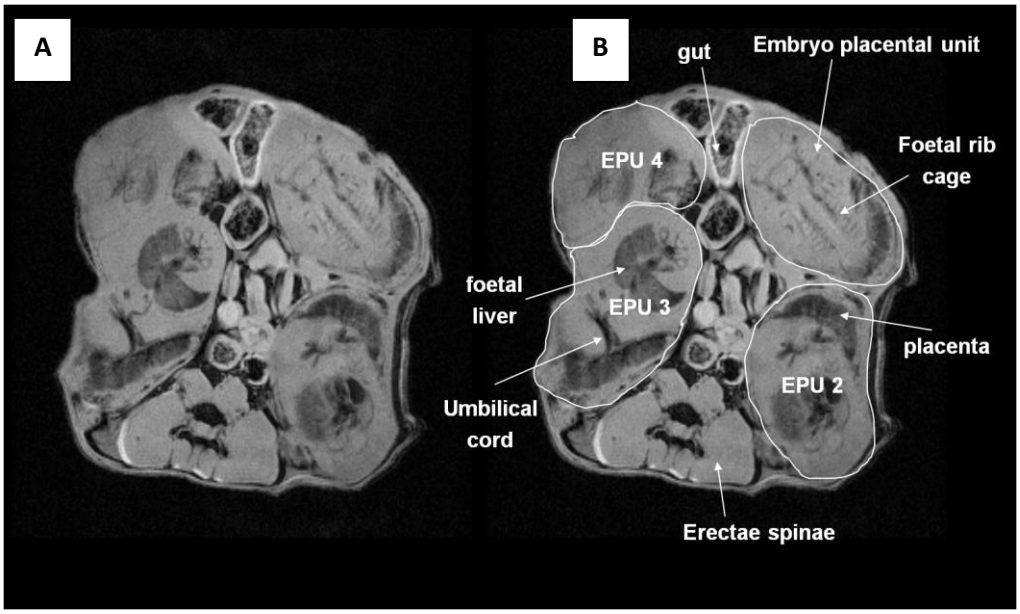


**Figure 6.1.2: Gradient Echo Fast Image (GEFI) of an axial slice of a C57BL/6JArc euthanized mouse at day 14.5 of gestation. A) unlabelled image and B) labelled image. Arrows show embryo placental unit (EPU), foetal rib cage, foetal liver, placenta, umbilical cord, and erectae spinae.**

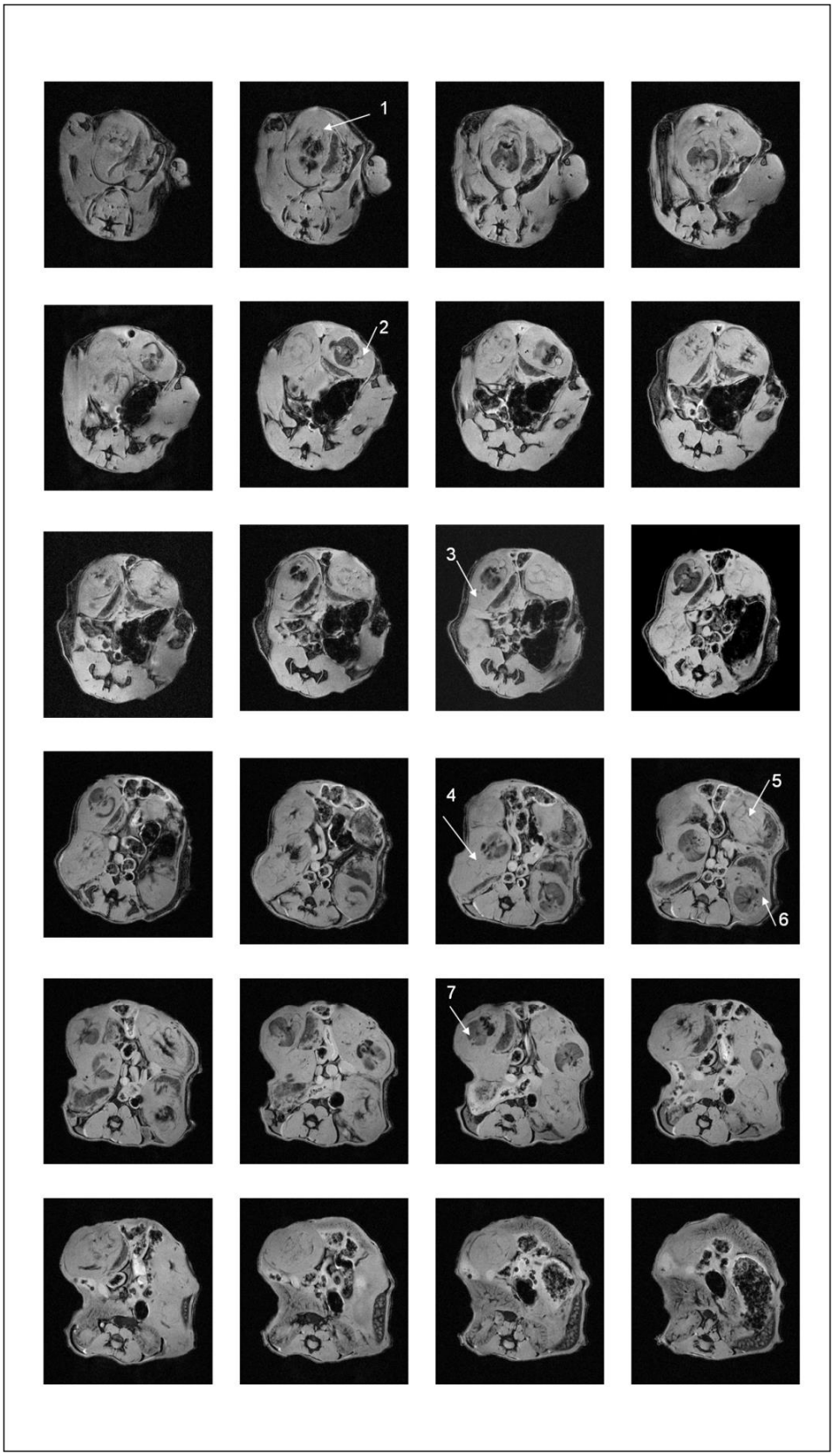


**Figure 6.1.3: Gradient Echo Fast Image of a contiguous series of 1 mm thick axial slices of a C57BL/6JArc euthanized mouse at day 14.5 of gestation. Every second slice from the abdominal cavity is shown. Numbered arrows refer to each of the seven embryo units.**

## 6.2 Diffusion Weighted Imaging

Selected slices were subject to the DWI sequence, with acquisitions made using 10 different diffusion gradient values per experiment. The images did not discriminate tissues as clearly as the GEFI images and were subject to low signal-to-noise ratios and blurring due to motion (Figure 6.2.1), with more blurring arising from slices that were closer to the chest cavity due to movement arising from respiration. (Figure 6.2.2) These disrupted images were unable to be used for analysis.

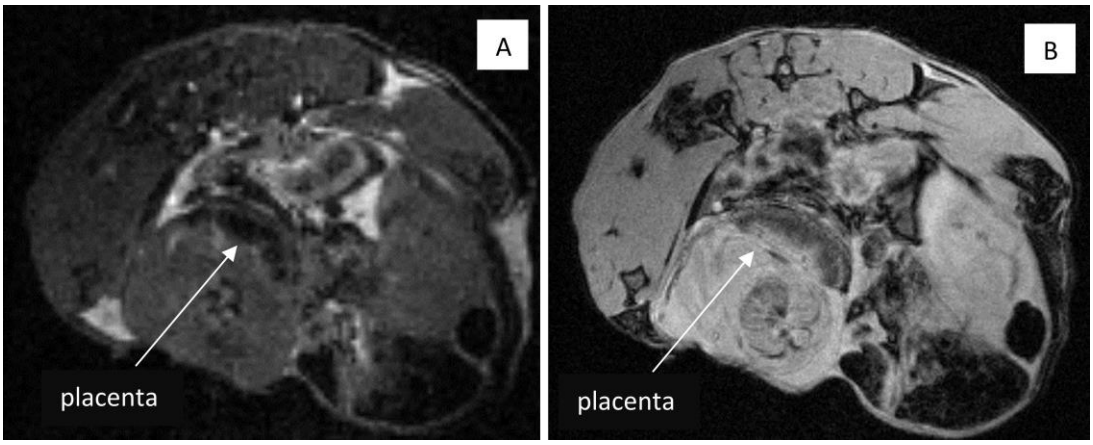


**Figure 6.2.1: Comparison of imaging protocols showing differences in resolution. A) Diffusion weighted $b_0$ image and B) GEFI image of the same axial slice across a normal pregnant C57BL/6JArc mouse.**

Using MATLAB an attempt was made to construct an ADC map of the clearer images. For each voxel, the signal attenuation versus the *b* value of the different gradient pulses used in the sequence was plotted and the equation E=A exp(-*bD*) was regressed onto the data in order to recover *D*, or the ADC, and a visual image of the relative ADC value per voxel was created. However no clear visual map could be obtained (Figure 6.2.3).

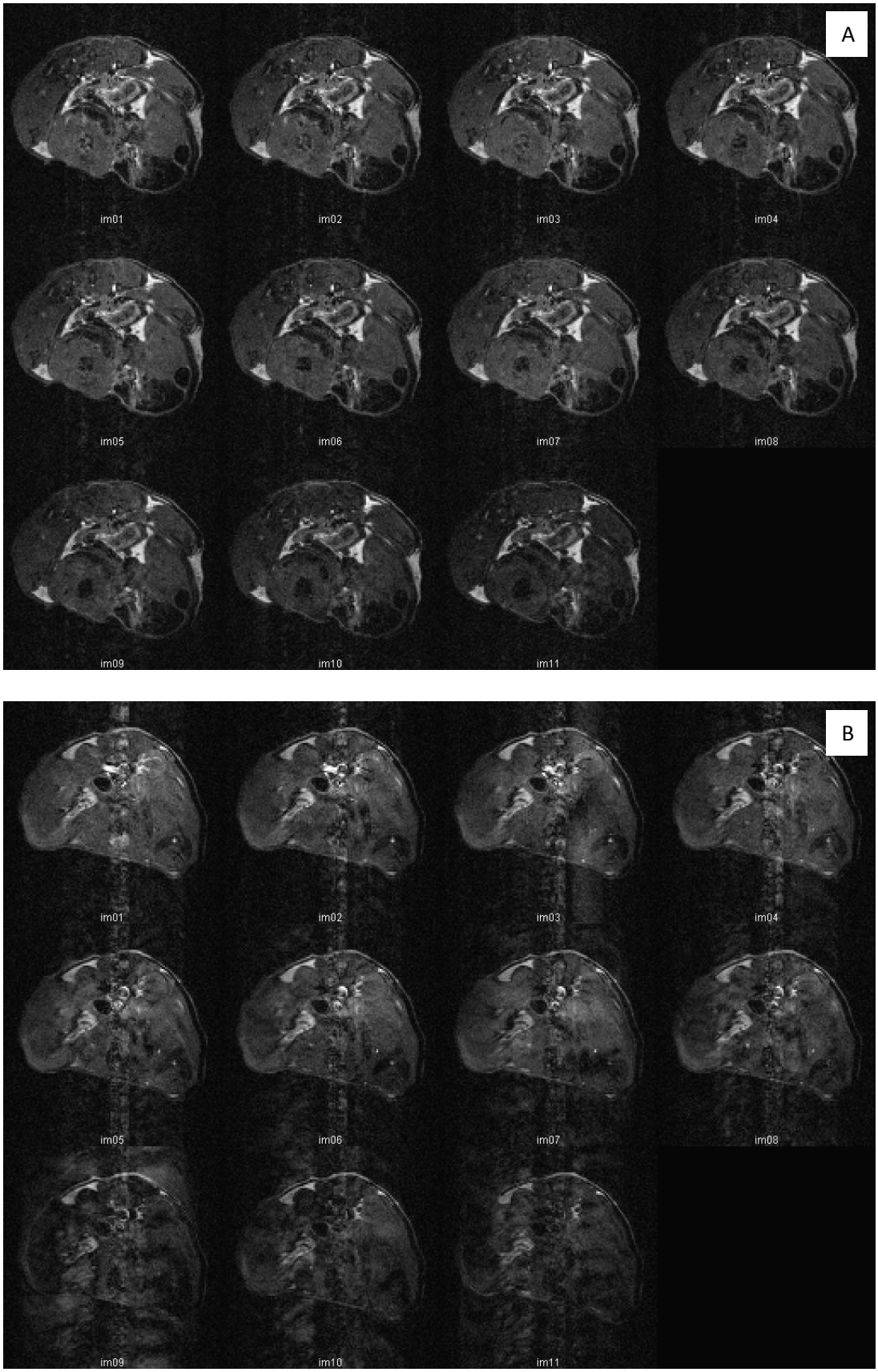


**Figure 6.2.2: Diffusion weighted images showing demonstrating that blurring is increased in slices closer to the chest cavity. A) a slice lower down the abdomen and B) a slice closer to the chest, showing the $b_0$ image and the images arising from the 10 different diffusion gradient values**

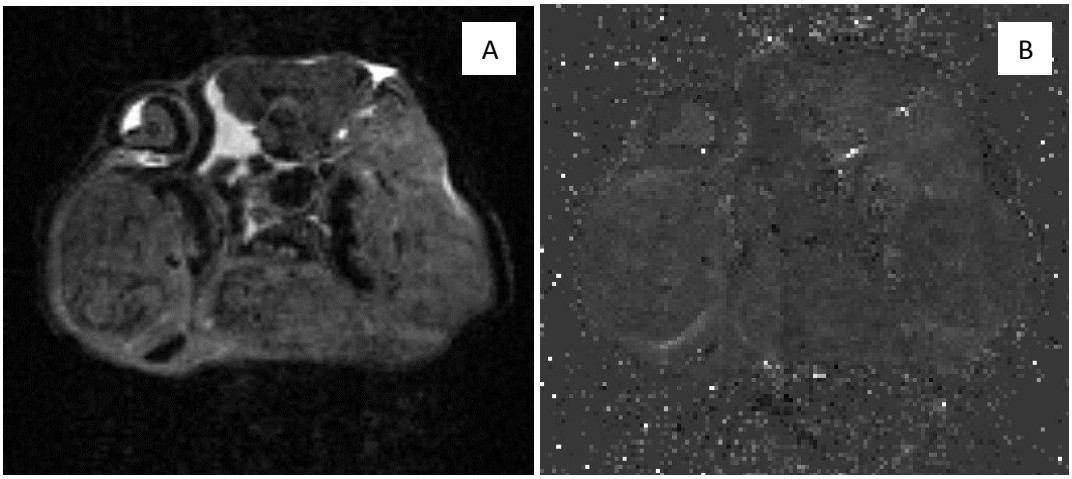


**Figure 6.2.3: Construction of ADC map. A) Diffusion weighted $b_0$ image and B) ADC map constructed from the corresponding series of gradient images showing low resolution due to a low signal-to-noise ratio**

As an alternative strategy, the average signal intensity of groups of 4 voxels was calculated. Using the $b_0$ image to identify the placenta, three regions of 4 voxels each were selected in each placenta and the average signal intensity plotted against the diffusion sensitive parameter *b*. (Figure 6.2.4). These plots proved very noisy and were unable to be fitted to a curve to derive the apparent diffusion coefficients.

The placenta shows up dark on the DWI image, and with the signal intensity at the initial $b_0$ value so low it is difficult to detect any signal attenuation by the increase in *b* value beyond noise. On re-examination of the images, in particular comparing the DWI images with the GEFI images, it could be seen that the dark region on the DWI image did not equate to the whole placenta, and that it was harder to discern the interface between the placenta and the foetus (Figure 6.2.1). This was further displayed upon observation and comparison of $1/T_2$ and $T_1$ maps with the DWI images (Figure 6.2.5). It became apparent that the selected points in the dark region of the placenta on the DWI images were in the junctional/decidual zone, whereas the labyrinth zone needed to be the target to measure blood flow. Therefore in subsequent analyses, points immediately below the dark region were selected

on the $b_0$ image for ADC analysis and these were later mapped against an overlay of the placental region as discerned from the $1/T_2$ map (Figure 6.2.6). The ADC plots of these lighter regions of the placenta were still subject to noise, but it appeared that measurements would be possible.

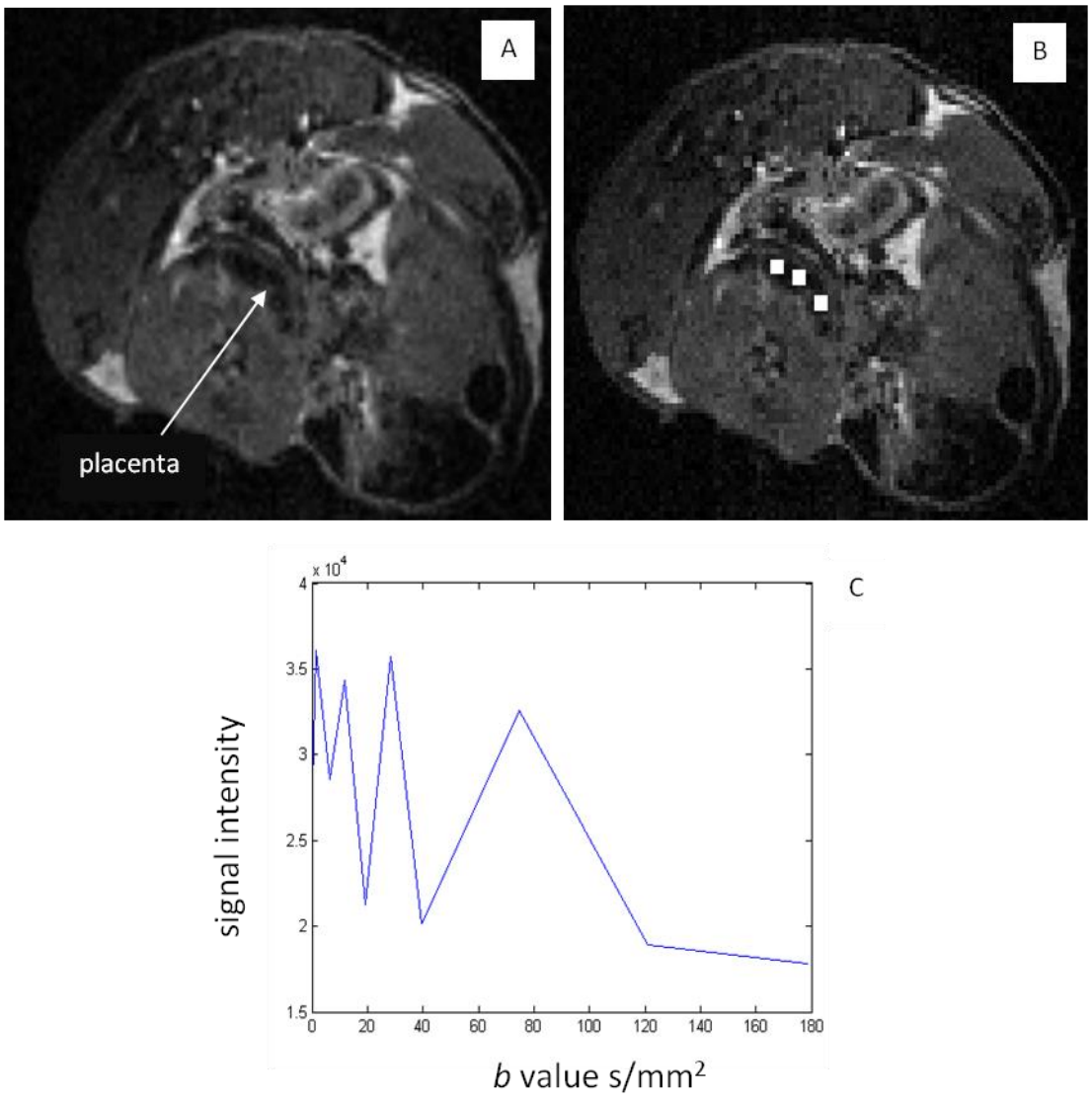


**Figure 6.2.4: Selection of regions for ADC calculation. A) Diffusion weighted $b_0$ image, B) image with overlay showing points selected for ADC calculation and C) representative ADC curve plotting signal intensity against the *b* value of the different gradient pulses used in the sequence. The low signal-to-noise ratio means a smooth curve is unable to be fitted to the data.**

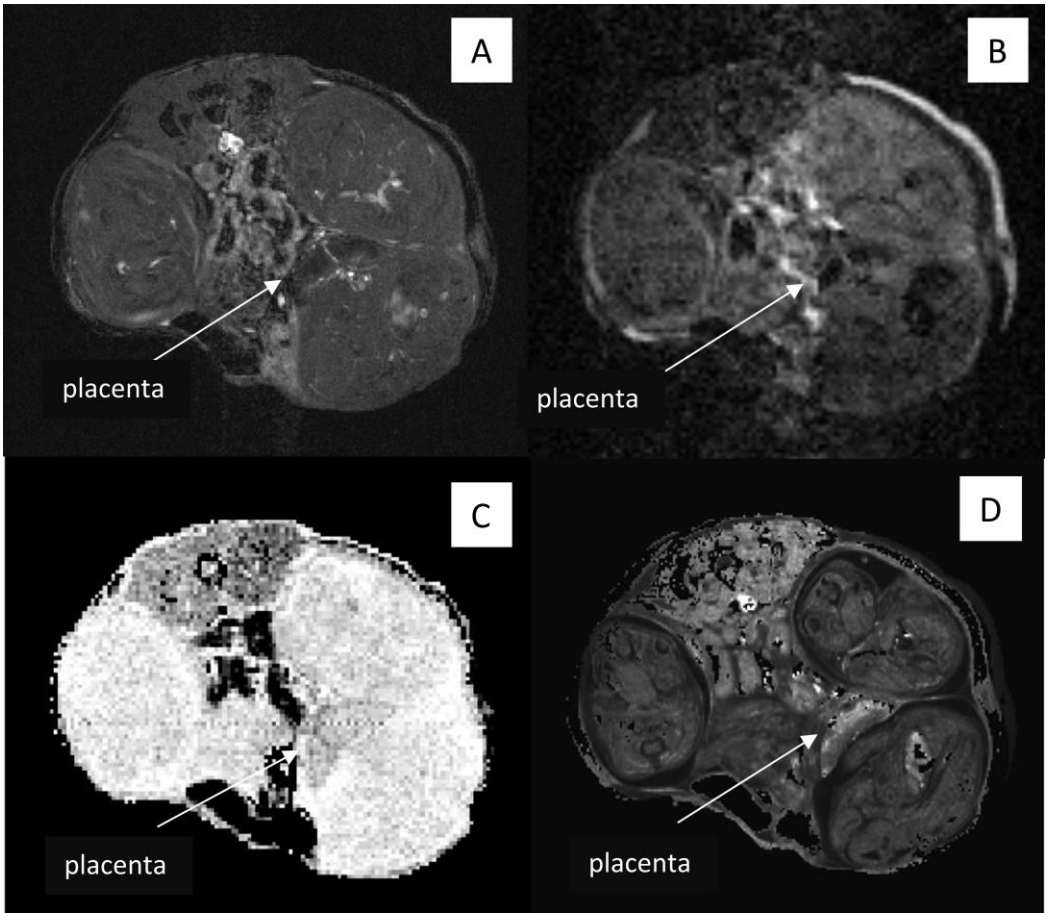


**Figure 6.2.5: Comparison of MRI images indicating differences in resolution of the placenta. A) GEFI image B) DWI image C) $T_1$ map and D) $1/T_2$ map from a single slice across the abdomen of a normal pregnant C57BL/6JArc mouse.**

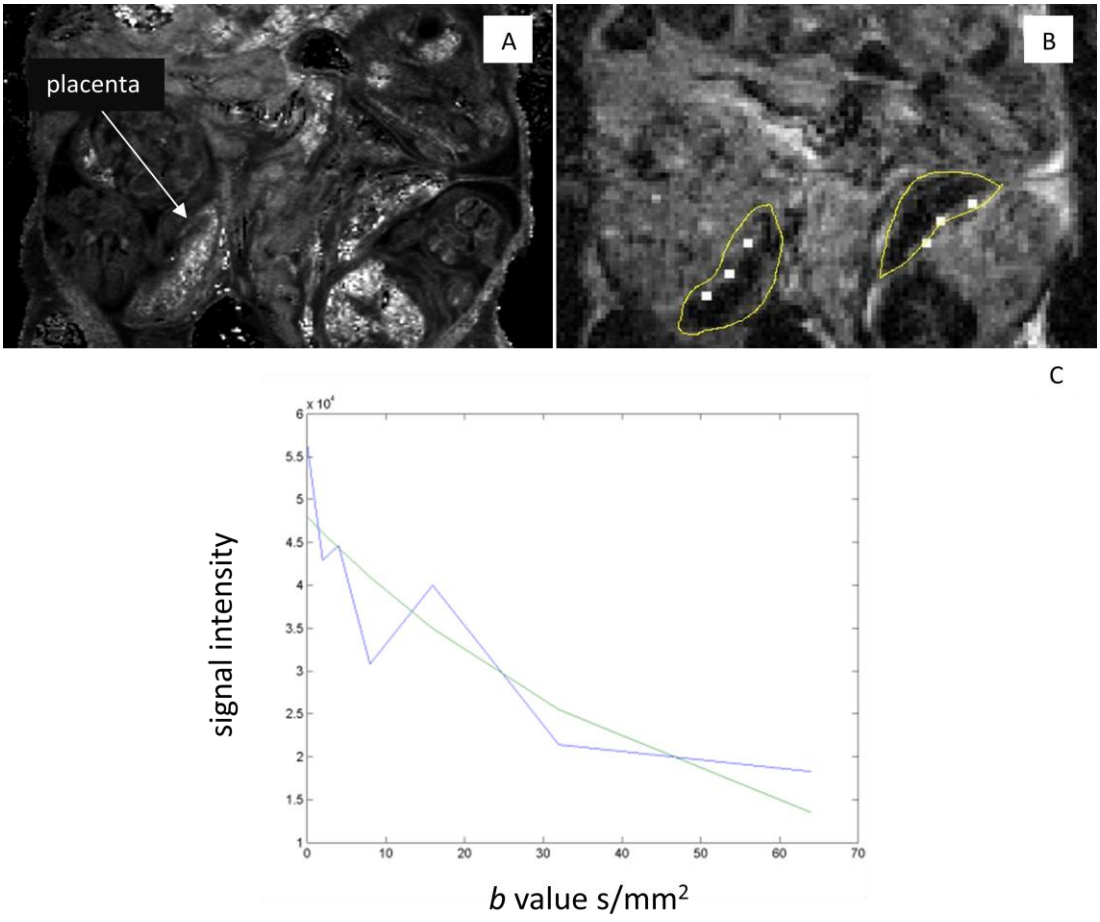


**Figure 6.2.6: Alteration of regions selected for ADC calculations. A) $1/T_2$ map of sagittal slice of a normal pregnant C57BL/6JArc mouse abdomen showing distinct regions of the placenta B) Diffusion weighted $b_0$ image with overlay from $1/T_2$ map showing new points selected for ADC calculation and C) representative ADC curve plotting signal intensity against the *b* value of the 10 different diffusion weighted images. The blue curve represents the actual measured data, and the green curve is the smoothed best fit plot representing the ADC.**

Part way through the study updated software (Paravision 5) enabled Echo Planar Imaging to be performed. EPI is performed using a pulse sequence in which multiple echoes of different phase steps are acquired using rephasing gradients instead of repeated 180° rf pulses following the 90° / 180° in a spin-echo sequence. As a result, an image can be acquired in 20-100 ms, allowing excellent temporal resolution and much reduced overall sequence acquisition times compared to the DWI and MSME sequences used. It was

expected that a marked reduction in acquisition time would enable the diffusion weighted sequence to be performed with parameters that would increase the signal-to-noise ratio.

After carrying out an EPI-Diffusion tensor sequence and examining the five $b_0$ images which are separated by approximately 15 seconds, it was observed that the embryo placental units were subject to movement within the abdomen (Figure 6.2.7).

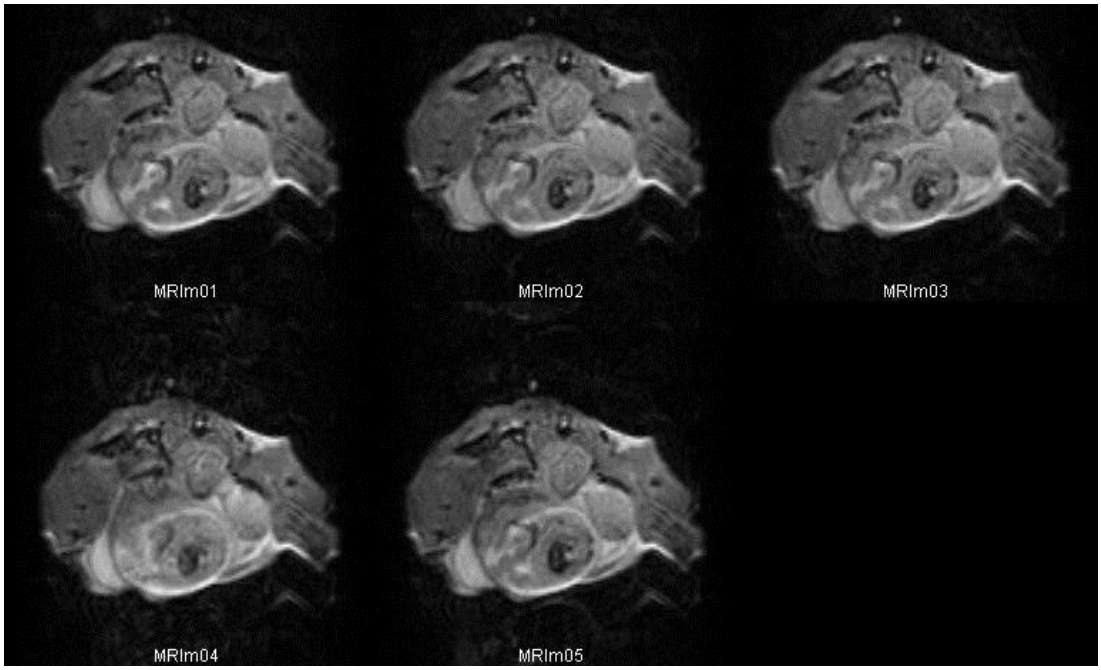


**Figure 6.2.7: Movement of embryo placental units. DTI sequence showing 5 $b_0$ images of a single slice of gestational day 17 C57BL/6JArc mouse abdomen scanned approximately 15 seconds apart. During this time the foetus moves position. An animation demonstrating the motion can be found at** https://db.tt/oV1vWyRa
**(NB must use windows explorer for the animation to display correctly)**

This movement of the embryo placental units had not been observed previously due to the slower acquisition time of the DWI and MSME sequences. On the DWI images which take longer to acquire, any movement will be averaged out and will only be discerned as a blurred image. This newly detected movement in the foetal placenta units explain the source of much of the blurring which hampered DWI analysis, but, unlike motion artefact

due to breathing, cannot be easily overcome. Foetal sedation by placental transfer of maternally administered anaesthetics is known to be variable and does not necessarily ensure an anesthetised or immobile foetus (Untergasser et al., 2007). A longer period of anaesthesia may allow equilibration of the isoflurane in foetal tissues, however does not reliably ensure this, and may lead to adverse effects on the foetus (Untergasser et al., 2007).

Diffusion analysis is inherently sensitive to motion as it is essentially detecting motion due to perfusion and diffusion of protons. Motion artefacts interfere with the signal attenuation and compromise the integrity of the data. While motion artefacts from respiration can be overcome by gating acquisition on respiration, unpredictable motion due to foetal movement are not easily surmounted.

In the DWI study on human placenta (Moore et al., 2000a), subject movement was acknowledged to present difficulties with many images that were affected by gross movement leading to artificially high signal attenuation being discarded. They also found difficulties with low signal-to-noise ratios, finding that at 0.5 T the image signal-to-noise was not large enough to allow a three parameter pixel by pixel fit of the IVIM parameters. The value of *D* was thus fixed at the value measured for the entire region of interest and each pixel was fitted for *D** and f only in order to produce pixel by pixel maps of the moving blood fraction. Moore *et al*. used EPI with a total imaging time of 220 s with an in-plane resolution of 3.5 mm x 2.5 mm, slice thickness 7 mm and data matrix 128 x 128. The region of interest for analysis was 50-100 pixels and avoided areas of major vessels. In comparison, the images of the mice placenta took 13 min to acquire, had an in plane resolution 0.24 mm, slice thickness of 1 mm, data matrix 128 x 128 giving a voxel size of 0.24 mm x 0.24 mm x 1 mm. The mice placenta measure approximately 5.5 mm x 2.5 mm. We selected regions of 4-9 pixels and given there are two or three major canals in mice

placenta, vessels were difficult to avoid. In the Moore study; data was able to be averaged, to increase the signal-to-noise ratio, from many more voxels in the selected region than was possible for the small mice placenta. Thus, even though the strength of the spectrometer used in this thesis (11.74 T) was greater than that in the Moore study on human placenta (0.5 T), we were unable to easily overcome the low signal-to-noise ratio problem.

Given the difficulties with the signal-to-noise ratio and given that any even small movement of the foetus would result in artifacts in signal attenuation, it was decided to discontinue the DWI studies for an alternative approach with $T_2$ mapping which had proved promising.

## 6.3 $T_2$ mapping

### 6.3.1 Distinct regions of $T_2$ contrast

$T_1$ and $T_2$ measurements were acquired on selected slices using an MSME sequence and MATLAB was used to generate $1/T_2$ maps from the acquired data (Figure 6.3.1). Three distinct morphological regions of contrast based on $T_2$ relaxation times were discerned in the MRI images of normal pregnant mouse placenta at gd 17.5 correlating to the labyrinth, junctional and decidual zones (Figure 6.3.1A and B). No variation of contrast within areas of the placenta was observed in the $T_1$ images (Figure 6.3.1C) and consequently the $T_1$ scans were not routinely performed. $T_2$ mapping on a pregnant mouse at gestational day 10.5 did not differentiate placental regions (Figure 6.3.1D).

As the maternal circulation to the mouse placenta is not established until day 10.5 of gestation (Georgiades et al., 2002), the possibility that the observed $T_2$ contrast was due to blood flow was further investigated.

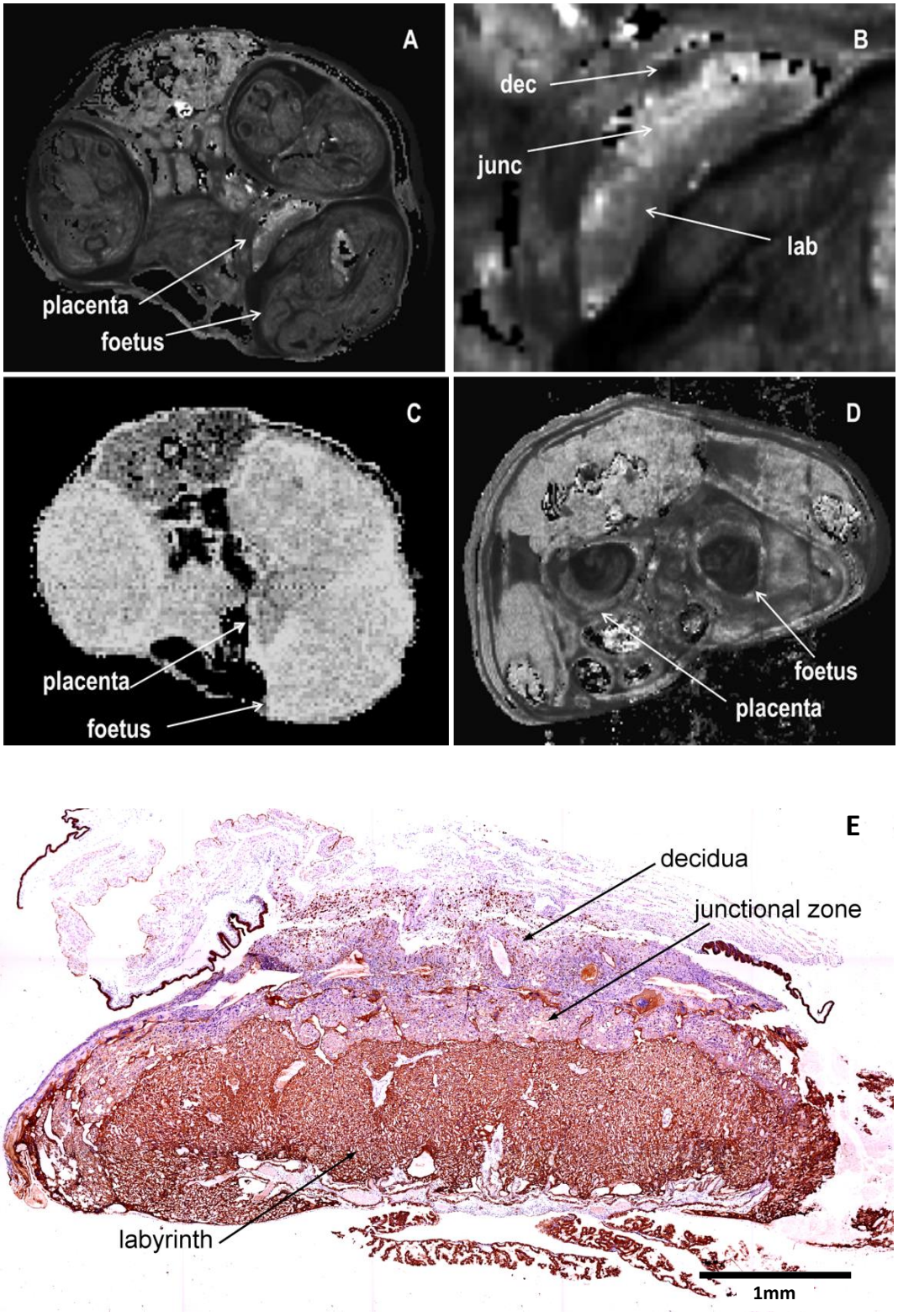


**Figure 6.3.1: Comparison of $1/T_1$ and $1/T_2$ MRI images with a histological section of a gestational day 17.5 normal pregnant C57BL/6JArc mouse. A) $1/T_2$ map of abdominal cross section B) Enlarged placenta from A) showing three distinct regions of labyrinth (lab), junctional zone (junc) and deciduas (dec); C) $T_1$ map of the same slice; D) $1/T_2$ map at gestational day 10.5; E) Histological section at gd 17 immunostained for cytokeratin, a marker for trophoblast cells.**

### 6.3.2 $T_2$ contrast abolished at loss of blood flow

To determine the contribution of perfusion to the contrast between regions in the $1/T_2$ map, additional $T_2$ measurements were acquired on the same slices of one normal pregnant mouse immediately after the blood flow was reduced to zero by terminal anaesthesia. Upon cessation of blood flow the difference in $T_2$ contrast between the three regions was substantially reduced (Figure 6.3.2). For quantification, $T_2$ values were calculated from three groups of four voxels selected from each region of interest for each of five individual placentas. There was a significant decrease in $T_2$ contrast in the labyrinth and a significant increase in the junctional region ($p$=0.003) upon loss of blood flow, whereas the $T_2$ values of the decidual region remained unchanged (Figure 6.3.3). The ratio of $T_2$lab/$T_2$junc was calculated to further clarify the observed changes, decreasing from 2.56 ± 0.14 during blood flow to 1.04 ± 0.14 after blood flow ceased.

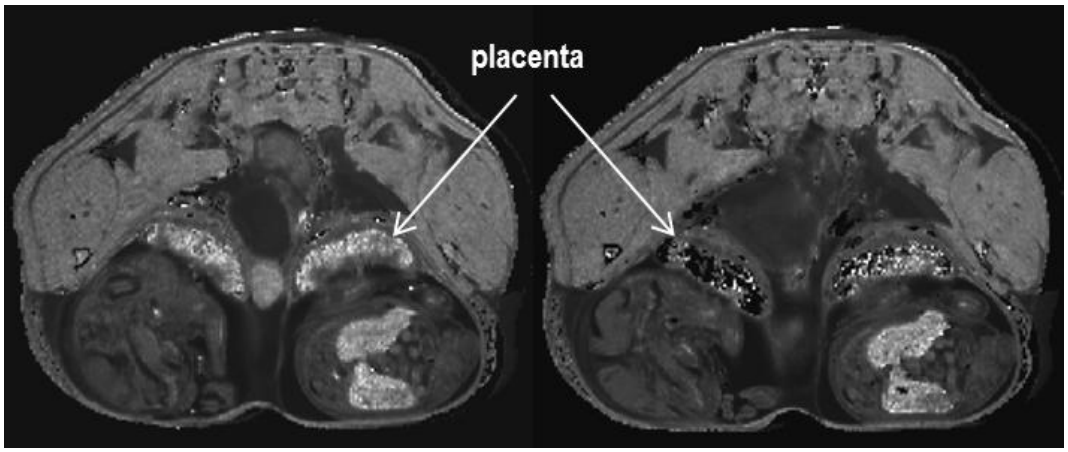


**Figure 6.3.2: $T_2$ contrast in the placenta is abolished at loss of blood flow. (A) $1/T_2$ map of gestational day 17.5 normal pregnant C57BL/6JArc mouse showing $T_2$ contrast in the different regions of the placenta. (B) $1/T_2$ map of same abdominal slice after blood flow had ceased.**

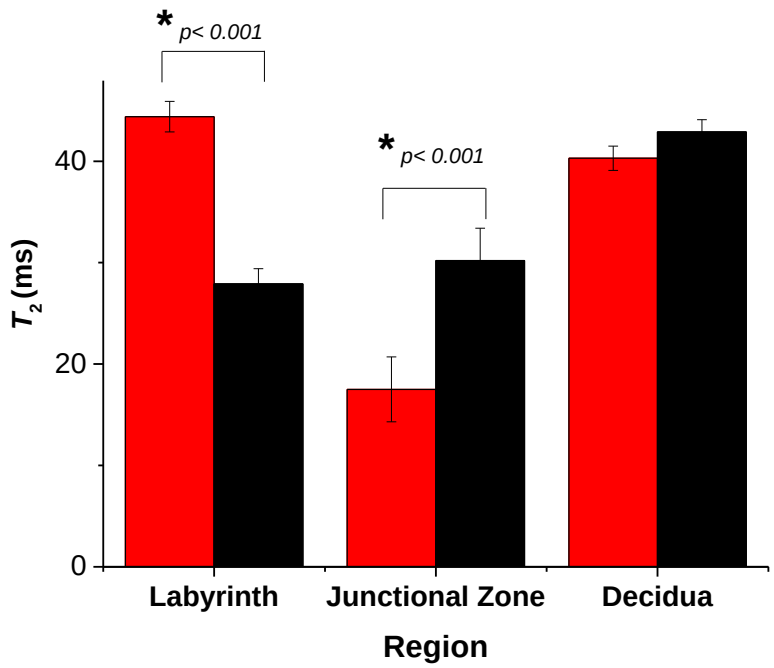


**Figure 6.3.3: Comparison of mean $T_2$ values from different regions of the placenta from a normal pregnant C57BL/6JArc mouse at day 17 of gestation during blood flow (red) and after blood flow has ceased (black). $T_2$ values were calculated from 3 groups of 4 voxels selected from each region of interest from the same 5 placentas before and after blood flow ceased.**

### 6.3.3 Pattern of $T_2$ contrast altered in perturbed pregnancies

Given that the observed $T_2$ contrast appeared to be related to blood flow within the placenta, investigations were carried out to determine whether morphological differences could be detected by $T_2$ mapping in the placenta of mice subjected to the two experimental models of preeclampsia; the RUPP model and the inflammatory cytokine imbalance model (TNF-α). Differences in the pattern of the regions of $T_2$ contrast in the placenta were observed between control, RUPP, and TNF-α treated mice (Figure 6.3.4). The ratio of $T_2$lab/ $T_2$junc was significantly altered in RUPP and TNF-α treated animals compared to control animals (Figure 6.3.5), and there was a trend for larger $T_2$ values in the junctional zone and decidua of RUPP and TNF-α treated animals (Figure 6.3.6). Sham-operated and saline-infused

controls were not significantly different to normal pregnant animals and for the purposes of analysis the three control groups were grouped together.

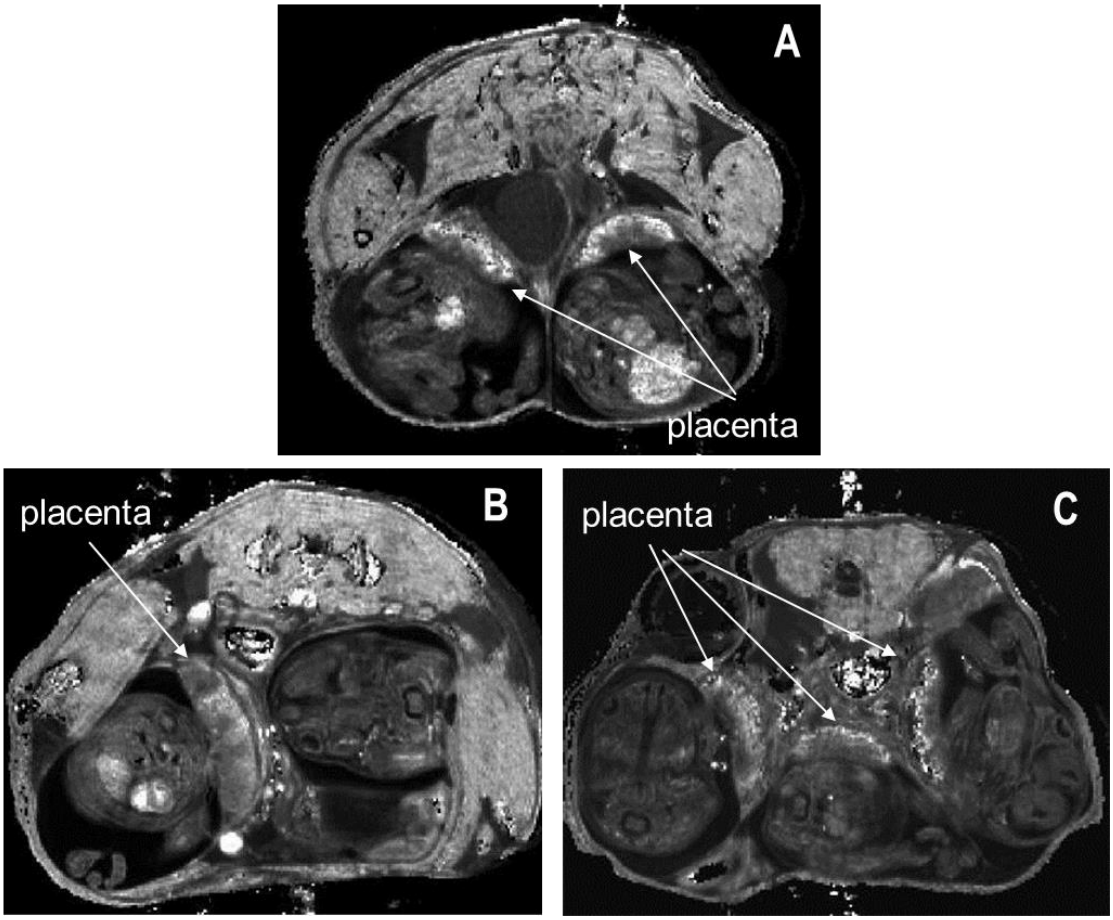


**Figure 6.3.4: The pattern of $T_2$ contrast is altered in perturbed pregnancies. (A) $1/T_2$ map of gestational day 17.5 pregnant C57BL/6JArc mouse showing contrast in the placenta of normal pregnant animal; (B) RUPP animal and (C) TNF-α treated mouse.**

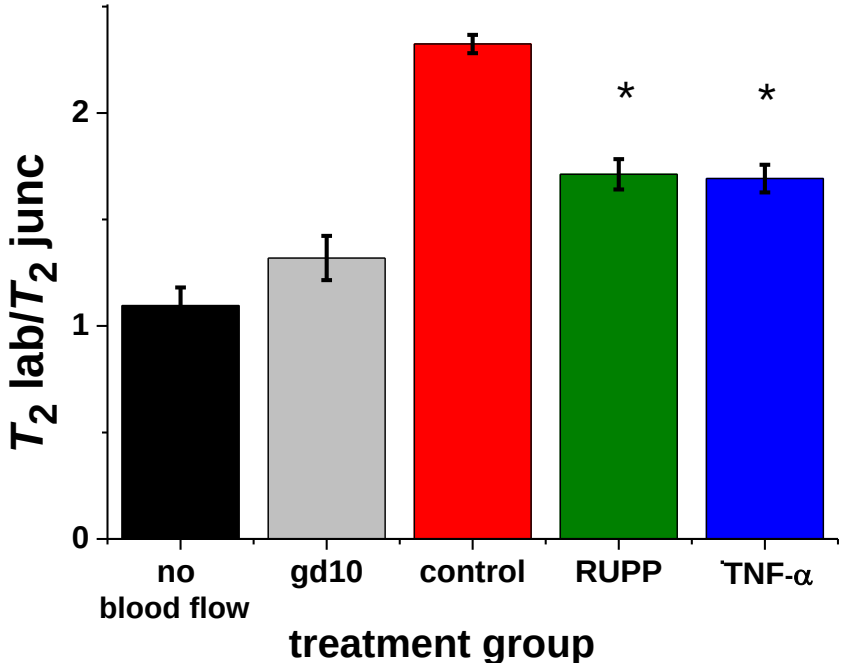


**Figure 6.3.5: Comparison of the ratio of $T_2$lab/ $T_2$junc values between treatment groups. $T_2$ values were measured at gestational day 17 of control (red) and perturbed pregnancy model animals (green and blue) and at loss of blood flow (black). $T_2$ values were also measured at gestational day 10, prior to establishment of maternal placental blood flow (grey). The ratio of $T_2$lab/ $T_2$junc were; no blood flow (n=1) 1.09 ± 0.09; gestational d10 (n=1) 1.32 ± 0.10; control (n=8) 2.35 ± 0.06; RUPP (n=3) 1.70 ± 0.16 (p=0.001); TNF-α (n=3) 1.74 ± 0.19 (p=0.001). $T_2$ values were calculated from 3 points in each region, from 2-5 placentas from each animal.**

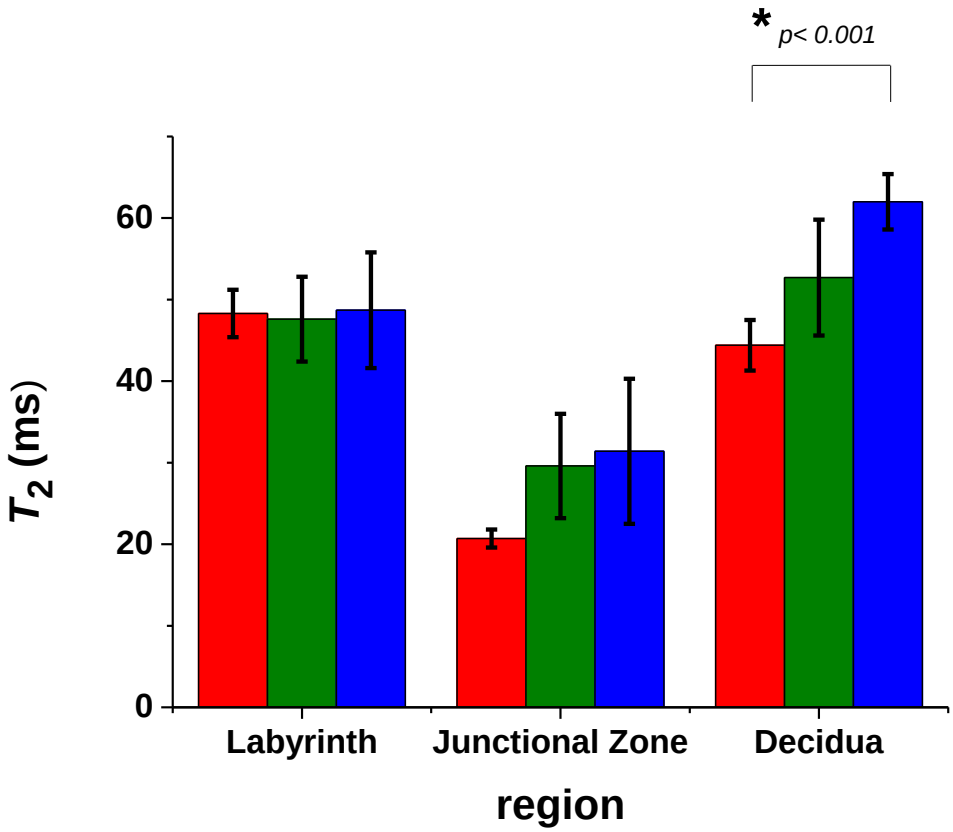


**Figure 6.3.6: Comparison of the $T_2$ values from different regions of the placenta. Control animals (*n*=8) are shown in red; RUPP animals (*n*=3) in green and TNF-α treated animals (*n*=3) in blue. $T_2$ values were calculated from 3 points in each of the labyrinth, junctional zone and decidua regions, from 2-5 placentas from each animal at day 17.5 of gestation.**

## 6.4 Discussion

This study has shown that higher resolution $T_2$ maps of mouse placenta can clearly differentiate between different regions of the placenta at time points after the maternal circulation is fully established. This differs from previous studies of $T_2$ relaxation times in humans using much lower field strengths, where the placenta was observed to be homogeneous (Gowland, 2005, Duncan et al., 1998). This is likely related to the diverse structure of the mouse placenta, with its distinct layers of labyrinth and junctional zone/decidua, compared to the more homogeneous villous structure of the human placenta.

The human studies have shown a correlation of $T_1$ and $T_2$ relaxation times with gestational age suggesting that changes in tissue structure or composition that occur with age influence relaxation times. A trend for shorter $T_1$ and $T_2$ in pregnancies complicated by preeclampsia and foetal growth restriction were also been reported, with another study by this group showing a significant correlation of $T_2$ with the fibrin volume density and the ratio of fibrin: villous volume density within a subset of placentas that were examined histologically within a week of scanning (Wright et al., 2011). A recent study by this group confirmed that $T_2$ of the placenta is shorter in pregnancies that deliver small for gestational age babies and further shows an association with impedance to flow in the uterine arteries as measured by Doppler ultrasound (Derwig et al., 2013).

The findings presented here show that the labyrinth has a $T_2$ value twice that of the junctional zone, with the observed contrast between these regions of the placenta being abolished on loss of blood flow. The decreased $T_2$lab/$T_2$junc ratio on loss of blood flow was due to both a decrease in the $T_2$ value in the labyrinth and an increase in the $T_2$ value in the junctional zone.

A possible explanation for the differences between regions and for the changes on loss of blood flow can be obtained by an examination of both the structure of the placenta and the influences on $T_2$ relaxation times. $T_2$ relaxation times of protons in tissue are sensitive to many physical, chemical and physiological parameters. Freely moving protons, in the form of free water gives rise to longer $T_2$ values whereas bound or tightly packed protons give rise to shorter $T_2$ values (Bottomley et al., 1984). In the labyrinth, essentially an intermeshed network of independent foetal and maternal blood vessels, there is an abundance of both freely moving protons, in the form of free water, and of blood cells containing mostly highly oxygenated haemoglobin. The junctional zone is dense with spongiotrophoblast and giant trophoblast cells. The longer $T_2$ value measured in the vascularised labyrinth reflects the abundance of freely moving protons in this region compared to the more cellularly dense junctional zone. Upon cessation of blood flow, the $T_2$ value in the labyrinth decreased and the $T_2$ value in the junctional zone increased. After cessation of blood flow the tissue continues to metabolise for some time, consuming $O_2$, producing $CO_2$ and generating deoxyhaemoglobin. The decrease in the $T_2$ value in the labyrinth can be accounted for by the blood oxygen level (BOLD) effect whereby an increase in the paramagnetic ion deoxyhaemoglobin gives rise to shorter $T_2$ relaxation times (Ogawa et al., 1990, Meyer et al., 1995), however in the junctional zone there are few haemoglobin containing blood cells and hence minimal paramagnetic effect of deoxyhaemoglobin on the $T_2$ value in this region. Conversely, due to the accumulation of $CO_2$ in the tissue and the consequent acidosis, the increase in free protons would account for the observed increase in the $T_2$ value in the junctional zone.

The effects of pH on $T_2$ values has been well documented in both muscle tissue of live patients (Jehenson et al., 1993) and in isolated muscle (Louie et al., 2009), with a clear correlation between decrease of intracellular pH and an increase in the $T_2$ relaxation time,

reflecting the increase in free protons. While acidosis would also occur in the labyrinth the predominant effect on the $T_2$ value in this region appears to be that of the paramagnetic deoxyhaemoglobin. Thus, the abolition of contrast between regions of the placenta upon complete loss of blood flow is consistent with the effects on $T_2$ relaxation times by both increases in deoxyhaemoglobin (hypoxia) and decreases in intracellular pH (acidosis).

The RUPP and the TNF-α treated mice also showed a decrease in contrast between the labyrinth and junctional zones, though this is primarily due to a trend for an increase in the $T_2$ value in the junctional zone alone with no change in the labyrinth observed. While the observed changes within each region have been limited to trends by the small number of mice in this study, the large number of individual placenta examined within each litter and the significance of the individual placental $T_2$lab/$T_2$junc ratio suggests that the trends are real. In the RUPP mice where blood flow is being artificially constricted, lower perfusion pressures are assumed to lead to hypoxia, and presumably, a greater proportion of deoxyhaemoglobin. In turn, this should lead to a lower $T_2$ value in the labyrinth, however this is not the case and the observed decrease in the $T_2$lab/$T_2$junc ratio is due solely to an increase in the $T_2$ value in the junctional zone. It could be speculated that, although reduced, the blood flow may be sufficient to prevent an accumulation of deoxyhaemoglobin in the labyrinth resulting in no observed change in the $T_2$ value. Alternatively, there may be a small increase in deoxyhaemoglobin tending to reduce $T_2$, however it is counteracted by a simultaneous increase in pH tending to increase $T_2$, thereby providing no net change. Conversely in the junctional zone, the observed increase in the $T_2$ value is likely to be a reflection of an increased acidosis in this region.

The quantitative analysis of the $T_2$ placental maps carried out here is similar to studies using the quantitative $T_2$ BOLD effect to determine the *in vivo* tissue oxygenation state in myocardial tissue (Ghugre et al., 2011). The BOLD effect using quantitative T2 relaxation

and has been considered to be potentially more specific than signal intensity measures such as traditional BOLD fMRI, allowing regional, longitudinal and cross-subject comparison (Ghugre and Wright, 2012). A recent study has used the quantitative $T_2$ BOLD effect to distinguish between ischaemic, non-ischaemic and normal myocardial segments in a clinical patient population exhibiting coronary artery disease (Manka et al., 2010).

In a review of the theoretical aspects of quantitative $T_2$ BOLD, it was concluded that to probe blood oxygenation levels in a given tissue, it is necessary to consider a multi-compartment model with the long and short $T_2$ components representing the vascular space and combination of intracellular and interstitial space respectively. Theoretical predictions and experimental work indicate that $T_{2\text{Long}}$ is sensitive to changes in oxygenation, but not $T_{2\text{Short}}$ (Ghugre and Wright, 2012).

This thesis did not distinguish two components of the measured $T_2$ value. This may offer a possible explanation as to why the $T_2$ values in the labyrinth of the RUPP animals did not decrease as expected. Due to the highly vascularised structure of the labyrinth, a single compartment approach may have concealed real changes in oxygenation. If determined as separate components, one would expect the $T_{2Long}$ value, representing the vascular space, to decrease consistent with a decrease in perfusion and expected lower oxygenation, while the $T_{2\text{Short}}$ value representing the intracellular and interstitial space would increase consistent with a decreased pH. By measuring a combined $T_2$, the changes have effectively been cancelled out, exhibiting as no change of $T_2$ in the labyrinth. Further studies to determine the separate $T_2$ components would clarify the issue.

One of the interesting features of the data presented here is that an increase in the inflammatory cytokine TNF-α shows a similar $T_2$ pattern to RUPP suggesting that metabolic changes in levels of tissue acidity may be a common feature in these two models. Further

studies involving the measurement of intracellular pH using $^{31}P$ MRI are warranted to confirm the tissue acidosis in these models.

## 6.5 Summary

This study has shown that higher resolution $T_2$ maps of mouse placenta can clearly differentiate between different regions of the placenta at time points after the maternal circulation is fully established. This study has shown that morphological differences related to blood flow can be detected by $T_2$ mapping in the placenta of both the artificially reduced perfusion (RUPP) and imbalance of inflammatory cytokines (TNF-α) experimental models. Observed differences are consistent with the effects on $T_2$ relaxation times by both increases in deoxyhaemoglobin (hypoxia) and decreases in intracellular pH (acidosis). That an increase in the inflammatory cytokine TNF-α shows a similar $T_2$ pattern to RUPP suggests that metabolic changes in levels of tissue acidity may be a common feature in these two very different models.

# Chapter 7 Visualisation of placental structure by MRI

## 7.1 High Resolution Placental Maps

High resolution GEFI images (voxel size, 50 x 50 x 50 μm) were taken of isolated fixed placenta in order to identify features of the placenta and to assess structural changes between treatment groups. Representative individual images distinguishing different regions of normal pregnant placenta are shown in Figure 7.1.1. The labyrinth, junctional zone, decidua, spiral arteries, central canal and umbilical vein and artery are clearly differentiated. A complete set of images from a single placenta are displayed in Appendix 2.

Figure 7.1.2 shows representative images of placenta from normal, RUPP and TNF-α infused animals. There was a wide variation in the internal composition of the major three zones of the placenta between individual placentas but no gross differences between the separate treatment groups were observed.

With the utilisation of 3D visualisation software (Amira™) it was possible to reconstruct 3D models of the placenta from the 2D images as shown in Figure 7.1.3.

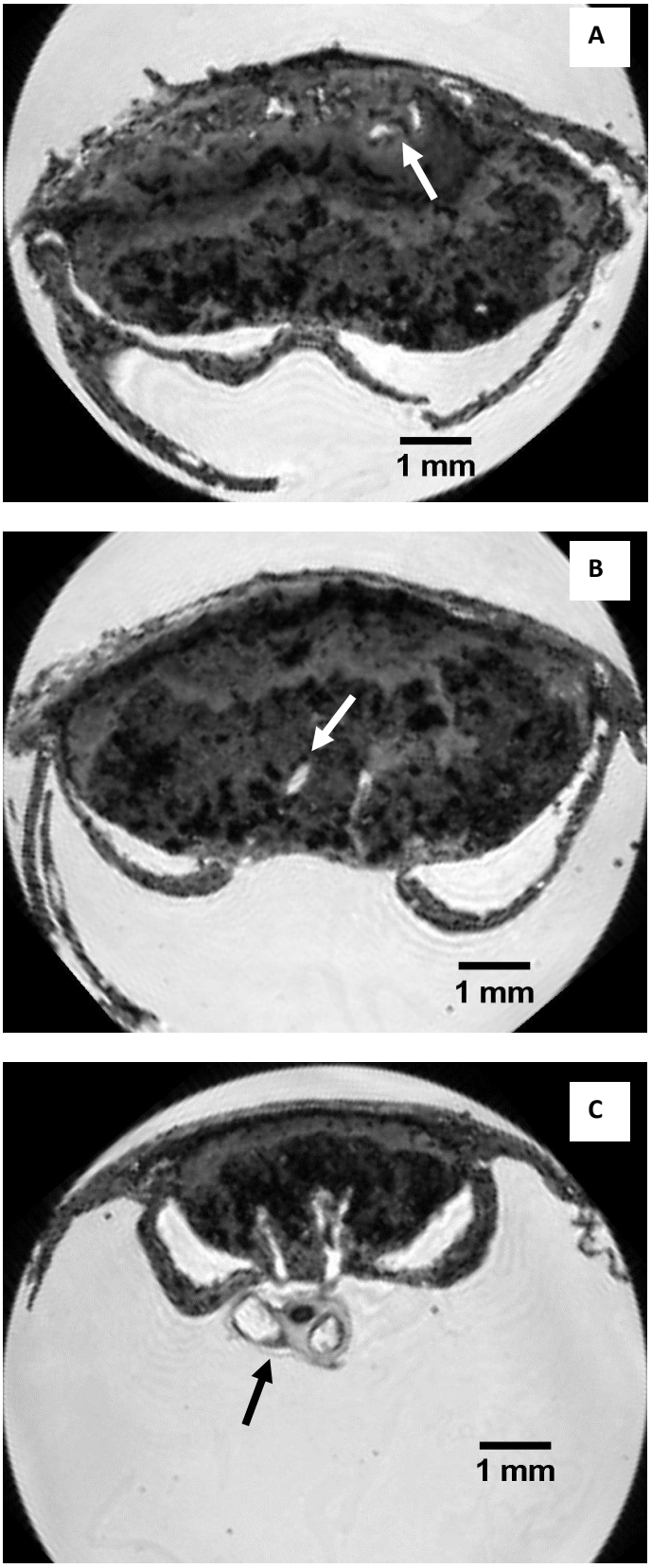


**Figure 7.1.1: High resolution (50 x 50 x 50 µm voxels) GEFI images of a normal pregnant gd 17 placenta. The labyrinth, junctional zone and decidua are clearly distinguished. A) shows spiral arteries in the decidua (arrow); B) shows two central canals (arrow); C) shows umbilical vein and artery (arrow).**

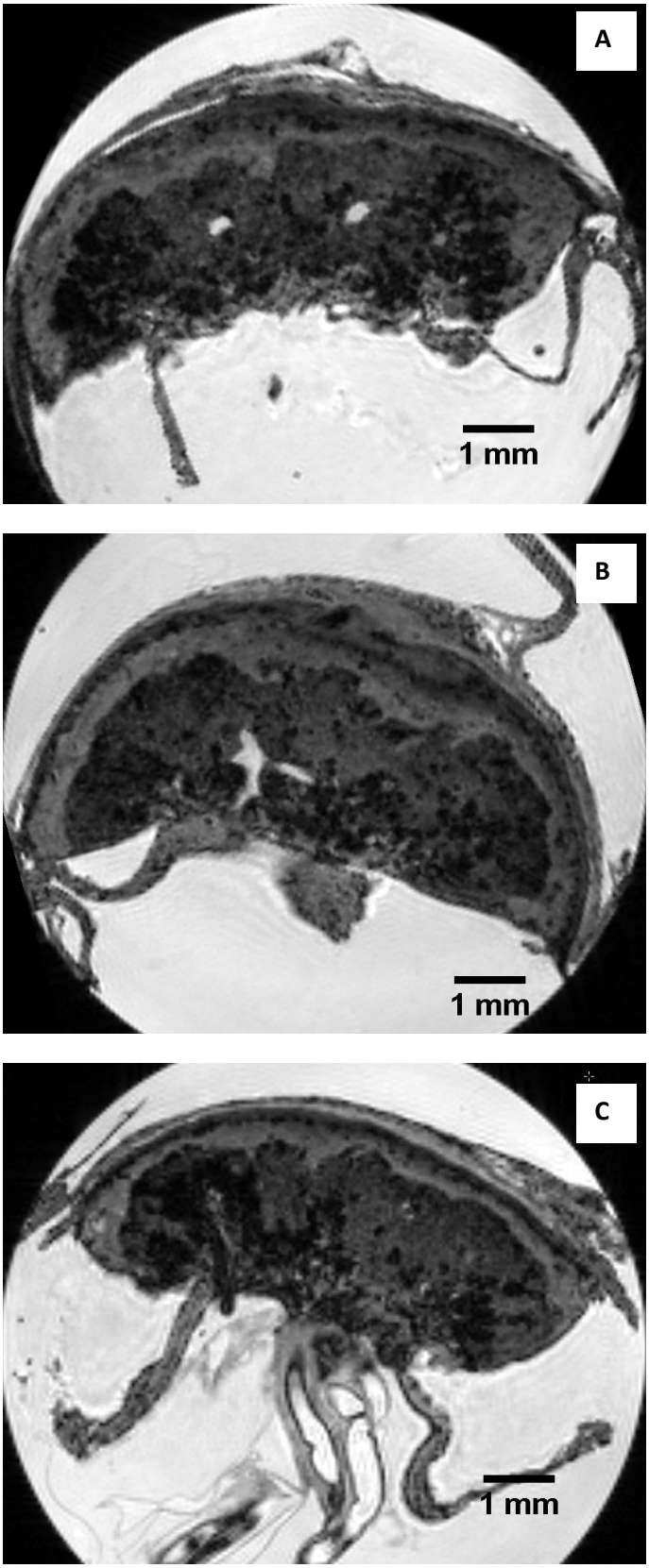


**Figure 7.1.2: Representative high resolution (50 x 50 x 50 µm voxels) GEFI images of placenta from A) normal, B) RUPP and C) TNF-α infused animals.**

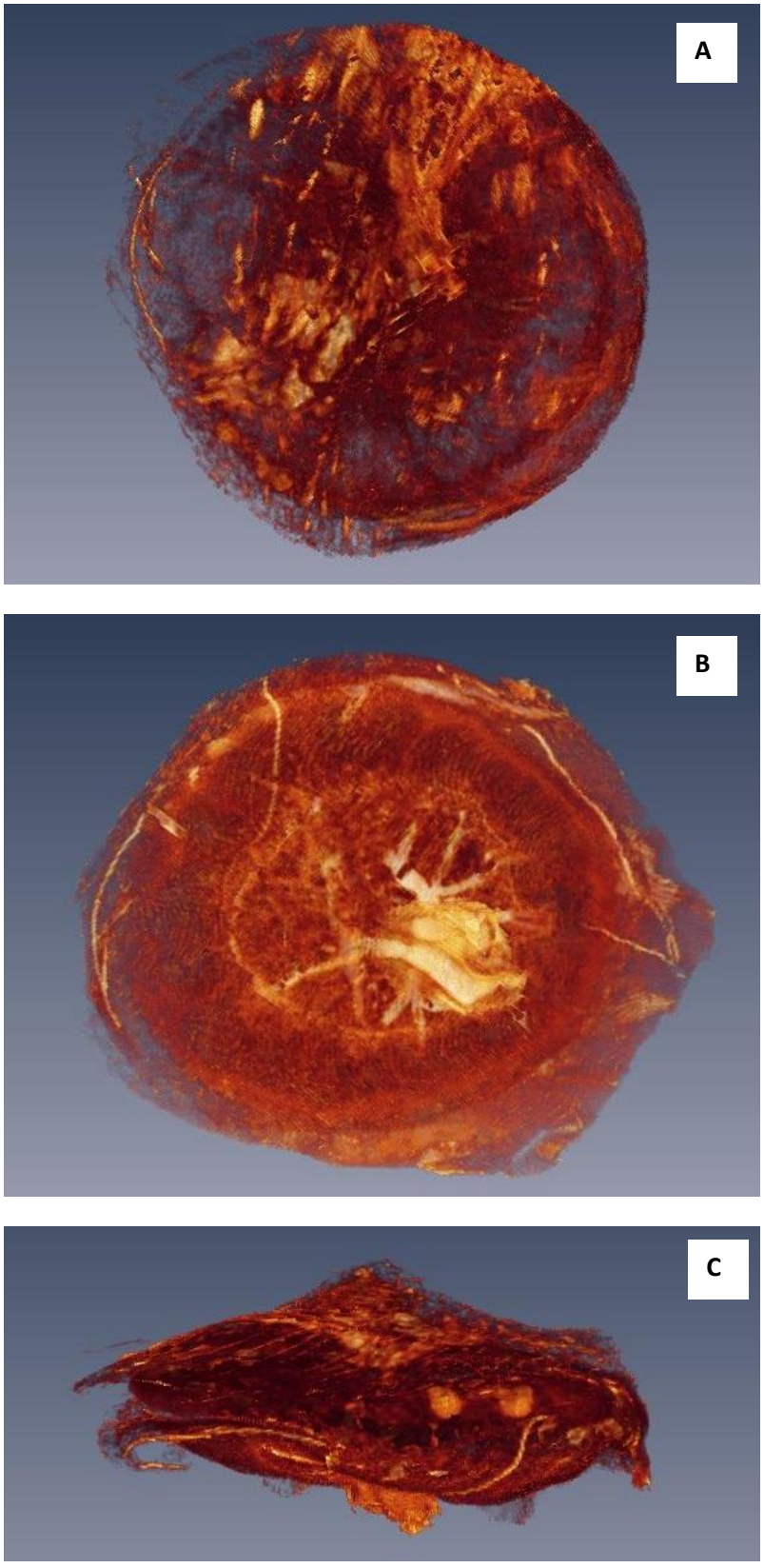


**Figure 7.1.3: 3D reconstruction from 2D MRI images of the placenta showing A) Maternal surface view, B) foetal surface view C) sideview. 3D volume rendering was performed using the visualisation software (Amira™).**

## 7.2 Volumetric Analysis of Placental Maps

The high resolution detail of internal structural features of the placenta indicated that it would be possible to segment the placenta into different regions for volume analysis. Segmentation of the 2D images into labelled placental regions; amniotic membrane, labyrinth, junctional zone and decidua were performed using Amira™ software. Segmentation used a combination of manual tools and algorithms based on voxel intensity thresholds to delineate structures within the placenta. Figures 7.2.1 and 7.2.2 show representative images with coloured overlays depicting the segmented data. 3D reconstruction of placentas was performed using the segmented label data. Each of the labelled regions are able to be visualised independently and can be combined to form a complete 3D model (Figure 7.2.3). Different colour ranges can be chosen including solid colours which can distinguish regions or ranges based on voxel intensity which allows definition of microstructure (Figure 7.2.4).

Segmentation of the data to visualize the maternal vasculature was possible (figure 7.2.5), affording the potential to investigate changes in spiral artery and central canal dimensions.

In order to test the feasibility of performing stereological analysis of the placenta from 3D models reconstructed from high resolution MRI images, volumetric analysis was carried out on the segmented data from multiple placentas of one normal, one RUPP and one TNF-α infused animal. Volume measurements of the labyrinth, junctional zone and decidua, and ratios of labyrinth/junctional zone are recorded in Table 7.1. Volume measurements of the decidua are highly variable as the labelling of this tissue included the uterine wall. The uterine wall in the mouse is a narrow structure and, in order to visualize the spiral arteries, the placentas were dissected with the uterine wall attached. Variable amounts

of uterine wall were collected with each placenta and more refined segmentation would be required to distinguish true decidua basalis from uterine wall tissue.

**Table 7.1: Volumetric analysis on the 3D segmented placentas**

| | Volume ± stdev ($mm^3$) | | | | Ratio Lab/Jun |
|---|---|---|---|---|---|
| **Treatment** | **Labyrinth** | **Junctional Zone** | **Decidua** | **Total volume** | |
| **Normal (n=5)** | 37.9 ± 2.9 | 17.1 ± 3.9 | 41.3 ± 5.2 | 96.2 ± 5.9 | 2.3 ± 0.7 |
| **TNF-α (n=5)** | 35.8 ± 1.6 | 13.5 ± 1.9 | 39.3 ± 10.3 | 88.7 ± 11.9 | 2.7 ± 0.5 |
| **RUPP (n=5)** | 34.3 ± 3.5 | 21.8 ± 4.0* | 38.5 ± 7.7 | 94.6 ± 9.0 | 1.6± 0.4 * |

* $p < 0.05$

The preliminary data suggests that there may be small changes in the volume of the junctional zone in the experimental model animals; however this would need to be validated further by examining placentas from multiple animals within each group. The reliability of comparative quantitative measurements within litters, between individual animals and between treatments groups is dependent on the accuracy of the segmentation. Various algorithms may be utilised to assist, but segmentation still remains a manual task that requires skill to master in order to obtain accurate data in a time efficient manner. Repetition of the initial segmentations would be warranted in order to be assured of accurate and reliable data.

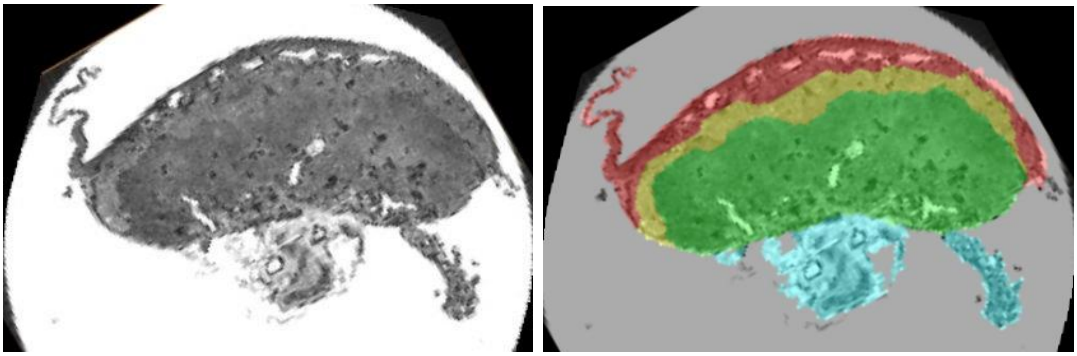

**Figure 7.2.1: GEFI image of normal mouse placenta showing overlay of the segmented labelled regions; decidua (red), junctional zone (yellow), labyrinth (green) and amniotic membrane (blue). Segmentation was performed using the visualisation software (Amira™)**

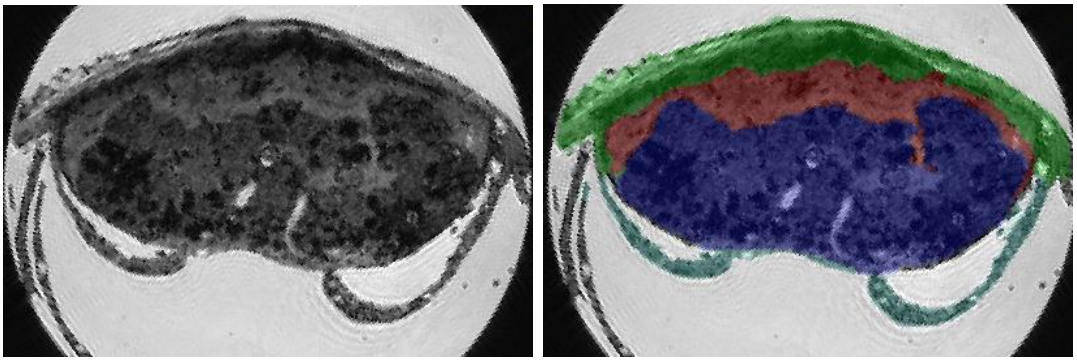

**Figure 7.2.2: GEFI image of a second normal mouse placenta showing overlay of the segmented labelled regions; decidua (green), junctional zone (red), labyrinth (purple) and amniotic membrane (blue). Segmentation was performed using the visualisation software (Amira™)**

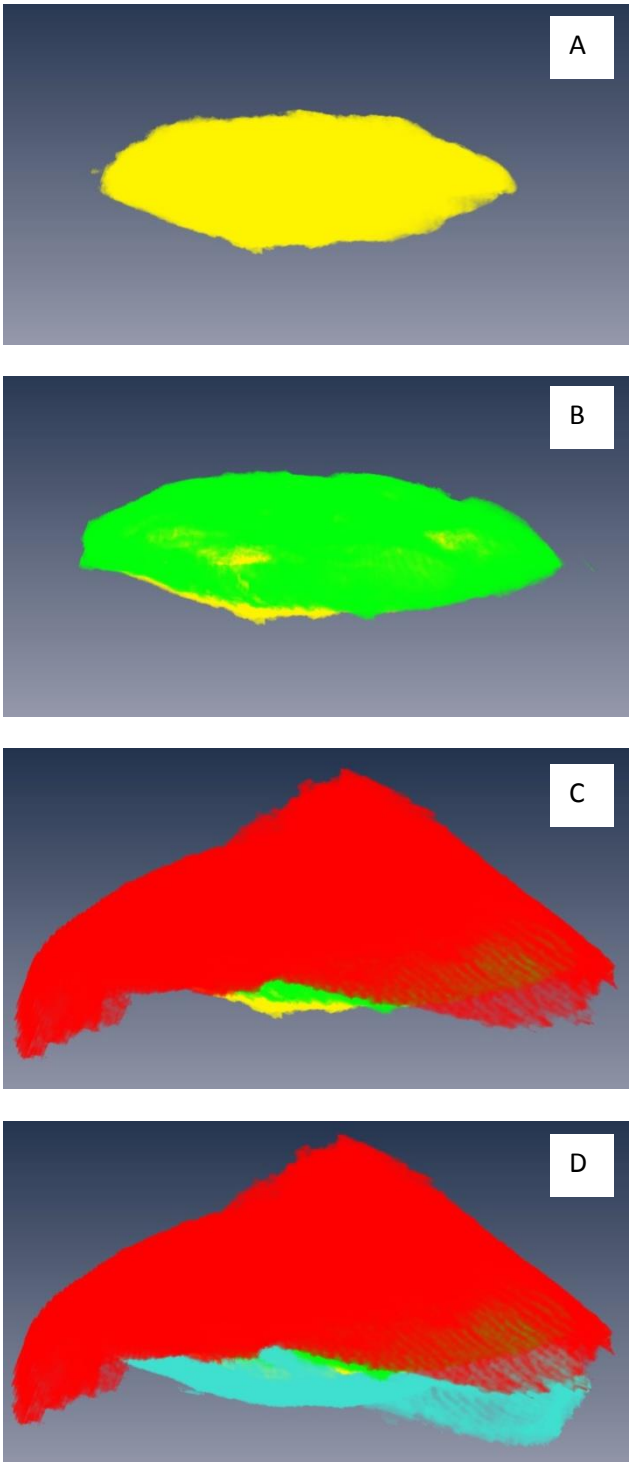


**Figure 7.2.3: 3D reconstruction of a placenta using segmented label data. Each of the regions can be visualized independently or combined. A) labyrinth (yellow) B) labyrinth and junctional zone (green); C) labyrinth, junctional zone and decidua (red); D) labyrinth, junctional zone, decidua and amniotic membrane (blue). 3D volume rendering was performed using the visualisation software (Amira™)**

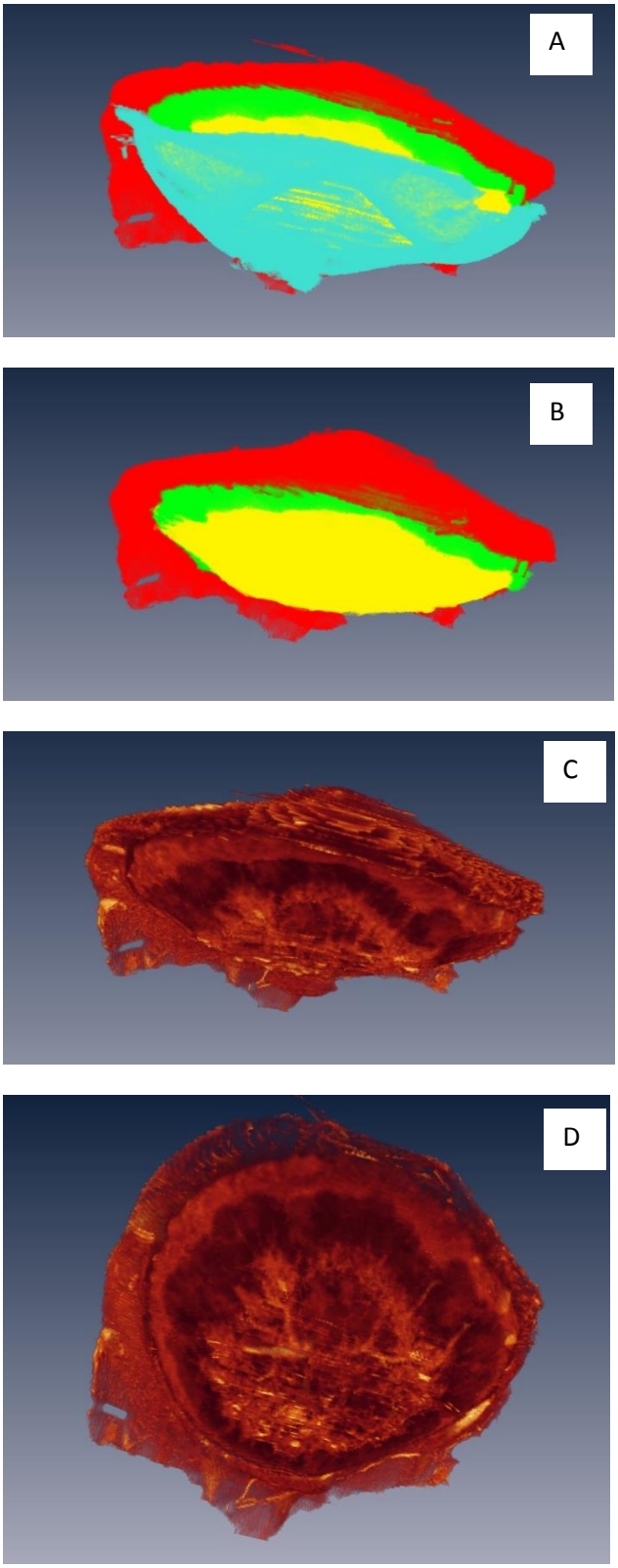


**Figure 7.2.4: 3D models are able to be viewed in multiple ways. 3D reconstruction of a placenta showing A) labyrinth (yellow), junctional zone (green), decidua (red) and amniotic membrane (blue); B) same as (A) but with amniotic layer removed; C) same as (B) but using colour range based on voxel intensity; D) same as (C) but with view changed to visualize the foetal surface. 3D volume rendering was performed using the visualisation software (Amira™)**

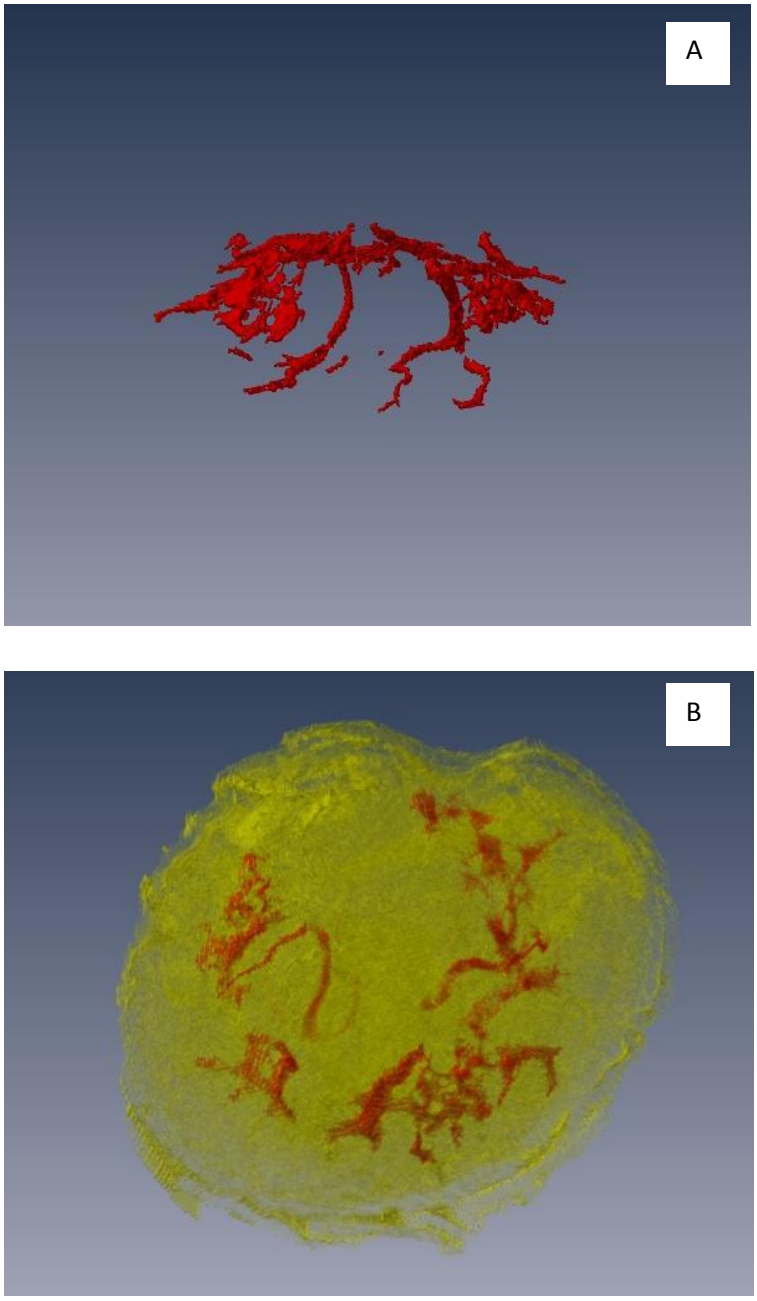


**Figure 7.2.5: Segmentation of the placental image data to identify maternal vasculature. A) Solid colour rendition of a sideview of the vasculature B) Placenta overlay showing maternal vasculature viewed from the maternal side. 3D volume rendering was performed using the visualisation software (Amira™)**

## 7.3 Summary

MRI was utilised to create a high resolution placental map which identifies many of the structural features of the placenta. This study documents that high resolution MRI data, combined with 3D visualisation software, can be successfully used to create 3D reconstructions of the placenta. The detail in the images is such that segmentation into regions of the placenta can be performed and quantitative analysis performed.

The data presented here demonstrates that it is feasible to measure and compare structural features of the placenta with this technique. Further it demonstrates that high resolution MRI followed by 3D reconstruction of a complete organ provides an alternative to conventional stereology which uses sampling and estimation tools to estimate parameters of 3D structures from 2D histological sections.

The preliminary data using multiple placentas from a single animal from each treatment group (control, RUPP, TNF-α) also suggests there may be measurable changes in the junctional zone of experimental model animals. While this remains to be validated with increased numbers, this innovative technique shows the potential to visualize and quantify placental structural change in experimental models of perturbed pregnancies.

# Chapter 8 Molecular changes: mRNA expression

Placental tissue from the experimental model animals was examined for molecular changes at the transcription level. Molecules targeted were the anti-angiogenic factor sFlt-1 and its membrane counterpart mFlt-1, as well as molecules involved in response to hypoxia (HIF-1α), inflammation (TLR-3 and TLR-4) and pH homeostasis (CLIC-3 and CLIC-4). Alterations in mRNA expression levels of *mFlt-1*, *sFlt-1*, *hif-1α*, *tlr-3, tlr-4, clic-3* and *clic-4* were determined using quantitative PCR and beta actin *bAct* as a normaliser gene.

## 8.1 Membrane and soluble Flt-1

There were no significant differences in the expression of either *sFlt-1* or *mFlt-1* between treatment groups (Figure 8.1.1 and 8.1.2).

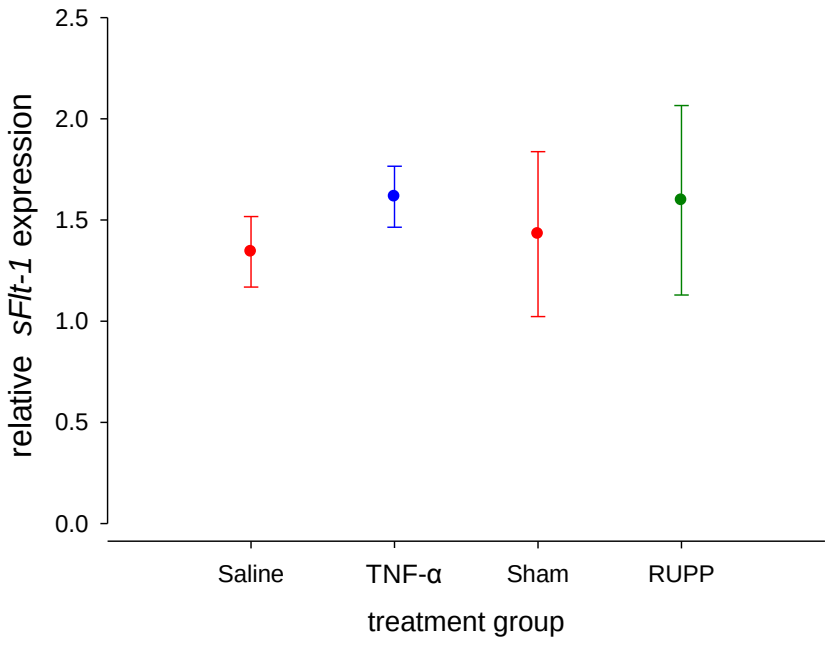


**Figure 8.1.1: Relative expression of *sFLt-1* between saline (n=4), TNF-α (n=8) sham operated (n=4) and RUPP (n=4) animals. Data is expressed as mean ± SEM and levels are relative to an individual saline sample and normalised to *bAct* expression levels.**

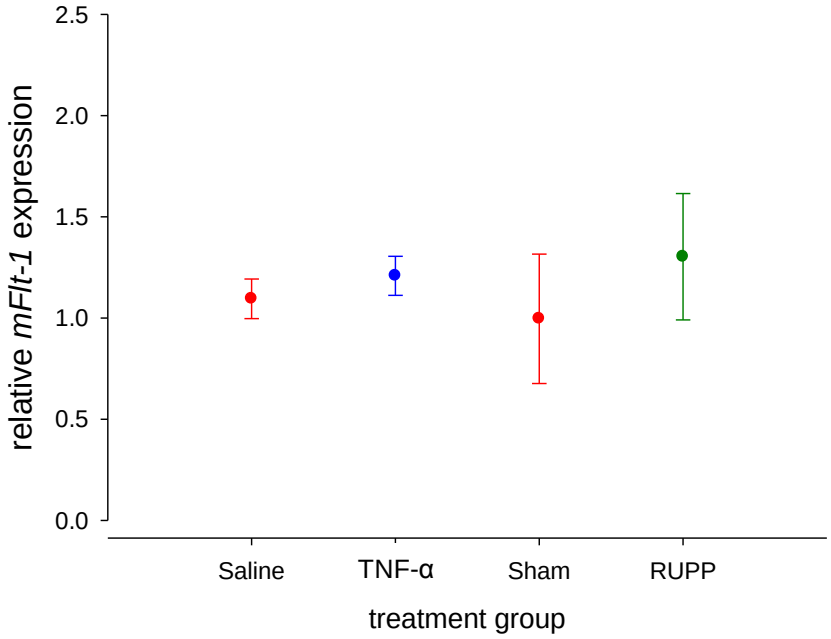


**Figure 8.1.2: Relative expression of *mFlt-1* between saline (n=4), TNF-α (n=8) sham operated (n=4) and RUPP (n=4) animals. Data is expressed as mean ± SEM and levels are relative to an individual saline sample and normalised to *bAct* expression levels.**

## 8.2 Hypoxia inducible factor 1 (HIF-1α)

Expression levels of *hif-1α* were significantly higher in TNF-α treated animals compared to saline control animals and in RUPP animals compared to sham operated animals (Figure 8.2.1). It is interesting to note that there were significantly higher expression levels in saline control animals as compared to sham control animals.

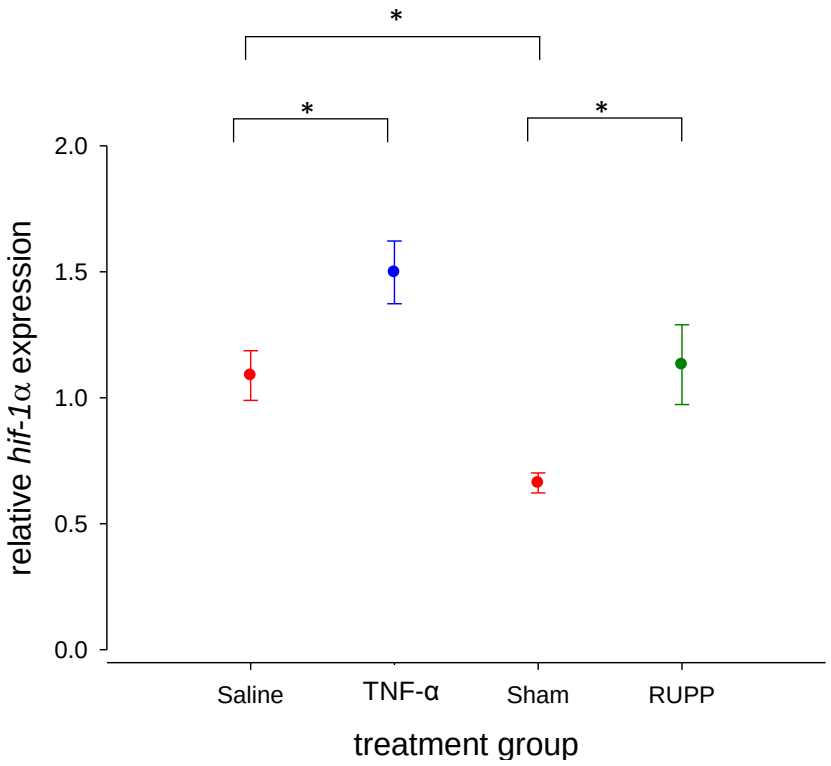


**Figure 8.2.1: Relative expression of *hif-1α* between saline (n=4), TNF-α (n=8) sham operated (n=4) and RUPP (n=4) animals. Data is expressed as mean ± SEM and levels are relative to an individual saline sample and normalised to *bAct* expression levels. (*p<0.01)**

## 8.3 Toll like receptors (TLR-3 and TLR-4)

There were no significant differences in the expression of *tlr-3* between treatment groups (Figure 8.3.1). There was a trend for expression levels of *tlr-4* to be higher in RUPP animals compared to sham, and interestingly a small, but significant difference in expression levels was found between sham control animals and animals implanted with either the saline or TNF-α osmotic pumps (Figure 8.3.2).

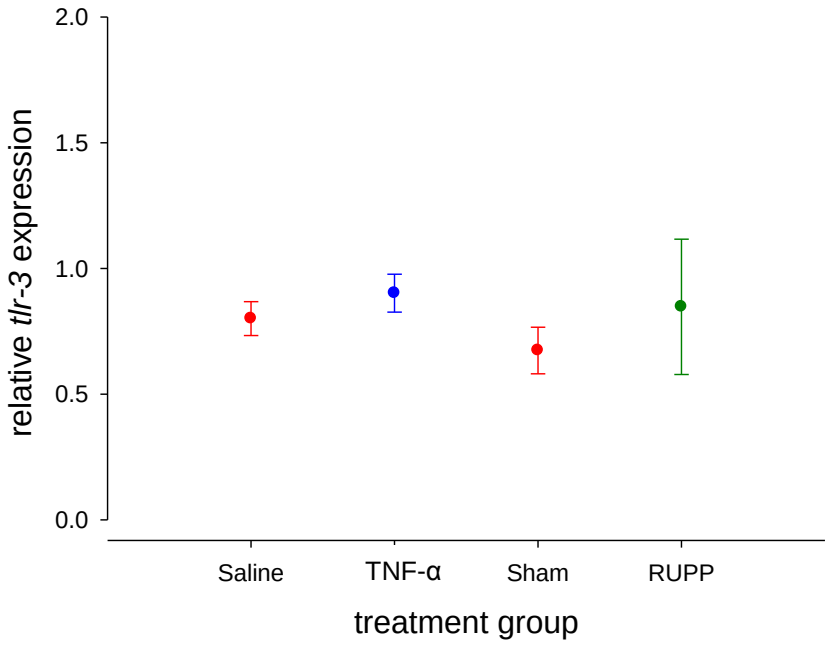


**Figure 8.3.1: Relative expression of *tlr-3* between saline (n=4), TNF-α (n=8) sham operated (n=4) and RUPP (n=4) animals. Data is expressed as mean ± SEM and levels are relative to an individual saline sample and normalised to *bAct* expression levels.**

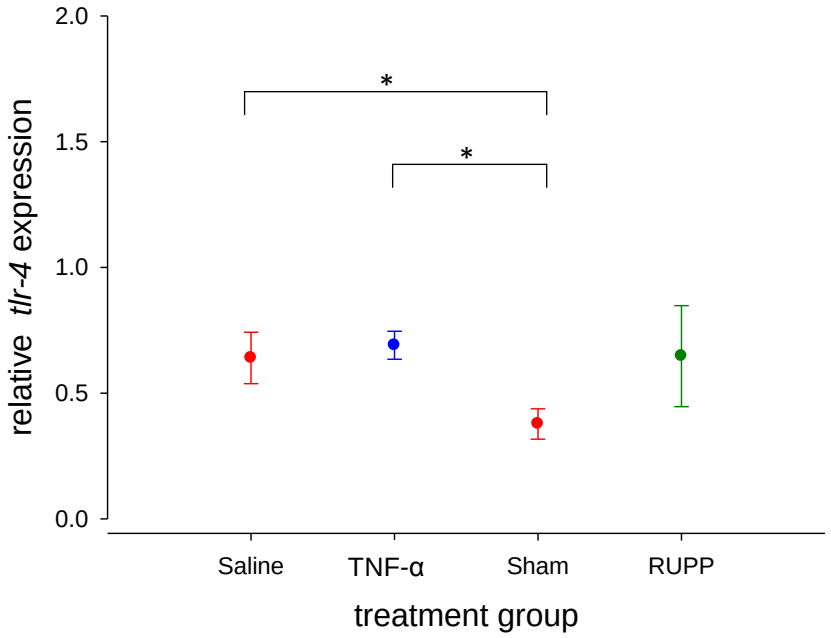


**Figure 8.3.2: Relative expression of *tlr-4* between saline (n=4), TNF-α (n=8) sham operated (n=4) and RUPP (n=4) animals. Data is expressed as mean ± SEM and levels are relative to an individual saline sample and normalised to *bAct* expression levels. (*p<0.05)**

## 8.4 Chloride intracellular channels (CLIC-3 and CLIC-4)

Expression levels of *Clic-3* were significantly decreased in TNF-α treated animals compared to saline control animals and there was a trend for expression levels to be lower in RUPP animals compared to sham operated animals (Figure 8.4.1).

There were no significant differences in *Clic-4* expression levels between treatment groups (Figure 8.4.2).

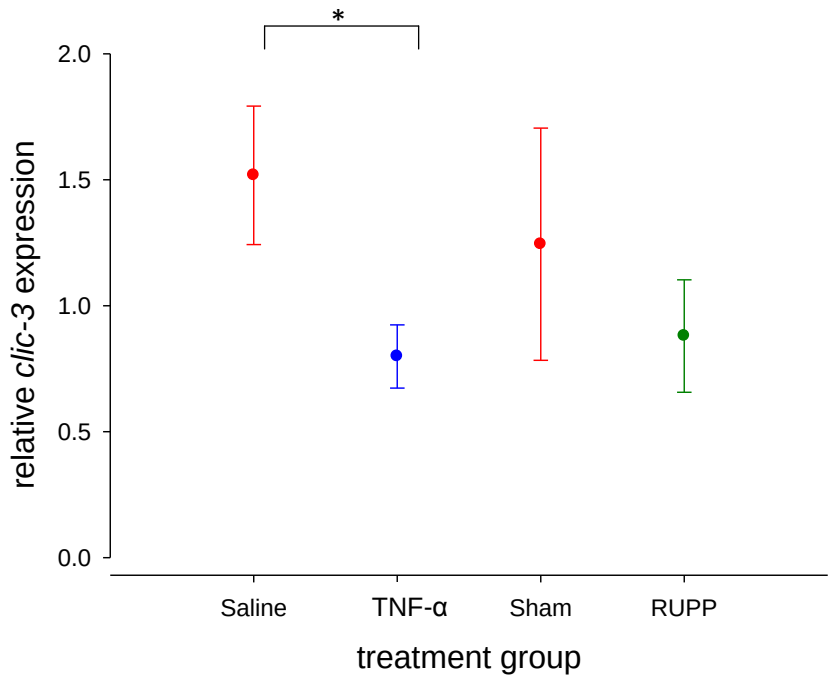


**Figure 8.4.1: Relative expression of *clic-3* between saline (n=4), TNF-α (n=8) sham operated (n=4) and RUPP (n=4) animals. Data is expressed as mean ± SEM and levels are relative to an individual saline sample and normalised to *bAct* expression levels. (*p<0.05)**

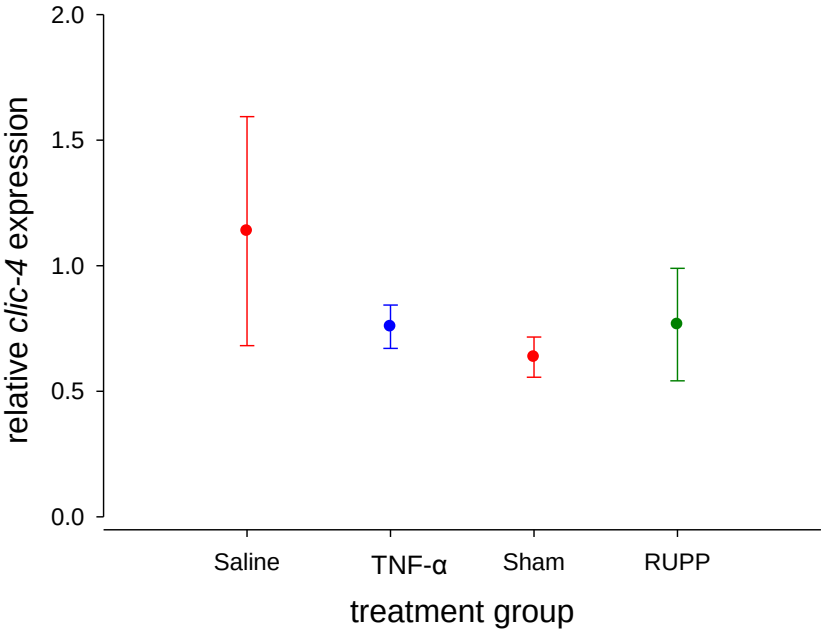


**Figure 8.4.2: Relative expression of *clic-4* between saline (n=4), TNF-α (n=8) sham operated (n=4) and RUPP (n=4) animals. Data is expressed as mean ± SEM and levels are relative to an individual saline sample and normalised to *bAct* expression levels.**

## 8.5 Correlations between factors

There was a significant and strong correlation between placental expression levels of *sFlt-1* and *mFlt-1* mRNA (Figure 8.5.1), indicating that expression of the soluble and membrane forms were tightly linked and that there was no differential regulation of expression of the soluble form of the receptor.

There was no relationship between the expression of placental *sFlt-1* mRNA and levels of sFlt-1 found in the maternal serum (Figure 8.5.2), suggesting that in this model the levels of sFlt-1 found in the maternal serum are not directly related to *de novo* synthesis of placental sFlt-1, but may reflect a more complex pathway of storage and release of the soluble form of the receptor from the placenta and from maternal tissue as has been discussed in Section 5.4.

There was a significant correlation between placental *hif-1α* mRNA expression and *sFlt-1* and *mFlt-1* mRNA expression (Figure 8.5.3 and Figure 8.5.4) and between placental *hif-1α* mRNA expression and *tlr-3* and *tlr-4* mRNA expression (Figure 8.5.5 and Figure 8.5.6), indicating that there is a relationship between the transcription factor HIF-1α and molecules involved in angiogenesis and inflammation. There was no correlation between *hif-1α* mRNA expression and *clic-3* or *clic-4* mRNA expression (data not shown).

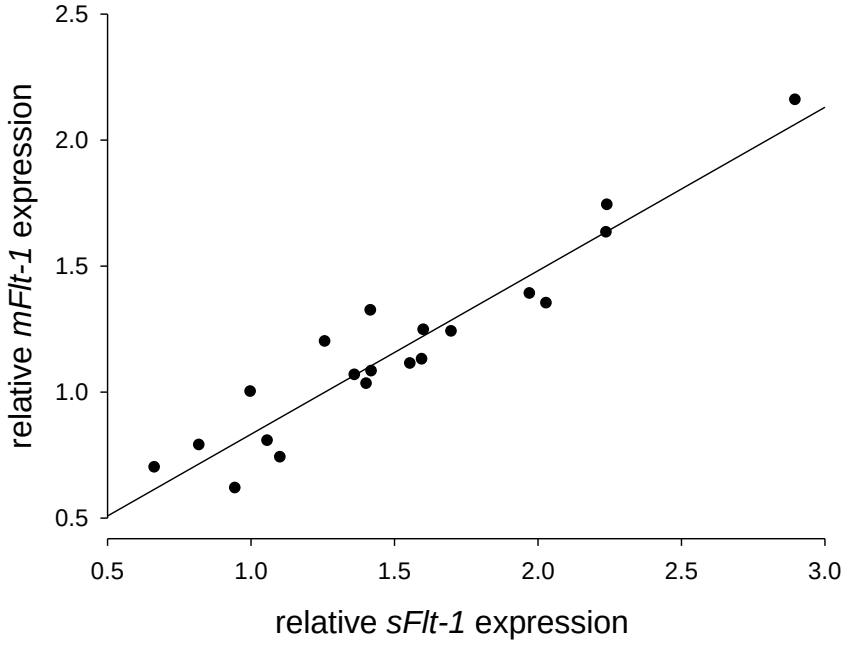


**Figure 8.5.1: Correlation between relative *sFlt-1* mRNA expression and *mFlt-1* expression in placental tissue at gestational day 17. ($r^2$=0.904; Pearsons correlation 0.923, p<0.001)**

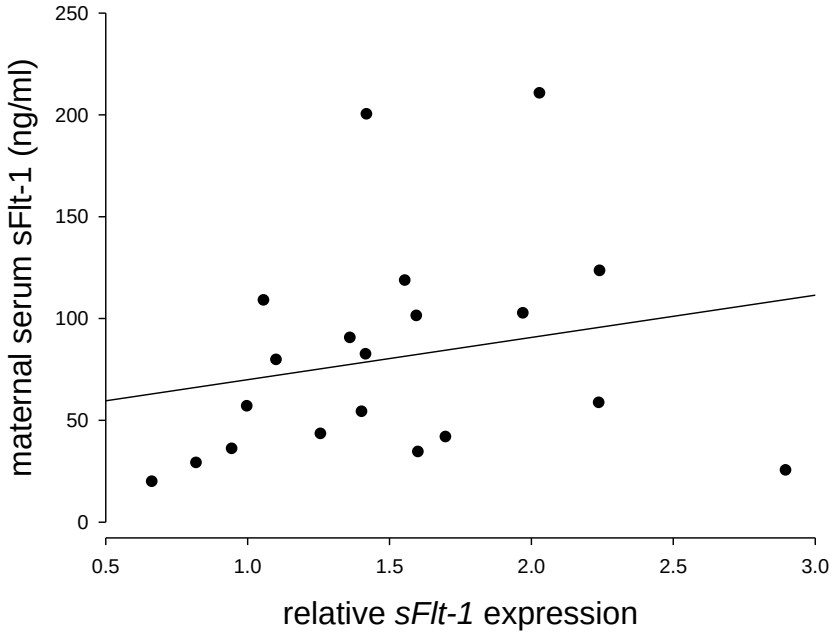


**Figure 8.5.2: Correlation between relative placental *sFlt-1* mRNA expression and levels of sFlt-1 protein in maternal serum at gestational day 17. ($r^2$=0.046) p=N.S**

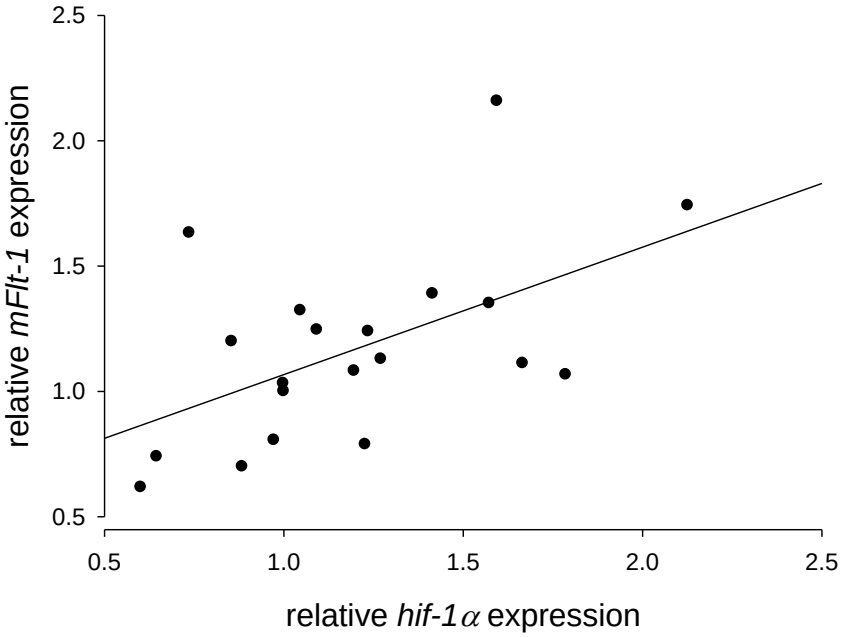


**Figure 8.5.3: Correlation between relative placental *hif-1α* mRNA expression and relative placental *mFlt-1* mRNA expression at gestational day 17. ($r^2$=0.291; Pearsons correlation 0.610, p<0.05)**

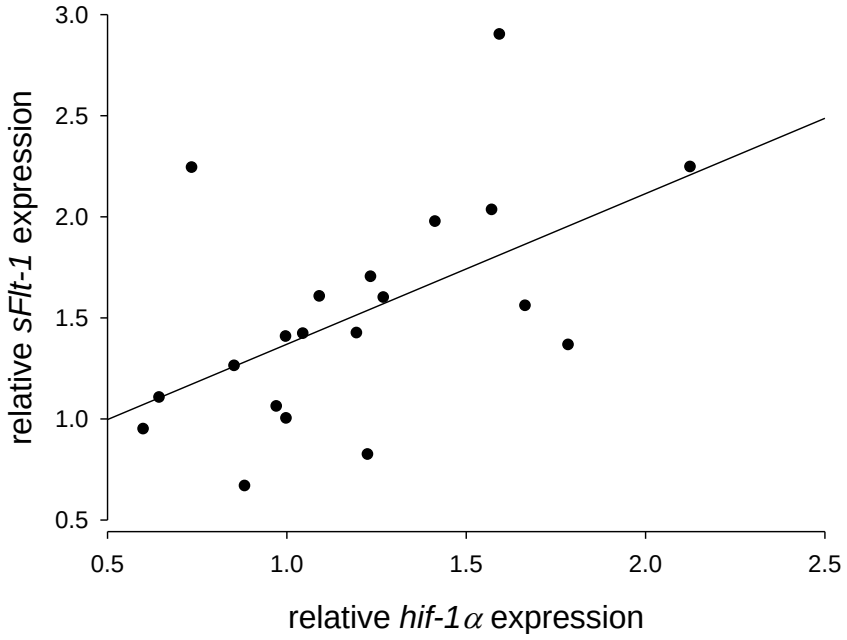


**Figure 8.5.4: Correlation between relative placental *hif-1α* mRNA expression and relative placental *sFlt-1* mRNA expression at gestational day 17. ($r^2$=0.291; Pearsons correlation 0.525, p<0.05)**

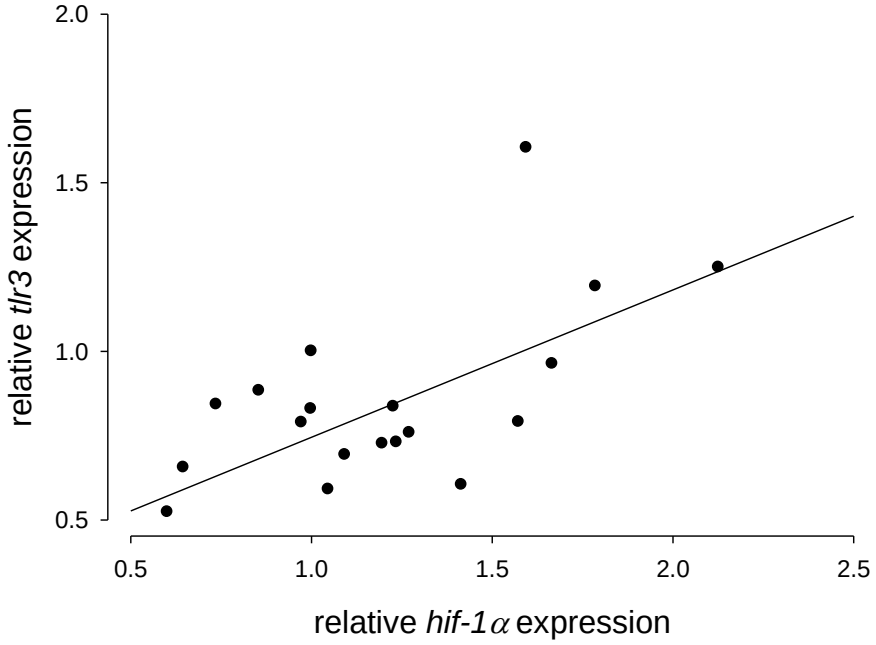


**Figure 8.5.5: Correlation between relative placental *hif-1α* mRNA expression and relative placental *tlr3* mRNA expression at gestational day 17. ($r^2$=0.399; Pearsons correlation 0.586 p<0.01)**

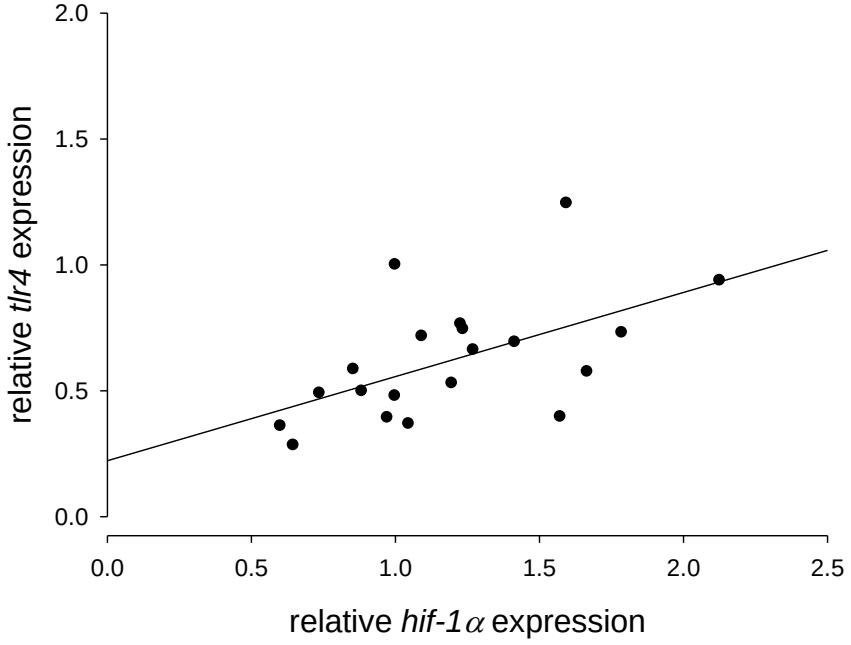


**Figure 8.5.6: Correlation between relative placental *hif-1α* mRNA expression and relative placental *tlr4* mRNA expression at gestational day 17. ($r^2$=0.305; Pearsons correlation 0.612 p<0.01)**

## 8.6 Discussion

***Membrane and soluble Flt-1***

The lack of significant differences between treatment groups for either *sFlt-1* or *mFlt-1* mRNA expression may indicate that, similarly to the serum concentrations of sFLt-1 (Section 5.4), the intervention time of four days is not long enough to see any statistically significantly changes. A recent study examining the differential expression of *sFlt-1* in individual placenta from normal pregnant mice observed that expression of *sFlt-1* was significantly different between litters (Surmon et al., 2014). It is possible that this inter-litter variation may hamper the detection of differences between the treatment groups, suggesting that greater numbers of animals are required to observe statistically significant differences between groups. Alternatively the results may suggest that any changes in release of sFlt-1 into the maternal circulation is not necessarily a result of changes in *sFlt-1* transcription, but could be due to increased translation or post translational release from a pre-existing pool, or proteolysis from the membrane form (Denizot et al., 2007, Searle et al., 2011, Sela et al., 2011).

There was more variability in the *sFlt-1* or *mFlt-1* mRNA expression in the abdominally operated animals (sham and RUPP) as compared to the animals receiving the subcutaneous infusion (saline and TNF-α). This may be related to the effects of localised response due to position of placenta in relation to the ligation or sham ligation, as compared to the systemic response to the TNF-α. Placental position was not accounted for in this study.

***Hypoxia inducible factor 1-α***

Expression levels of *hif-1α* were significantly higher in TNF-α treated and RUPP animals compared to control animals. It is interesting to note that there were significantly higher expression levels in saline control animals as compared to sham control animals. This may indicate that the implant of the mini-osmotic pump alone causes an inflammatory response with release of inflammatory cytokines, as suggested by the maternal serum sFlt-1 trends (Section 5.4).

The increased expression of *sFlt-1* by placental villous explants under hypoxic conditions has been demonstrated by others to be mediated by the transcription factor HIF-1α (Nevo et al., 2006). The data presented here is consistent with this temporal sequence of events, even though downstream effects on *sFlt-1* mRNA expression is not observed in this model, perhaps due to inadequate time of intervention or small numbers. Alternatively, HIF-1α may regulate other factors that are released into the maternal circulation such as endothelin (Minchenko and Caro, 2000) and soluble endoglin (Sanchez-Elsner et al., 2002), and elicit the maternal hypertensive response.

While levels of oxygen primarily regulate HIF-1α activity by either affecting its stability or its transcriptional ability, *de novo* synthesis of HIF-1α is largely dependent upon non-hypoxic mechanisms such as growth factors and inflammatory stimuli. *Hif-1α* mRNA expression has previously been reported to be only modestly increased in tissues from rodents exposed to hypoxia (Wiener et al., 1996) and has more recently been shown to be upregulated by TNF-α in airway smooth muscle cells through an NFκB sensitive pathway (Tsapournioti et al., 2013). Stimulation of TLR-4 through a NF-κB dependent process has also been reported to increase gene expression of *hif-1α* and in turn to upregulate gene transcription of *tnf-α*

(Kim et al., 2007). Thus under inflammatory conditions, a positive feedback process to upregulate *hif-1α* expression may operate.

The correlation between *hif-1α* expression and *mFlt-1*, *sFlt-1*, *tlr3* and *tlr-4* expression is another line of evidence supporting the growing body of work showing that there is a link between the transcription factor and molecules involved in angiogenesis (Tal, 2012, Tal et al., 2010, Nevo et al., 2006) and inflammation (Sumbayev and Nicholas, 2010, Kim et al., 2010, Raicevic et al., 2010, Young et al., 2010).

***Toll-like receptors (TLR-3 and TLR-4)***

There were no significant differences between treatment groups for *tlr-3* mRNA expression levels and while there was a trend for expression levels of *tlr-4* to be higher in RUPP animals compared to sham, and a significant difference in expression levels between sham control animals and animals implanted with either the saline or TNF-α osmotic pumps, it is noted that the fold change in expression is minimal across all groups (less than the >1.5-2 fold change traditionally considered biologically meaningful in the study of disease mechanisms) and it was concluded that no relevant upregulation of *tlr-3* or *tlr-4* transcription occurs within the time frame of the experiment.

***Chloride intracellular channels (CLIC-3 and CLIC-4)***

Expression levels of *Clic-3* were significantly lower in TNF-α treated animals compared to saline control animals and there was a trend for expression levels to be lower in RUPP animals compared to sham operated animals. There were no significant differences between treatment groups for *Clic-4* mRNA expression levels. The data from this experimental animal model are contrary to those presented in a human study which found that clic3 mRNA was significantly increased in preeclamptic placentas (Murthi et al., 2012).

## 8.7 Summary

This study demonstrates that maternal infusion of the inflammatory cytokine TNF-α and restriction of blood flow to the placenta (RUPP) upregulates placental HIF-1α at the mRNA and protein level (Section 9.2.3).

While this study showed no significant differences between treatment groups for either *sFlt-1* or *mFlt-1* mRNA expression, it is possible that the time frame is too short to see any HIF-1α mediated effects on their expression. Alternatively, HIF-1α may regulate other factors that are released into the maternal circulation and attenuate the maternal hypertensive response.

This study indicates that in the TNF-α and RUPP experimental animal models, no upregulation of the *tlr3* or *tlr4* transcription occurs within the time frame of the experiment, indicating that post-transcriptional regulation of these signalling molecules in the inflammatory pathway are likely to explain the upregulation of protein expression observed (Section 9.2.2).

This study found expression levels of *Clic-3* mRNA significantly decreased in TNF-α treated animals in contrast to the increased protein expression levels observed in the junctional zone (Section 9.2.4). This discrepancy may arise because of sampling issues, given that mRNA results reflect total placental values, while protein expression reflects immunolocalization. No changes were observed in RUPP animals or for *Clic-4.*

# Chapter 9 Molecular Changes: Protein Expression

Immunohistochemistry of fixed placental sections was undertaken in order to obtain localisation and expression data of a small set of molecules of interest; namely the trophoblast marker cytokeratin, the hypoxia inducible transcription factor HIF-1α, the anti angiogenic factor sFlt-1, the inflammation signalling molecules toll-like receptors TLR-3, and TLR-3 and the $H^+/Cl^-$ co transporter CLIC-3.

## 9.1 Localisation of Molecules by Immunostaining and Visualization with DAB

Background staining, using the chromogenic substrate diaminobenzidine (DAB) as visualisation reagent, is shown in Figure 9.1.1. A typical selected area showing labyrinth, junctional zone and decidua is shown. Figure 9.1.2 shows typical staining for cytokeratin. In the labyrinth (Figure 9.1.2) staining is prominently observed in trophoblasts around the edge of the maternal blood space. Identification of giant trophoblast cells in the junctional zone is shown in Figure 9.1.2c and Figure 9.1.2c identifies cytokeratin positive trophoblast that have invaded into the interstitium of the proximal decidua. Figure 9.1.3 shows localisation of TLR-3 and Figure 9.1.4 shows a typical staining pattern for TLR-4. Staining for the both TLR-3 and TLR-4 was found throughout the placenta, but with more prominent staining in trophoblast cells lining the maternal blood space in the labyrinth and in trophoblast cells around the spiral arteries in the decidua. A representative image documenting HIF-1α localisation to the nucleus in cells in all placental regions is shown in Figure 9.1.5. CLIC-3 staining is shown in Figure 9.1.6, localising the protein most predominantly to perinuclear areas in the junctional zone. Staining for sFlt-1 was problematic, with no successful specific staining obtained.

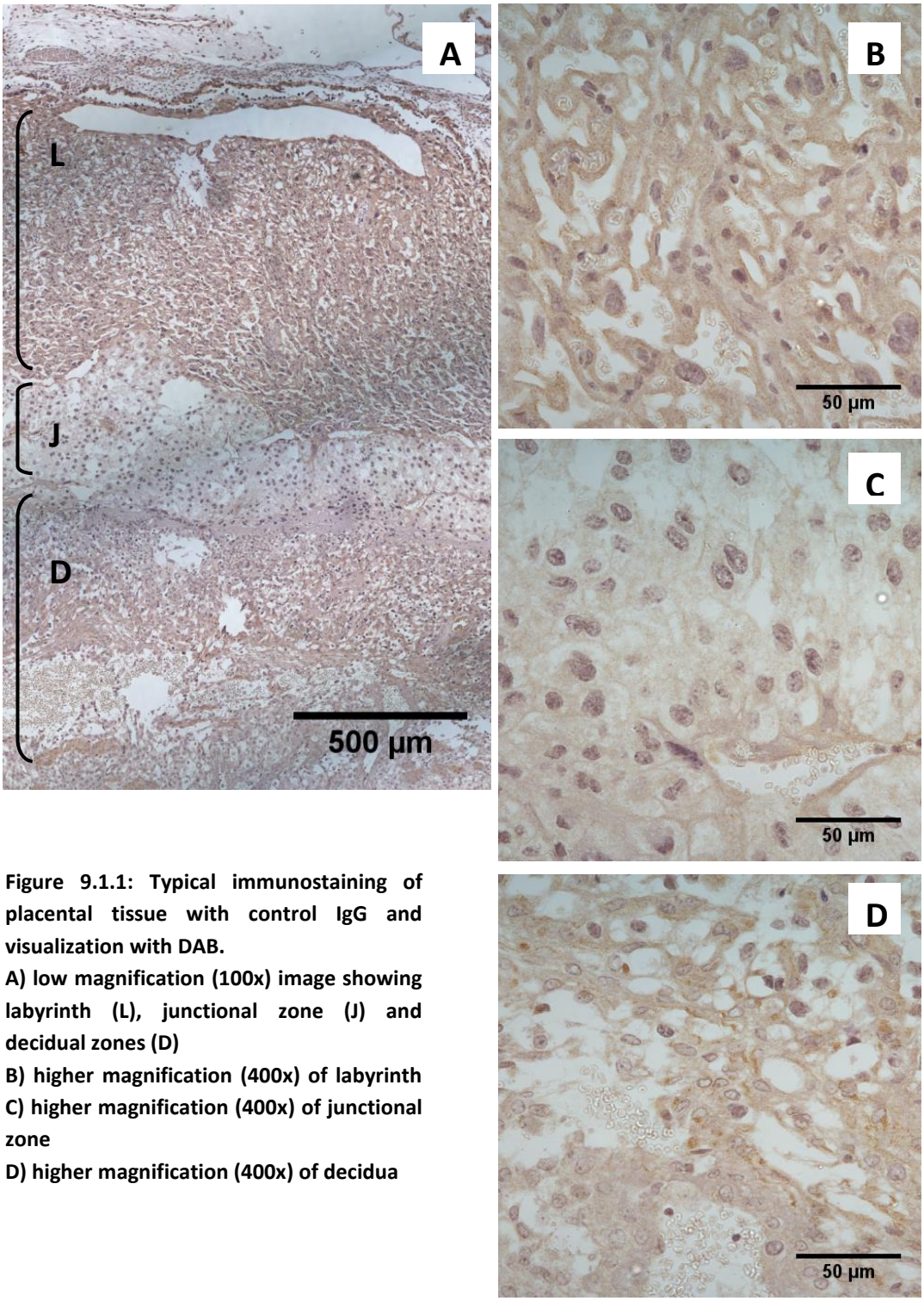


**Figure 9.1.1: Typical immunostaining of placental tissue with control IgG and visualization with DAB.**
**A) low magnification (100x) image showing labyrinth (L), junctional zone (J) and decidual zones (D)**
**B) higher magnification (400x) of labyrinth**
**C) higher magnification (400x) of junctional zone**
**D) higher magnification (400x) of decidua**

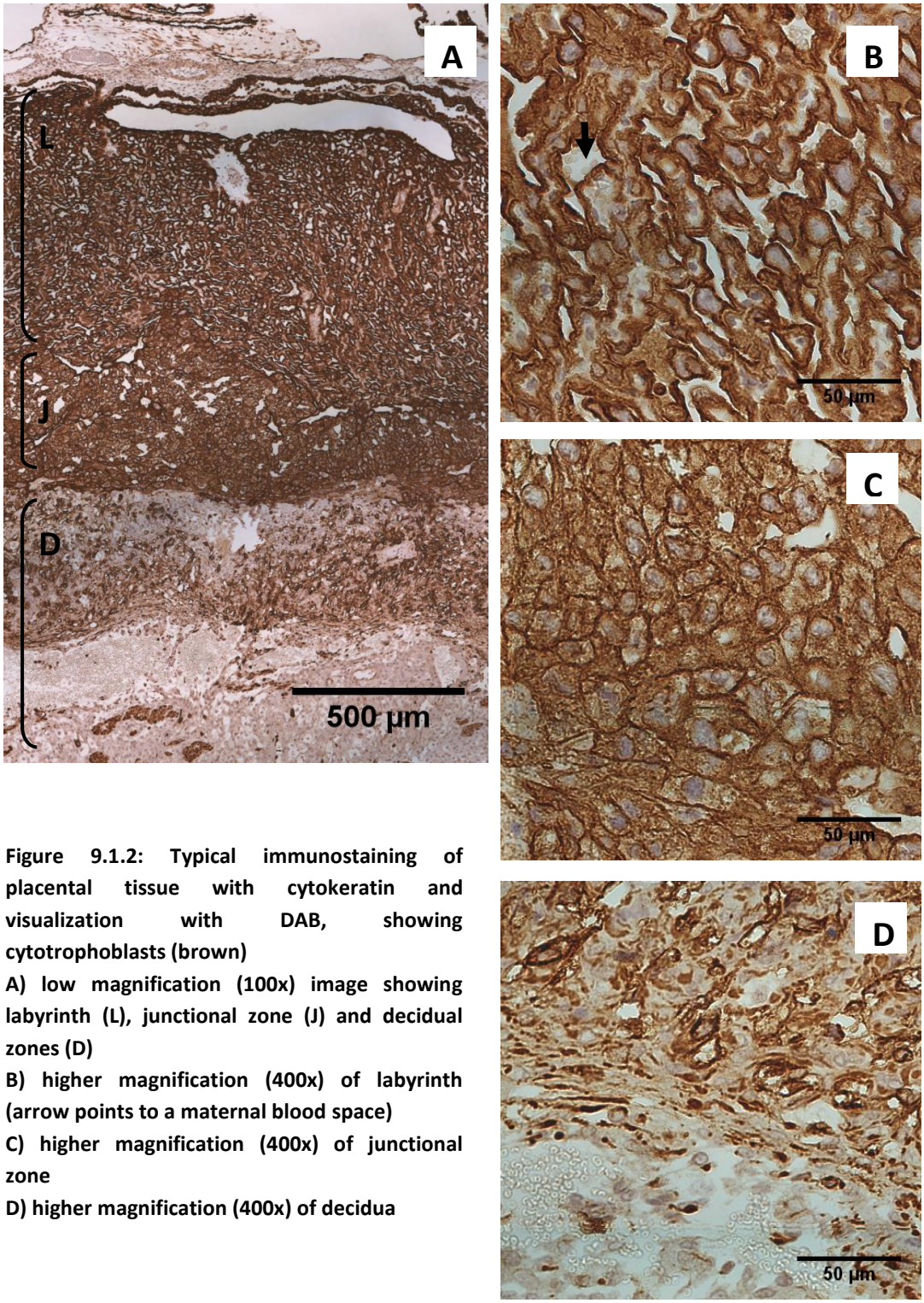


**Figure 9.1.2: Typical immunostaining of placental tissue with cytokeratin and visualization with DAB, showing cytotrophoblasts (brown)**

**A) low magnification (100x) image showing labyrinth (L), junctional zone (J) and decidual zones (D)**

**B) higher magnification (400x) of labyrinth (arrow points to a maternal blood space)**

**C) higher magnification (400x) of junctional zone**

**D) higher magnification (400x) of decidua**

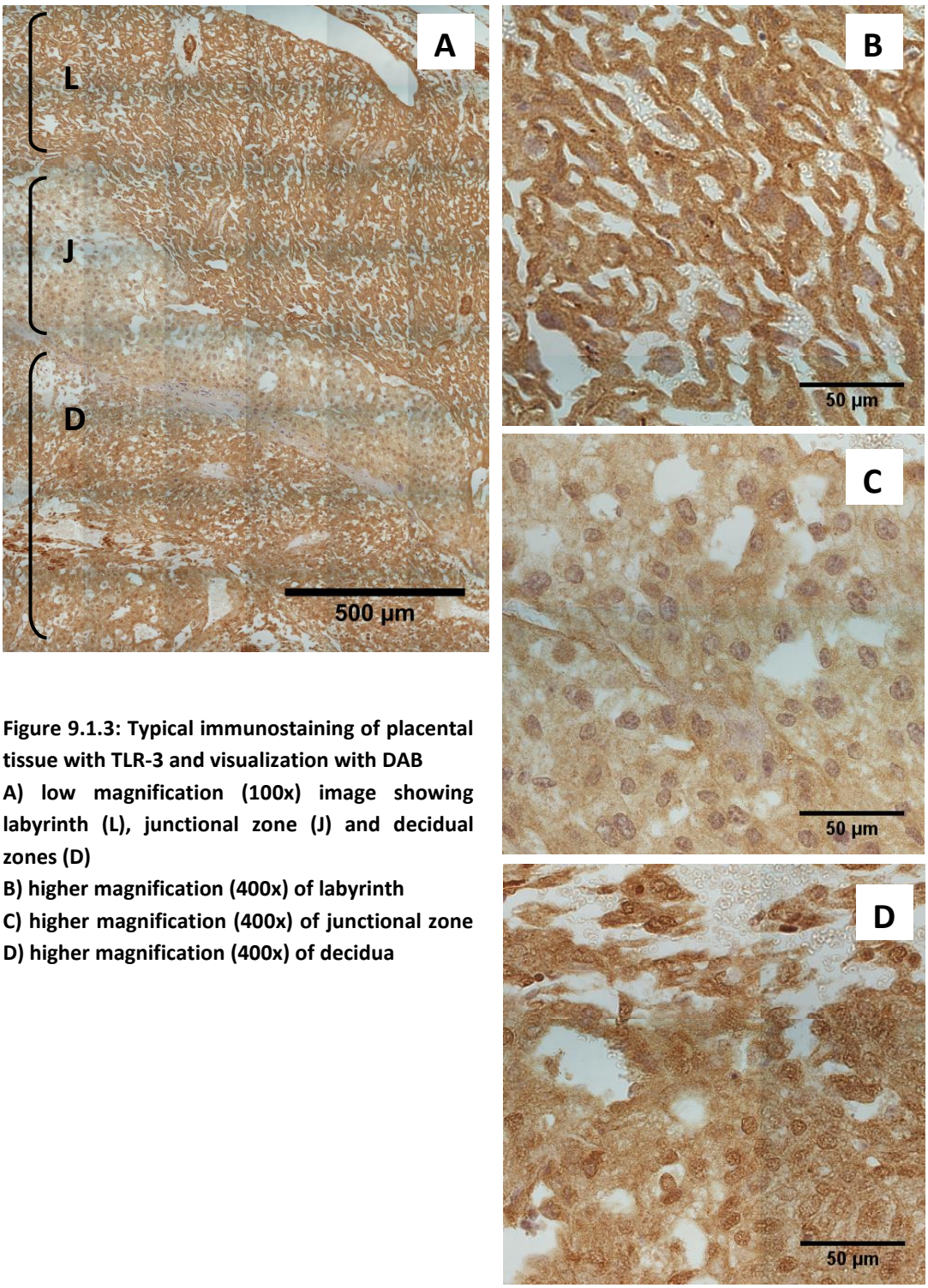


**Figure 9.1.3: Typical immunostaining of placental tissue with TLR-3 and visualization with DAB**
**A) low magnification (100x) image showing labyrinth (L), junctional zone (J) and decidual zones (D)**
**B) higher magnification (400x) of labyrinth**
**C) higher magnification (400x) of junctional zone**
**D) higher magnification (400x) of decidua**

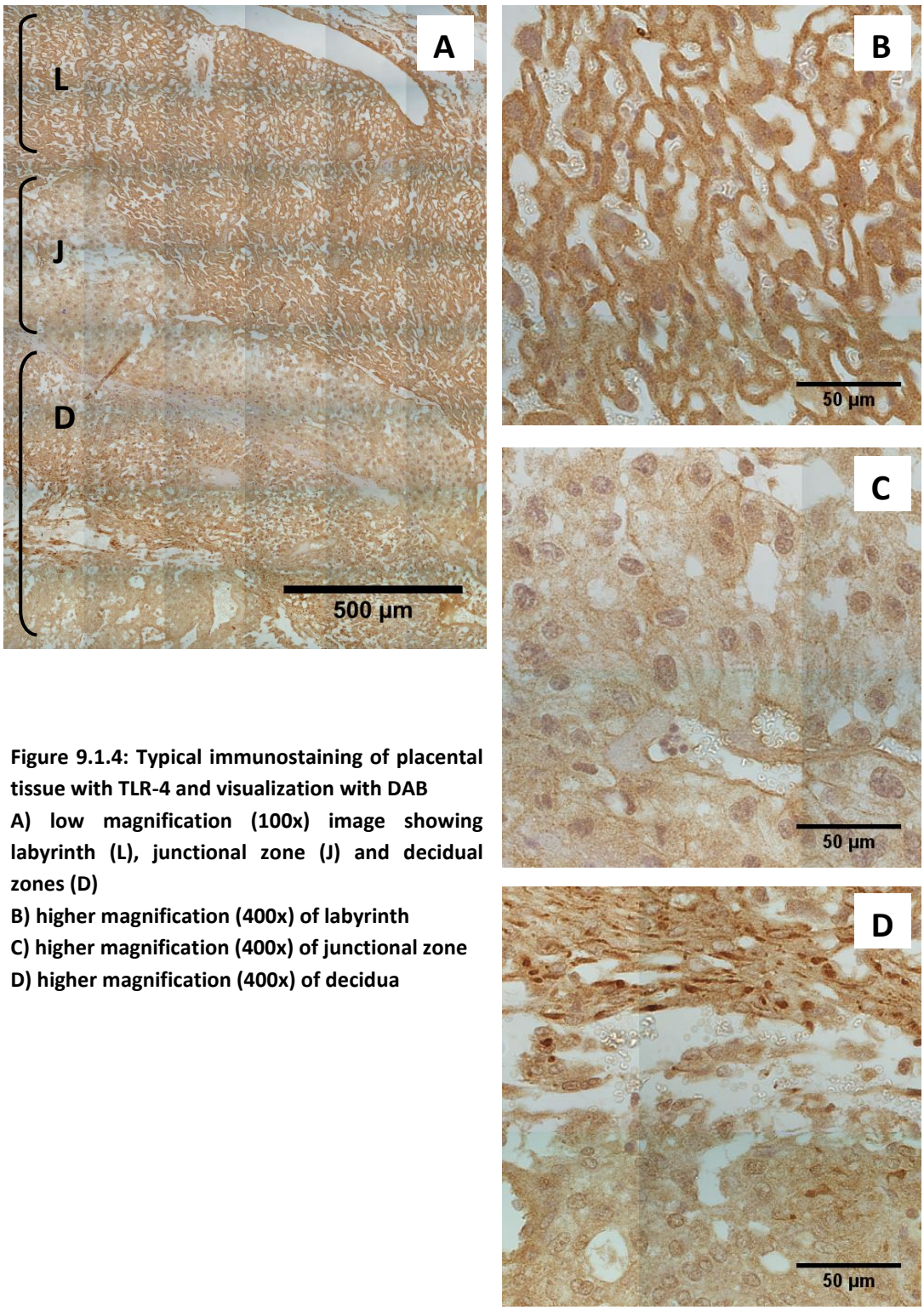


**Figure 9.1.4: Typical immunostaining of placental tissue with TLR-4 and visualization with DAB**
**A) low magnification (100x) image showing labyrinth (L), junctional zone (J) and decidual zones (D)**
**B) higher magnification (400x) of labyrinth**
**C) higher magnification (400x) of junctional zone**
**D) higher magnification (400x) of decidua**

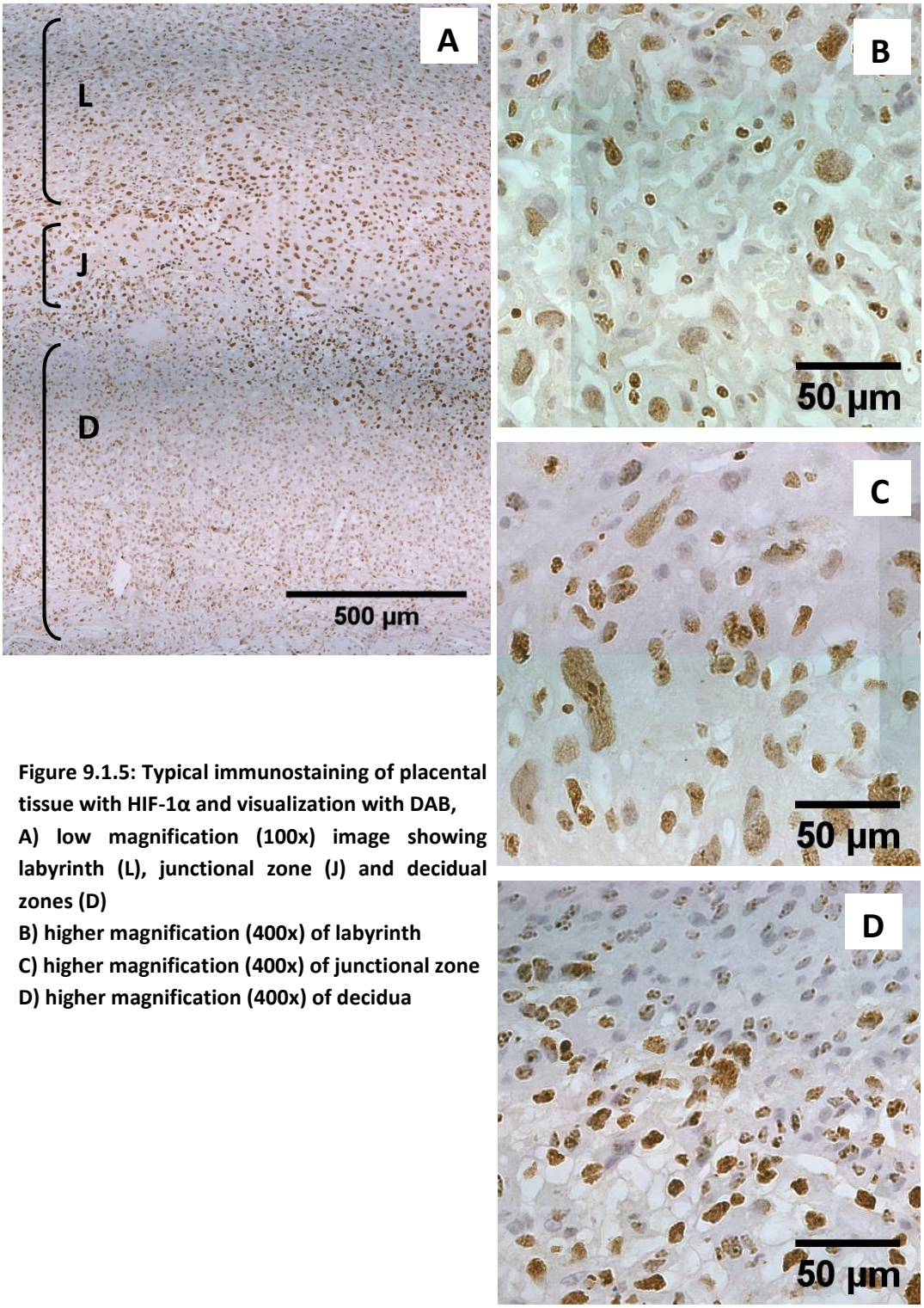


**Figure 9.1.5: Typical immunostaining of placental tissue with HIF-1α and visualization with DAB,**
**A) low magnification (100x) image showing labyrinth (L), junctional zone (J) and decidual zones (D)**
**B) higher magnification (400x) of labyrinth**
**C) higher magnification (400x) of junctional zone**
**D) higher magnification (400x) of decidua**

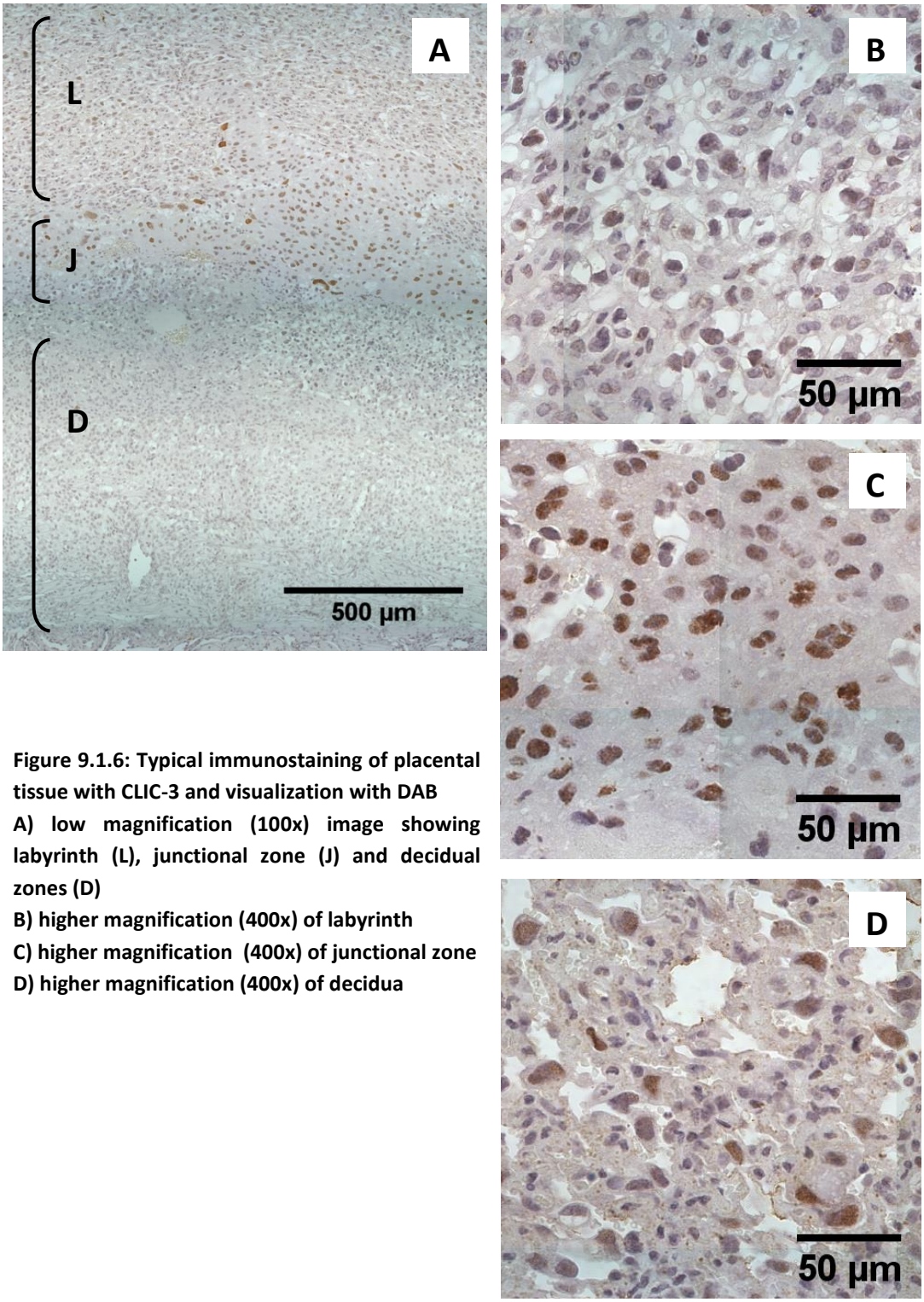


**Figure 9.1.6: Typical immunostaining of placental tissue with CLIC-3 and visualization with DAB**
**A) low magnification (100x) image showing labyrinth (L), junctional zone (J) and decidual zones (D)**
**B) higher magnification (400x) of labyrinth**
**C) higher magnification (400x) of junctional zone**
**D) higher magnification (400x) of decidua**

## 9.2 Quantification by Fluorescent Staining

### 9.2.1 Cytokeratin

There was increased cytokeratin staining in labyrinth of TNF-α and RUPP placentas compared to control placentas (Figure 9.2.1) Cytokeratin is a marker for trophoblast cells, however does not distinguish between sub-types of trophoblast.

### 9.2.2 Toll-like receptors (TLR-3 and TLR-4)

TLR-3 expression was upregulated in the labyrinth of TNF-α treated animals; with a trend for an increase in RUPP animals (Figure 9.2.2). There was also a significant increase in TLR-3 expression in the decidua of RUPP animals with a trend for an increase in TNF-α animals. A trend for an increase in the junctional zone of both TNF-α and RUPP animals was observed. TLR-4 expression was increased in the labyrinth and decidua of TNF-α treated animals as compared to control. No change was seen in RUPP animals (Figure 9.2.3).

### 9.2.3 Hypoxia inducible factor 1α (HIF-1α)

HIF-1α expression was upregulated in all three zones of the placenta in RUPP animals and in the labyrinth of TNF-α treated animals (Figure 9.2.4).

### 9.2.4 Chloride intracellular channel-3 (CLIC-3)

CLIC-3 expression was significantly increased in the junctional zone of TNF-α treated animals, with no change observed in RUPP animals (Figure 9.2.5). No change was observed in the labyrinth or the decidua.

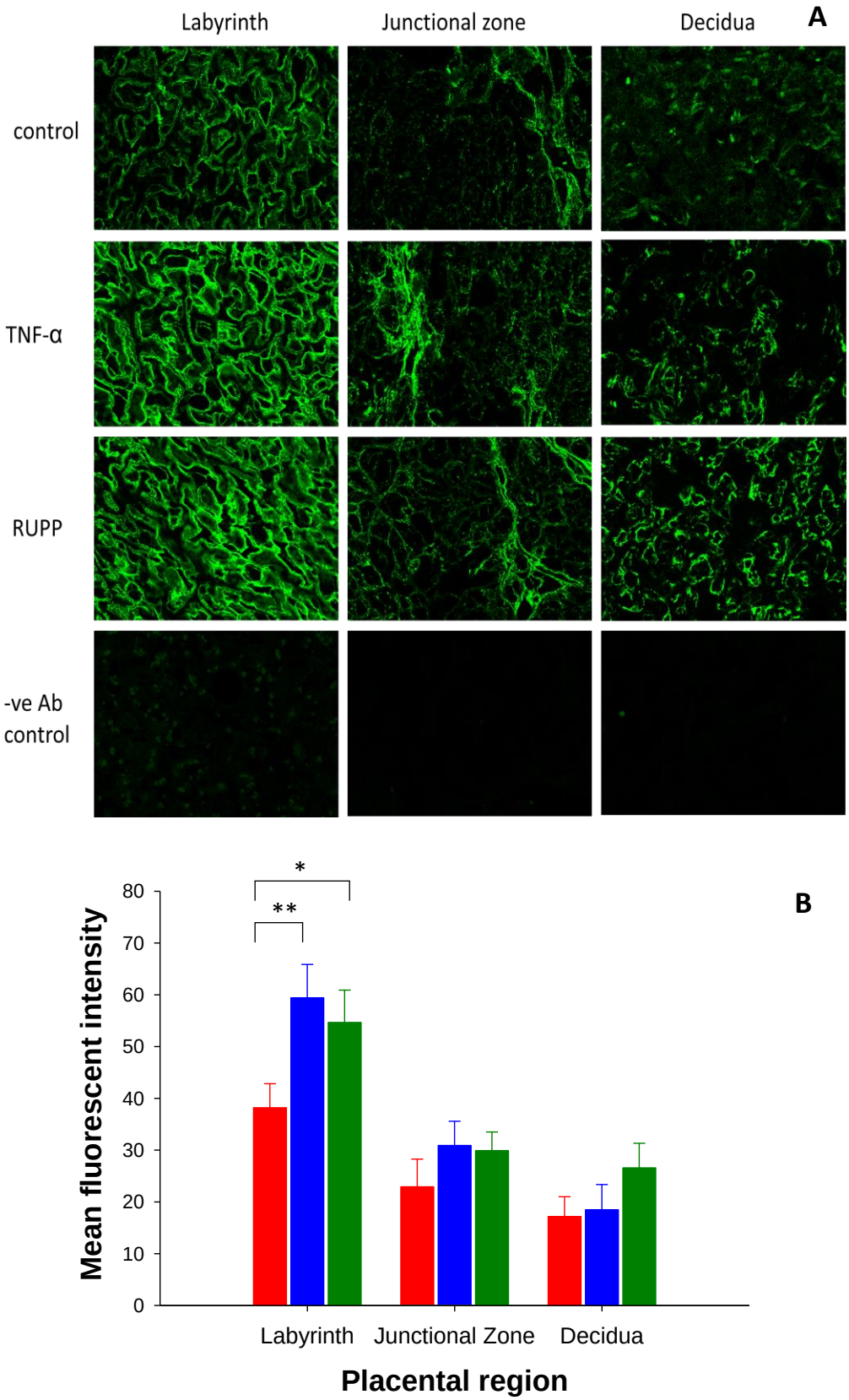


**Figure 9.2.1: Immunofluorescent staining of placental tissue for Cytokeratin. A) Sample images at 400x magnification are shown for treatment groups and placental regions as indicated. B) Mean fluorescent intensity ±SEM in the different placental regions for Control (n=3, red), TNF-α (n=3, blue) and RUPP (n=3, green) treated animals. (* p<0.05, **p<0.01)**

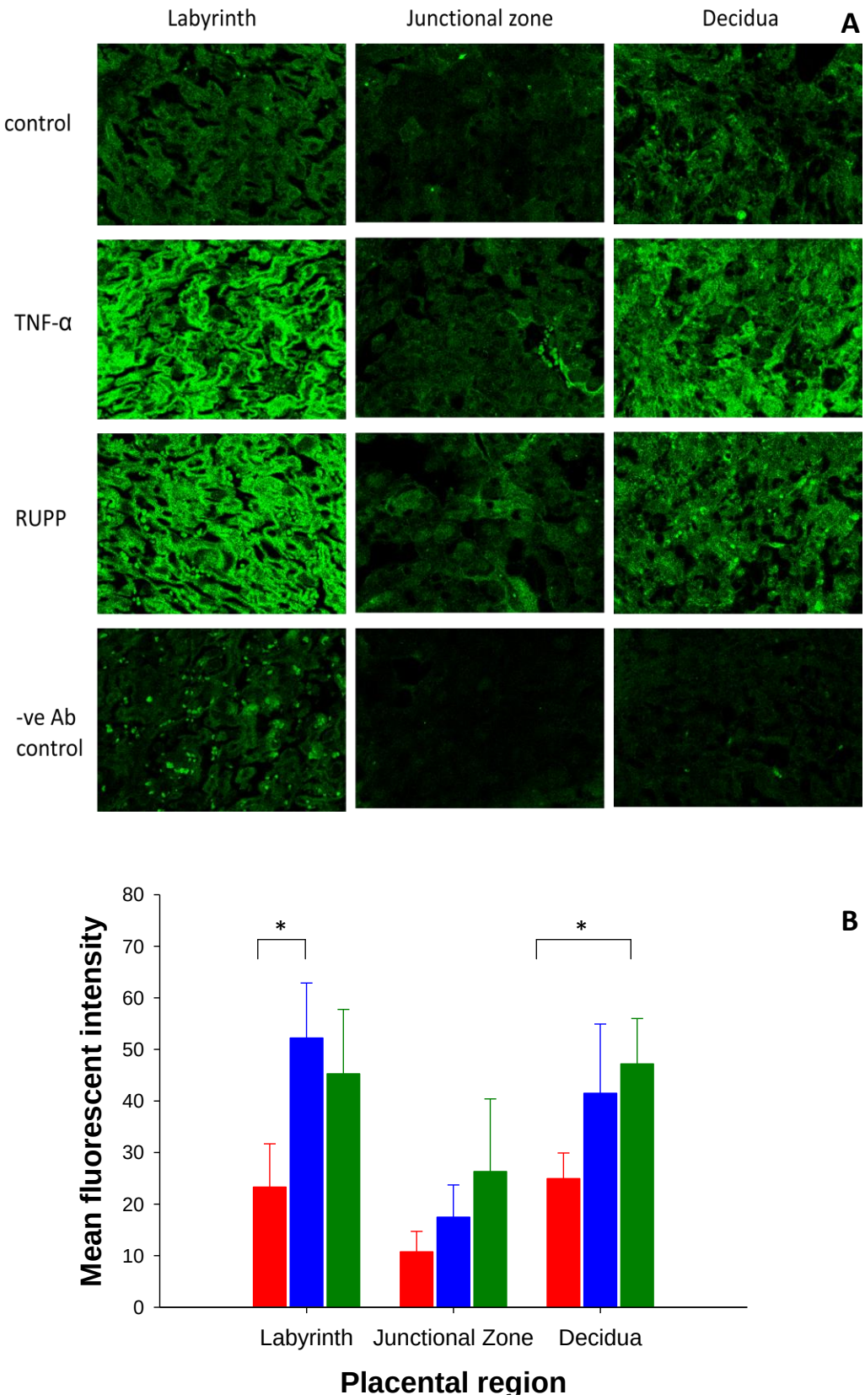


**Figure 9.2.2: Immunofluorescent staining of placental tissue for TLR-3. A) Sample images at 400x magnification are shown for treatment groups and placental regions as indicated. B) Mean fluorescent intensity ±SEM in the different placental regions for Control (n=3, red), TNF-α (n=3, blue) and RUPP (n=3, green) treated animals. (* p<0.05)**

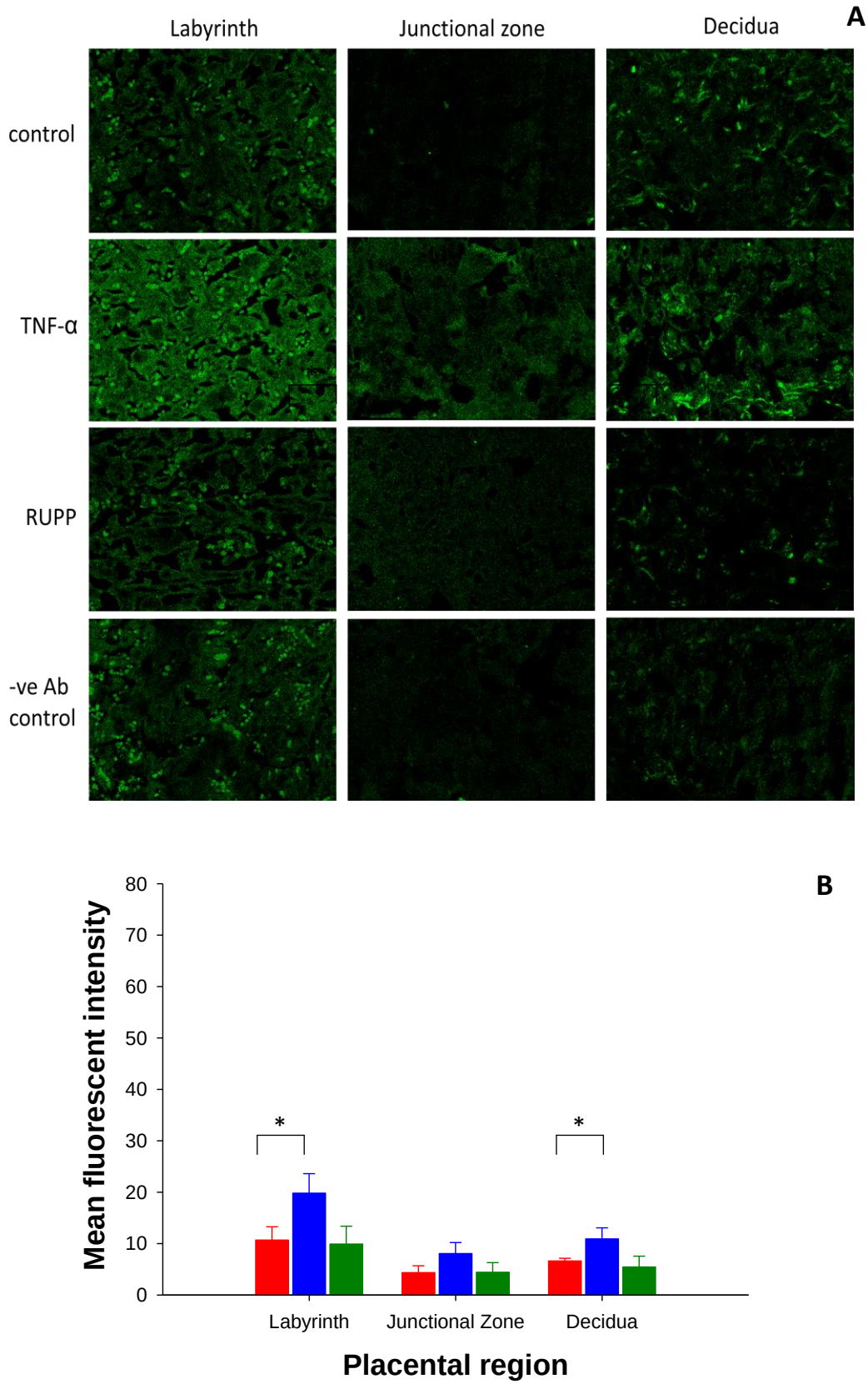


**Figure 9.2.3: Immunofluorescent staining of placental tissue for TLR-4. A) Sample images at 400x magnification are shown for treatment groups and placental regions as indicated. B) Mean fluorescent intensity ±SEM in the different placental regions for Control (n=3, red), TNF-α (n=3, blue) and RUPP (n=3, green) treated animals. (* p<0.05)**

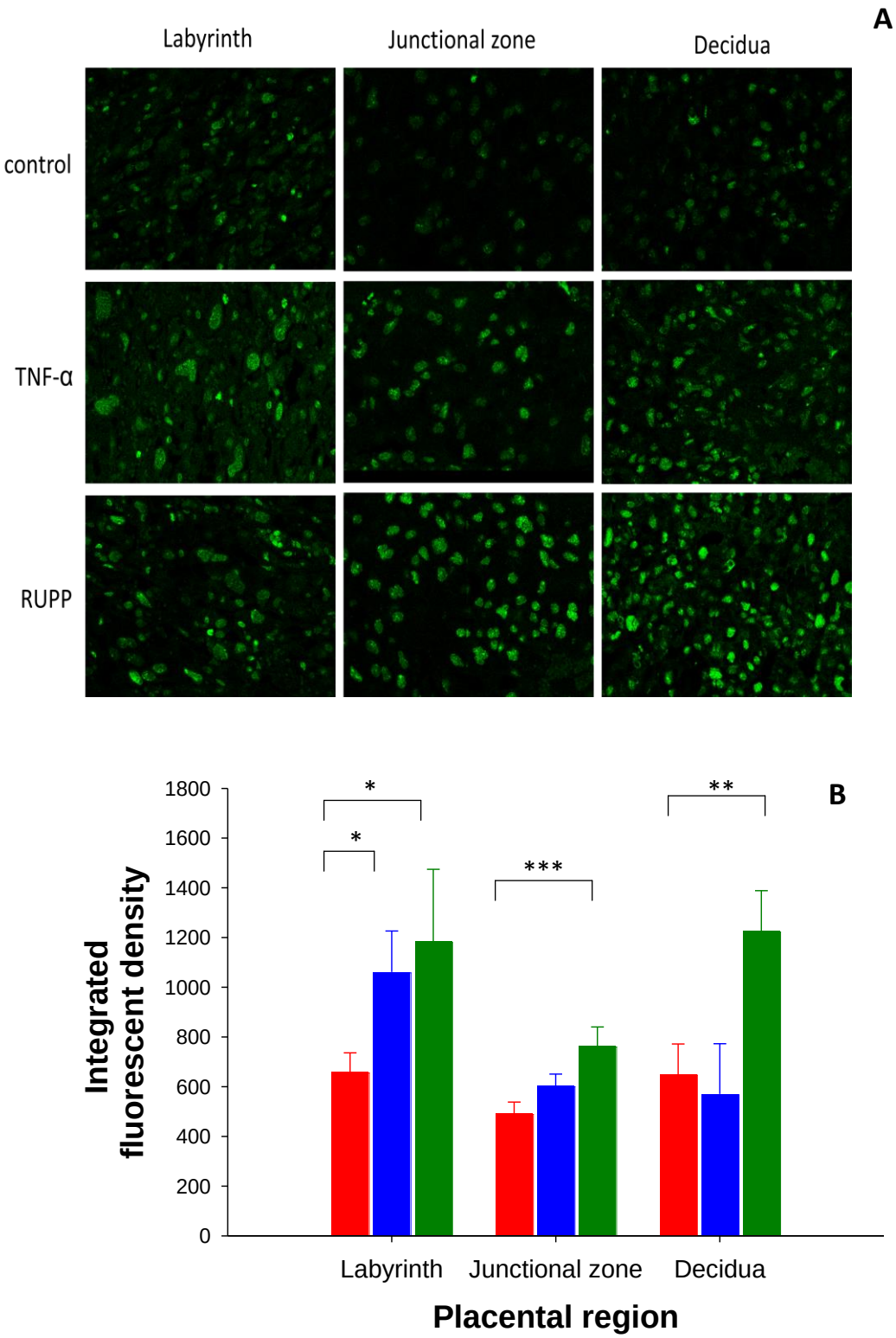


**Figure 9.2.4: Immunofluorescent staining of placental tissue for HIF-1α. A) Sample images at 400x magnification are shown for treatment groups and placental regions as indicated. B) Integrated fluorescent density ±SEM in the different placental regions for Control (n=3, red), TNF-α (n=3, blue) and RUPP (n=3, green) treated animals. (* p<0.05, **p<0.01, **p<0.001)**

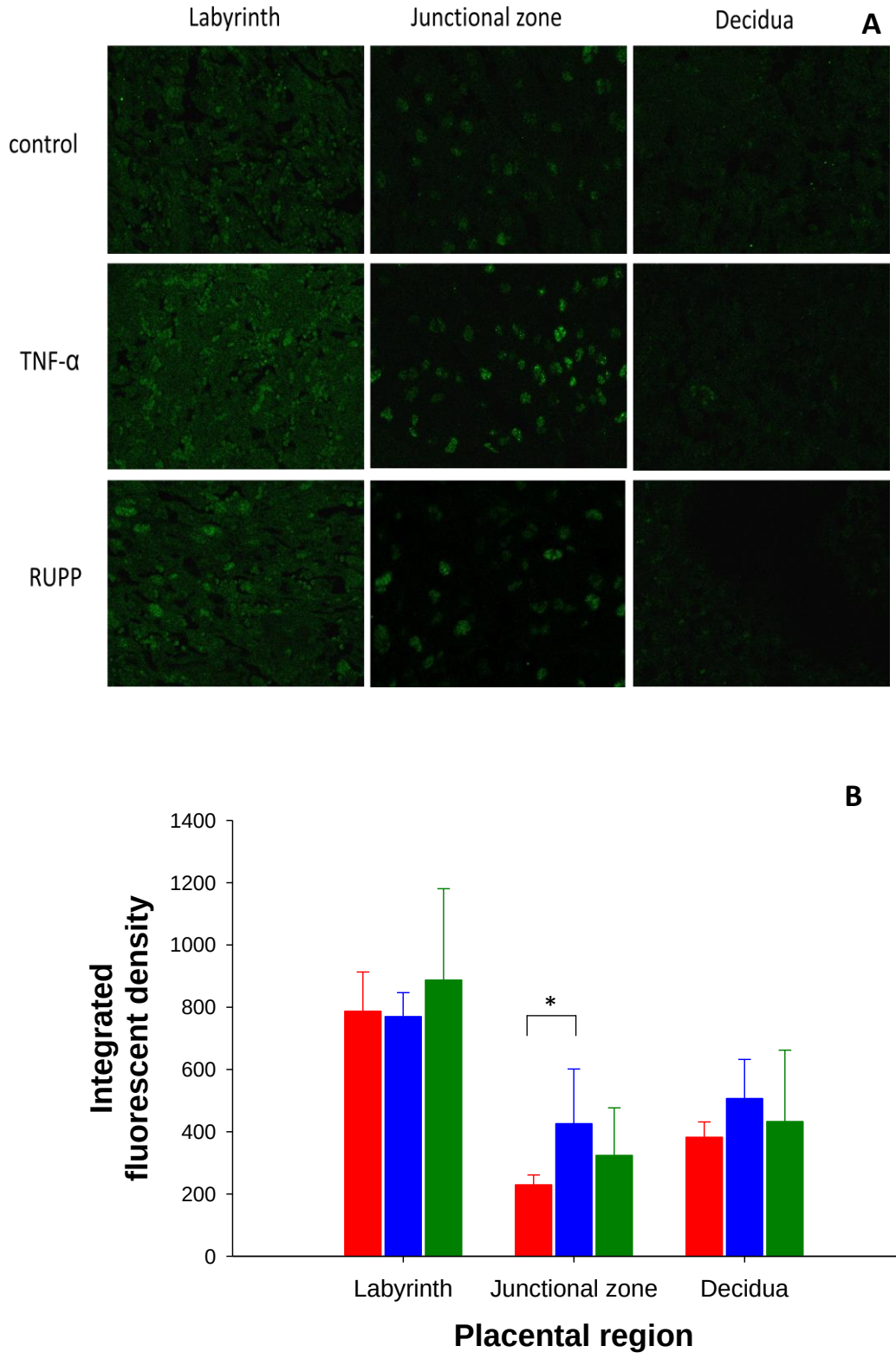


**Figure 9.2.5: Immunofluorescent staining of placental tissue for CLIC-3. A) Sample images at 400x magnification are shown for treatment groups and placental regions as indicated. B) Integrated fluorescent density ±SEM in the different placental regions for Control (n=3, red), TNF-α (n=3, blue) and RUPP (n=3, green) treated animals. (* p<0.05)**

## 9.3 Discussion

***Cytokeratin***

The increased cytokeratin expression in the labyrinth of TNF-α and RUPP placentas compared to control placentas was unexpected. Cytokeratin is a marker for trophoblast cells, however does not distinguish between sub-types. It is possible that there is a modulation of trophoblast differentiation in this experimental model which is reflected by an increase in cytokeratin staining. The use of markers that can distinguish between subtypes (Simmons et al., 2007) would be warranted to further investigate this possibility.

***Toll-like receptors (TLR-3 and TLR-4)***

These results show that infusion of pro-inflammatory cytokines in the TNF-α model leads to upregulation of both TLR-3 and TLR-4 in the placenta, primarily in the trophoblasts of the labyrinth. Additionally, ischaemic stress brought about by reduction of blood flow to the placenta (RUPP) also resulted in increased levels of TLR-3 in the decidua

TLR's may be considered as sentinels for tissue damage (Mollen et al., 2006), activated through molecular indicators of infection or injury and initiating pathways that repair the wound and protect from further damage (Huebener and Schwabe, 2013). Their role in inflammation-induced angiogenesis is being elucidated (Grote et al., 2011) and it has also been suggested that the ability of trophoblast to successfully 'orchestrate' their inflammatory environment and regulate the differentiation and activation of immune cells through TLR is a key to successful pregnancy (Koga et al., 2009).

The placenta holds an immunologically unique position at the interface between mother and 'foreign' foetus and it seems plausible that the inflammatory response and TLR

pathways play a key role in not only implantation, but in the inflammation driven angiogenesis of early development of the placenta. The results presented here, while showing no mechanistic process, support a role for TLR in the development of this experimental model of preeclampsia.

***Hypoxia inducible factor 1α (HIF-1α)***

These results show that HIF-1α protein is upregulated in the placenta of these experimental mice under conditions of restricted blood flow to the placenta (RUPP model) and also by inflammatory insult to the placenta (TNF-α model). In hypoxic conditions HIF-1α is stabilised and protected from ubiquitin-proteasome degradation, therefore increased levels in the RUPP animals may reflect increased stability rather than increased translation or transcription. The upregulation seen in the TNF-α animals may be due to increased protein synthesis via increased translation, as it has been reported that TNF-α increases HIF-1α protein expression via Internal Ribosome Entry Site (IRES) dependent translation (Zhou et al., 2004). IRES dependent translation occurs under conditions where protein translation is usually repressed to conserve cellular energy such as hypoxia, nutrient deprivation, heat shock or apoptosis (Lang et al., 2002, Ozretić et al., 2012). It is increasingly seen as having relevance in inflammation (Rübsamen et al., 2012) and may be an important mechanism of translational control in the hypoxic environment of the developing placenta.

***Chloride intracellular channel-3 (CLIC-3)***

These results demonstrate that there is significant upregulation of CLIC-3 expression in the junctional zone of the placenta in the TNF-α infused animals compared to control animals.

Expression of CLIC-3 was analysed using integrated fluorescent intensity (the mean intensity above the threshold multiplied by the percentage area above the threshold). Analysed in this manner, the integrated fluorescent intensity is higher in the labyrinth than in the junctional zone, however, by visual inspection it is clear that the perinuclear staining in the junctional zone has a higher intensity than in the labyrinth. This incongruity reflects a larger percentage of area with staining rather than a higher mean intensity. Examination of the data (not shown) indicates that while there is no change in mean fluorescent intensity in any zones upon TNF-α or RUPP treatment, the percentage area above the fluorescent threshold increases in the junctional zone of the TNF-α animals. These findings may reflect changes in localisation of the CLIC-3 molecule.

CLIC-3 exists in both a soluble and integral membrane form and may be more active as an ion channel at low pH, with oxidising conditions favouring the transition from soluble, globular form to a membrane bound form (Littler et al., 2010). It is possible that in the junctional zone CLIC-3 is more prominent as the membrane ion channel form and localises to the nuclear membrane, whereas in the labyrinth and decidua the molecule exists diffusely in the cytoplasm as the soluble globular form. Upon changes brought about by the infusion of the inflammatory cytokine TNF-α, CLIC-3 may have increased expression of the soluble form in the junctional zone (increased diffuse staining throughout the region. The unchanged or decreased expression levels of *clic-3* mRNA observed in TNF-α treated animals (Section 8.4) would be consistent with changes in form or localisation of CLIC-3 protein rather than increased protein synthesis.

This study demonstrates that placental changes in CLIC-3 expression in the TNF-α infused animals are localised to the junctional zone which predominantly consists of glycogen trophoblast cells. Further studies to examine changes in localisation would be required to

help ascertain the precise function of CLIC-3 in the placenta and its role in the pH homeostasis associated with the possible acidosis as detected by MRI (Section 6.3).

## 9.4 Summary

These results show that infusion of the pro-inflammatory cytokine TNF-α leads to an upregulation of both TLR-3 and TLR-4 expression in the placenta, primarily in the trophoblasts of the labyrinth. Additionally, an upregulation of TLR-3 was observed in the decidua upon the ischaemic stress in the placenta brought about by the reduction of blood flow to the placenta (RUPP). As there was no upregulation of mRNA (Section 8.3) the increased protein expression is likely to be explained by post-transcriptional regulation of these important signalling molecules in the inflammatory pathway.

This study demonstrates that maternal infusion of the inflammatory cytokine TNF-α upregulates the key placental transcription, HIF-1α, at both the protein and the mRNA level (Section 8.2). In addition these results show that HIF-1 protein expression and mRNA (Section 8.2) is upregulated in the placenta of these experimental mice under conditions of restricted blood flow to the placenta (RUPP).

These results demonstrate that there is upregulation of the chloride intracellular channel protein CLIC-3 expression in the junctional zone of the placenta in the TNF-α infused animals, suggesting that molecular changes in the placenta as a result of the increased inflammatory cytokines are affecting molecules such a CLIC-3 which are involved in pH homeostasis in the tissue.

# Chapter 10 Discussion

## 10.1 Clinical Features of Experimental Preeclampsia

This study investigated the establishment of a TNF-α infusion model of preeclampsia in order to determine whether an imbalance in pro-inflammatory cytokines alters placental metabolism and development in such a way that placental blood flow is affected. A RUPP model of preeclampsia was investigated as a perturbed blood flow control model. While RUPP and TNF-α infusion have previously been used as models for preeclampsia in other animals, this study is the first report of their employment in mice. The results presented in Chapters 4 and 5 demonstrate that infusion of the inflammatory cytokine TNF-α is an experimental model for hypertension in pregnancy. Hypertension was not definitively confirmed for the RUPP model, however as the RUPP model was primarily a control for the MRI analysis of blood flow in the placenta this does not detract appreciably from this study. Both experimental models exhibited proteinuria. Maternal serum sFlt-1 levels were grossly elevated in all pregnant animals tested, however no differences compared to controls were observed in either the RUPP or inflammatory cytokine models of preeclampsia. Other markers of human preeclampsia such as endoglin or AT1-AA were not identified in this work.

The hypertension characteristic of preeclampsia appears to be mediated by endothelial dysfunction, with sFlt-1 considered a key contributing factor (Maynard et al., 2003b). However in the TNF-α experimental model presented here, sFlt-1 does not appear to be the mediating factor. The lack of significant increase of sFlt-1 in the experimental model animals may be a consequence of insufficient time span between intervention at gd 13 and plasma collection at gd 17. Other groups have also reported hypertension in the absence of sFlt-1 increase, with one study observing that only rats undergoing RUPP from gd 14-19,

but not from gd 12-17 demonstrated sFlt-1 increase in parallel with the hypertension (Banek et al., 2012), indicating that timing may be crucial. Alternatively the lack of difference in sFlt-1 in the experimental models presented here may be due to the concept discussed in Chapter 5, that levels of sFlt-1 measured in maternal serum may not necessarily be a true reflection of placental release, and that other factors act to affect levels of sFlt-1 in maternal plasma. Either way maternal serum sFlt-1 is not a reliable marker of disease in mouse models.

In the human disease a number of biomarkers have been identified including sFlt-1/PlGf ratio, soluble endoglin (sEng), pregnancy associated protein (PAPP-A), placental protein 13 (PP13), free foetal haemoglobin (HbF) and alpha-1 microglobin (A1M) (Anderson et al., 2012). More recently, metabolomics which measures metabolites in maternal blood or urine as a final downstream product of gene expression (Kenny et al., 2010, Austdal et al., 2014) or Multiple'omics' which look for a combination of 11 serum markers (Liu et al., 2013) have been considered for their predictive value in early identification of the disease. Angiotensin II type I receptor autoantibodies (AT1-AA) which are found in increased concentrations in patients with hypertensive disorders have also been considered not only as markers but, like sFlt-1 and sEng, as effectors of the maternal hypertensive response (Xia and Kellems, 2013). More recently small non-coding RNAs called microRNAs (miRNAs) have been found to be altered in the circulation of preeclamptic women (Anton et al., 2013, Xu et al., 2014b, Doridot et al., 2014, Betoni et al., 2013). Many of the factors released from the placenta such as sEng, AT1-AA, endothelin, nitric oxide, COMT or 2ME and other metabolic molecules such as uric acid have all been highlighted as having profound effects on the maternal endothelium and blood pressure regulation (LaMarca, 2012) and may be markers of, or contribute to, the experimental hypertension observed in this thesis.

## 10.2 MRI evaluation of blood flow

In this study high field strength (11.74 Tesla) MRI was used to investigate whether structural heterogeneities in the placenta could be discerned by $T_2$ mapping and to determine if blood flow and blood oxygenation was a determinant of any observed differences in $T_2$ relaxation times. Further it was investigated whether $T_2$ mapping was capable of detecting changes in morphology or perfusion in the two mouse models of preeclampsia. The results presented in Chapter 6 have shown that morphological differences related to blood flow can be detected by $T_2$ mapping in the placentas of both the RUPP and TNF-α models. The findings show that the labyrinth has a $T_2$ relaxation time twice that of the junctional zone, with the observed contrast between these regions of the placenta being abolished on loss of blood flow. The abolition of contrast between regions of the placenta upon complete loss of blood flow is consistent with the effects on $T_2$ relaxation times by both increases in deoxyhaemoglobin (hypoxia) and decreases in intracellular pH (acidosis). The fact that an increase in inflammatory cytokine shows a similar $T_2$ pattern to RUPP suggests that metabolic changes in levels of tissue acidity may be a common feature in these two models. Verification of the inferred acidosis would be valuable for understanding the mechanism of these models, as it would implicate intracellular acidosis in the regulation of signalling pathways leading to the downstream effects on the maternal system.

Structural abnormalities in the placenta have been proposed to result in reduced placental perfusion (Redman and Sargent, 2009) or ischaemia-reperfusion injury (Burton et al., 2009), and to lead to placental oxidative stress, cellular damage and inflammation. The subsequent release of anti-angiogenic and other toxic compounds into the maternal circulation has been shown to lead to endothelial dysfunction and the maternal hypertensive response in the preeclamptic pregnancy (Maynard et al., 2008). The signalling

pathways leading to the release of the anti-angiogenic molecules are as yet unclear, but may involve both oxygen dependent elements such as hypoxia inducible factor-1 (HIF-1) (Nevo et al., 2006) or Jumonji domain-containing protein 6 (Jmjd6) (Boeckel et al., 2011), and non-oxygen dependent mechanisms such as toll-like receptor-3 (TLR-3) and NF-κB pathways (Nakada et al., 2009). The MRI data presented in this thesis suggests that pH dependent mechanisms may also play a significant role. Many studies have shown that acidosis and hypoxia have a linked role in some signalling pathways (Kubasiak et al., 2002, Graham et al., 2004, Zheng et al., 2005, Boedtkjer et al., 2011) and the MRI results would be in keeping with these findings.

Recently it has been reported that coupling factor 6 (CF6) activation of ectopic ATP synthase leads to increased sFlt-1 through intracellular acidosis induced c-Src signalling (Sasaki et al., 2004). CF6 is found in the circulation, has higher levels in spontaneously hypertensive rats and its release from the surface of endothelial cells is stimulated by TNF-α (Sasaki et al., 2004). Acidosis has also been reported to affect splicing of VEGF-A isoforms through modulation of splicing proteins (Elias and Dias, 2008) and to upregulate VEGF in brain tumours (Fukumura et al., 2001). These reports suggest that acidosis has an ability to modulate angiogenesis. To maintain homeostasis cells respond to increased intracellular pH by extruding the protons from the cell by way of pH regulating pumps, transporters and exchangers, thereby making the extracellular space acidic. Acidic extracellular pH has been reported to induce matrix metalloproteinase-9 (MMP9) expression in mouse metastatic melanoma cells through phospholipase D-mitogen-activated protein kinase signalling (Kato et al., 2005). MMP9 is known to be involved in trophoblast invasion and tissue remodelling and angiogenesis in the placenta (Plaks et al., 2013). The MRI data presented in this thesis implicating changes in tissue acidity suggests that pH dependent mechanisms may be as equally important as hypoxia in the perturbed placenta.

## 10.3 Placental changes

This thesis investigated the effects of exogenous TNF-α infusion and RUPP in the pregnant mouse on placental morphology and on placental changes in molecular markers of hypoxia, inflammation and pH homeostasis. Results suggest common pathways between the two models and an interdependence of hypoxia, inflammation, and metabolic changes in the physiological development and pathology of the placenta.

### 10.3.1 Structural changes (MRI)

Structural changes in both human and mice placenta have previously been assessed using stereological techniques on 2D histological sections (as reviewed in Section 1.4.1),), though no stereological assessment of placenta from mouse models of preeclampsia have been carried out Histological visualisation of the placenta was performed in this study and is documented in Appendix 3, however no stereological assessment of the histological sections was performed. Instead, the results of a preliminary investigation into the use of high resolution MRI images to assess structural changes, was presented. While an in vivo assessment of putative functional placental tissue volume in IUGR in human foetuses using Diffusion Tensor MRI has recently been reported (Javor et al., 2013), this is the first report of a high resolution in vitro assessment of the placenta in any species.

Using 50 µm voxel resolution scans the complete isolated fixed placenta was imaged and 3D models were reconstructed from the segmented data, enabling quantitative assessment of structural features. The technique has the potential to quantify volume changes of regions of the placenta such as labyrinth, junctional zone, proximal decidua, and maternal vasculature. Preliminary data suggests there may be measurable changes in the junctional zone of experimental model animals, but this remains to be validated with increased numbers.

This innovative technique has the potential to visualize and quantify placental structural change in experimental models of perturbed pregnancies and could prove to be a powerful tool in examining placental morphology.

### 10.3.2 Molecular changes (mRNA and protein expression)

In Chapters 8 and 9 the results of an investigation of changes at the molecular level were presented. Quantitative pCR was employed to examine changes in expression levels of mRNA and immunohistochemistry was employed to localise any protein expression changes to the labyrinth, junctional zones or decidua. Molecules that were targeted were the anti angiogenic molecule sFlt-1 (sVEGFR-1) and its membrane counterpart mFlt-1, and molecules involved in response to hypoxia (HIF-1-α), inflammation (TLR-3 and TLR-4) and pH homeostasis (CLIC-3 and CLIC-4).

***Anti angiogenic molecules***

Neither *sFlt-1* nor *mFlt-1* mRNA was upregulated in either experimental model. Protein expression by immunohistochemistry was unable to be assessed due to lack of suitable antibodies. A tight correlation between expression levels of *sFlt-1* and *mFlt-1* mRNA indicated that there was no differential regulation of expression of the soluble form. There was no relationship between expression levels of placental *sFlt-1* mRNA and concentrations of sFlt-1 found in the maternal serum suggesting that in this model the levels of sFlt-1 found in the maternal serum are not directly related to *de novo* synthesis of placental sFlt-1, but may reflect a more complex pathway of storage and release of the soluble form of the receptor from the placenta and from maternal tissue.

One recent study that examined sFlt-1 release from rat placental explants cultured under normoxia and hypoxia found that both TNF-α and sFlt-1 protein expression was increased

under hypoxic conditions, however upon inhibition of TNF-α with the soluble inhibitor etanercept concentrations of sFlt-1 did not decrease, indicating that TNF-α did not have a direct effect on release of sFlt-1 into the culture media (Murphy et al., 2013). This same study found that administration of TNF-α to pregnant rats increased both mean arterial blood pressure and serum sFlt-1 after 5 days, however inhibiting TNF-α with etanercept decreased sFlt-1 production but did not attenuate the induced hypertension in rats subject to 5 days placental ischaemia (RUPP) (Murphy et al., 2013).

This finding along with the results presented here that demonstrate TNF-α induced hypertension in pregnancy in the absence of any significant serum sFlt-1 increase suggest that the relationship between the inflammatory cytokine TNF-α, the anti-angiogenic molecule sFlt-1 and hypertension is not straightforward. TNF-α is known to inhibit trophoblast-like cells integration into maternal endothelial cellular networks in a process that involves the inhibition of MMP-2 and a failure of the integrin switch from α6β4 to α1β1 (Xu et al., 2011, Xu et al., 2014a). It is more likely that the effects of the inflammatory cytokine work at a more subtle level in the developing placenta, affecting the regulation of trophoblast differentiation, angiogenesis and villi formation, and thus blood flow.

***Hypoxia inducible factor***

The transcription factor hypoxia inducible factor (HIF-1) has emerged as a key molecule in placental development, regulating angiogenesis and trophoblast differentiation (Genbacev et al., 1997). It is also emerging as one of the 'signalling drivers' of toll-like receptor dependent and allergic inflammation (Sumbayev and Nicholas, 2010). HIF-1 activates the transcription of many genes that code for proteins that are involved in angiogenesis, glucose metabolism, cell proliferation/survival and invasion (Semenza, 2003). HIFs are not only involved in the regulation a number of genes in response to chronic or acute low

oxygen environments, but are also activated by non-hypoxic stimuli such as growth factors, the renin-angiotensin system, reactive oxygen species (ROS) and by inflammatory stimuli under normoxic conditions. Recently the Krebs cycle intermediate succinate has been identified as an activator of HIF-1α. Succinate concentrations increase when there is a shift to reliance on the glycolytic rather than tricarboxylic acid (TCA) cycle pathway (McGettrick and O'Neill, 2013). Succinate acts by inhibiting PHD and thus stabilizing HIF-1α in a non-oxygen dependent manner (Tannahill et al., 2013, Palsson-Mcdermott and O'Neill, 2013), thus providing a means of metabolic regulation of this key transcription factor.

The results presented here show that *hif-1α* mRNA expression is upregulated in the placenta of these experimental mice under conditions of restricted blood flow to the placenta (RUPP model) and also by inflammatory insult to the placenta (TNF-α model). Other studies have reported levels of *hif-1α* mRNA in cells to be unchanged (Wenger et al., 1997, Olmos et al., 2007) or only modestly increased (Wiener et al., 1996) following induced hypoxia, while inflammatory stimuli such as TNF-α (Tsapournioti et al., 2013) or TLR-4 activation (Frede et al., 2006) have been demonstrated to upregulate *hif-1α* mRNA. It is possible that the pathway to upregulation of *hif-1α* mRNA in the RUPP model is via oxidative, inflammatory or metabolic stress caused by ischaemia rather than by hypoxia *per se*.

Protein expression of HIF-1α was also upregulated in all three zones of the placenta in the RUPP model. It is unclear whether this involves increased translation or increased stabilisation of the protein. In well oxygenated cells HIF-1α is targeted for ubiquitin-proteasome degradation by the $O_2$ dependent hydroxylation of two proline residue by a family of HIF prolyl hydroxylases (PHDs) (Berra et al., 2006). The results presented here are consistent with an increased stability of HIF-1α due to hypoxia or succinate inhibition of the PHD hydroxylation, however given the increase in *hif-1α* mRNA, upregulation of translation

may also be involved. It is notable that reactive oxygen species (ROS) also regulate PHD activity (Berra et al., 2006), providing another pathway for molecules of oxidative and inflammatory stress to regulate HIF-1α. It has also been proposed that extracellular acidosis may modulate HIF-1α stabilization by protecting HIF-1α from proteasomal degradation (Chiche et al., 2010). Whether acidosis is a contributing factor in the results presented here remains to be confirmed.

The increased HIF-1α expression observed in the labyrinth of TNF-α infused animals may be due to increased protein synthesis via increased translation as it has been reported that TNF-α increases HIF-1α protein expression via Internal Ribosome Entry Site (IRES) dependent translation (Zhou et al., 2004). This mechanism may well be at work to increase protein translation in the RUPP model also. Cells under stress conditions such as hypoxia, nutrient deprivation, heat shock or apoptosis generally repress protein synthesis in an effort to conserve energy (Ozretić et al., 2012). IRES dependent translation enables escape of this physiological control of translation and is increasingly seen as having relevance in inflammation (Rübsamen et al., 2012), but would also be an important mechanism of translational control in the hypoxic and energetically demanding environment of the developing placenta.

***Toll-like receptors***

TLR-3 and 4 are members of the family of Toll-like receptors that are part of the innate immune system, traditionally regarded as activating inflammatory pathways in response to invading pathogens. Increasingly though, TLR's are being considered as sentinels for tissue damage, activated by molecular indicators of infection or injury and initiating pathways that repair the wound and protect from further damage (Mollen et al., 2006, Huebener and Schwabe, 2013). Their role in inflammation induced angiogenesis is being elucidated (Grote

et al., 2011), along with their function in the development of preeclampsia (Chatterjee et al., 2012, Sado et al., 2011, Tinsley et al., 2009, Kim et al., 2005, Koga et al., 2009).

Expression of *tlr-3* and *tlr-4* mRNA showed no significant change in either model, however TLR-3 and TLR-4 protein was upregulated in the labyrinth of TNF-α infused animals. TLR-4 was increased in the decidua of TNF-α infused animals with a trend for increase of TLR-3. TLR-3 was upregulated in the decidua of RUPP animals, and a trend for an increase in the junctional zone was observed in both TNF-α infused and RUPP animals.

The observed differences between the mRNA and protein expression results may be a consequence of the fact that mRNA analyses was on total placenta, but protein expression looked at regional changes. Alternatively these results suggest that post transcriptional regulation of TLR-3 and TLR-4 expression is a predominant feature in this experimental model. Regulation of protein translation, among other post-translational checkpoints, has been considered as important in modulating the strength and duration of the inflammatory response and for turning the system off in a timely and efficient manner (Carpenter et al., 2014). Notable is the pH-dependent phosphorylation of elongation factor 2 that regulates protein synthesis at the elongation stage (Dorovkov et al., 2002). It is both conceivable and consistent with the results presented here that metabolic changes due to ischaemia (RUPP model) or inflammatory insult (TNF-α model) have resulted in an acidosis driven upregulation of the signalling molecules TLR-3 and TLR-4.

TLR-4 protein expression has been shown to be increased in the interstitial trophoblasts of patients with preeclampsia (Kim, 2005) and TLR-3 has been shown to upregulate sFlt-1 in trophoblast cells (Nakada et al., 2009). TLR-3 activation during pregnancy causes pre-eclampsia-like signs in rats (Tinsley et al., 2009) and activation of TLR-3 by double-stranded RNA (dsRNA) and TLR7 and 8 by single stranded RNA (ssRNA), either of viral or damaged

cell origin, has been shown to contribute to preeclampsia in both humans and in a mice model (Chatterjee et al., 2012).

TLR-4 deficient mice are resistant to chronic hypoxia-induced pulmonary hypertension (Young et al., 2010) and inhibition of TLR-4 activity has been shown to decrease hypertension in spontaneously hypertensive rats (Bomfim et al., 2012). Recently it has been proposed that TLRs have a role in programming of vascular dysfunction in preeclampsia (Thompson and Webb, 2013). They propose that danger signals mobilized by the placenta or foetal tissues during complicated pregnancy activate the foetal innate immune system through TLRs and thereby potentiate the generation of ROS (reactive oxygen species) and orchestrate foetal adaptive responses, including changes in gene expression, which later translate to vascular dysfunction.

The role of TLRs in oxidative stress driven inflammation (Gill, 2010) and ischaemia-reperfusion injury (Arumagam, 2009) clearly shows their role in responding to cellular danger and it has been suggested that the ability of trophoblast to successfully orchestrate their inflammatory environment and regulate immune cells differentiation and activation through TLR is a key to successful pregnancy (Koga et al., 2009). Cellular injury and 'stress' result in the unmasking or release of damage associated molecular patterns (DAMPs) such as nucleic acids, extracellular matrix fragments, cytoskeleton components, small molecules like ATP and uric acid, as well as large proteins such as heat shock proteins (HSPs), S100 proteins or high mobility group box protein 1 (HMGB1) (Huebner, 2011). These DAMPS activate TLRs to induce pathways to restore tissue integrity (Grote et al., 2011, Huebener and Schwabe, 2013). The developing placenta is under hypoxic stress, apoptotic stress, remodelling stress, immunological stress and as such would release DAMPs that could potentially activate TLRs as a normal part of the development process, especially with respect to the vasculogenesis/angiogenesis of this highly vascularised tissue. This process

would need to be highly tuned and regulated in the changing cellular environment of development, and if unbalanced for any reason, for example sustained infection or temporally inappropriate sets of endogenous ligands, maladaptive regulation of TLRs, inflammatory cytokines or angiogenic molecules may eventuate resulting in an abnormal or pathological placentation.

***Chloride intracellular channels***

This thesis also examined the expression of one group of molecules that may potentially have a role in pH homeostasis in the placenta and in any acidosis driven responses in the perturbed placenta. CLIC-3 and CLIC-4 are chloride intracellular channel proteins that function as $H^+/Cl^-$ co transporters, but may also function as enzymes or redox proteins (Littler et al., 2010, Stauber and Jentsch, 2013). CLIC-3 interacts with extracellular signal-regulated kinase (ERK7), (Qian et al., 1999) and since ERK7 is known to inhibit DNA synthesis, it may be possible that CLIC-3 is involved in transcription regulation either via directly interacting with ERK7 or by conducting ions and regulating osmolarity and intracellular pH in the cells (Singh, 2010). The placenta has much higher levels of expression of CLIC-3 relative to other tissues (Qian et al., 1999) and recently increased levels of CLIC-3 mRNA and protein have been found in placentas from pregnancies affected by preeclampsia (Murthi et al., 2012).

The results presented here show that expression levels of CLIC-3 mRNA were significantly decreased in TNF-α treated animals compared to saline control animals and there was a trend for expression levels to be lower in RUPP animals compared to sham operated animals. However protein expression was upregulated in the junctional zone of the TNF-α animals. The discrepancy between the mRNA and protein expression results is due perhaps to changes in localisation of CLIC-3. The mRNA expression levels are an average from the

whole placenta, while the protein expression examines immunolocalisation. CLIC-3 exists in both a soluble and integral membrane form and it is possible that in the junctional zone CLIC-3 is more prominent as the membrane ion channel form and localises to the nuclear membrane, whereas in the labyrinth and decidua the molecule exists diffusely in the cytoplasm as the soluble globular form. CLIC-3 may be more active as an ion channel at low pH, with oxidising conditions favouring the transition from soluble, globular form to a membrane bound form (Littler et al., 2010). It is plausible, and consistent with the results, that in the experimental animals, an acidosis in the junctional zone drives CLIC-3 into the membrane ion channel form, concentrating the molecule on the nuclear membrane. This would explain why in the DAB stained sections, little CLIC-3 was found in the labyrinth or decidua, yet using the more sensitive fluorescent staining, protein was detected in the labyrinth and decidua, with the integrated fluorescent intensity (mean above threshold/area) higher in the labyrinth than the junctional zone, while visually the intensity is higher in the junctional zone.

This study demonstrates that alterations in expression and localisation of the $H^+/Cl^-$ co transporter CLIC-3 are found in the placenta upon inflammatory cytokine (TNF-α) infusion, consistent with the metabolic change observed by MRI. Whether CLIC-3 has been upregulated in response to the conjectured acidosis in order to deal with an increase in $H^+$ ions within the cell, or whether it has a signalling function in association with ERK7 remain to be determined. More recently CLIC-3 has been shown to be involved in integrin recycling, invasion and activation of Src signalling in tumour cells (Dozynkiewicz et al., 2012). Given the very high level of CLIC 3 expression in placenta as compared to other tissues it is possible that CLIC-3 has a role in invasion of trophoblast cells in the remodelling involved in the developing placenta.

### 10.3.3 Links between TLR, HIF-1α and metabolic changes in preeclampsia

Recently there has been growing interest in the interplay between immunity, inflammation, and metabolic changes. Research is being directed towards the role of innate immunity in the sensing of metabolic imbalance, as would occur in infection and tissue injury, and in the role of pattern recognition receptors such as TLRs and NOD-like receptors in the restoration of homeostasis following such insults (Tannahill and O'Neill, 2011, McGettrick and O'Neill, 2013). This interplay may be of prime importance in the environment of the developing placenta. Others have discussed the interdependence of hypoxic and innate immune responses (Nizet and Johnson, 2009) and deliberated on the interplay of hypoxia and a dysfunctional immune system as key contributors to the aetiology and mechanisms of preeclampsia (Sharma et al., 2010). The results presented in this thesis indicate that acidosis may also be implicated in the pathophysiology of preeclampsia, supporting an interdependence of hypoxia, inflammation, and metabolic changes in physiological development and pathology of the placenta.

The transcription factor HIF-1α is a key molecule in this link between metabolic changes and inflammation, and has emerged as a significant molecule in placental development, regulating angiogenesis and trophoblast differentiation. HIF-α activation results in upregulation of glycolytic enzymes in response to cellular energy requirements when oxygen is low. A shift in metabolism towards glycolysis leads to a rise in succinate along with a decrease in intracellular pH (Palsson-Mcdermott and O'Neill, 2013). Succinate has recently been identified as an activator of HIF-1α. Succinate acts by inhibiting prolyl hydroxylase (PHD) and thus stabilizing HIF-1α in a non-oxygen dependent manner (Tannahill et al., 2013, Palsson-Mcdermott and O'Neill, 2013).

TLRs, as highly conserved molecules sensing the environment, directing angiogenesis and responding to danger at the same time, would also seem to be a prime component of embryonic development. TLR-4 activation by LPS also increases glycolysis and alters the TCA cycle whereby there is an increase in succinate (McGettrick and O'Neill, 2013, O'Neill, 2014) possibly being the mechanism responsible for the upregulation of HIF-1α in response to stimulation of TLR-4 (Frede et al., 2006). Recently LPS induced succinate has been demonstrated to have a signalling role that induces IL-1β through HIF-1α (Tannahill et al., 2013).

Succinate may be a key signalling molecule providing cross talk between the energy demanding requirements of a placenta developing in a low oxygen environment and the immunological demands of a foetus invading and establishing within maternal tissue. Succinate links TLR-4's function in 'sensing the environment' with HIF-1's transcriptional activity, thus providing a pathway important in maintaining homeostasis in the dynamic environment of placental development.

In placental development the environment is constantly changing, not least with respect to the oxygen concentration in the tissue. During the first trimester there is a steep gradient in the oxygen concentration from the decidua to the placenta and the oxygen tension determines whether cytotrophoblasts proliferate or invade, thereby regulating placental growth and cellular architecture (Genbacev et al., 1997). During development concentrations of oxygen and other metabolic components, such as succinate, will alter, especially when maternal arterial blood starts to reach the intervillous space at the end of the first trimester. Hypoxia and the HIF-1α signalling pathway could be considered the driving forces behind the angiogenesis that is essential to the function of this organ, with normal development of the placenta probably dependent on temporal changes in oxygen

levels and on the temporal regulation of the HIF-1α -signalling pathways. HIF-1α signalling activity is regulated by metabolites (oxygen and succinate) and by inflammation. Additional regulation of HIF-1α activity by the oxygen dependent factor inhibiting HIF-1 (FIH) allows for different sets of HIF activated genes to be expressed in response to varying oxygen concentrations (Dayan et al., 2009). Normal development would be highly dependent on temporal changes in gene activation dependent on fine control of the HIF-1α signalling pathway. Premature oxygenation or prolonged hypoxia, sustained high levels of succinate, maladaptive activation of TLR (perhaps due to sustained infection or autoimmune inflammation) would all have repercussions on the sets of genes activated and the structural and functional development of the placenta.

A recent study of gene activation in mesothelioma cells has shown that different signal proteins were activated under acidic conditions compared with those at pH 7.4, suggesting that when pH homeostasis is disrupted different signalling pathways may be activated (Fukamachi et al., 2013). Tumours, inflammation loci, and infarction areas, are known to be acidified, as a result of increased reliance on glycolysis for energy production under conditions when there is insufficient vascularisation and hence oxygen, or when energy demands are high due to cellular stress (Palsson-Mcdermott and O'Neill, 2013). Inflammation involves cellular stress due to the induction of the catalytic activity of dozens of kinases and molecular oxygen consuming enzymes and is associated with decreased local oxygen availability (Sumbayev and Nicholas, 2010). Both these situations, insufficient vascularisation and cellular stress are found in the developing placenta and the regulation of signal transduction, gene expression, and cellular functions under acidic conditions may have relevance to the pathogenesis of the preeclamptic placentas.

## 10.4 Future directions

A number of issues remain to be clarified in the animal models presented here including definitive confirmation of hypertension in the RUPP model by telemetry, confirmation of intracellular acidosis by $^{31}P$ magnetic resonance spectroscopy or other means, and validation of the stereological changes observed by MRI and 3D modelling using increased numbers of animals. Additionally an examination of timing in the experimental models is warranted with respect to clarifying the apparent lack of involvement of sFLT-1 in mediating the observed hypertension.

Endothelial dysfunction of the maternal vasculature mediated by factors released by the placenta appears to be cause of the hypertension characteristic of preeclampsia (LaMarca, 2012). In the experimental models presented here the prominent mediating factor does not, contrary to expectation, appear to be sFlt-1, and identification of other factors including $AT_1$-AA, miRNAs and other metabolic elements such as succinate would be merited.

Succinate increases in cells shifting from oxidative phosphorylation towards glycolysis when oxygen levels are low. This shift is accompanied by an increase in $H^+$ ions leading to a decrease in intracellular pH (Palsson-Mcdermott and O'Neill, 2013). Intravenous administration of succinate causes hypertension in mice (He et al., 2004) and humans (Zuckerbrod and Graef, 1950) and circulating succinate has been found to be elevated in rodent models of hypertension and metabolic disease (Sadagopan et al., 2007). Succinate has also been found to be a ligand for GPR91, a G protein coupled receptor, and signalling through this receptor results in hypertension via the renin-angiotensin system (Pluznick, 2013). Succinate is rapidly released to the extracellular compartment after tissue injury and unprogrammed cell death (Rubic et al., 2008) and to be increased during ischaemic hypoxia

(Pluznick, 2013). It has been shown to act as an 'alarmin' that activates dendritic cells and works in synergy with TLR ligand to induce the production of inflammatory cytokines (Rubic et al., 2008). Given this association between succinate, hypoxia, acidosis, TLR and hypertension, an examination of whether serum levels of succinate are altered in the experimental models of hypertension in pregnancy presented in this thesis and elsewhere would be warranted.

Small non-coding RNAs (miRNAs) that play a critical role in post-transcriptional gene regulation and may potentially contribute to inter-cellular signalling are found stabilized in the circulation within exosomes, microparticles, apoptotic bodies or in lipoprotein complexes (Zampetaki et al., 2012). Variations in circulating levels have been associated with a variety of clinical conditions, including cardiovascular diseases (van Empel et al., 2012) and recently the question has arisen of whether they are not only diagnostic of cardiovascular disease but whether they mediate the adverse effects of the disease (van Empel et al., 2012). Given that a subset of miRNAs are regulated by hypoxia and that placental hypoxia is associated with preeclampsia the possibility has been recently put forward that miRNAs may play a role in the pathogenesis of preeclampsia (Li et al., 2014). A variation in miRNA expression accompanies placental changes in preeclampsia (Anton et al., 2013, Xu et al., 2014b, Doridot et al., 2014, Betoni et al., 2013) and whether this is a cause of the changes or a response to changes, or both remains undetermined. Either way the effect would be an alteration in the transcriptome and proteome of target cells. Placental microparticles and exosomes that may be released as part of the placental oxidative and inflammatory stress response have been implicated in preeclampsia (Redman and Sargent, 2008, Redman and Sargent, 2009), with a hypothesis that these microvesicles are active in the maternal circulation providing either immunoregulatory (normal pregnancy) or pro-inflammatory, anti-angiogenic (preeclampsia) signals (Redman et al.,

2012). It is conceivable that miRNAs within released microvesicles, if truly active in an inter-cell signalling sense, may play a significant regulatory role on the translational activity of an array of proteins within the endothelium of the maternal cardiovascular system and the kidney and in this manner lead to the endothelial dysfunction and hypertension that is characteristic of preeclampsia. It is possible that what may be an adaptive response in the placenta becomes a pathological response when the miRNAs enter the maternal circulation. Future work could involve determining whether miRNAs are altered in the maternal serum of the TNF-α model animals and whether they may be the mediator of the observed hypertension.

Angiotensin II type-1 receptor autoantibodies ($AT_1$-AA), produced by women with preeclampsia (Wallukat et al., 1999) and increasingly being associated with hypertensive disorders (Xia and Kellems, 2013), may be a molecule relevant in this model. Both TNF-α induced hypertension and RUPP induced hypertension have been associated with the increased production of $AT_1$-AA (LaMarca et al., 2008b) and injection of $AT_1$-AA in pregnant mice leads to an increase in circulating TNF-α (Irani et al., 2010) pointing to a positive feedback cycle. Administration of TNF-α neutralizing antibodies results in a decrease of the preeclampsia like features seen in the $AT_1$-AA injected pregnant mice (Irani et al., 2010). Whether the circulating $AT_1$-AA disturb the circulatory renin-angiotensin system (RAS) effecting the maternal endothelial dysfunction leading to the hypertensive response or whether they play a role in the placental RAS system and the pathogenesis of placental changes in preeclampsia, has recently been reflected upon (Seki, 2014). Given the association of $AT_1$-AA with TNF-α, it would be informative to investigate their presence in the experimental models presented here.

The source of the $AT_1$ autoantibodies is still unclear, however it has been proposed that autophagy-related processing of self-proteins may provide a source of immunostimulatory molecules and autoantigens by delivering both foreign and self-derived proteins to autolysosomes where they can be processed and presented to TLRs or loaded onto the major histocompatibility complex and presented as autoantigens (Anders and Schlondorff, 2010). Autophagy as a response by nutritionally deprived or stressed cells appears to be a mechanism to maintain homeostasis and recover from stress (Hoyer-Hansen and Jaattela, 2007, Benbrook and Long, 2012) and its involvement in extravillous trophoblast (EVT) invasion and vascular remodelling under physiological conditions of low oxygen has recently been described (Nakashima et al., 2013). The role of autophagy in the placenta, its links with placental oxidative and endoplasmic reticulum stress and its possible role in modulating the inflammatory response and in the generation of new DAMPS stimulating TLR or other immunostimulatory molecules such as $AT_1$-AA in preeclampsia is another area ripe for investigation.

# Chapter 11 Conclusion

This thesis has demonstrated that an imbalance in the inflammatory cytokine, TNF-α, results in hypertension and proteinuria in an experimental mouse model of preeclampsia. The anti-angiogenic molecule sFlt-1 was shown to be an unreliable marker for disease in this model, suggesting that there may be other mediators of the observed hypertension in these experimental animals.

This thesis has demonstrated for the first time that morphological differences or abnormalities related to blood flow can be detected by live MRI scanning of the placenta of mice subject to experimental models of preeclampsia and may be used to analyse changes quantitatively. This technology has the potential to be used when studying the dynamic changes in the placenta of pregnancies complicated by preeclampsia. Additionally, preliminary data shows that 3D modelling using high resolution images of fixed placenta can yield quantitative data of morphological changes. MRI can now be used to examine placental changes in other physiological models of perturbed pregnancies.

Analysis of the MRI images suggests changes involve both increases in deoxyhaemoglobin (hypoxia) and decreases in intracellular pH (acidosis) and suggests that pH dependent mechanisms may be as equally important as hypoxia in the perturbed placenta. The results also indicate that the metabolic changes in the placenta in response to both decreased blood flow (RUPP) and inflammatory cytokine (TNF-α) infusion involve upregulation of both TLR-3 and TLR-4 protein expression and upregulation of HIF-1α mRNA and protein. Alterations in expression and localisation of the $H^+/Cl^-$ co transporter CLIC-3 are demonstrated in the placenta upon inflammatory cytokine (TNF-α) infusion, consistent with the metabolic change (acidosis) observed by MRI.

These results support a role for maladaptive regulation of TLR and HIF-1α in response to metabolic changes, brought about by either alterations in blood flow or an imbalance in inflammatory cytokines. Alterations in these key molecules that respond to changes in the cellular environment may be implicated in the abnormal development of the placenta that leads to the maternal signs of hypertension and proteinuria.

# Appendix 1: Proteomic Identification of Molecular Changes

## Introduction

Molecular change in tissues can be assessed by examining changes in both protein and mRNA expression and localisation. To screen for and identify global differences in proteins between treatment groups, a powerful tool can be found using a functional proteomic approach. In this approach a combination of two dimensional (2D) gel electrophoresis, followed by excision of protein spots of interest and tandem liquid chromatography and mass spectroscopy (LC-MS/MS) is used to identify functional changes in protein expression between treatment conditions.

## Methods

Placental tissue (2-4 placentas from a single control and a single TNF-α treated animal) were mechanically disrupted in the deep frozen state using the Mikro Dismembrator (Sartorius BBI, Bethleham PA, USA). The pulverised tissue was separated into soluble and membrane fractions by homogenisation in a hypotonic lysis buffer containing protease inhibitors followed by ultracentrifugation. Proteins in the soluble and membrane fractions were solubilised in 2DE buffer and resolved using 2D gel electrophoresis (Butt and Coorssen, 2006). Gels were stained with Coomassie Brilliant Blue and imaged using the FLA-9000 (FujiFilm/GE Health Science) and comparative analysis of the 2DE gel images between treatment groups was carried out using Delta 2D software (version 4.1, DECODEN, Gerifswald, Germany). Unique protein spots were excised manually, subject to in gel tryptic digestion and peptides extracted into formic acid/acetonitrile and analysed by tandem liquid chromatography/mass spectrometry (LC-MS/MS) (Wright et al., 2014) .

## Results

In total 34 protein spots were excised from the TNF-α treated and saline control placenta gels. Identified spots are shown on Figure A1.1. Two unique proteins were identified; Desmin from the saline control animal and 14-3-3 protein zeta/delta alternatively known as protein kinase C inhibitor protein 1 (KCIP-1) from the TNF-α treated animal (see Table A1.1). Four proteins appearing as unique spots at the same molecular weight but different isoelectric points(pI) in the saline and TNF-α gels were identified as the same protein but with a pI shift toward the acidic in the TNF-α treated animals (see Table A1.2).

**Table A1.1: Identification of unique proteins**

| Protein | abbreviation | function | Treatment group |
|---|---|---|---|
| Desmin | DES | maintain muscle fibre strength | control |
| 14-3-3 protein zeta/delta | | Regulation of signalling proteins | TNF-α |

**Table A1.2: Identification of the pI shifted proteins**

| Protein | abreviation | Alternate names | abreviations |
|---|---|---|---|
| 78 kDa glucose regulated protein | GRP78 | Heat shock 70 kDa protein<br>Immunoglobulin heavy chain binding protein 5 | HSP5<br><br>BiP |
| Protein disulphide isomerase | PDIA1 | Endoplasmic reticulum resident protein 59<br>Prolyl 4-hydroxylase subunit β | ERp59<br><br>P55 |
| ATP synthase subunit beta | ATP5b | | |
| Annexin V | | Calphobindin I, Endonexin II<br>Lipocortin V<br>Placental anticoagulant protein 4<br>Placental anticoagulant protein I<br>Thromboplaston inhibitor<br>Vascular anticoagulant-alpha | CBP-1<br><br>PP4<br>PAP-I<br><br>VAC-alpha |

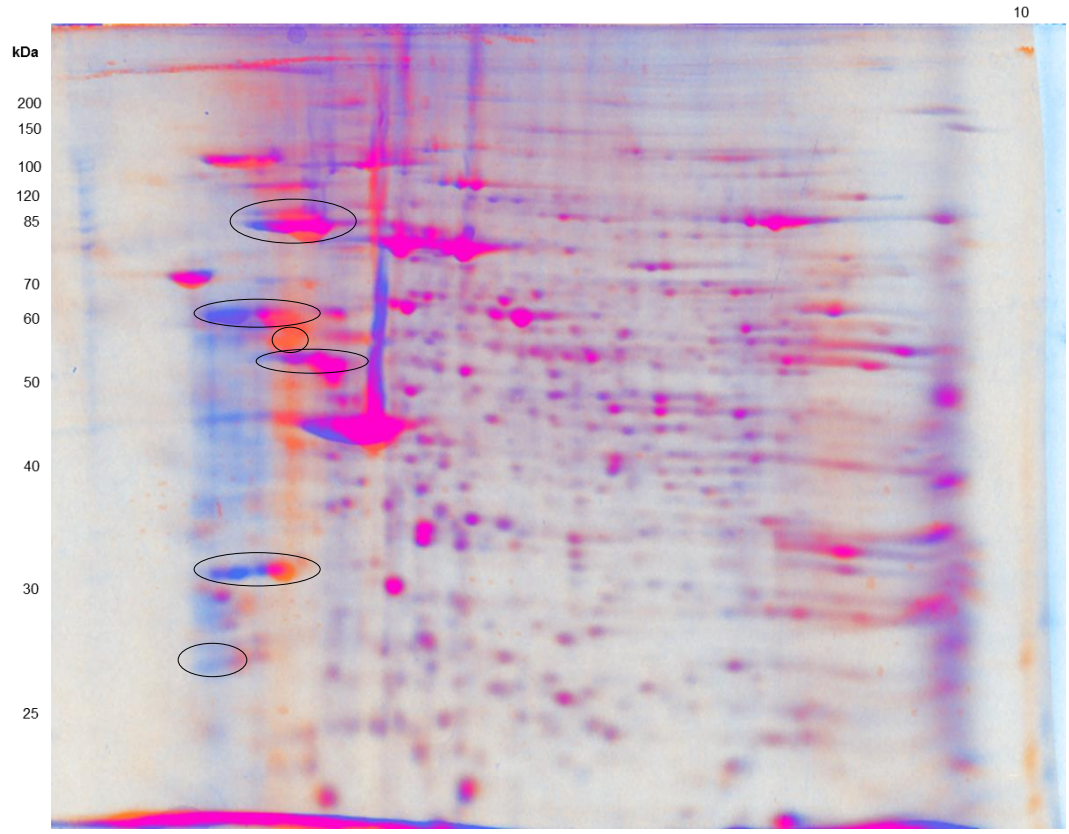


**Figure A1.1: 2D gel of membrane fraction of the placenta, circles indicate identified proteins, blue identifies spots that are unique to TNF-α sample #201, orange identifies spots that are unique to saline sample #217, pink identifies common spots.**

## Protein Descriptions

Desmin are class-III intermediate filaments generally found in muscle cells, where they have a role in helping to maintain muscle fibre strength. Desmin proteins connect rod-like structures called Z-discs to one another, linking neighbouring sarcomeres and forming myofibrils, the basic unit of muscle fibres.

14-3-3 protein zeta/delta is a member of the 14-3-3 protein family that are implicated in the regulation of a large spectrum of both general and specialised signalling pathways such as the apoptotic pathway. It binds to a large number of partners, including kinases, phosphatases, and transmembrane receptors, generally resulting in the modulation of their activity.

Grp78 probably plays a role in facilitating the assembly of multimeric protein complexes inside the endoplasmic reticulum (ER). It is involved in the correct folding of proteins and degradation of misfolded proteins. Grp78 is part of a large chaperone multiprotein complex including PDIA6.

ATP synthase subunit β is part of the ATP synthase complex which is involved in the synthesis of ATP in mitochondria. An ectopic ATP synthase has been identified on the cell membrane which appears to involve the same subunits as that in the mitochondrial enzyme complex.

Protein disulphide isomerise catalyses the formation, breakage and rearrangement of disulfide bonds. At the cell surface, it acts as a reductase that cleaves disulfide bonds of proteins attached to the cell. It may therefore cause structural modifications of exofacial proteins. Inside the cell, it seems to form/rearrange disulfide bonds of nascent proteins. At high concentrations, it functions as a chaperone that inhibits aggregation of misfolded proteins. At low concentrations, it facilitates aggregation (anti-chaperone activity). It is implicated in correct folding and trafficking of proteins.

PDI is also known as prolyl 4-hydroxylase subunit β and is part of the prolyl hydroxylase domain-containing proteins (PHDs) that play pivotal roles in the oxygen dependent regulation of hypoxia-inducible factor (HIF 1-α).

Annexin V belongs to the annexin family of calcium-dependent phospholipid binding proteins some of which have been implicated in membrane-related events along exocytotic and endocytotic pathways. Annexin 5 is a phospholipase A2 and protein kinase C inhibitory protein with calcium channel activity and a potential role in cellular signal transduction, inflammation, growth and differentiation.

## Discussion

The results presented here, while preliminary and requiring repetition with both replicate samples and replicate animals, appear to indicate changes in molecular expression (pI shift) which may be related to changes in activity of proteins involved in pH homeostasis and the correct folding and trafficking of proteins.

The chaperone proteins, protein disulfide isomerise (PDI) and glucose regulated protein (Grp78), have been previously shown to be phosphorylated by the serine-threonine kinase Akt *in vitro*, leading to an acidic shift in their isoelectric point and sphingosine-dependent kinases and casein kinase II have been shown to phosphorylate PDI *in vivo* (Barati et al., 2006). While the physiological role of ER chaperone phosphorylation is unclear, it may represent a mechanism for regulation of chaperone function. Phosphorylation of PDI has been shown to be differentially regulated by TNF-α stimulation (Yanagida et al., 2000) and ischemia-reperfusion in rat heart (Sakai et al., 2003), however this activity may be related to its function as subunit of PHD and its role on oxygen dependent regulation of HIF-1α rather than its function as a chaperone protein. These results suggest that TNF-α infusion may result in changes in the phosphorylation of PDI and Grp78, affecting their function.

The preliminary results presented here also suggest that that TNF-α infusion may result in changes in the phosphorylation of ATP synthase subunit β. The expression of the catalytic unit β-$F_1$-ATPase is tightly regulated at post-transcriptional levels during mammalian development and in the cell cycle (Willers and Cuezva, 2011) and phosphorylation of $F(_1)F(_0)$ ATP synthase subunit β attenuates its activity (Kane et al., 2010). The mitochondrial $F(_1)F(_0)$ ATP synthase translocates to the cell surface and has high activity in tumour-like acidic and hypoxic environments (Ma et al., 2010). Binding of coupling factor 6 (CF6) to ectopic ATP synthase leads to intracellular acidosis (Osanai et al., 2012), and induces insulin resistance, mild glucose intolerance and elevated blood pressure in mice. ATP synthase

inhibition leads to increase in expression of Grp78 and PDI and blocking ectopic ATP synthase activity has been shown to activate the unfolded protein response (Chang et al., 2012). It is possible that a change in ATP synthase subunit β phosphorylation induced by TNF-α may affect the function of ATP synthase activity, leading to acidosis or ER stress.

Persistent oxidative stress and protein misfolding initiate apoptotic cascades and are now known to play predominant roles in the pathogenesis of multiple human diseases including diabetes, atherosclerosis, and neurodegenerative diseases (Malhotra and Kaufman, 2007) **.** Recently it has proposed that preeclampsia is a disease of protein misfolding and aggregation (transthyretin misfolding) brought about by local changes in pH at membranes, and hypoxia induced oxidative stress and ER stress (Kalkunte et al., 2013). It was demonstrated that transthyretin is aggregated in preeclampsia and that native transthyretin, which is present in reduced levels in preeclamptic sera, inhibits preeclampsia–like features in a preclinical mouse model of the disease (IL 10-/- knockout mice given preeclamptic sera), including new onset proteinuria, increased blood pressure, glomerular endotheliosis and production of anti-angiogenic factors (Kalkunte et al., 2013). It was speculated that local changes in pH at membranes, and hypoxia induced oxidative stress and ER stress may be responsible for transthyretin misfolding and aggregation.

Here I present preliminary evidence of post transcriptional modifications leading to a pI shift in two proteins who have a chaperone function and are involved in the correct folding and trafficking of proteins, PDI and Grp78, in placentas from a mouse infused with the inflammatory cytokine (TNF-α). I also show post transcriptional modifications leading to a pI shift in ATP synthase subunit β, a molecule involved in both pH homeostasis and the unfolded protein response. Given that the MRI changes presented in Section 6.3 implicate changes in pH homeostasis in the experimental models used here, these preliminary results are of interest, and warrant validation in future work.

# Appendix 2: MRI Images of Complete Placenta

$^{1}$H MRI images were taken using a Bruker Avance 11.74 Tesla wide-bore spectrometer with micro-imaging probe capable of generating gradients of 0.45 T/m. A Gradient Echo (GEFI) sequence was used to obtain a series of images across the complete fixed placenta using the following parameters; Echo time 8 ms, Repetition time 40 ms, excitation pulse angle 58.4 degrees, 16 averages with 3D 50 µm isotropic voxels, a field of view (FOV) of 11 mm x 11 mm x 20 mm and an MTX of 220 x 220 x 400. Scans typically took 16 h.

These images were used to reconstruct a 3D model of the placenta in Amira™ 3D Analysis software (FEI Visualization Sciences Group, Mérignac Cedex, France). MRI image sets from each placenta were imported into the software, segmented into regions and volume reconstruction and volume analysis performed (see Chapter 7). A complete set of images from a representative placenta is shown below.

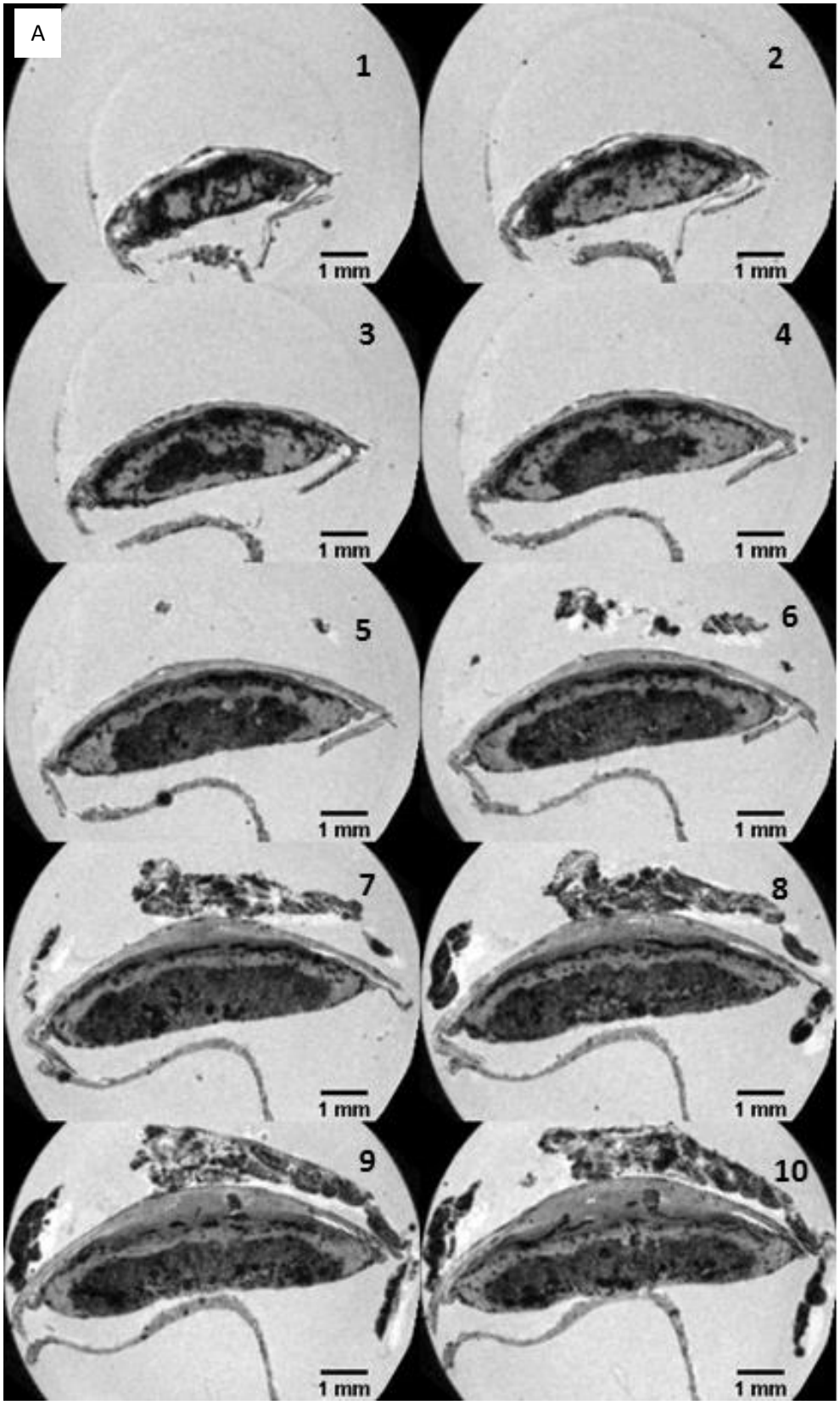


**Figure A2.1: Contiguous series of $^{1}$H MRI images of a placenta from a normal pregnant C57BL/6JArc mouse. A gestational day placenta was formalin fixed and infused with Magnevist™ contrast agent. A) slices 1-10.**

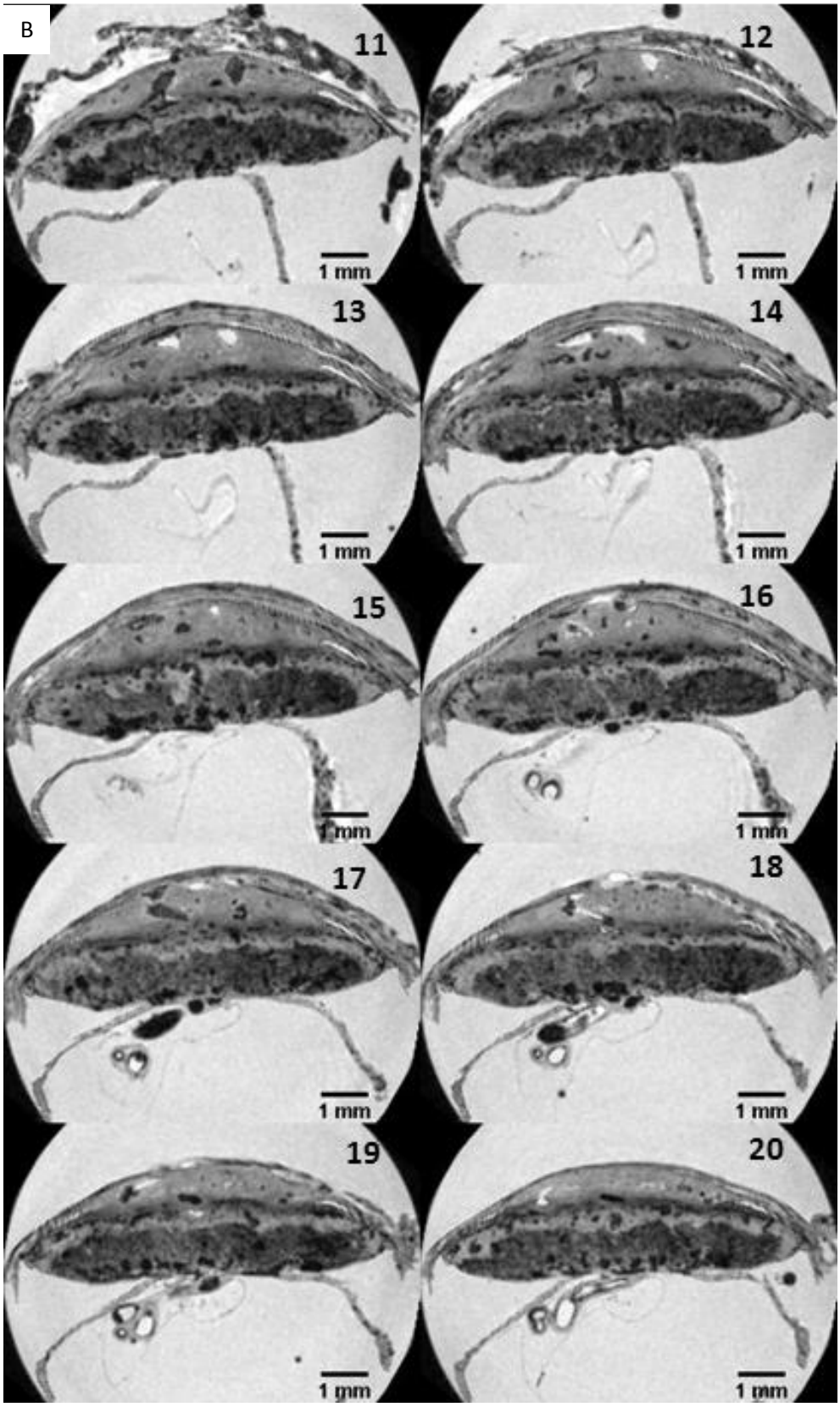


**Figure A2.1: Contiguous series of $^{1}$H MRI images of a placenta from a normal pregnant C57BL/6JArc mouse. A gestational day placenta was formalin fixed and infused with Magnevist™ contrast agent. B) slices 11-20.**

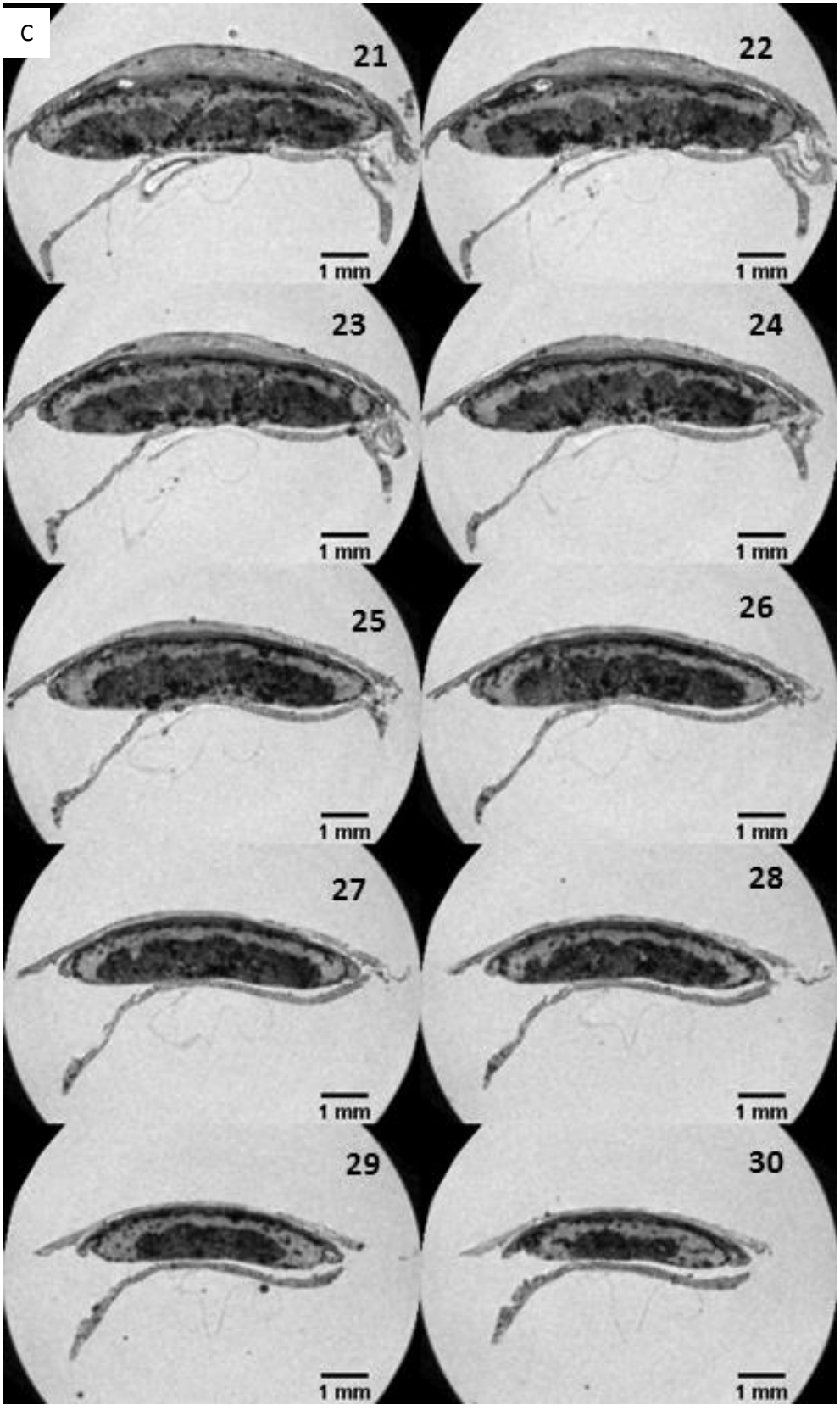


**Figure A2.1: Contiguous series of $^{1}$H MRI of a placenta from a normal pregnant C57BL/6JArc mouse. A gestational day 17 placenta was formalin fixed and infused with Magnevist™ contrast agent. C) slices 21-30.**

# Appendix 3: Placental Histology

Placental histology was carried out in order to visualize the structural components of the placenta. Both Haematoxylin and Eosin (H&E) staining and Periodic acid-Schiff (PAS) staining (which identifies glycogen trophoblast cells) was performed using placenta at gd 14 and gd 17.

Figures A3.1-A3.3 show H&E and PAS of a gd 14 placenta. The labyrinth, junctional zone and decidua are clearly identified with the PAS staining showing localisation of giant trophoblast cells in the junctional zone, as well as PAS +ve trophoblast cells in the decidua. Features such as the central canal, umbilical vein and artery and spiral arteries are clearly seen. FigureA3.4 shows a higher resolution image of these features.

Figure A3.5 shows a montage of H&E stained sections across a whole normal pregnant gd 17 placenta at a section distance of 100 uM, creating a coarse map of the placenta.

Figure A3.6 shows a higher resolution image of a normal gd 17 section showing labyrinth, junctional zone and decidua and Figure A3.7 shows detail of the labyrinth with identification of the maternal and foetal blood spaces.

Figures A3.8-A3.12 show comparison of H&E and PAS sections from gd 17 normal pregnant, TNF-α infused, RUPP, sham, and saline infused placentas. Figure A3.13 shows a higher resolution comparison of H&E stained normal, TNF-α and RUPP placentas and Figure A3.14 shows a higher resolution comparison of PAS stained normal, TNF-α and RUPP placentas. Comparison of the normal and experimental animals showed no gross structural differences between models. Any small changes in structural features would require determination by rigorous stereological assessment and was beyond the scope of this thesis. It was observed however that the RUPP animals appeared to have more PAS +ve

staining for glycogen trophoblast cells in the decidua than the control animals. As no stereological assessment of this was carried out, any change between treatment groups remains speculative. PAS also stains uNK cells but these were not distinguished in this study.

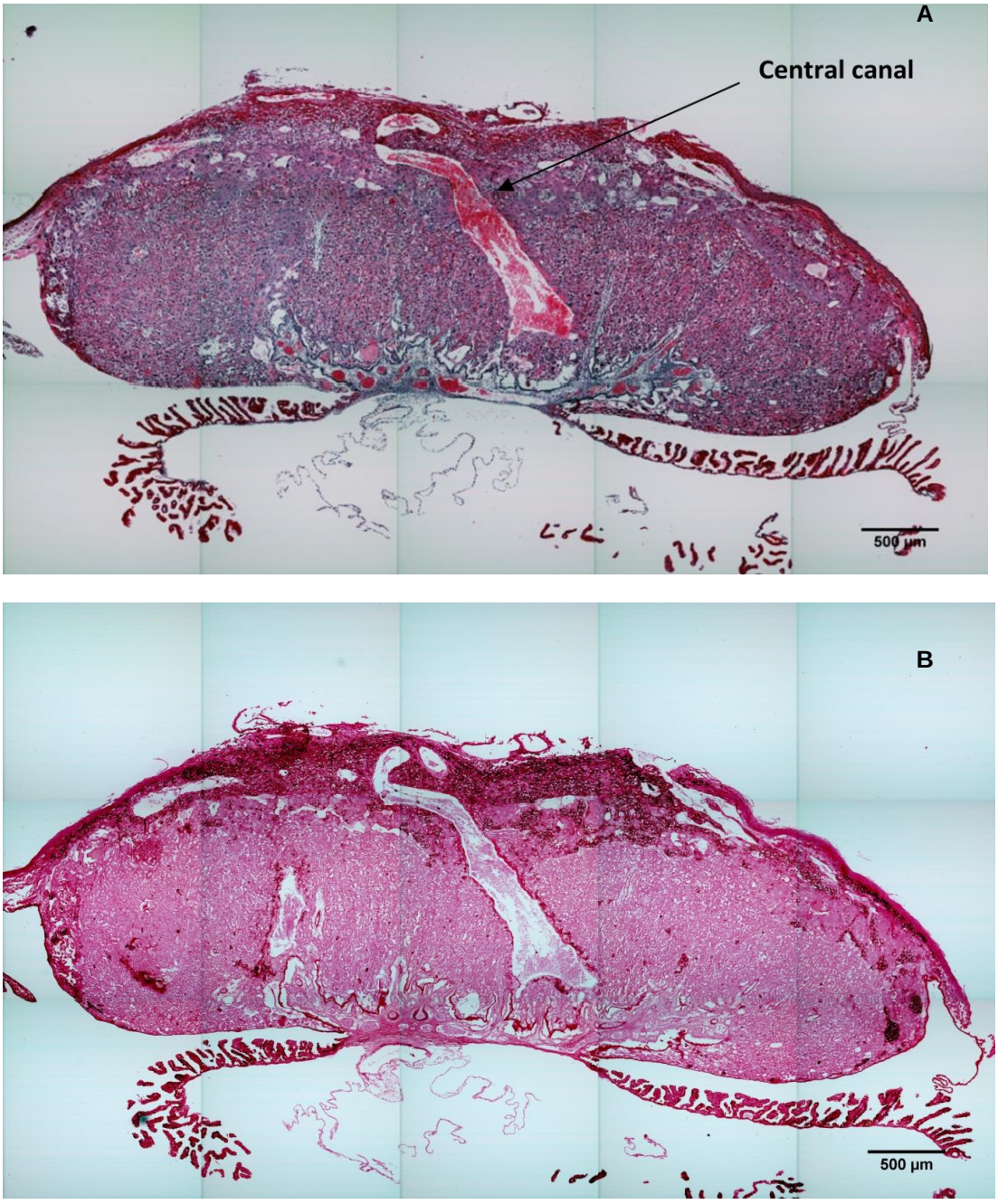


**Figure A3.1: Histological section of a placenta from a normal pregnant C57BL/6JArc mouse showing central canal. A) H&E and B) PAS stain of gestational day 14 placenta. Images (100x magnification) were taken with a Zeiss LSM 510 confocal microscope in tile scan mode.**

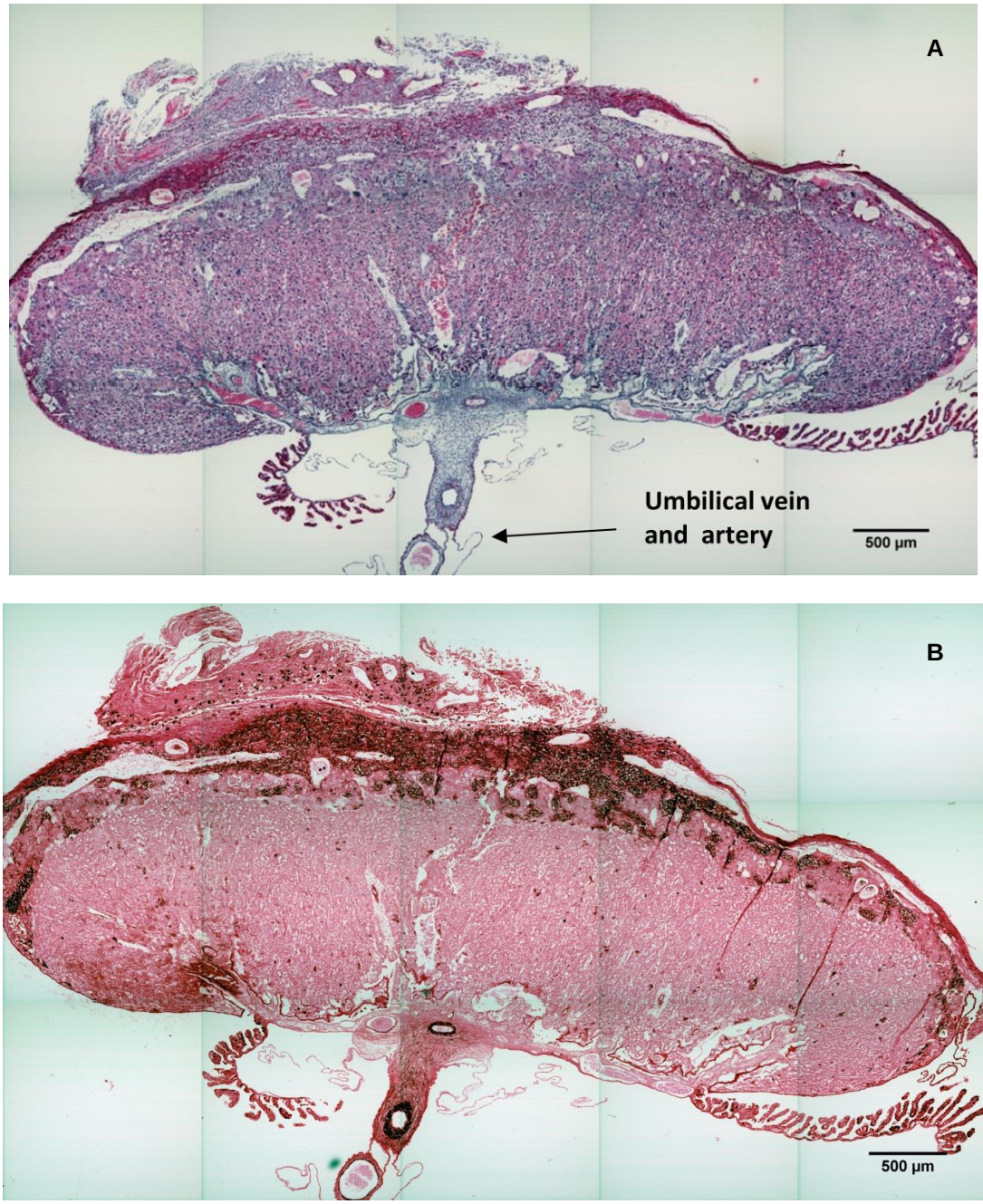


**Figure A3.2: Histological section of a placenta from a normal pregnant C57BL/6JArc mouse showing umbilical vein and artery. A) H&E and B) PAS stain of gestational day 14 placenta. Images (100x magnification) were taken with a Zeiss LSM 510 confocal microscope in tile scan mode.**

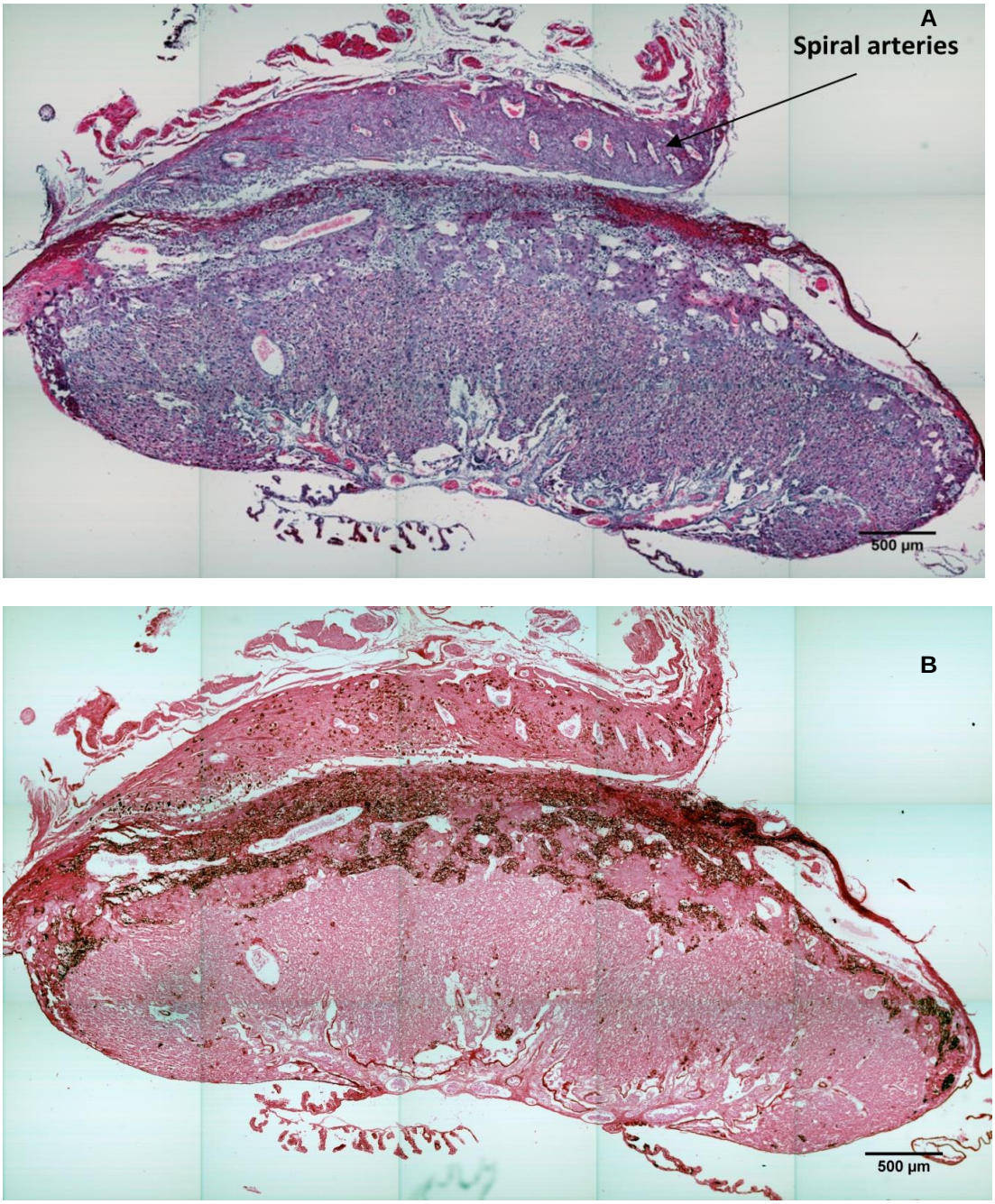


**Figure A3.3: Histological section of a placenta from a normal pregnant C57BL/6JArc mouse showing spiral arteries in the decidua. A) H&E and B) PAS stain of gestational day 14 placenta. Images (100x magnification) were taken with a Zeiss LSM 510 confocal microscope in tile scan mode.**

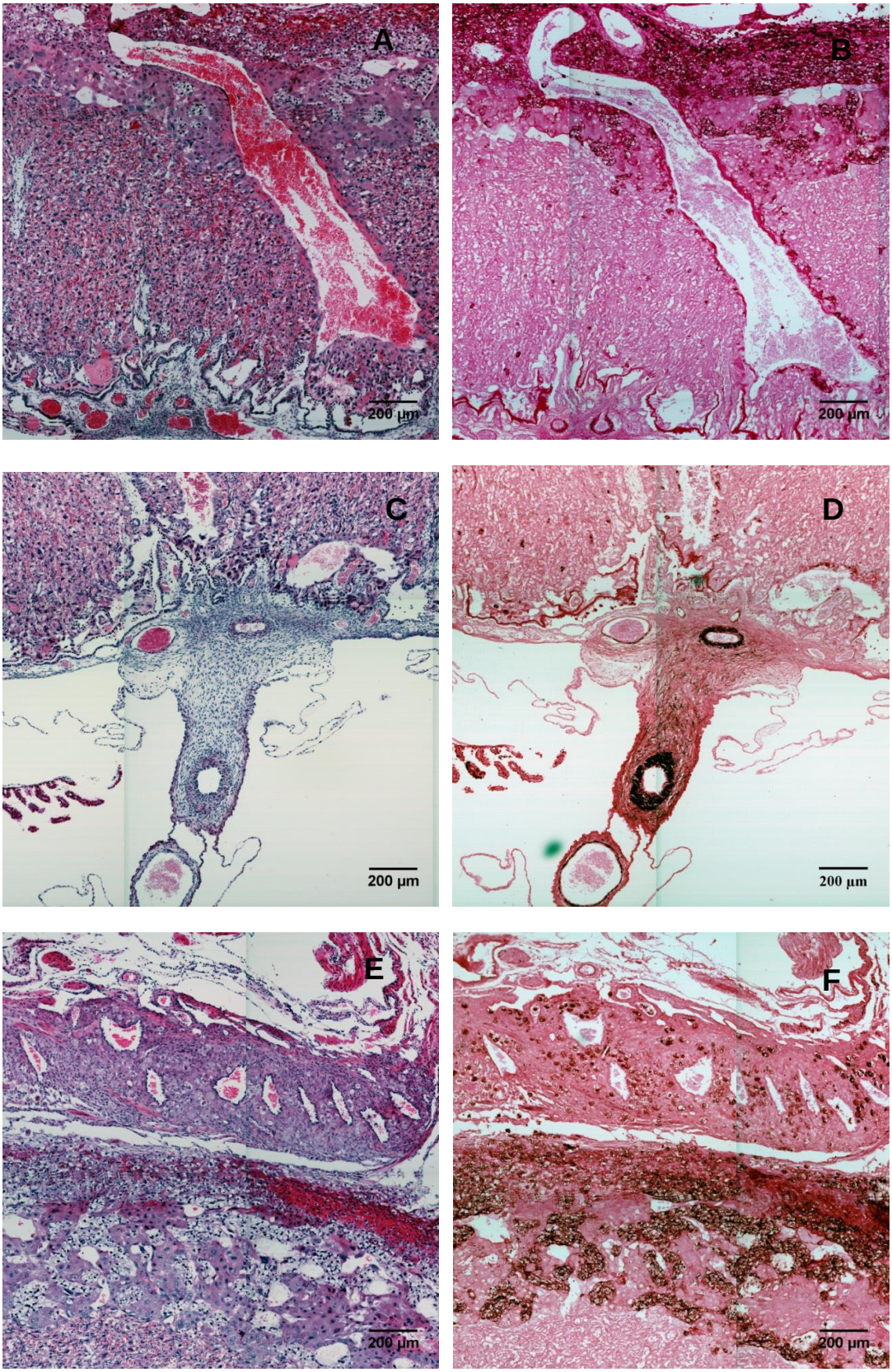


**Figure A3.4: Higher magnification of features in the placenta from a normal pregnant C57BL/6JArc mouse. H&E (A, C, E) and PAS (B, D, F) stain at gestational day 14, showing central canal (A, B), umbilical vein and artery (C, D) and spiral arteries in the decidua (E, F). Images (100x magnifications) were taken with a Zeiss LSM 510 confocal microscope in tile scan mode.**

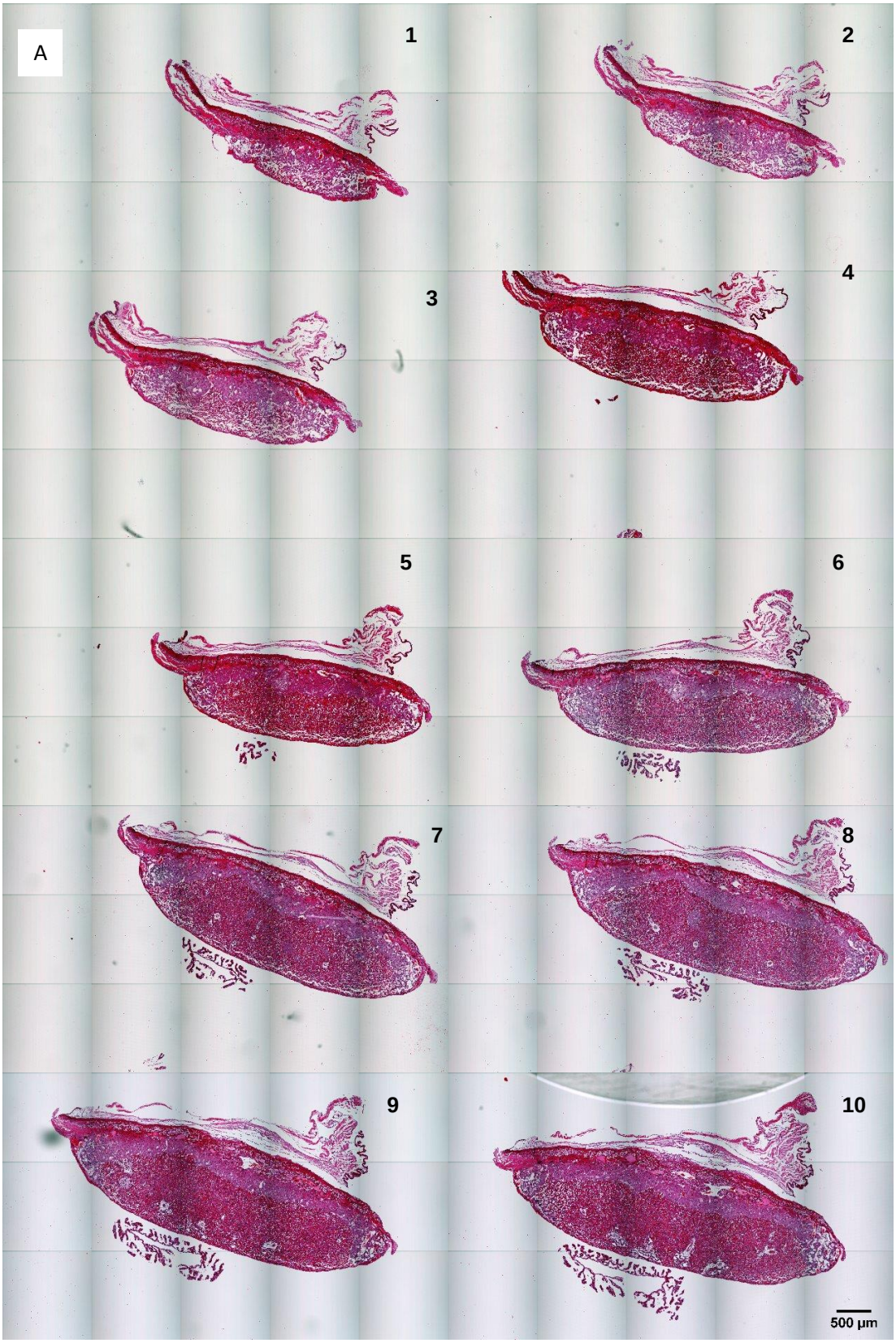


**Figure A3.5: H&E map of a placenta from a normal pregnant C57BL/6JArc mouse. Library of sections (10 µm) across the complete gestational day 17 placenta with intersection distance of 100 µm. Images (100x magnification) were taken with a Zeiss LSM 510 confocal microscope in tile scan mode. A) Section 1-10.**

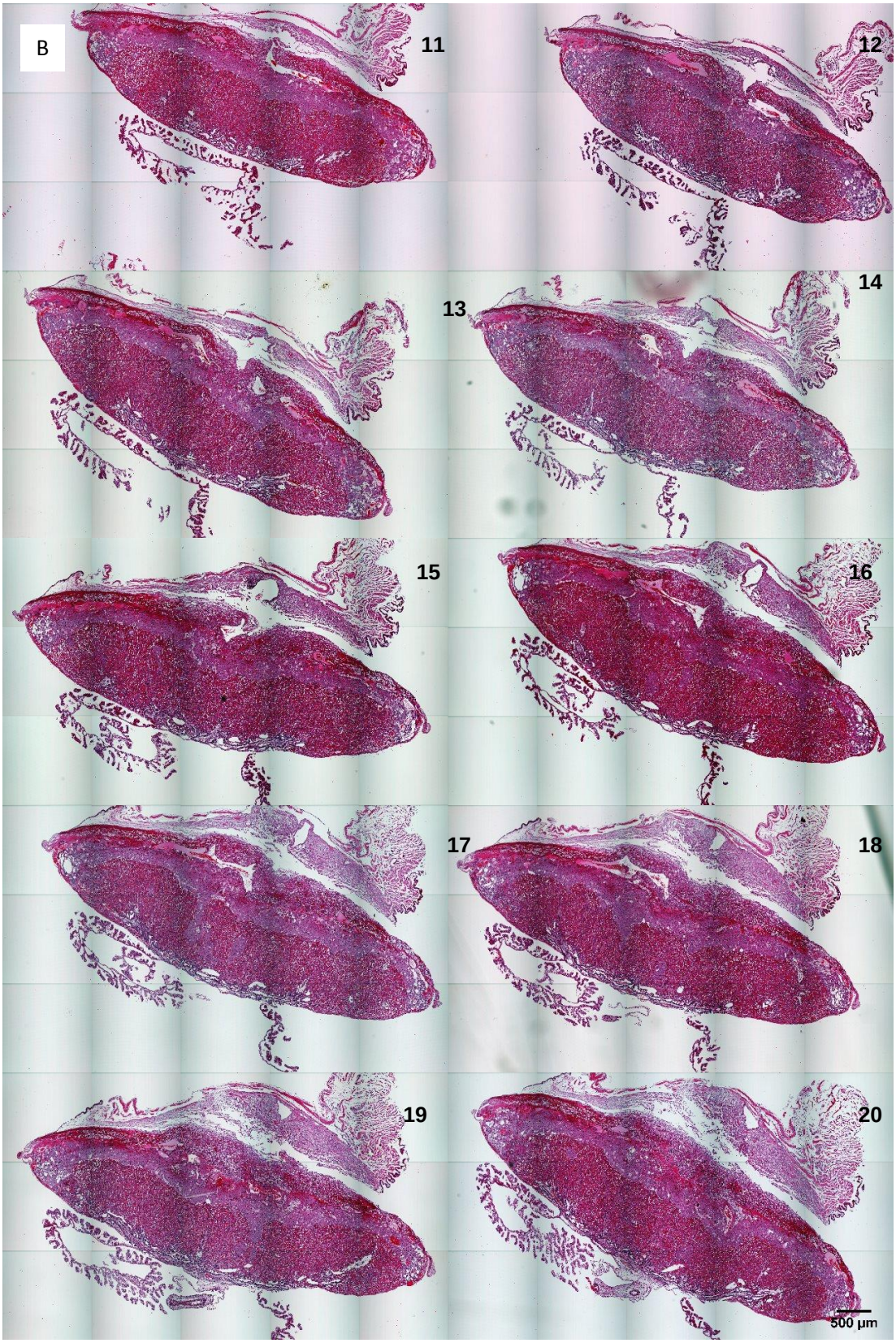


**Figure A3.5: H&E stain of a placenta from a normal pregnant C57BL/6JArc mouse. Library of sections (10 µm) across the complete gestational day 17 placenta with intersection distance of 100 µm. Images (100x magnification) were taken with a Zeiss LSM 510 confocal microscope in tile scan mode. B) Section 11-20.**

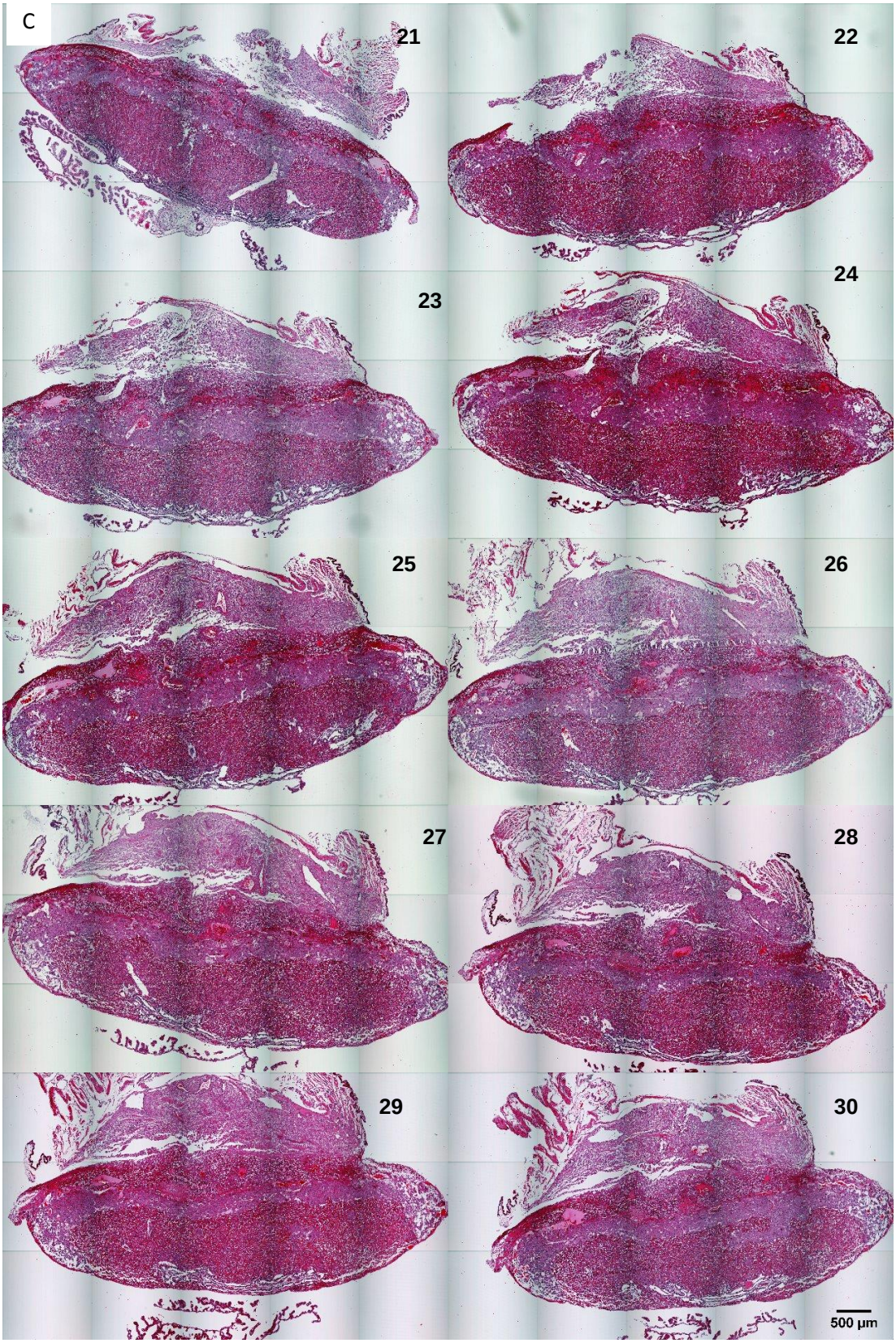


**Figure A3.5: H&E stain of a placenta from a normal pregnant C57BL/6JArc mouse. Library of sections (10 µm) across the complete gestational day 17 placenta with intersection distance of 100 µm. Images (100x magnification) were taken with a Zeiss LSM 510 confocal microscope in tile scan mode. C) Section 21-30.**

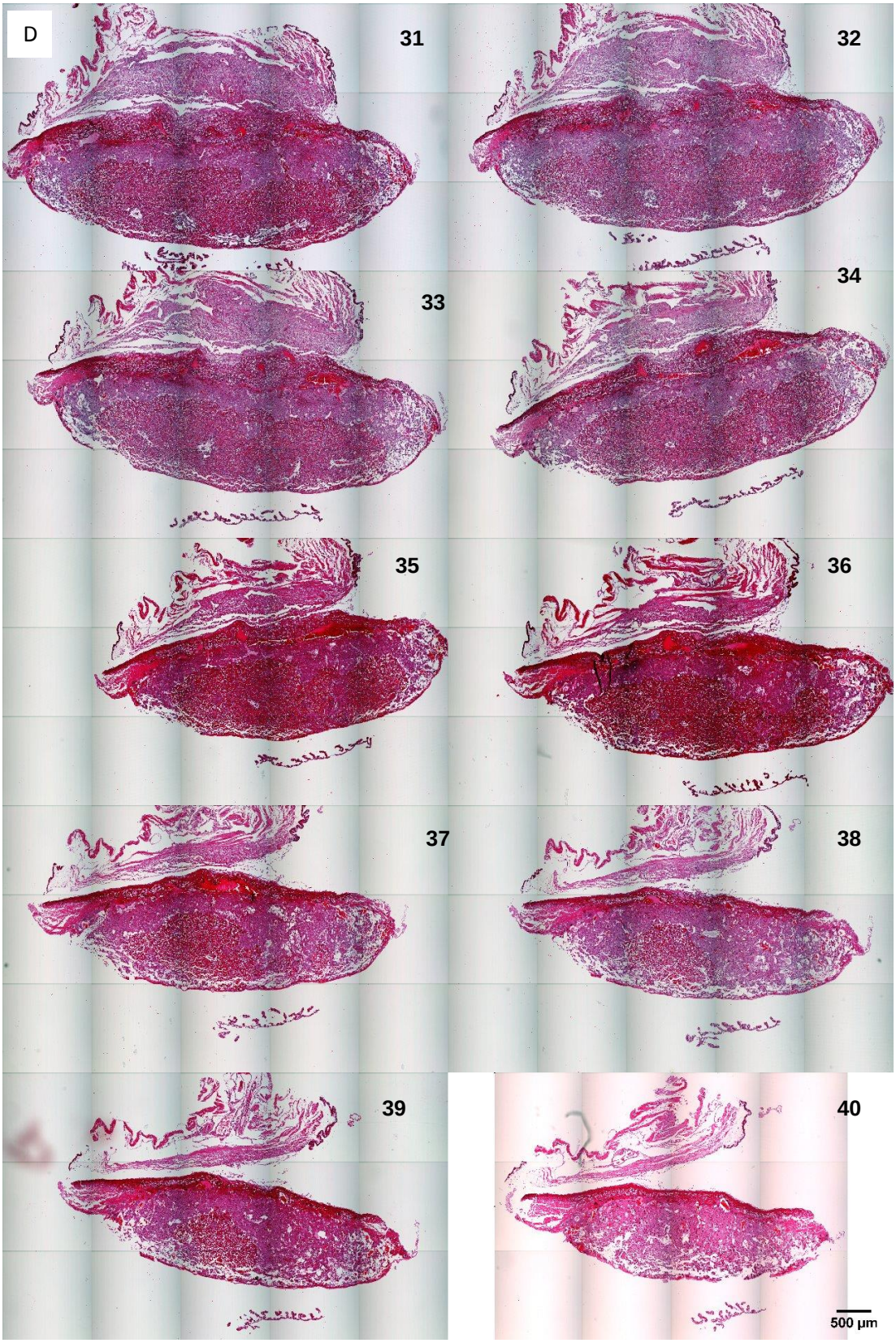


**Figure A3.5: H&E stain of a placenta from a normal pregnant C57BL/6JArc mouse. Library of sections (10 µm) across the complete gestational day 17 placenta with intersection distance of 100 µm. Images (100x magnification) were taken with a Zeiss LSM 510 confocal microscope in tile scan mode. D) Section 31-40.**

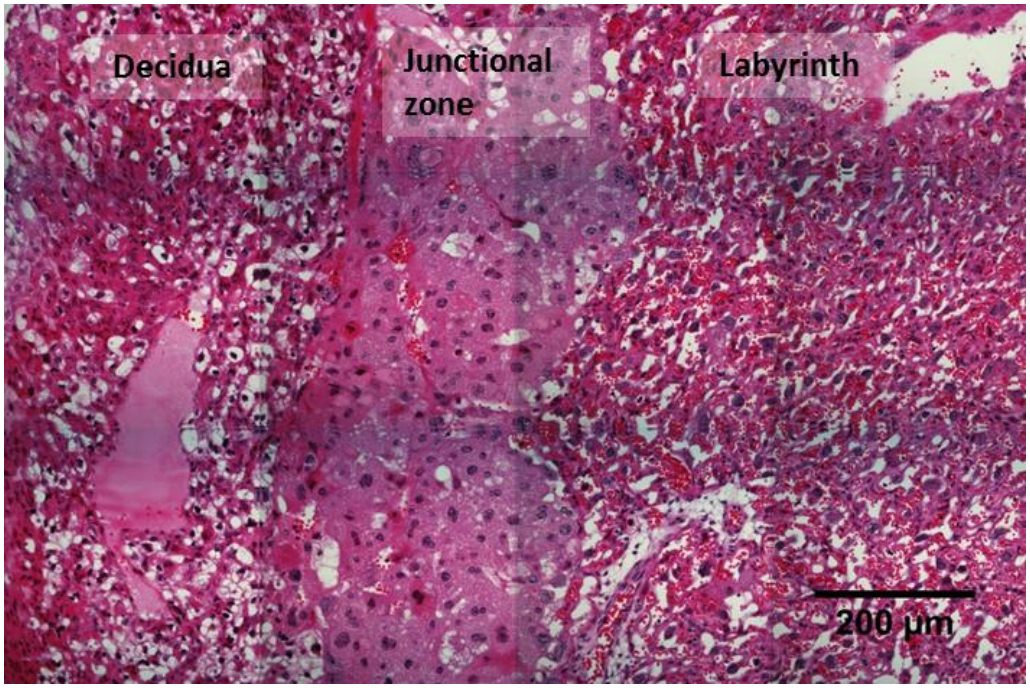


**Figure A3.6: Higher resolution H&E stain of a normal pregnant C57BL/6JArc mouse placenta at gestational day 17 showing decidua, junctional zone and labyrinth. Image (400x magnification) taken with Zeiss LSM 510 confocal microscope in tile scan mode.**

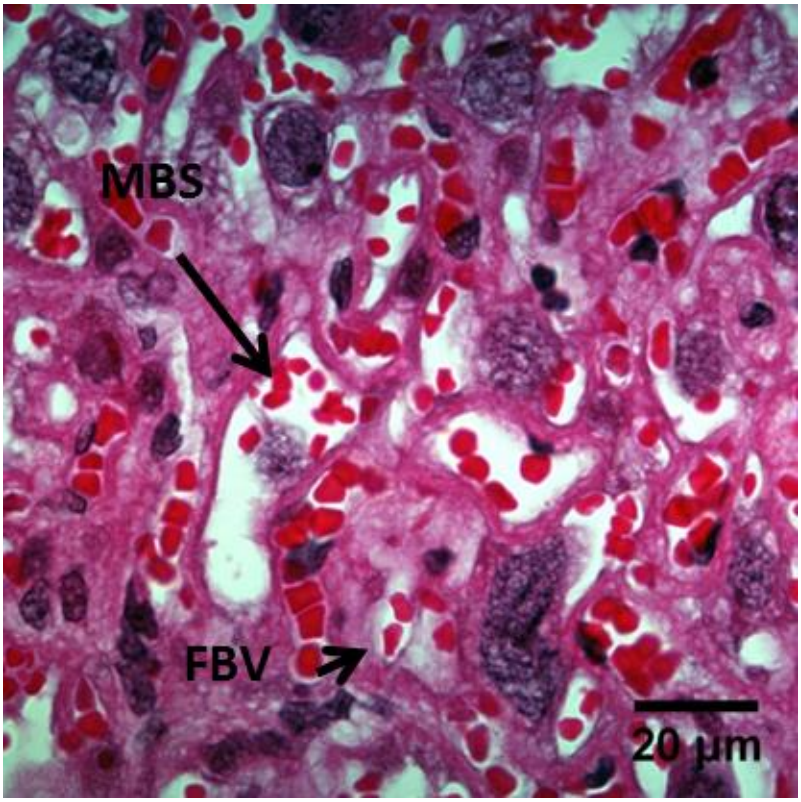


**Figure A3.7: Higher resolution H&E stain of labyrinth showing maternal blood space (MBS) and foetal blood vessels (FBV). Image (400x magnification) taken with Zeiss LSM 510 confocal microscope.**

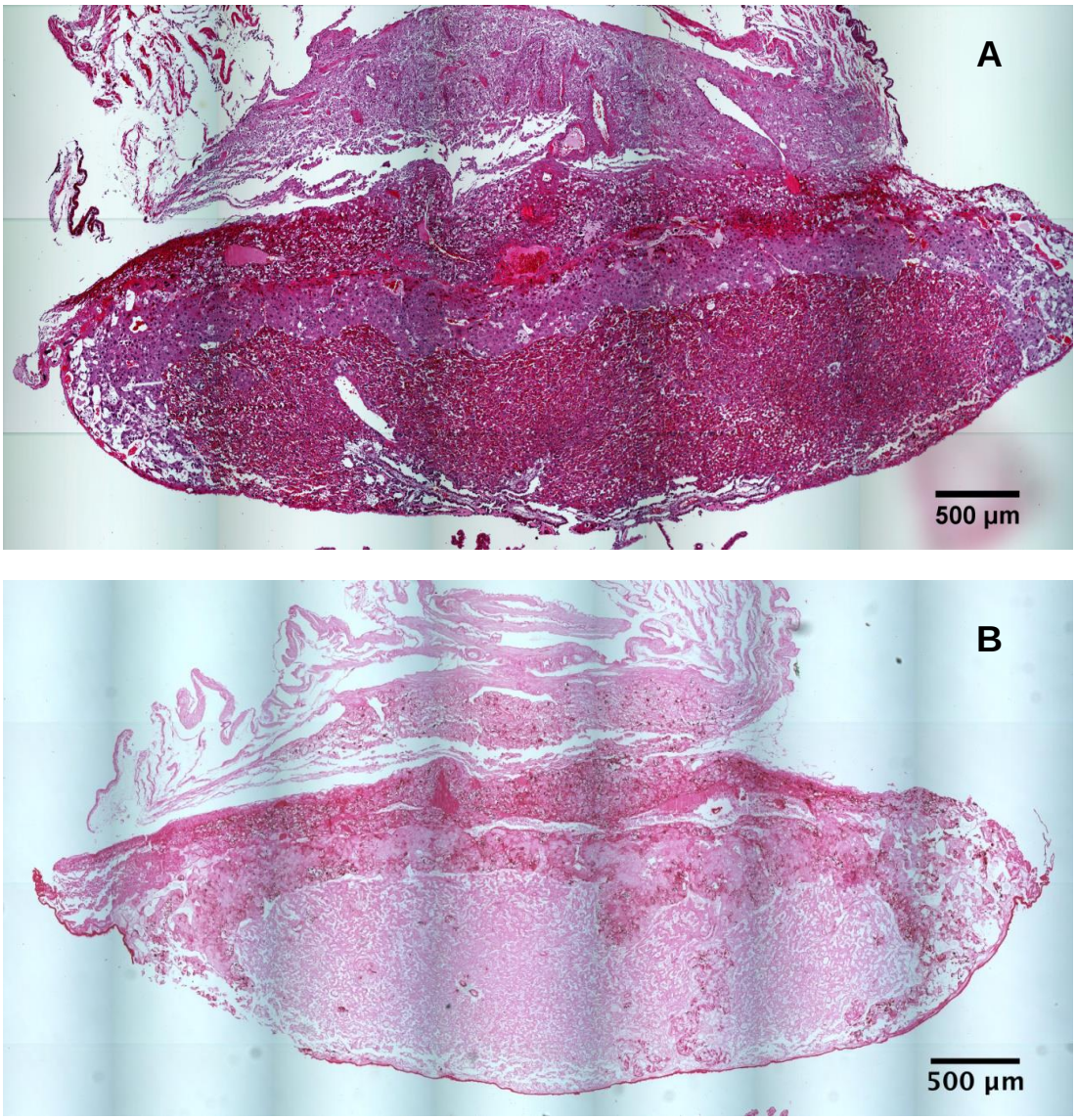


**Figure A3.8: Comparison of H&E (A) and PAS (B) stain of a placenta from a normal pregnant C57BL/6JArc mouse at gestational day 17. Image (100x magnification) taken with Zeiss LSM 510 confocal microscope in tile scan mode.**

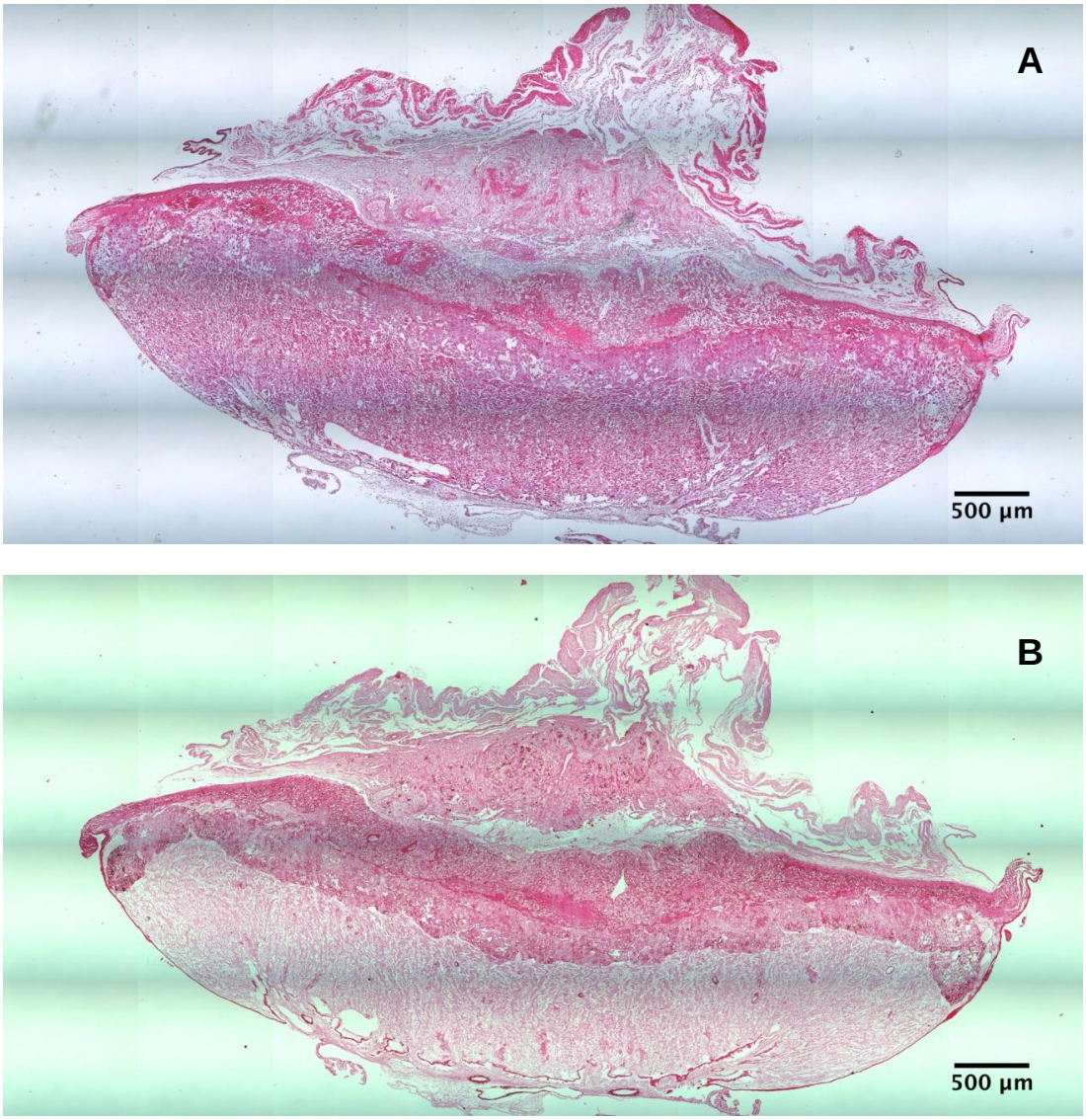


**Figure A3.9: Comparison of H&E (A) and PAS (B) stain of a placenta from a TNF-α infused C57BL/6JArc mouse at gestational day 17. Image (100x magnification) taken with Zeiss LSM 510 confocal microscope in tile scan mode.**

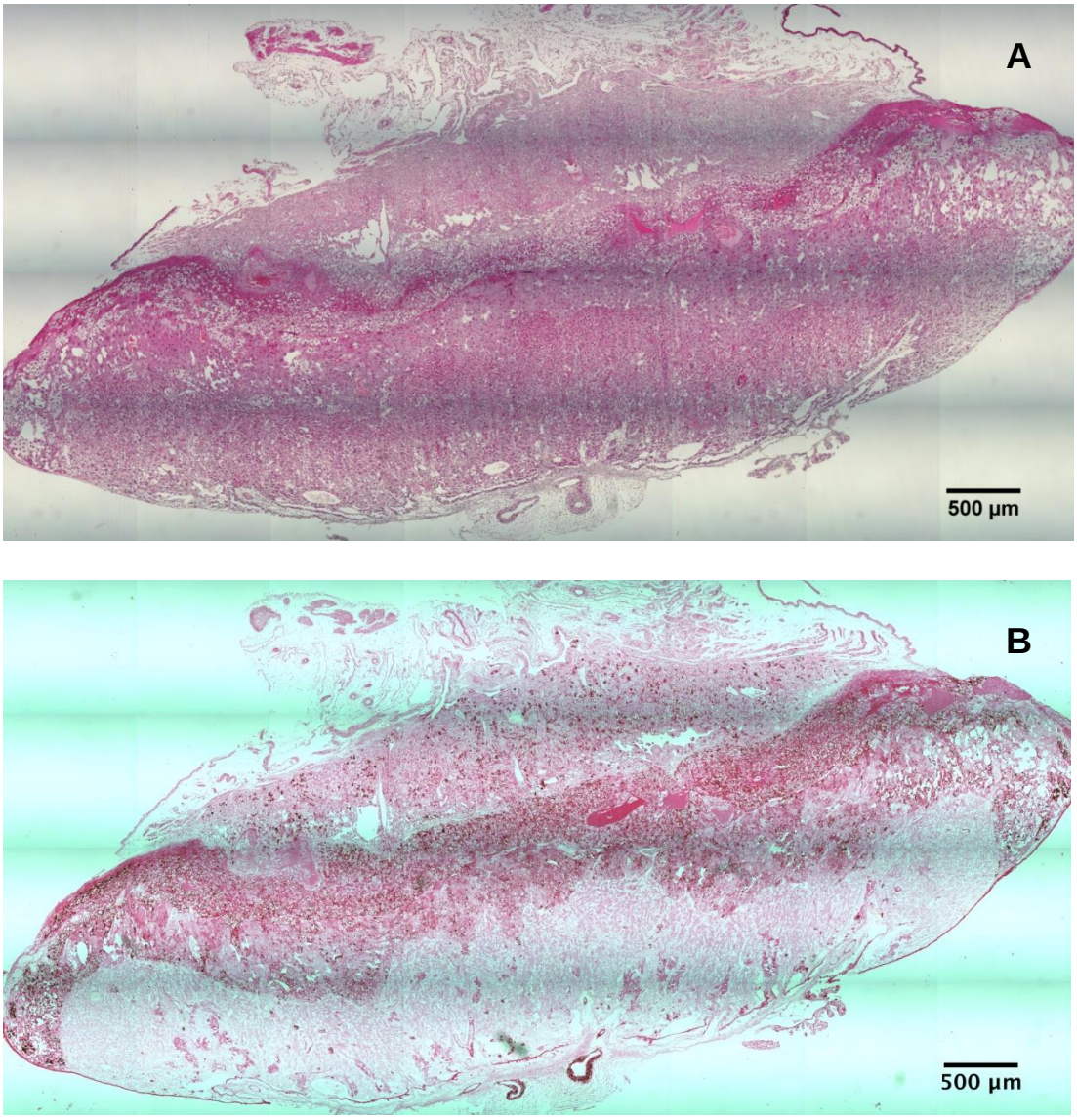


**Figure A3.10 Comparison of H&E (A) and PAS (B) stain of a placenta from a RUPP C57BL/6JArc mouse at gestational day 17. Image (100x magnification) taken with Zeiss LSM 510 confocal microscope in tile scan mode.**

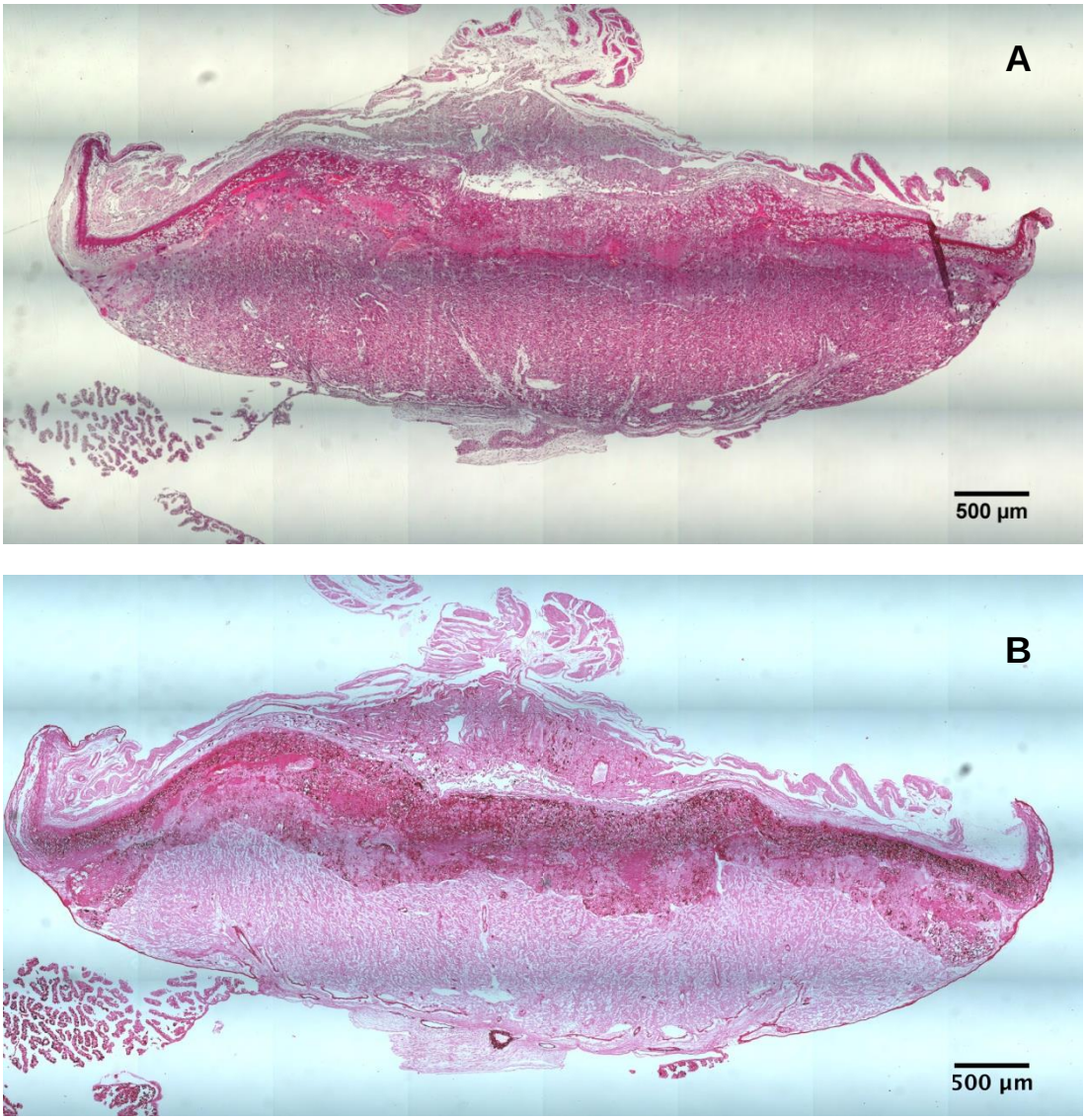


**Figure A3.11: Comparison of H&E (A) and PAS (B) stain of a placenta from a sham operated C57BL/6JArc mouse at gestational day 17. Image (100x magnification) taken with Zeiss LSM 510 confocal microscope in tile scan mode.**

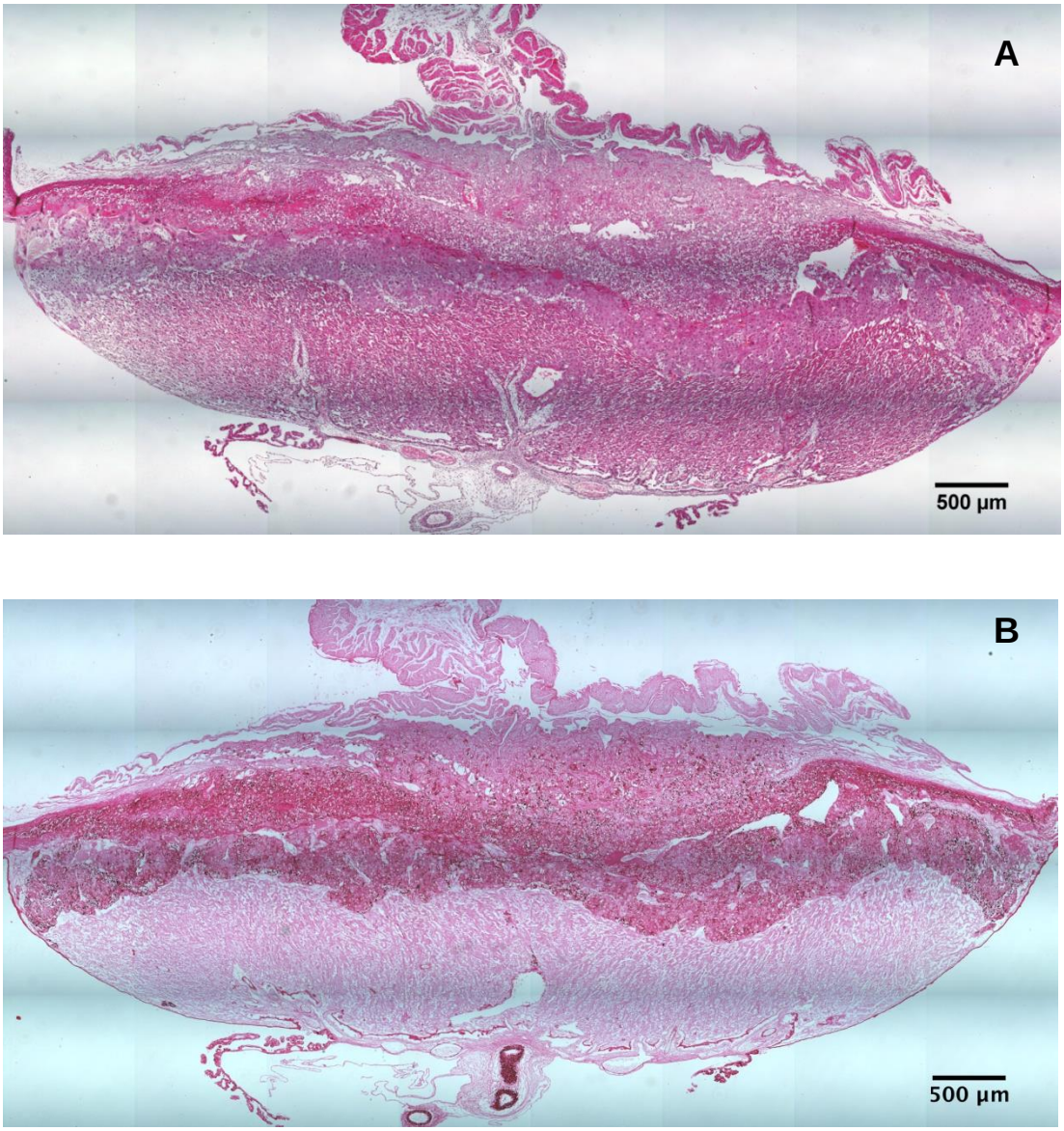


**Figure A3.12: Comparison of H&E (A) and PAS (B) stain of a placenta from a saline infused pregnant C57BL/6JArc mouse at gestational day 17. Image (100x magnification) taken with Zeiss LSM 510 confocal microscope in tile scan mode.**

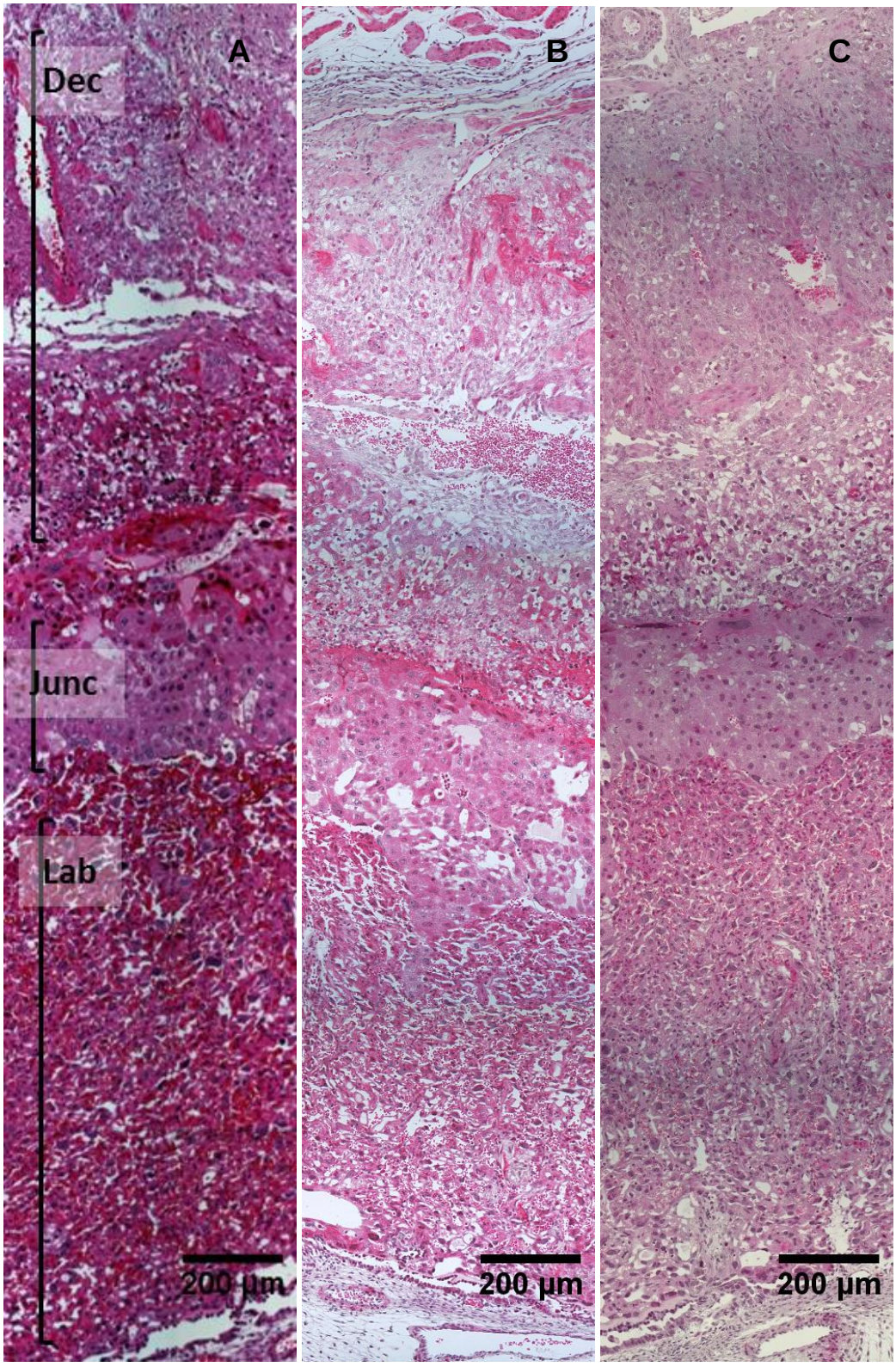


**Figure A3.13: Higher resolution comparison of H&E stained placenta from A) normal, B) TNF-α infused and C) RUPP C57BL/6JArc mice at gestational day 17. Images show all three regions of the placenta; decidua (Dec), Junctional zone (Junc) and Labyrinth (Lab). Image (100x magnification) taken with Zeiss LSM 510 confocal microscope in tile scan mode.**

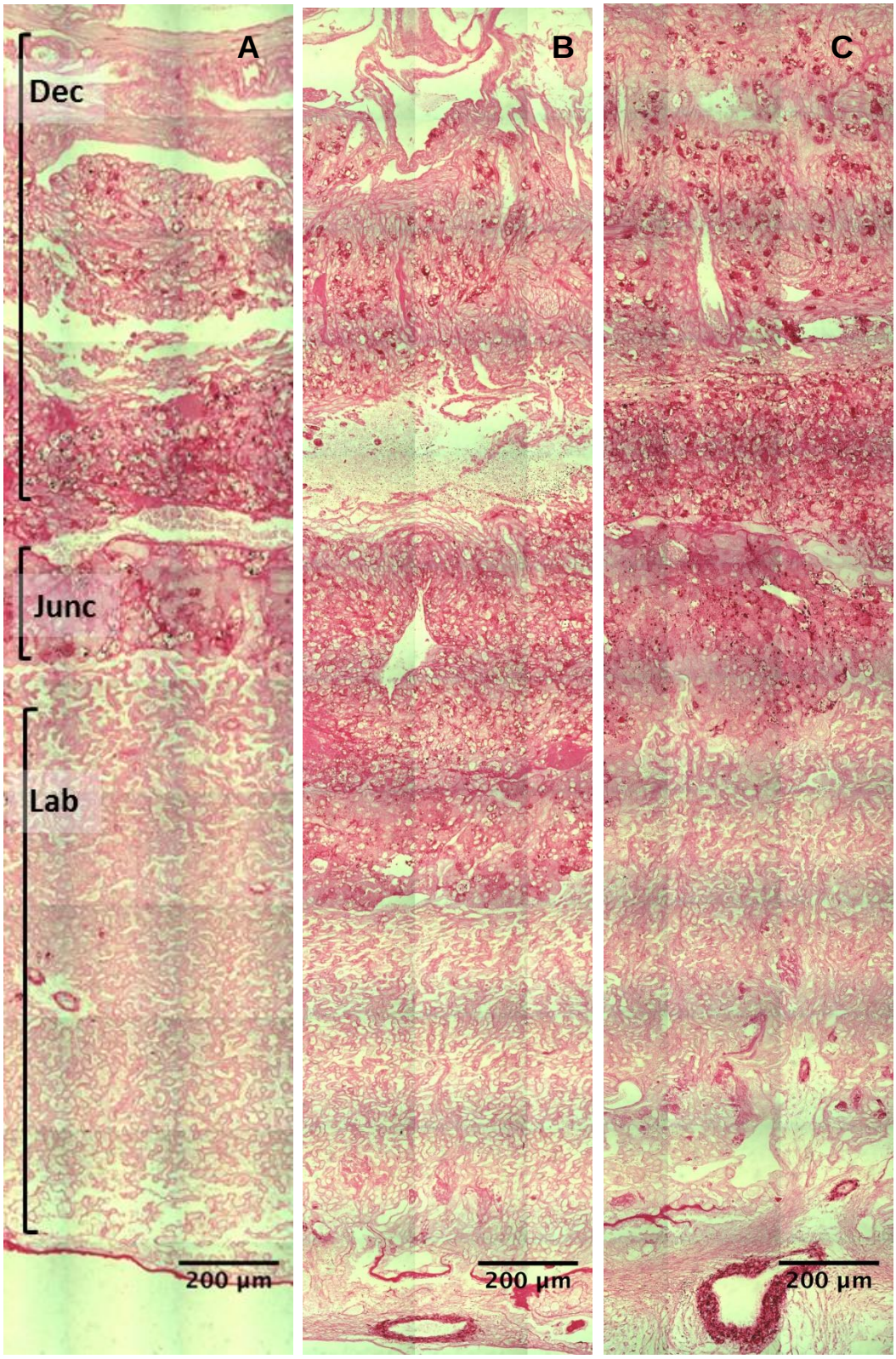


**Figure A3.14: Higher resolution comparison of PAS stained placenta from A) normal pregnant, B) TNF-α infused and C) RUPP C57BL/6JArc mice at gestational day 17. Image shows all three regions of the placenta; decidua (Dec), Junctional zone (Junc) and Labyrinth (Lab) with glycogen trophoblast cells (dark pink). Image (100x magnification) taken with Zeiss LSM 510 confocal microscope in tile scan mode.**

# Appendix 4: List of Scientific Papers

**Publications**

1. Magnetic Resonance Imaging Detects Placental Hypoxia And Acidosis In Mouse Models Of Perturbed Pregnancies
   **Bobek, G**., Stait-Gardner, T., Surmon, L., Makris, A., Lind, J. M., Price, W. S. & Hennessy, A. 2013. *PLoS One,* 8**,** e59971.

2. Placental Regulation of Inflammation and Hypoxia after TNF-α Infusion in Mice
   **Bobek, G**., Surmon, L., Mirabito, K.M., Makris, A. & Hennessy, A.2015 *American Journal of Reproductive Immunology (accepted July, 2015)*

3. The Expression Of Placental Soluble Fms-Like Tyrosine Kinase 1 In Mouse Placenta Varies Significantly Across Different Litters From Normal Pregnant Mice.
   Surmon, L., **Bobek, G**., Chiu, C. L., Young, S., Makris, A., Lind, J. M. & Hennessy, A. 2014. *Hypertens Pregnancy.*33 (3), 371

4. Variability In mRNA Expression Of Fms-Like Tyrosine Kinase-1 Variants In Normal And Preeclamptic Placenta
   Surmon, L., **Bobek, G**., Makris, A., Chiu, C. L., Lind, C. A., Lind, J. M. & Hennessy, A. 2014. *BMC Res Notes,* 7**,** 154.

**Abstracts**

5. Dynamic Studies on Changes in Placental Structure and Blood Flow in an Animal Model of Preeclampsia using High Resolution MRI
   **Bobek, G**., Stait-Gardner,T., Bahman,B., Preis,J., Price,W., Hennessy,A. 2009. *Placenta* 30(9), A40 *(IFPA, Adelaide)*

6. Differential timing of induced hypertension in 2 mouse models of preeclampsia
   **Bobek, G**., Surmon, L., Stait-Gardner,.T., Price, W., Makris, A., Hennessy, A. 2010. *Pregnancy Hypertension,* 1, S69. (*ISSHP, Melbourne)*

7. Molecular Changes Of Cell Adhesion And Invasion Markers In Two Mouse Models Of Preeclampsia
   Xu, B , **Bobek, G**., Surmon, L., Makris, A., Hennessy, A. 2011. *Placenta,* 32**,** A88. (*IFPA Norway)*

*8.* Morphological Differences In Murine Placenta Detected By Magnetic Resonance Imaging Measurements Of $T_2$ Relaxation Times In Mouse Models Of Preeclampsia. **Bobek, G**., Stait-Gardner, T., Surmon, L., Makris, A., Price, W. S. & Hennessy, A. 2012. *Pregnancy Hypertension,* 2**,** 200 (ISSHP, Geneva)

9. Magnetic Resonance Imaging Measurements Of $T_2$ Relaxation Times Within Contrasting Regions Of Murine Placenta Is Dependent Upon Blood Flow
**Bobek, G**., Stait-Gardner,.T., Surmon, L., Makris, A., Price, W., Hennessy, A. 2012. *Pregnancy Hypertension,* 2, 286. *(ISSHP, Geneva)*

10. Variability In mRNA Expression And Colocalisation Of Jmjd6 And Different Flt-1 Variants In Normal And Preeclamptic Human Placenta
Surmon, L., **Bobek, G**., Makris, A., Lind, J., Hennessy, A. 2012. *Pregnancy Hypertension, 2, 240. (ISSHP, Geneva)*

*11.* Sex-dependent differences in expression of Flt-1 variants and Jmjd6 in mouse placenta.
Surmon, L., Young, S., **Bobek, G**., Chiu, C. L., Xu, B., Makris, A., Lind, J. M. & Hennessy, A. 2012. *Pregnancy Hypertension,* 2**,** 206. (ISSHP, Geneva)

*12.* sFlt-1 Controlled By CPAP In A Pregnant Patient With Chronic Hypertension.
Daly, A. L., Robertson, A., Johnson, P., Middleton, S., **Bobek, G**., Sullivan, C. & Hennessy, A. 2012. *Pregnancy Hypertension,* 2**,** 327. (ISSHP, Geneva)

13. Immunofluorescent Localisation Of Molecules Involved In Response To Both Inflammation And Changes In Oxygen And Acidity Levels In Mice Placenta
**Bobek, G**., Stait-Gardner,.T., Surmon, L., Makris, A., Lind, JM., Price, W., Hennessy, A. 2013. *Proceedings of HBPRCA Melbourne,* H-023.

14. The Protective Effect of Apolipoprotein A-1 on Mean Arterial Pressure in an in vivo model of cytokine-induced hypertension in pregnancy.
Charlton, FS., **Bobek, G**., Mirabito, K., Xu, B., Makris, A., Rye, K., Hennessy, A. 2013, *Proceedings HBPRCA Melbourne,* H-024

15. High Resolution Magnetic Resonance Imaging Of Placentas And Lizard Brains At The University Of Western Sydney Node Of The National Imaging Facility
Stait-Gardner,.T., Hennessy, A., **Bobek, G**., Keogh, S., Hoops, D., Price, W. 2013. *Proceedings of ANZMAG Brisbane*

# References


ABITBOL, M. M. 1981. A simplified technique to produce toxemia in the pregnant dog. *Am J Obstet Gynecol,* 139**,** 526-34.

ABITBOL, M. M. 1982. Simplified technique to produce toxemia in the rat: considerations on cause of toxemia. *Clin Exp Hypertens B,* 1**,** 93-103.

ABITBOL, M. M., GALLO, G. R., PIRANI, C. L. & OBER, W. B. 1976. Production of experimental toxemia in the pregnant rabbit. *Am J Obstet Gynecol,* 124**,** 460-70.

ABITBOL, M. M., OBER, M. B., GALLO, G. R., DRISCOLL, S. G. & PIRANI, C. L. 1977. Experimental toxemia of pregnancy in the monkey, with a preliminary report on renin and aldosterone. *Am J Pathol,* 86**,** 573-90.

ADAMSON, S. L., LU, Y., WHITELEY, K. J., HOLMYARD, D., HEMBERGER, M., PFARRER, C. & CROSS, J. C. 2002. Interactions between trophoblast cells and the maternal and fetal circulation in the mouse placenta. *Dev Biol,* 250**,** 358-73.

ADELMAN, D. M., GERTSENSTEIN, M., NAGY, A., SIMON, M. C. & MALTEPE, E. 2000. Placental cell fates are regulated in vivo by HIF-mediated hypoxia responses. *Genes Dev,* 14**,** 3191-203.

AGATISA, P. K., NESS, R. B., ROBERTS, J. M., COSTANTINO, J. P., KULLER, L. H. & MCLAUGHLIN, M. K. 2004. Impairment of endothelial function in women with a history of preeclampsia: An indicator of cardiovascular risk. *American Journal of Physiology - Heart and Circulatory Physiology,* 286**,** H1389-H1393.

AHMAD, S. & AHMED, A. 2004. Elevated placental soluble vascular endothelial growth factor receptor-1 inhibits angiogenesis in preeclampsia. *Circ Res,* 95**,** 884-91.

AHMAD, S. & AHMED, A. 2005. Antiangiogenic effect of soluble vascular endothelial growth factor receptor-1 in placental angiogenesis. *Endothelium,* 12**,** 89-95.

AHMED, A., DUNK, C., AHMAD, S. & KHALIQ, A. 2000. Regulation of placental vascular endothelial growth factor (VEGF) and placenta growth factor (PIGF) and soluble Flt-1 by oxygen - A review. *Placenta,* 21**,** S16-S24.

AHMED, A., SINGH, J., KHAN, Y., SESHAN, S. V. & GIRARDI, G. 2010. A new mouse model to explore therapies for preeclampsia. *PLoS ONE,* 5**,** e13663.

ALEXANDER, B. T., COCKRELL, K. L., MASSEY, M. B., BENNETT, W. A. & GRANGER, J. P. 2002. Tumor necrosis factor-alpha-induced hypertension in pregnant rats results in decreased renal neuronal nitric oxide synthase expression. *Am J Hypertens,* 15**,** 170-5.

ALEXANDER, B. T., KASSAB, S. E., MILLER, M. T., ABRAM, S. R., RECKELHOFF, J. F., BENNETT, W. A. & GRANGER, J. P. 2000. Reduced uterine perfusion pressure during pregnancy in the rat is associated with increases in arterial pressure and changes in renal nitric oxide. *Hypertension,* 37**,** 1191-5.

ANDERS, H. J. & SCHLONDORFF, D. O. 2010. Innate immune receptors and autophagy: Implications for autoimmune kidney injury. *Kidney International,* 78**,** 29-37.

ANDERSON, K. V., BOKLA, L. & NUSSLEIN-VOLHARD, C. 1985. Establishment of dorsal-ventral polarity in the Drosophila embryo: the induction of polarity by the Toll gene product. *Cell,* 42**,** 791-8.

ANDERSON, U. D., OLSSON, M. G., KRISTENSEN, K. H., ÅKERSTRÖM, B. & HANSSON, S. R. 2012. Review: Biochemical markers to predict preeclampsia. *Placenta,* 33**,** S42-S47.

ANTON, L., OLARERIN-GEORGE, A. O., SCHWARTZ, N., SRINIVAS, S., BASTEK, J., HOGENESCH, J. B. & ELOVITZ, M. A. 2013. MiR-210 inhibits trophoblast invasion and is a serum biomarker for preeclampsia. *American Journal of Pathology,* 183**,** 1437-1445.

ARAKI-TAGUCHI, M., NOMURA, S., INO, K., SUMIGAMA, S., YAMAMOTO, E., KOTANI-ITO, T., HAYAKAWA, H., KAJIYAMA, H., SHIBATA, K., ITAKURA, A. & KIKKAWA, F. 2008. Angiotensin II mimics the hypoxic effect on regulating trophoblast proliferation and differentiation in human placental explant cultures. *Life Sciences,* 82**,** 59-67.

ARUMUGAM, T. V., OKUN, E., TANG, S. C., THUNDYIL, J., TAYLOR, S. M. & WOODRUFF, T. M. 2009. Toll-like receptors in ischemia-reperfusion injury. *Shock,* 32**,** 4-16.

AUSTDAL, M., SKRASTAD, R. B., GUNDERSEN, A. S., AUSTGULEN, R., IVERSEN, A. C. & BATHEN, T. F. 2014. Metabolomic biomarkers in serum and urine in women with preeclampsia. *PLoS ONE,* 9.

BANEK, C. T., BAUER, A. J., GINGERY, A. & GILBERT, J. S. 2012. Timing of ischemic insult alters fetal growth trajectory, maternal angiogenic balance, and markers of renal oxidative stress in the pregnant rat. *American Journal of Physiology - Regulatory Integrative and Comparative Physiology,* 303**,** R658-R664.

BARATI, M. T., RANE, M. J., KLEIN, J. B. & MCLEISH, K. R. 2006. A proteomic screen identified stress-induced chaperone proteins as targets of Akt phosphorylation in mesangial cells. *J Proteome Res,* 5**,** 1636-46.

BAUER, S., POLLHEIMER, J., HARTMANN, J., HUSSLEIN, P., APLIN, J. D. & KNOFLER, M. 2004. Tumor necrosis factor-alpha inhibits trophoblast migration through elevation of plasminogen activator inhibitor-1 in first-trimester villous explant cultures. *J Clin Endocrinol Metab,* 89**,** 812-22.

BENBROOK, D. M. & LONG, A. 2012. Integration of autophagy, proteasomal degradation, unfolded protein response and apoptosis. *Exp Oncol,* 34**,** 286-97.

BERGMANN, A., AHMAD, S., CUDMORE, M., GRUBER, A. D., WITTSCHEN, P., LINDENMAIER, W., CHRISTOFORI, G., GROSS, V., GONZALVES, A. C. D. C., GRÃ¶NE, H., AHMED, A. & WEICH, H. A. 2010. Reduction of circulating soluble Flt-1 alleviates preeclampsia-like symptoms in a mouse model. *Journal of Cellular and Molecular Medicine,* 14**,** 1857-1867.

BERRA, E., GINOUVÈS, A. & POUYSSÉGUR, J. 2006. The hypoxia-inducible-factor hydroxylases bring fresh air into hypoxia signalling. *EMBO Reports,* 7**,** 41-45.

BETONI, J. S., DERR, K., PAHL, M. C., ROGERS, L., MULLER, C. L., PACKARD, R. E., CAREY, D. J., KUIVANIEMI, H. & TROMP, G. 2013. MicroRNA analysis in placentas from patients with preeclampsia: Comparison of new and published results. *Hypertension in Pregnancy,* 32**,** 321-339.

BISCHOF, P. 2001. Endocrine, paracrine and autocrine regulation of trophoblastic metalloproteinases. *Early Pregnancy,* 5**,** 30-1.

BOECKEL, J. N., GUARANI, V., KOYANAGI, M., ROEXE, T., LENGELING, A., SCHERMULY, R. T., GELLERT, P., BRAUN, T., ZEIHER, A. & DIMMELER, S. 2011. Jumonji domain-containing protein 6 (Jmjd6) is required for angiogenic sprouting and regulates splicing of VEGF-receptor 1. *Proceedings of the National Academy of Sciences of the United States of America,* 108**,** 3276-3281.

BOEDTKJER, E., PRAETORIUS, J., MATCHKOV, V. V., STANKEVICIUS, E., MOGENSEN, S., FUCHTBAUER, A. C., SIMONSEN, U., FUCHTBAUER, E. M. & AALKJAER, C. 2011. Disruption of Na+,HCO(3)(-) cotransporter NBCn1 (slc4a7) inhibits NO-mediated vasorelaxation, smooth muscle Ca(2)(+) sensitivity, and hypertension development in mice. *Circulation,* 124**,** 1819-29.

BOHLENDER, J., GANTEN, D. & LUFT, F. C. 2000. Rats transgenic for human renin and human angiotensinogen as a model for gestational hypertension. *Journal of the American Society of Nephrology,* 11**,** 2056-2061.

BOMFIM, G. F., DOS SANTOS, R. A., OLIVEIRA, M. A., GIACHINI, F. R., AKAMINE, E. H., TOSTES, R. C., FORTES, Z. B., WEBB, R. C. & CARVALHO, M. H. C. 2012. Toll-like

receptor 4 contributes to blood pressure regulation and vascular contraction in spontaneously hypertensive rats. *Clinical Science,* 122**,** 535-543.
BOTTOMLEY, P. A., FOSTER, T. H., ARGERSINGER, R. E. & PFEIFER, L. M. 1984. A review of normal tissue hydrogen NMR relaxation times and relaxation mechanisms from 1-100 MHz: dependence on tissue type, NMR frequency, temperature, species, excision, and age. *Med Phys,* 11**,** 425-48.
BOYD, P. A. & SCOTT, A. 1985. Quantitative structural studies on human placentas associated with pre-eclampsia, essential hypertension and intrauterine growth retardation. *Br J Obstet Gynaecol,* 92**,** 714-21.
BRADFORD, M. M. 1976. A rapid and sensitive method for the quantitation of microgram quantities of protein utilizing the principle of protein-dye binding. *Anal Biochem,* 72**,** 248-54.
BROSENS, I. A., ROBERTSON, W. B. & DIXON, H. G. 1972. The role of the spiral arteries in the pathogenesis of preeclampsia. *Obstet Gynecol Annu,* 1**,** 177-91.
BROWNE, J. C. & VEALL, N. 1953. The maternal placental blood flow in normotensive and hypertensive women. *J Obstet Gynaecol Br Emp,* 60**,** 141-7.
BURKE, S. D., BARRETTE, V. F., BIANCO, J., THORNE, J. G., YAMADA, A. T., PANG, S. C., ADAMS, M. A. & CROY, B. A. 2010. Spiral arterial remodeling is not essential for normal blood pressure regulation in pregnant mice. *Hypertension,* 55**,** 729-37.
BURTON, G. J., RESHETNIKOVA, O. S., MILOVANOV, A. P. & TELESHOVA, O. V. 1996. Stereological evaluation of vascular adaptations in human placental villi to differing forms of hypoxic stress. *Placenta,* 17**,** 49-55.
BURTON, G. J., WOODS, A. W., JAUNIAUX, E. & KINGDOM, J. C. 2009. Rheological and physiological consequences of conversion of the maternal spiral arteries for uteroplacental blood flow during human pregnancy. *Placenta,* 30**,** 473-82.
BUTT, R. & COORSSEN, J. R. 2006. Pre-extraction sample handling by automated frozen disruption significantly improves subsequent proteomic analyses. *Journal of Proteome Research,* 5**,** 437-448.
BYTAUTIENE, E., LU, F., TAMAYO, E. H., HANKINS, G. D. V., LONGO, M., KUBLICKIENE, K. & SAADE, G. R. 2010. Long-term maternal cardiovascular function in a mouse model of sFlt-1-induced preeclampsia. *American Journal of Physiology - Heart and Circulatory Physiology,* 298.
CANIGGIA, I. & WINTER, J. L. 2002. Adriana and Luisa Castellucci Award Lecture 2001 Hypoxia Inducible Factor-1: Oxygen regulation of trophoblast differentiation in normal and pre-eclamptic pregnancies - A review. *Placenta,* 23**,** S47-S57.
CARLSTROM, M., WENTZEL, P., SKÃ¸TT, O., PERSSON, A. E. G. & ERIKSSON, U. J. 2009. Angiogenesis inhibition causes hypertension and placental dysfunction in a rat model of preeclampsia. *Journal of Hypertension,* 27**,** 829-837.
CARPENTER, S., RICCI, E. P., MERCIER, B. C., MOORE, M. J. & FITZGERALD, K. A. 2014. Post-transcriptional regulation of gene expression in innate immunity. *Nat Rev Immunol,* 14**,** 361-76.
CARTER, A. M. 2007. Animal models of human placentation--a review. *Placenta,* 28 Suppl A**,** S41-7.
CHAKRABORTY, D., RUMI, M. A. K. & SOARES, M. J. 2012. NK cells, hypoxia and trophoblast cell differentiation. *Cell Cycle,* 11**,** 2427-2430.
CHALOUHI, G. E., DELOISON, B., SIAUVE, N., AIMOT, S., BALVAY, D., CUENOD, C. A., VILLE, Y., CLÉMENT, O. & SALOMON, L. J. 2011. Dynamic contrast-enhanced magnetic resonance imaging: Definitive imaging of placental function? *Seminars in Fetal and Neonatal Medicine,* 16**,** 22-28.

CHANG, H. Y., HUANG, H. C., HUANG, T. C., YANG, P. C., WANG, Y. C. & JUAN, H. F. 2012. Ectopic ATP synthase blockade suppresses lung adenocarcinoma growth by activating the unfolded protein response. *Cancer Res,* 72**,** 4696-706.

CHARLTON, F., TOOHER, J., RYE, K. A. & HENNESSY, A. 2014. Cardiovascular risk, lipids and pregnancy: Preeclampsia and the risk of later life cardiovascular disease. *Heart Lung and Circulation,* 23**,** 203-212.

CHARNOCK-JONES, D. S., KAUFMANN, P. & MAYHEW, T. M. 2004. Aspects of human fetoplacental vasculogenesis and angiogenesis. I. Molecular regulation. *Placenta,* 25**,** 103-13.

CHATTERJEE, P., CHIASSON, V. L., KOPRIVA, S. E., YOUNG, K. J., CHATTERJEE, V., JONES, K. A. & MITCHELL, B. M. 2011. Interleukin 10 deficiency exacerbates toll-like receptor 3-induced preeclampsia-like symptoms in mice. *Hypertension,* 58**,** 489-496.

CHATTERJEE, P., WEAVER, L. E., DOERSCH, K. M., KOPRIVA, S. E., CHIASSON, V. L., ALLEN, S. J., NARAYANAN, A. M., YOUNG, K. J., JONES, K. A., KUEHL, T. J. & MITCHELL, B. M. 2012. Placental toll-like receptor 3 and toll-like receptor 7/8 activation contributes to preeclampsia in humans and mice. *PLoS ONE,* 7.

CHEN, S. & LI, X. 2012. Functional magnetic resonance imaging for imaging neural activity in the human brain: the annual progress. *Comput Math Methods Med,* 2012**,** 613465.

CHICHE, J., BRAHIMI-HORN, M. C. & POUYSSÉGUR, J. 2010. Tumour hypoxia induces a metabolic shift causing acidosis: A common feature in cancer. *Journal of Cellular and Molecular Medicine,* 14**,** 771-794.

CHIU, C. L., MORGAN, C. T., LUPTON, S. J. & LIND, J. M. 2013. Parent of origin influences the cardiac expression of vascular endothelial growth factor (Vegfa). *BMC Medical Genetics,* 14.

CLARK, D. E., SMITH, S. K., HE, Y., DAY, K. A., LICENCE, D. R., CORPS, A. N., LAMMOGLIA, R. & CHARNOCK-JONES, D. S. 1998. A vascular endothelial growth factor antagonist is produced by the human placenta and released into the maternal circulation. *Biol Reprod,* 59**,** 1540-8.

COAN, P. M., FERGUSON-SMITH, A. C. & BURTON, G. J. 2004. Developmental dynamics of the definitive mouse placenta assessed by stereology. *Biol Reprod,* 70**,** 1806-13.

CONDE-AGUDELO, A., VILLAR, J. & LINDHEIMER, M. 2008. Maternal infection and risk of preeclampsia: Systematic review and metaanalysis. *American Journal of Obstetrics and Gynecology,* 198**,** 7-22.

CROOK, N. & ROBINSON, L. 2009. A review of the safety implications of magnetic resonance imaging at field strengths of 3 Tesla and above. *Radiography,* 15**,** 351-356.

CROSS, J. C., WERB, Z. & FISHER, S. J. 1994. Implantation and the placenta: key pieces of the development puzzle. *Science,* 266**,** 1508-18.

DAMODARAM, M., STORY, L., EIXARCH, E., PATEL, A., MCGUINNESS, A., ALLSOP, J., WYATT-ASHMEAD, J., KUMAR, S. & RUTHERFORD, M. 2010. Placental MRI in Intrauterine Fetal Growth Restriction. *Placenta,* 31**,** 491-498.

DART, A. M. & KINGWELL, B. A. 2001. Pulse pressure - A review of mechanisms and clinical relevance. *Journal of the American College of Cardiology,* 37**,** 975-984.

DAVIS, E. F., LAZDAM, M., LEWANDOWSKI, A. J., WORTON, S. A., KELLY, B., KENWORTHY, Y., ADWANI, S., WILKINSON, A. R., MCCORMICK, K., SARGENT, I., REDMAN, C. & LEESON, P. 2012. Cardiovascular risk factors in children and young adults born to preeclamptic pregnancies: A systematic review. *Pediatrics,* 129**,** e1552-e1561.

DAVISSON, R. L., HOFFMANN, D. S., BUTZ, G. M., ALDAPE, G., SCHLAGER, G., MERRILL, D. C., SETHI, S., WEISS, R. M. & BATES, J. N. 2002. Discovery of a spontaneous genetic mouse model of preeclampsia. *Hypertension,* 39**,** 337-42.

DAYAN, F., MONTICELLI, M., POUYSSÉGUR, J. & PÉCOU, E. 2009. Gene regulation in response to graded hypoxia: The non-redundant roles of the oxygen sensors PHD and FIH in the HIF pathway. *Journal of Theoretical Biology,* 259**,** 304-316.

DAYAN, F., ROUX, D., BRAHIMI-HORN, M. C., POUYSSEGUR, J. & MAZURE, N. M. 2006. The oxygen sensor factor-inhibiting hypoxia-inducible factor-1 controls expression of distinct genes through the bifunctional transcriptional character of hypoxia-inducible factor-1α. *Cancer Research,* 66**,** 3688-3698.

DEMIR, R., SEVAL, Y. & HUPPERTZ, B. 2007. Vasculogenesis and angiogenesis in the early human placenta. *Acta Histochemica,* 109**,** 257-265.

DENIZOT, Y., LEGUYADER, A., CORNU, E., LASKAR, M., ORSEL, I., VINCENT, C. & NATHAN, N. 2007. Release of soluble vascular endothelial growth factor receptor-1 (sFlt-1) during coronary artery bypass surgery. *Journal of Cardiothoracic Surgery,* 2.

DENNIS, S. C., GEVERS, W. & OPIE, L. H. 1991. Protons in ischemia: Where do they come from; Where do they go to? *Journal of Molecular and Cellular Cardiology,* 23**,** 1077-1086.

DERWIG, I., BARKER, G. J., POON, L., ZELAYA, F., GOWLAND, P., LYTHGOE, D. J. & NICOLAIDES, K. 2013. Association of placental T2 relaxation times and uterine artery Doppler ultrasound measures of placental blood flow. *Placenta,* 34**,** 474-9.

DORIDOT, L., HOURY, D., GAILLARD, H., CHELBI, S. T., BARBAUX, S. & VAIMAN, D. 2014. miR-34A expression, epigenetic regulation, and function in human placental diseases. *Epigenetics,* 9**,** 142-151.

DOROVKOV, M. V., PAVUR, K. S., PETROV, A. N. & RYAZANOV, A. G. 2002. Regulation of elongation factor-2 kinase by pH. *Biochemistry,* 41**,** 13444-13450.

DOZYNKIEWICZ, M. A., JAMIESON, N. B., MACPHERSON, I., GRINDLAY, J., VAN DEN BERGHE, P. V., VON THUN, A., MORTON, J. P., GOURLEY, C., TIMPSON, P., NIXON, C., MCKAY, C. J., CARTER, R., STRACHAN, D., ANDERSON, K., SANSOM, O. J., CASWELL, P. T. & NORMAN, J. C. 2012. Rab25 and CLIC3 collaborate to promote integrin recycling from late endosomes/lysosomes and drive cancer progression. *Developmental cell,* 22**,** 131-145.

DUCKITT, K. & HARRINGTON, D. 2005. Risk factors for pre-eclampsia at antenatal booking: Systematic review of controlled studies. *British Medical Journal,* 330**,** 565-567.

DULEY, L. 2009. The Global Impact of Pre-eclampsia and Eclampsia. *Seminars in Perinatology,* 33**,** 130-137.

DUNCAN, K. R., GOWLAND, P., FRANCIS, S., MOORE, R., BAKER, P. N. & JOHNSON, I. R. 1998. The investigation of placental relaxation and estimation of placental perfusion using echo-planar magnetic resonance imaging. *Placenta,* 19**,** 539-43.

EGBOR, M., ANSARI, T., MORRIS, N., GREEN, C. J. & SIBBONS, P. D. 2006. Pre-eclampsia and Fetal Growth Restriction: How Morphometrically Different is the Placenta? *Placenta,* 27**,** 727-734.

ELIAS, A. P. & DIAS, S. 2008. Microenvironment changes (in pH) affect VEGF alternative splicing. *Cancer Microenvironment,* 1**,** 131-139.

ELICEIRI, B. P. 2001. Integrin and growth factor receptor crosstalk. *Circulation Research,* 89**,** 1104-1110.

ERLEBACHER, A. 2013. Immunology of the Maternal-Fetal Interface. *Annual Review of Immunology,* 31**,** 387-411.

ESPINOZA, J. 2012. The need to redefine preeclampsia. *Expert Opinion on Medical Diagnostics,* 6**,** 347-357.

FAAS, M. M., SCHUILING, G. A., BALLER, J. F., VISSCHER, C. A. & BAKKER, W. W. 1994. A new animal model for human preeclampsia: ultra-low-dose endotoxin infusion in pregnant rats. *Am J Obstet Gynecol,* 171**,** 158-64.

FALCAO, S., STOYANOVA, E., CLOUTIER, G., MAURICE, R. L., GUTKOWSKA, J. & LAVOIE, J. L. 2009. Mice overexpressing both human angiotensinogen and human renin as a model of superimposed preeclampsia on chronic hypertension. *Hypertension,* 54**,** 1401-1407.

FAURE, E., THOMAS, L., XU, H., MEDVEDEV, A., EQUILS, O. & ARDITI, M. 2001. Bacterial lipopolysaccharide and IFN-gamma induce Toll-like receptor 2 and Toll-like receptor 4 expression in human endothelial cells: role of NF-kappa B activation. *J Immunol,* 166**,** 2018-24.

FEST, S., ALDO, P. B., ABRAHAMS, V. M., VISINTIN, I., ALVERO, A., CHEN, R., CHAVEZ, S. L., ROMERO, R. & MOR, G. 2007. Trophoblast-macrophage interactions: A regulatory network for the protection of pregnancy. *American Journal of Reproductive Immunology,* 57**,** 55-66.

FREDE, S., STOCKMANN, C., FREITAG, P. & FANDREY, J. 2006. Bacterial lipopolysaccharide induces HIF-1 activation in human monocytes via p44/42 MAPK and NF-kappaB. *Biochem J,* 396**,** 517-27.

FUKAMACHI, T., IKEDA, S., WANG, X., SAITO, H., TAGAWA, M. & KOBAYASHI, H. 2013. Gene expressions for signal transduction under acidic conditions. *Genes,* 4**,** 65-85.

FUKUMURA, D., XU, L., CHEN, Y., GOHONGI, T., SEED, B. & JAIN, R. K. 2001. Hypoxia and acidosis independently up-regulate vascular endothelial growth factor transcription in brain tumors in vivo. *Cancer Research,* 61**,** 6020-6024.

GENBACEV, O., ZHOU, Y., LUDLOW, J. W. & FISHER, S. J. 1997. Regulation of human placental development by oxygen tension. *Science,* 277**,** 1669-72.

GEORGIADES, P., FERGUSON-SMITH, A. C. & BURTON, G. J. 2002. Comparative developmental anatomy of the murine and human definitive placentae. *Placenta,* 23**,** 3-19.

GHAJAR, C. M., GEORGE, S. C. & PUTNAM, A. J. 2008. Matrix metalloproteinase control of capillary morphogenesis. *Critical Reviews in Eukaryotic Gene Expression,* 18**,** 251-278.

GHUGRE, N. R., RAMANAN, V., POP, M., YANG, Y., BARRY, J., QIANG, B., CONNELLY, K. A., DICK, A. J. & WRIGHT, G. A. 2011. Myocardial BOLD imaging at 3 T using quantitative T 2: Application in a myocardial infarct model. *Magnetic Resonance in Medicine,* 66**,** 1739-1747.

GHUGRE, N. R. & WRIGHT, G. A. 2012. Myocardial BOLD imaging with T2 relaxation. *Open Medical Imaging Journal,* 6**,** 18-30.

GILBERT, J. S., BABCOCK, S. A. & GRANGER, J. P. 2007. Hypertension produced by reduced uterine perfusion in pregnant rats is associated with increased soluble fms-like tyrosine kinase-1 expression. *Hypertension,* 50**,** 1142-7.

GILL, R., TSUNG, A. & BILLIAR, T. 2010. Linking oxidative stress to inflammation: Toll-like receptors. *Free Radical Biology and Medicine,* 48**,** 1121-1132.

GINOUVÈS, A., ILC, K., MACÍAS, N., POUYSSÉGUR, J. & BERRA, E. 2008. PHDs overactivation during chronic hypoxia "desensitizes" HIFα and protects cells from necrosis. *Proceedings of the National Academy of Sciences of the United States of America,* 105**,** 4745-4750.

GIRARDI, G., YARILIN, D., THURMAN, J. M., HOLERS, V. M. & SALMON, J. E. 2006. Complement activation induces dysregulation of angiogenic factors and causes fetal rejection and growth restriction. *Journal of Experimental Medicine,* 203**,** 2165-2175.

GIRSH, E., PLAKS, V., GILAD, A. A., NEVO, N., SCHECHTMAN, E., NEEMAN, M. & DEKEL, N. 2007. Cloprostenol, a prostaglandin F(2alpha) analog, induces hypoxia in rat placenta: BOLD contrast MRI. *NMR Biomed,* 20**,** 28-39.

GOLDMAN-WOHL, D. & YAGEL, S. 2008. NK cells and pre-eclampsia. *Reproductive biomedicine online,* 16**,** 227-231.
GOWLAND, P. 2005. Placental MRI. *Seminars in Fetal and Neonatal Medicine,* 10**,** 485-490.
GOWLAND, P. A., FRANCIS, S. T., DUNCAN, K. R., FREEMAN, A. J., ISSA, B., MOORE, R. J., BOWTELL, R. W., BAKER, P. N., JOHNSON, I. R. & WORTHINGTON, B. S. 1998. In vivo perfusion measurements in the human placenta using echo planar imaging at 0.5 T. *Magnetic Resonance in Medicine,* 40**,** 467-473.
GRAHAM, R. M., FRAZIER, D. P., THOMPSON, J. W., HALIKO, S., LI, H., WASSERLAUF, B. J., SPIGA, M. G., BISHOPRIC, N. H. & WEBSTER, K. A. 2004. A unique pathway of cardiac myocyte death caused by hypoxia-acidosis. *Journal of Experimental Biology,* 207**,** 3189-3200.
GROTE, K., SCHUTT, H. & SCHIEFFER, B. 2011. Toll-like receptors in angiogenesis. *ScientificWorldJournal,* 11**,** 981-91.
HADDAD, J. J. & LAND, S. C. 2001. A non-hypoxic, ROS-sensitive pathway mediates TNF-α-dependent regulation of HIF-1α. *FEBS Letters,* 505**,** 269-274.
HAYAKAWA, S., FUJIKAWA, T., FUKUOKA, H., CHISIMA, F., KARASAKI-SUZUKI, M., OHKOSHI, E., OHI, H., KIYOSHI FUJII, T., TOCHIGI, M., SATOH, K., SHIMIZU, T., NISHINARITA, S., NEMOTO, N. & SAKURAI, I. 2000. Murine fetal resorption and experimental pre-eclampsia are induced by both excessive Th1 and Th2 activation. *J Reprod Immunol,* 47**,** 121-38.
HE, W., MIAO, F. J. P., LIN, D. C. H., SCHWANDNER, R. T., WANG, Z., GAO, J., CHEN, J. L., TLAN, H. & LING, L. 2004. Citric acid cycle intermediates as ligands for orphan G-protein-coupled receptors. *Nature,* 429**,** 188-193.
HE, Y., SMITH, S. K., DAY, K. A., CLARK, D. E., LICENCE, D. R. & CHARNOCK-JONES, D. S. 1999. Alternative splicing of vascular endothelial growth factor (VEGF)-R1 (FLT-1) pre-mRNA is important for the regulation of VEGF activity. *Mol Endocrinol,* 13**,** 537-45.
HENNESSY, A., PILMORE, H. L., SIMMONS, L. A. & PAINTER, D. M. 1999. A deficiency of placental IL-10 in preeclampsia. *J Immunol,* 163**,** 3491-5.
HIGGINBOTHAM, M. B., MORRIS, K. G., WILLIAMS, S., MCHALE, P. A., COLEMAN, R. E. & COBB, F. R. 1986. Regulation of stroke volume during submaximal and maximal upright exercise in normal man. *Circulation Research,* 58**,** 281-291.
HIRASHIMA, C., OHKUCHI, A., ARAI, F., TAKAHASHI, K., SUZUKI, H., WATANABE, T., KARIO, K., MATSUBARA, S. & SUZUKI, M. 2005. Establishing reference values for both total soluble Fms-like tyrosine kinase 1 and free placental growth factor in pregnant women. *Hypertension Research,* 28**,** 727-732.
HIRSILA, M., KOIVUNEN, P., GUNZLER, V., KIVIRIKKO, K. I. & MYLLYHARJU, J. 2003. Characterization of the human prolyl 4-hydroxylases that modify the hypoxia-inducible factor. *J Biol Chem,* 278**,** 30772-80.
HOWARD, C. & REED, N. B. 2005. Unbiased Stereology: Three Dimensional Measurement in Microscopy.
HOYER-HANSEN, M. & JAATTELA, M. 2007. Connecting endoplasmic reticulum stress to autophagy by unfolded protein response and calcium. *Cell Death Differ,* 14**,** 1576-82.
HSU, P. & NANAN, R. K. H. 2014. Innate and adaptive immune interactions at the fetal-maternal interface in healthy human pregnancy and pre-eclampsia. *Frontiers in Immunology,* 5.
HUCKLE, W. R. & ROCHE, R. I. 2004. Post-transcriptional control of expression of sFlt-1, an endogenous inhibitor of vascular endothelial growth factor. *J Cell Biochem,* 93**,** 120-32.
HUEBENER, P. & SCHWABE, R. F. 2013. Regulation of wound healing and organ fibrosis by toll-like receptors. *Biochim Biophys Acta,* 1832**,** 1005-17.

HUPPERTZ, B. 2008. The anatomy of the normal placenta. *Journal of Clinical Pathology,* 61**,** 1296-302.

HUPPERTZ, B., GAUSTER, M., ORENDI, K., KÖNIG, J. & MOSER, G. 2009. Oxygen as modulator of trophoblast invasion. *Journal of Anatomy,* 215**,** 14-20.

HUPPERTZ, B. & PEETERS, L. L. H. 2005. Vascular biology in implantation and placentation. *Angiogenesis,* 8**,** 157-167.

HUPPERTZ, B., WEISS, G. & MOSER, G. 2013. Trophoblast invasion and oxygenation of the placenta: measurements versus presumptions. *Journal of reproductive immunology*.

IANOSI-IRIMIE, M., VU, H. V., WHITBRED, J. M., PRIDJIAN, C. A., NADIG, J. D., WILLIAMS, M. Y., WRENN, D. C., PRIDJIAN, G. & PUSCHETT, J. B. 2005. A rat model of preeclampsia. *Clin Exp Hypertens,* 27**,** 605-17.

IKEDA, E., ACHEN, M. G., BREIER, G. & RISAU, W. 1995. Hypoxia-induced transcriptional activation and increased mRNA stability of vascular endothelial growth factor in C6 glioma cells. *J Biol Chem,* 270**,** 19761-6.

IMHOF, B. A. & AURRAND-LIONS, M. 2006. Angiogenesis and inflammation face off. *Nature Medicine,* 12**,** 171-172.

IMTIYAZ, H. Z. & SIMON, M. C. 2010. Hypoxia-inducible factors as essential regulators of inflammation. *Current topics in microbiology and immunology,* 345**,** 105-120.

IRANI, R. A., ZHANG, Y., ZHOU, C. C., BLACKWELL, S. C., HICKS, M. J., RAMIN, S. M., KELLEMS, R. E. & XIA, Y. 2010. Autoantibody-mediated angiotensin receptor activation contributes to preeclampsia through tumor necrosis factor-alpha signaling. *Hypertension,* 55**,** 1246-53.

JAUNIAUX, E., WATSON, A. L., HEMPSTOCK, J., BAO, Y. P., SKEPPER, J. N. & BURTON, G. J. 2000. Onset of maternal arterial blood flow and placental oxidative stress. A possible factor in human early pregnancy failure. *Am J Pathol,* 157**,** 2111-22.

JAVOR, D., NASEL, C., SCHWEIM, T., DEKAN, S., CHALUBINSKI, K. & PRAYER, D. 2013. In vivo assessment of putative functional placental tissue volume in placental intrauterine growth restriction (IUGR) in human fetuses using diffusion tensor magnetic resonance imaging. *Placenta,* 34**,** 676-80.

JEHENSON, P., LEROY-WILLIG, A., DE KERVILER, E., DUBOC, D. & SYROTA, A. 1993. MR imaging as a potential diagnostic test for metabolic myopathies: importance of variations in the T2 of muscle with exercise. *AJR Am J Roentgenol,* 161**,** 347-51.

JUNG, J. J., TIWARI, A., INAMDAR, S. M., THOMAS, C. P., GOEL, A. & CHOUDHURY, A. 2012. Secretion of Soluble Vascular Endothelial Growth Factor Receptor 1 (sVEGFR1/sFlt1) Requires Arf1, Arf6, and Rab11 GTPases. *PLoS ONE,* 7.

KALKUNTE, S., BOIJ, R., NORRIS, W., FRIEDMAN, J., LAI, Z., KURTIS, J., LIM, K. H., PADBURY, J. F., MATTHIESEN, L. & SHARMA, S. 2010. Sera from preeclampsia patients elicit symptoms of human disease in mice and provide a basis for an in vitro predictive assay. *Am J Pathol,* 177**,** 2387-98.

KALKUNTE, S. S., NEUBECK, S., NORRIS, W. E., CHENG, S. B., KOSTADINOV, S., VU HOANG, D., AHMED, A., VON EGGELING, F., SHAIKH, Z., PADBURY, J., BERG, G., OLOFSSON, A., MARKERT, U. R. & SHARMA, S. 2013. Transthyretin is dysregulated in preeclampsia, and its native form prevents the onset of disease in a preclinical mouse model. *American Journal of Pathology,* 183**,** 1425-1436.

KANASAKI, K. & KALLURI, R. 2009. The biology of preeclampsia. *Kidney International,* 76**,** 831-837.

KANASAKI, K., PALMSTEN, K., SUGIMOTO, H., AHMAD, S., HAMANO, Y., XIE, L., PARRY, S., AUGUSTIN, H. G., GATTONE JR, V. H., FOLKMAN, J., STRAUSS, J. F. & KALLURI, R. 2008. Deficiency in catechol-O-methyltransferase and 2-methoxyoestradiol is associated with pre-eclampsia. *Nature,* 453**,** 1117-1121.

KANE, L. A., YOUNGMAN, M. J., JENSEN, R. E. & VAN EYK, J. E. 2010. Phosphorylation of the F(1)F(o) ATP synthase beta subunit: functional and structural consequences assessed in a model system. *Circ Res,* 106**,** 504-13.

KARUMANCHI, S. A., MAYNARD, S. E., STILLMAN, I. E., EPSTEIN, F. H. & SUKHATME, V. P. 2005. Preeclampsia: a renal perspective. *Kidney Int,* 67**,** 2101-13.

KATO, Y., LAMBERT, C. A., COLIGE, A. C., MINEUR, P., NOËL, A., FRANKENNE, F., FOIDART, J. M., BABA, M., HATA, R. I., MIYAZAKI, K. & TSUKUDA, M. 2005. Acidic extracellular pH induces matrix metalloproteinase-9 expression in mouse metastatic melanoma cells through the phospholipase D-mitogen-activated protein kinase signaling. *Journal of Biological Chemistry,* 280**,** 10938-10944.

KAUFMANN, P., BLACK, S. & HUPPERTZ, B. 2003. Endovascular trophoblast invasion: implications for the pathogenesis of intrauterine growth retardation and preeclampsia. *Biol Reprod,* 69**,** 1-7.

KAWAI, T. & AKIRA, S. 2009. The roles of TLRs, RLRs and NLRs in pathogen recognition. *International Immunology,* 21**,** 317-337.

KEELER, J. 2010. *Understanding NMR spectroscopy,* Chichester, U.K., John Wiley and Sons.

KENDALL, R. L., WANG, G. & THOMAS, K. A. 1996. Identification of a natural soluble form of the vascular endothelial growth factor receptor, FLT-1, and its heterodimerization with KDR. *Biochem Biophys Res Commun,* 226**,** 324-8.

KENNY, L. C., BROADHURST, D. I., DUNN, W., BROWN, M., NORTH, R. A., MCCOWAN, L., ROBERTS, C., COOPER, G. J., KELL, D. B., BAKER, P. N. & SCREENING FOR PREGNANCY ENDPOINTS, C. 2010. Robust early pregnancy prediction of later preeclampsia using metabolomic biomarkers. *Hypertension,* 56**,** 741-9.

KIM, H. Y., KIM, Y. H., NAM, B. H., KONG, H. J., KIM, H. H., KIM, Y. J., AN, W. G. & CHEONG, J. 2007. HIF-1α expression in response to lipopolysaccaride mediates induction of hepatic inflammatory cytokine TNFα. *Experimental Cell Research,* 313**,** 1866-1876.

KIM, S. Y., CHOI, Y. J., JOUNG, S. M., LEE, B. H., JUNG, Y. S. & LEE, J. Y. 2010. Hypoxic stress up-regulates the expression of Toll-like receptor 4 in macrophages via hypoxia-inducible factor. *Immunology,* 129**,** 516-24.

KIM, Y. M., ROMERO, R., OH, S. Y., KIM, C. J., KILBURN, B. A., ARMANT, D. R., NIEN, J. K., GOMEZ, R., MAZOR, M., SAITO, S., ABRAHAMS, V. M. & MOR, G. 2005. Toll-like receptor 4: a potential link between "danger signals," the innate immune system, and preeclampsia? *Am J Obstet Gynecol,* 193**,** 921-7.

KNÖFLER, M. & POLLHEIMER, J. 2012. IFPA Award in Placentology Lecture: Molecular regulation of human trophoblast invasion. *Placenta,* 33**,** S55-S62.

KOGA, K., ALDO, P. B. & MOR, G. 2009. Toll-like receptors and pregnancy: Trophoblast as modulators of the immune response. *Journal of Obstetrics and Gynaecology Research,* 35**,** 191-202.

KOGA, K. & MOR, G. 2010. Toll-Like Receptors at the Maternal-Fetal Interface in Normal Pregnancy and Pregnancy Disorders. *American Journal of Reproductive Immunology,* 63**,** 587-600.

KUBASIAK, L. A., HERNANDEZ, O. M., BISHOPRIC, N. H. & WEBSTER, K. A. 2002. Hypoxia and acidosis activate cardiac myocyte death through the Bcl-2 family protein BNIP3. *Proceedings of the National Academy of Sciences of the United States of America,* 99**,** 12825-12830.

LAGADIC-GOSSMANN, D., HUC, L. & LECUREUR, V. 2004. Alterations of intracellular pH homeostasis in apoptosis: Origins and roles. *Cell Death and Differentiation,* 11**,** 953-961.

LAMARCA, B. 2012. Endothelial dysfunction. An important mediator in the pathophysiology of hypertension during pre-eclampsia. *Minerva Ginecologica,* 64**,** 309-320.

LAMARCA, B., PARRISH, M., RAY, L. F., MURPHY, S. R., ROBERTS, L., GLOVER, P., WALLUKAT, G., WENZEL, K., COCKRELL, K., MARTIN, J. N., RYAN, M. J. & DECHEND, R. 2009. Hypertension in response to autoantibodies to the angiotensin II type i receptor (AT1-AA) in pregnant rats: Role of endothelin-1. *Hypertension,* 54**,** 905-909.

LAMARCA, B., PARRISH, M. R. & WALLACE, K. 2012. Agonistic autoantibodies to the angiotensin II type i receptor cause pathophysiologic characteristics of preeclampsia. *Gender Medicine,* 9**,** 139-146.

LAMARCA, B., SPEED, J., FOURNIER, L., BABCOCK, S. A., BERRY, H., COCKRELL, K. & GRANGER, J. P. 2008a. Hypertension in response to chronic reductions in uterine perfusion in pregnant rats: effect of tumor necrosis factor-alpha blockade. *Hypertension,* 52**,** 1161-7.

LAMARCA, B., WALLUKAT, G., LLINAS, M., HERSE, F., DECHEND, R. & GRANGER, J. P. 2008b. Autoantibodies to the angiotensin type I receptor in response to placental ischemia and tumor necrosis factor alpha in pregnant rats. *Hypertension,* 52**,** 1168-72.

LAMARCA, B. B., BENNETT, W. A., ALEXANDER, B. T., COCKRELL, K. & GRANGER, J. P. 2005. Hypertension produced by reductions in uterine perfusion in the pregnant rat: role of tumor necrosis factor-alpha. *Hypertension,* 46**,** 1022-5.

LANDO, D., PEET, D. J., GORMAN, J. J., WHELAN, D. A., WHITELAW, M. L. & BRUICK, R. K. 2002. FIH-1 is an asparaginyl hydroxylase enzyme that regulates the transcriptional activity of hypoxia-inducible factor. *Genes and Development,* 16**,** 1466-1471.

LANG, K. J. D., KAPPEL, A. & GOODALL, G. J. 2002. Hypoxia-inducible factor-1α mRNA contains an internal ribosome entry site that allows efficient translation during normoxia and hypoxia. *Molecular Biology of the Cell,* 13**,** 1792-1801.

LE BIHAN, D. 2007. The 'wet mind': water and functional neuroimaging. *Phys Med Biol,* 52**,** R57-90.

LE BIHAN, D., BRETON, E., LALLEMAND, D., AUBIN, M. L., VIGNAUD, J. & LAVAL-JEANTET, M. 1988. Separation of diffusion and perfusion in intravoxel incoherent motion MR imaging. *Radiology,* 168**,** 497-505.

LE BIHAN, D., BRETON, E., LALLEMAND, D., GRENIER, P., CABANIS, E. & LAVAL-JEANTET, M. 1986. MR imaging of intravoxel incoherent motions: application to diffusion and perfusion in neurologic disorders. *Radiology,* 161**,** 401-7.

LEBER, A., TELES, A. & ZENCLUSSEN, A. C. 2010. Regulatory T Cells and Their Role in Pregnancy. *American Journal of Reproductive Immunology,* 63**,** 445-459.

LEMAITRE, B. 2004. The road to Toll. *Nat Rev Immunol,* 4**,** 521-7.

LENO-DURAN, E., HATTA, K., BIANCO, J., YAMADA, Ã. T., RUIZ-RUIZ, C., OLIVARES, E. G. & CROY, B. A. 2010. Fetal-placental hypoxia does not result from failure of spiral arterial modification in mice. *Placenta,* 31**,** 731-737.

LEVINE, R. J., MAYNARD, S. E., QIAN, C., LIM, K. H., ENGLAND, L. J., YU, K. F., SCHISTERMAN, E. F., THADHANI, R., SACHS, B. P., EPSTEIN, F. H., SIBAI, B. M., SUKHATME, V. P. & KARUMANCHI, S. A. 2004. Circulating angiogenic factors and the risk of preeclampsia. *N Engl J Med,* 350**,** 672-83.

LEVITT, M. 2008. *Spin Dynamics - Basics of Nuclear Magnetic Resonance,* Chichester, Wiley.

LI, J. Y. Z., YONG, T. Y., MICHAEL, M. Z. & GLEADLE, J. M. 2014. MicroRNAs: Are they the missing link between hypoxia and pre-eclampsia? *Hypertension in Pregnancy,* 33**,** 102-114.

LITTLER, D. R., HARROP, S. J., GOODCHILD, S. C., PHANG, J. M., MYNOTT, A. V., JIANG, L., VALENZUELA, S. M., MAZZANTI, M., BROWN, L. J., BREIT, S. N. & CURMI, P. M. G. 2010. The enigma of the CLIC proteins: Ion channels, redox proteins, enzymes, scaffolding proteins? *FEBS Letters,* 584**,** 2093-2101.

LIU, L. Y., YANG, T., JI, J., WEN, Q., MORGAN, A. A., JIN, B., CHEN, G., LYELL, D. J., STEVENSON, D. K., LING, X. B. & BUTTE, A. J. 2013. Integrating multiple 'omics'

analyses identifies serological protein biomarkers for preeclampsia. *BMC Medicine,* 11.
LIVAK, K. J. & SCHMITTGEN, T. D. 2001. Analysis of relative gene expression data using real-time quantitative PCR and the 2(-Delta Delta C(T)) Method. *Methods,* 25**,** 402-8.
LOUIE, E. A., GOCHBERG, D. F., DOES, M. D. & DAMON, B. M. 2009. Transverse relaxation and magnetization transfer in skeletal muscle: effect of pH. *Magn Reson Med,* 61**,** 560-9.
LU, F., LONGO, M., TAMAYO, E., MANER, W., AL-HENDY, A., ANDERSON, G. D., HANKINS, G. D. V. & SAADE, G. R. 2007. The effect of over-expression of sFlt-1 on blood pressure and the occurrence of other manifestations of preeclampsia in unrestrained conscious pregnant mice. *American Journal of Obstetrics and Gynecology,* 196.
LU, J., ZHANG, S., NAKANO, H., SIMMONS, D. G., WANG, S., KONG, S., WANG, Q., SHEN, L., TU, Z., WANG, W., WANG, B., WANG, H., WANG, Y., VAN ES, J. H., CLEVERS, H., LEONE, G. & CROSS, J. C. 2013. A Positive Feedback Loop Involving Gcm1 and Fzd5 Directs Chorionic Branching Morphogenesis in the Placenta. *PLoS Biology,* 11.
LUCIANI, A., VIGNAUD, A., CAVET, M., NHIEU, J. T., MALLAT, A., RUEL, L., LAURENT, A., DEUX, J. F., BRUGIERES, P. & RAHMOUNI, A. 2008. Liver cirrhosis: intravoxel incoherent motion MR imaging--pilot study. *Radiology,* 249**,** 891-9.
MA, Z., CAO, M., LIU, Y., HE, Y., WANG, Y., YANG, C., WANG, W., DU, Y., ZHOU, M. & GAO, F. 2010. Mitochondrial F1Fo-ATP synthase translocates to cell surface in hepatocytes and has high activity in tumor-like acidic and hypoxic environment. *Acta Biochimica et Biophysica Sinica,* 42**,** 530-537.
MAKRIS, A., THORNTON, C., THOMPSON, J., THOMSON, S., MARTIN, R., OGLE, R., WAUGH, R., MCKENZIE, P., KIRWAN, P. & HENNESSY, A. 2007. Uteroplacental ischemia results in proteinuric hypertension and elevated sFLT-1. *Kidney Int,* 71**,** 977-84.
MALHOTRA, J. D. & KAUFMAN, R. J. 2007. Endoplasmic reticulum stress and oxidative stress: a vicious cycle or a double-edged sword? *Antioxid Redox Signal,* 9**,** 2277-93.
MANDRIOTA, S. J. & PEPPER, M. S. 1998. Regulation of angiopoietin-2 mRNA levels in bovine microvascular endothelial cells by cytokines and hypoxia. *Circ Res,* 83**,** 852-9.
MANKA, R., PAETSCH, I., SCHNACKENBURG, B., GEBKER, R., FLECK, E. & JAHNKE, C. 2010. BOLD cardiovascular magnetic resonance at 3.0 tesla in myocardial ischemia. *J Cardiovasc Magn Reson,* 12**,** 54.
MATZINGER, P. 2002. The danger model: a renewed sense of self. *Science,* 296**,** 301-5.
MAXWELL, P. H., WIESENER, M. S., CHANG, G. W., CLIFFORD, S. C., VAUX, E. C., COCKMAN, M. E., WYKOFF, C. C., PUGH, C. W., MAHER, E. R. & RATCLIFFE, P. J. 1999. The tumour suppressor protein VHL targets hypoxia-inducible factors for oxygen-dependent proteolysis. *Nature,* 399**,** 271-5.
MAYHEW, T. M. 2003. Changes in fetal capillaries during preplacental hypoxia: Growth, shape remodelling and villous capillarization in placentae from high-altitude pregnancies. *Placenta,* 24**,** 191-198.
MAYHEW, T. M. 2009. A stereological perspective on placental morphology in normal and complicated pregnancies. *J Anat,* 215**,** 77-90.
MAYHEW, T. M., MANWANI, R., OHADIKE, C., WIJESEKARA, J. & BAKER, P. N. 2007. The Placenta in Pre-eclampsia and Intrauterine Growth Restriction: Studies on Exchange Surface Areas, Diffusion Distances and Villous Membrane Diffusive Conductances. *Placenta,* 28**,** 233-238.
MAYHEW, T. M., WIJESEKARA, J., BAKER, P. N. & ONG, S. S. 2004. Morphometric evidence that villous development and fetoplacental angiogenesis are compromised by intrauterine growth restriction but not by pre-eclampsia. *Placenta,* 25**,** 829-833.

MAYNARD, S., EPSTEIN, F. H. & KARUMANCHI, S. A. 2008. Preeclampsia and angiogenic imbalance. *Annu Rev Med,* 59**,** 61-78.

MAYNARD, S. E., MIN, J. Y., MERCHAN, J., LIM, K. H., LI, J., MONDAL, S., LIBERMANN, T. A., MORGAN, J. P., SELLKE, F. W., STILLMAN, I. E., EPSTEIN, F. H., SUKHATME, V. P. & KARUMANCHI, S. A. 2003a. Excess placental soluble fms-like tyrosine kinase 1 (sFlt1) may contribute to endothelial dysfunction hypertension, and proteinuria in preeclampsia. *Journal of Clinical Investigation,* 111**,** 649-658.

MAYNARD, S. E., MIN, J. Y., MERCHAN, J., LIM, K. H., LI, J., MONDAL, S., LIBERMANN, T. A., MORGAN, J. P., SELLKE, F. W., STILLMAN, I. E., EPSTEIN, F. H., SUKHATME, V. P. & KARUMANCHI, S. A. 2003b. Excess placental soluble fms-like tyrosine kinase 1 (sFlt1) may contribute to endothelial dysfunction, hypertension, and proteinuria in preeclampsia. *J Clin Invest,* 111**,** 649-58.

MAYNARD, S. E., VENKATESHA, S., THADHANI, R. & KARUMANCHI, S. A. 2005. Soluble Fms-like tyrosine kinase 1 and endothelial dysfunction in the pathogenesis of preeclampsia. *Pediatr Res,* 57**,** 1R-7R.

MCARDLE, A. M., DENTON, K. M., MADUWEGEDERA, D., MORITZ, K., FLOWER, R. L. & ROBERTS, C. T. 2009. Ontogeny of placental structural development and expression of the renin-angiotensin system and 11beta-HSD2 genes in the rabbit. *Placenta,* 30**,** 590-8.

MCGETTRICK, A. F. & O'NEILL, L. A. J. 2013. How metabolism generates signals during innate immunity and inflammation. *Journal of Biological Chemistry,* 288**,** 22893-22898.

MEYER, M. E., YU, O., ECLANCHER, B., GRUCKER, D. & CHAMBRON, J. 1995. NMR relaxation rates and blood oxygenation level. *Magn Reson Med,* 34**,** 234-41.

MINASSIAN, C., THOMAS, S. L., WILLIAMS, D. J., CAMPBELL, O. & SMEETH, L. 2013. Acute Maternal Infection and Risk of Pre-Eclampsia: A Population-Based Case-Control Study. *PLoS ONE,* 8**,** e73047.

MINCHENKO, A. & CARO, J. 2000. Regulation of endothelin-1 gene expression in human microvascular endothelial cells by hypoxia and cobalt: role of hypoxia responsive element. *Mol Cell Biochem,* 208**,** 53-62.

MOLLEN, K. P., ANAND, R. J., TSUNG, A., PRINCE, J. M., LEVY, R. M. & BILLIAR, T. R. 2006. Emerging paradigm: Toll-like receptor 4 - Sentinel for the detection of tissue damage. *Shock,* 26**,** 430-437.

MONEY, T. T., KING, R. G., WONG, M. H., STEVENSON, J. L., KALIONIS, B., ERWICH, J. J. H. M., HUISMAN, M. A., TIMMER, A., HIDEN, U., DESOYE, G. & GUDE, N. M. 2007. Expression and Cellular Localisation of Chloride Intracellular Channel 3 in Human Placenta and Fetal Membranes. *Placenta,* 28**,** 429-436.

MOORE, R. J., ISSA, B., TOKARCZUK, P., DUNCAN, K. R., BOULBY, P., BAKER, P. N., BOWTELL, R. W., WORTHINGTON, B. S., JOHNSON, I. R. & GOWLAND, P. A. 2000a. In vivo intravoxel incoherent motion measurements in the human placenta using echo-planar imaging at 0.5 T. *Magnetic Resonance in Medicine,* 43**,** 295-302.

MOORE, R. J., STRACHAN, B. K., TYLER, D. J., DUNCAN, K. R., BAKER, P. N., WORTHINGTON, B. S., JOHNSON, I. R. & GOWLAND, P. A. 2000g. In utero perfusing fraction maps in normal and growth restricted pregnancy measured using IVIM echo-planar MRI. *Placenta,* 21**,** 726-732.

MOUTON, P. R. (ed.) 2002. *Principles and Practices of Unbiased Stereology: An Introduction for Bioscientists,* Baltimore: The John Hopkins University Press.

MU, J. & ADAMSON, S. L. 2006. Developmental changes in hemodynamics of uterine artery, utero- and umbilicoplacental, and vitelline circulations in mouse throughout gestation. *Am J Physiol Heart Circ Physiol,* 291**,** H1421-8.

MUNTENER, M. & HSU, Y. C. 1977. Development of trophoblast and placenta of the mouse. A reinvestigation with regard to the in vitro culture of mouse trophoblast and placenta. *Acta Anat (Basel),* 98**,** 241-52.

MURPHY, S. R., LAMARCA, B. B. D., COCKRELL, K. & GRANGER, J. P. 2010. Role of endothelin in mediating soluble fms-like tyrosine kinase 1-induced hypertension in pregnant rats. *Hypertension,* 55**,** 394-398.

MURPHY, S. R., LAMARCA, B. B. D., PARRISH, M., COCKRELL, K. & GRANGER, J. P. 2013. Control of soluble fms-like tyrosine-1 (sFlt-1) production response to placental ischemia/hypoxia: Role of tumor necrosis factor-α. *American Journal of Physiology - Regulatory Integrative and Comparative Physiology,* 304**,** R130-R135.

MURTHI, P., STEVENSON, J. L., MONEY, T. T., BORG, A. J., BRENNECKE, S. P. & GUDE, N. M. 2012. Placental CLIC3 is increased in fetal growth restriction and pre-eclampsia affected human pregnancies. *Placenta,* 33**,** 741-744.

MUZIO, M., BOSISIO, D., POLENTARUTTI, N., D'AMICO, G., STOPPACCIARO, A., MANCINELLI, R., VAN'T VEER, C., PENTON-ROL, G., RUCO, L. P., ALLAVENA, P. & MANTOVANI, A. 2000. Differential expression and regulation of toll-like receptors (TLR) in human leukocytes: Selective expression of TLR3 in dendritic cells. *Journal of Immunology,* 164**,** 5998-6004.

NAGAMATSU, T., FUJII, T., KUSUMI, M., ZOU, L., YAMASHITA, T., OSUGA, Y., MOMOEDA, M., KOZUMA, S. & TAKETANI, Y. 2004. Cytotrophoblasts up-regulate soluble Fms-like tyrosine kinase-1 expression under reduced oxygen: An implication for the placental vascular development and the pathophysiology of preeclampsia. *Endocrinology,* 145**,** 4838-4845.

NAKADA, E., WALLEY, K. R., NAKADA, T., HU, Y., VON DADELSZEN, P. & BOYD, J. H. 2009. Toll-like Receptor-3 Stimulation Upregulates sFLT-1 Production by Trophoblast Cells. *Placenta,* 30**,** 774-779.

NAKASHIMA, A., YAMANAKA-TATEMATSU, M., FUJITA, N., KOIZUMI, K., SHIMA, T., YOSHIDA, T., NIKAIDO, T., OKAMOTO, A., YOSHIMORI, T. & SAITO, S. 2013. Impaired autophagy by soluble endoglin, under physiological hypoxia in early pregnant period, is involved in poor placentation in preeclampsia. *Autophagy,* 9**,** 303-16.

NESS, R. B. & ROBERTS, J. M. 1996. Heterogeneous causes constituting the single syndrome of preeclampsia: A hypothesis and its implications. *American Journal of Obstetrics and Gynecology,* 175**,** 1365-1370.

NEVO, O., SOLEYMANLOU, N., WU, Y., XU, J., KINGDOM, J., MANY, A., ZAMUDIO, S. & CANIGGIA, I. 2006. Increased expression of sFlt-1 in in vivo and in vitro models of human placental hypoxia is mediated by HIF-1. *Am J Physiol Regul Integr Comp Physiol,* 291**,** R1085-93.

NISHIZAWA, H., HASEGAWA, K., SUZUKI, M., ACHIWA, Y., KATO, T., SAITO, K., KURAHASHI, H. & UDAGAWA, Y. 2008. Mouse model for allogeneic immune reaction against fetus recapitulates human pre-eclampsia. *The journal of obstetrics and gynaecology research,* 34**,** 1-6.

NIZET, V. & JOHNSON, R. S. 2009. Interdependence of hypoxic and innate immune responses. *Nature Reviews Immunology,* 9**,** 609-617.

NOLTE, I., GORBEY, S., BOLL, H., FIGUEIREDO, G., GRODEN, C., LEMMER, B. & BROCKMANN, M. A. 2011. Maintained functionality of an implantable radiotelemetric blood pressure and heart rate sensor after magnetic resonance imaging in rats. *Physiol Meas,* 32**,** 1941-51.

NUSSLEIN-VOLHARD, C. & WIESCHAUS, E. 1980. Mutations affecting segment number and polarity in Drosophila. *Nature,* 287**,** 795-801.

O'NEILL, L. A. 2014. Glycolytic reprogramming by TLRs in dendritic cells. *Nat Immunol,* 15**,** 314-5.

OGAWA, S., LEE, T. M., NAYAK, A. S. & GLYNN, P. 1990. Oxygenation-sensitive contrast in magnetic resonance image of rodent brain at high magnetic fields. *Magn Reson Med,* 14**,** 68-78.

OLMOS, G., CONDE, I., ARENAS, I., DEL PESO, L., CASTELLANOS, C., LANDAZURI, M. O. & LUCIO-CAZANA, J. 2007. Accumulation of hypoxia-inducible factor-1alpha through a novel electrophilic, thiol antioxidant-sensitive mechanism. *Cell Signal,* 19**,** 2098-105.

ONOGI, A., NARUSE, K., SADO, T., TSUNEMI, T., SHIGETOMI, H., NOGUCHI, T., YAMADA, Y., AKASAKI, M., OI, H. & KOBAYASHI, H. 2011. Hypoxia inhibits invasion of extravillous trophoblast cells through reduction of matrix metalloproteinase (MMP)-2 activation in the early first trimester of human pregnancy. *Placenta,* 32**,** 665-670.

ORANGE, S., RASKO, J. E., THOMPSON, J. F., VAUGHAN, J., OLIVE, E., PEDLER, M., HORVATH, J. S. & HENNESSY, A. 2005. Interleukin-10 regulates arterial pressure in early primate pregnancy. *Cytokine,* 29**,** 176-85.

ORIJ, R., BRUL, S. & SMITS, G. J. 2011. Intracellular pH is a tightly controlled signal in yeast. *Biochimica et Biophysica Acta - General Subjects,* 1810**,** 933-944.

OSANAI, T., TANAKA, M., MAGOTA, K., TOMITA, H. & OKUMURA, K. 2012. Coupling factor 6-induced activation of ecto-F 1F o complex induces insulin resistance, mild glucose intolerance and elevated blood pressure in mice. *Diabetologia,* 55**,** 520-529.

OZRETIĆ, P., BISIO, A., INGA, A. & LEVANAT, S. 2012. The growing relevance of cap-independent translation initiation in cancer-related genes. *Periodicum Biologorum,* 114**,** 471-478.

PALSSON-MCDERMOTT, E. M. & O'NEILL, L. A. J. 2013. The Warburg effect then and now: From cancer to inflammatory diseases. *BioEssays,* 35**,** 965-973.

PAPAGEORGHIOU, A. T., YU, C. K., CICERO, S., BOWER, S. & NICOLAIDES, K. H. 2002. Second-trimester uterine artery Doppler screening in unselected populations: a review. *J Matern Fetal Neonatal Med,* 12**,** 78-88.

PATEL, J., LANDERS, K., MORTIMER, R. H. & RICHARD, K. 2010. Regulation of hypoxia inducible factors (HIF) in hypoxia and normoxia during placental development. *Placenta,* 31**,** 951-7.

PETERSEN, E. T., ZIMINE, I., HO, Y. C. & GOLAY, X. 2006. Non-invasive measurement of perfusion: a critical review of arterial spin labelling techniques. *Br J Radiol,* 79**,** 688-701.

PIJNENBORG, R., VERCRUYSSE, L. & HANSSENS, M. 2006. The uterine spiral arteries in human pregnancy: facts and controversies. *Placenta,* 27**,** 939-58.

PLAKS, V., RINKENBERGER, J., DAI, J., FLANNERY, M., SUND, M., KANASAKI, K., NI, W., KALLURI, R. & WERB, Z. 2013. Matrix metalloproteinase-9 deficiency phenocopies features of preeclampsia and intrauterine growth restriction. *Proceedings of the National Academy of Sciences of the United States of America,* 110**,** 11109-11114.

PLAKS, V., SAPOZNIK, S., BERKOVITZ, E., HAFFNER-KRAUSZ, R., DEKEL, N., HARMELIN, A. & NEEMAN, M. 2011. Functional phenotyping of the maternal albumin turnover in the mouse placenta by dynamic contrast-enhanced MRI. *Molecular Imaging and Biology,* 13**,** 481-492.

PLUZNICK, J. L. 2013. Renal and cardiovascular sensory receptors and blood pressure regulation. *American Journal of Physiology - Renal Physiology,* 305**,** F439-F444.

POLLHEIMER, J., FOCK, V. & KNÖFLER, M. 2014. Review: The ADAM metalloproteinases - Novel regulators of trophoblast invasion? *Placenta,* 35**,** S57-S63.

POUYSSÉGUR, J., DAYAN, F. & MAZURE, N. M. 2006. Hypoxia signalling in cancer and approaches to enforce tumour regression. *Nature,* 441**,** 437-443.

PRICE, W. S. 1997. Pulsed-field gradient nuclear magnetic resonance as a tool for studying translational diffusion: Part 1. Basic theory. *Concepts in Magnetic Resonance,* 9**,** 299-335.
PRICE, W. S. 2009. *NMR studies of translational motion,* Cambridge ; New York, Cambridge University Press.
PUGH, C. W. & RATCLIFFE, P. J. 2003. Regulation of angiogenesis by hypoxia: role of the HIF system. *Nat Med,* 9**,** 677-84.
QAYYUM, A. 2009. Diffusion-weighted imaging in the abdomen and pelvis: concepts and applications. *Radiographics,* 29**,** 1797-810.
QIAN, Z., OKUHARA, D., ABE, M. K. & ROSNER, M. R. 1999. Molecular cloning and characterization of a mitogen-activated protein kinase-associated intracellular chloride channel. *J Biol Chem,* 274**,** 1621-7.
RAFFETTO, J. D. & KHALIL, R. A. 2008. Matrix metalloproteinases and their inhibitors in vascular remodeling and vascular disease. *Biochemical Pharmacology,* 75**,** 346-359.
RAICEVIC, G., ROUAS, R., NAJAR, M., STORDEUR, P., ID BOUFKER, H., BRON, D., MARTIAT, P., GOLDMAN, M., NEVESSIGNSKY, M. T. & LAGNEAUX, L. 2010. Inflammation modifies the pattern and the function of Toll-like receptors expressed by human mesenchymal stromal cells. *Human Immunology,* 71**,** 235-244.
RAJAKUMAR, A., BRANDON, H. M., DAFTARY, A., NESS, R. & CONRAD, K. P. 2004. Evidence for the functional activity of hypoxia-inducible transcription factors overexpressed in preeclamptic placentae. *Placenta,* 25**,** 763-9.
RAJAKUMAR, A., JEYABALAN, A., MARKOVIC, N., NESS, R., GILMOUR, C. & CONRAD, K. P. 2007. Placental HIF-1 alpha, HIF-2 alpha, membrane and soluble VEGF receptor-1 proteins are not increased in normotensive pregnancies complicated by late-onset intrauterine growth restriction. *Am J Physiol Regul Integr Comp Physiol,* 293**,** R766-74.
REDMAN, C. W. 1991. Current topic: pre-eclampsia and the placenta. *Placenta,* 12**,** 301-8.
REDMAN, C. W. & SARGENT, I. L. 2005. Latest advances in understanding preeclampsia. *Science,* 308**,** 1592-4.
REDMAN, C. W. & SARGENT, I. L. 2008. Circulating microparticles in normal pregnancy and pre-eclampsia. *Placenta,* 29 Suppl A**,** S73-7.
REDMAN, C. W. & SARGENT, I. L. 2009. Placental stress and pre-eclampsia: a revised view. *Placenta,* 30 Suppl A**,** S38-42.
REDMAN, C. W., SARGENT, I. L. & STAFF, A. C. 2014. IFPA senior award lecture: Making sense of pre-eclampsia - Two placental causes of preeclampsia? *Placenta,* 35**,** S20-S25.
REDMAN, C. W., TANNETTA, D. S., DRAGOVIC, R. A., GARDINER, C., SOUTHCOMBE, J. H., COLLETT, G. P. & SARGENT, I. L. 2012. Review: Does size matter? Placental debris and the pathophysiology of pre-eclampsia. *Placenta,* 33 Suppl**,** S48-54.
REDMAN, C. W. G. & SARGENT, I. L. 2010. Immunology of Pre-Eclampsia. *American Journal of Reproductive Immunology,* 63**,** 534-543.
REISSE, J. 1983. Relaxation processes in nuclear magnetic resonance. *In:* LAMBERT, J. B. & RIDDELL, F. G. (eds.) *The Multinuclear approach to NMR spectroscopy.* D. Reidel Publishing Company.
RILEY, J. K. & NELSON, D. M. 2010. Toll-like Receptors in Pregnancy Disorders and Placental Dysfunction. *Clin Rev Allergy Immunol,* 39**,** 185-93.
ROBERGS, R. A., GHIASVAND, F. & PARKER, D. 2004. Biochemistry of exercise-induced metabolic acidosis. *American Journal of Physiology - Regulatory Integrative and Comparative Physiology,* 287**,** R502-R516.
ROBERTS, J. M. & GAMMILL, H. S. 2005. Preeclampsia: Recent insights. *Hypertension,* 46**,** 1243-1249.

ROBERTS, J. M. & HUBEL, C. A. 2009. The Two Stage Model of Preeclampsia: Variations on the Theme. *Placenta,* 30**,** 32-37.

RODESCH, F., SIMON, P., DONNER, C. & JAUNIAUX, E. 1992. Oxygen measurements in endometrial and trophoblastic tissues during early pregnancy. *Obstet Gynecol,* 80**,** 283-5.

ROLFO, A., MANY, A., RACANO, A., TAL, R., TAGLIAFERRO, A., IETTA, F., WANG, J., POST, M. & CANIGGIA, I. 2010. Abnormalities in oxygen sensing define early and late onset preeclampsia as distinct pathologies. *PLoS ONE,* 5**,** e13288.

ROSARIO, G. X., KONNO, T. & SOARES, M. J. 2008. Maternal hypoxia activates endovascular trophoblast cell invasion. *Dev Biol,* 314**,** 362-75.

ROSENBERG, V. A., BUHIMSCHI, I. A., LOCKWOOD, C. J., PAIDAS, M. J., DULAY, A. T., RAMMA, W., ABDEL-RAZEQ, S. S., ZHAO, G., AHMAD, S., AHMED, A. & BUHIMSCHI, C. S. 2011. Heparin elevates circulating soluble fms-like tyrosine kinase-1 immunoreactivity in pregnant women receiving anticoagulation therapy. *Circulation,* 124**,** 2543-2553.

ROSSANT, J. & CROSS, J. C. 2001. Placental development: lessons from mouse mutants. *Nat Rev Genet,* 2**,** 538-48.

RUBIC, T., LAMETSCHWANDTNER, G., JOST, S., HINTEREGGER, S., KUND, J., CARBALLIDO-PERRIG, N., SCHWÄRZLER, C., JUNT, T., VOSHOL, H., MEINGASSNER, J. G., MAO, X., WERNER, G., ROT, A. & CARBALLIDO, J. M. 2008. Triggering the succinate receptor GPR91 on dendritic cells enhances immunity. *Nature Immunology,* 9**,** 1261-1269.

RÜBSAMEN, D., BLEES, J. S., SCHULZ, K., DÖRING, C., HANSMANN, M. L., HEIDE, H., WEIGERT, A., SCHMID, T. & BRÜNE, B. 2012. IRES-dependent translation of egr2 is induced under inflammatory conditions. *RNA,* 18**,** 1910-1920.

SADAGOPAN, N., LI, W., ROBERDS, S. L., MAJOR, T., PRESTON, G. M., YU, Y. & TONES, M. A. 2007. Circulating Succinate is Elevated in Rodent Models of Hypertension and Metabolic Disease. *American Journal of Hypertension,* 20**,** 1209-1215.

SADO, T., NARUSE, K., NOGUCHI, T., HARUTA, S., YOSHIDA, S., TANASE, Y., KITANAKA, T., OI, H. & KOBAYASHI, H. 2011. Inflammatory pattern recognition receptors and their ligands: Factors contributing to the pathogenesis of preeclampsia. *Inflammation Research,* 60**,** 509-520.

SAITO, S., SHIOZAKI, A., SASAKI, Y., NAKASHIMA, A., SHIMA, T. & ITO, M. 2007. Regulatory T cells and regulatory natural killer (NK) cells play important roles in feto-maternal tolerance. *Semin Immunopathol,* 29**,** 115-22.

SAKAI, J., ISHIKAWA, H., KOJIMA, S., SATOH, H., YAMAMOTO, S. & KANAOKA, M. 2003. Proteomic analysis of rat heart in ischemia and ischemia-reperfusion using fluorescence two-dimensional difference gel electrophoresis. *Proteomics,* 3**,** 1318-24.

SALOMON, L. J., SIAUVE, N., TAILLIEU, F., BALVAY, D., VAYSSETTES, C., FRIJA, G., VILLE, Y., CUENOD, C. A. & CLEMENT, O. 2006. In vivo dynamic MRI measurement of the noradrenaline-induced reduction in placental blood flow in mice. *Placenta,* 27**,** 1007-13.

SANCHEZ-ELSNER, T., BOTELLA, L. M., VELASCO, B., LANGA, C. & BERNABEU, C. 2002. Endoglin expression is regulated by transcriptional cooperation between the hypoxia and transforming growth factor-beta pathways. *J Biol Chem,* 277**,** 43799-808.

SARGENT, I. L., BORZYCHOWSKI, A. M. & REDMAN, C. W. 2006. Immunoregulation in normal pregnancy and pre-eclampsia: an overview. *Reproductive biomedicine online,* 13**,** 680-686.

SARTORI-CINTRA, A. R., MARA, C. S., ARGOLO, D. L. & COIMBRA, I. B. 2012. Regulation of hypoxia-inducible factor-1alpha (HIF-1alpha) expression by interleukin-1beta (IL-1

beta), insulin-like growth factors I (IGF-I) and II (IGF-II) in human osteoarthritic chondrocytes. *Clinics (Sao Paulo),* 67**,** 35-40.
SASAKI, S., OSANAI, T., TOMITA, H., MATSUNAGA, T., MAGOTA, K. & OKUMURA, K. 2004. Tumor necrosis factor α as an endogenous stimulator for circulating coupling factor 6. *Cardiovascular Research,* 62**,** 578-586.
SCHEFFLER, K. & HENNIG, J. 2001. T(1) quantification with inversion recovery TrueFISP. *Magn Reson Med,* 45**,** 720-3.
SCHIFF, E., FRIEDMAN, S. A., BAUMANN, P., SIBAI, B. M. & ROMERO, R. 1994. Tumor necrosis factor-alpha in pregnancies associated with preeclampsia or small-for-gestational-age newborns. *Am J Obstet Gynecol,* 170**,** 1224-9.
SCHMID, M., SOLLWEDEL, A., THUERE, C., WAFULA, P. O., ZENCLUSSEN, M. L., MÃ¼LLER, D. N., GRATZE, P., WOICIECHOWSKY, C., VOLK, H. D. & ZENCLUSSEN, A. C. 2007. Murine Pre-Eclampsia Induced by Unspecific Activation of the Immune System Correlates with Alterations in the eNOS and AT1 Receptor Expression in the Kidneys and Placenta. *Placenta,* 28**,** 688-700.
SEARLE, J., MOCKEL, M., GWOSC, S., DATWYLER, S. A., QADRI, F., ALBERT, G. I., HOLERT, F., ISBRUCH, A., KLUG, L., MULLER, D. N., DECHEND, R., MULLER, R., VOLLERT, J. O., SLAGMAN, A., MUELLER, C. & HERSE, F. 2011. Heparin strongly induces soluble fms-like tyrosine kinase 1 release in vivo and in vitro-brief report. *Arteriosclerosis, Thrombosis, and Vascular Biology,* 31**,** 2972-2974.
SEKI, E., TSUTSUI, H., IIMURO, Y., NAKA, T., SON, G., AKIRA, S., KISHIMOTO, T., NAKANISHI, K. & FUJIMOTO, J. 2005. Contribution of Toll-like receptor/myeloid differentiation factor 88 signaling to murine liver regeneration. *Hepatology,* 41**,** 443-50.
SEKI, H. 2014. The role of the renin-angiotensin system in the pathogenesis of preeclampsia - New insights into the renin-angiotensin system in preeclampsia. *Medical Hypotheses,* 82**,** 362-367.
SELA, S., NATANSON-YARON, S., ZCHARIA, E., VLODAVSKY, I., YAGEL, S. & KESHET, E. 2011. Local retention versus systemic release of soluble VEGF receptor-1 are mediated by heparin-binding and regulated by heparanase. *Circulation Research*.
SEMENZA, G. 2002. Signal transduction to hypoxia-inducible factor 1. *Biochem Pharmacol,* 64**,** 993-8.
SEMENZA, G. L. 2003. Targeting HIF-1 for cancer therapy. *Nat Rev Cancer,* 3**,** 721-32.
SEONG, S. Y. & MATZINGER, P. 2004. Hydrophobicity: an ancient damage-associated molecular pattern that initiates innate immune responses. *Nat Rev Immunol,* 4**,** 469-78.
SHARMA, S., NORRIS, W. E. & KALKUNTE, S. 2010. Beyond the threshold: An etiological bridge between hypoxia and immunity in preeclampsia. *Journal of reproductive immunology,* 85**,** 112-116.
SHIBUYA, M. 2011. Involvement of Flt-1 (VEGF receptor-1) in cancer and preeclampsia. *Proceedings of the Japan Academy. Series B, Physical and biological sciences,* 87**,** 167-178.
SHOKRY, M., OMRAN, O. M., HASSAN, H. I., ELSEDFY, G. O. & HUSSEIN, M. R. A. 2009. Expression of matrix metalloproteinases 2 and 9 in human trophoblasts of normal and preeclamptic placentas: Preliminary findings. *Experimental and Molecular Pathology,* 87**,** 219-225.
SIBAI, B. M. 2003. Diagnosis and management of gestational hypertension and preeclampsia. *Obstetrics and Gynecology,* 102**,** 181-192.
SIMMONS, D. G., FORTIER, A. L. & CROSS, J. C. 2007. Diverse subtypes and developmental origins of trophoblast giant cells in the mouse placenta. *Dev Biol,* 304**,** 567-78.
SINGH, H. 2010. Two decades with dimorphic Chloride Intracellular Channels (CLICs). *FEBS Letters,* 584**,** 2112-2121.

SMITH, J. A. 2010. Hazards, Safety, and Anesthetic Considerations for Magnetic Resonance Imaging. *Topics in Companion Animal Medicine,* 25**,** 98-106.
SOTO, E., ROMERO, R., KUSANOVIC, J. P., OGGE, G., HUSSEIN, Y., YEO, L., HASSAN, S. S., KIM, C. J. & CHAIWORAPONGSA, T. 2012. Late-onset preeclampsia is associated with an imbalance of angiogenic and anti-angiogenic factors in patients with and without placental lesions consistent with maternal underperfusion. *J Matern Fetal Neonatal Med,* 25**,** 498-507.
STAUBER, T. & JENTSCH, T. J. 2013. Chloride in vesicular trafficking and function. *Annual Review of Physiology,* 75**,** 453-477.
STEJSKAL, E. O. 1965. Use of spin echoes in a pulsed magnetic-field gradient to study anisotropie, restricted diffusion and flow. *The Journal of Chemical Physics,* 43**,** 3597-3603.
STEJSKAL, E. O. & TANNER, J. E. 1965. Spin diffusion measurements: Spin echoes in the presence of a time-dependent field gradient. *The Journal of Chemical Physics,* 42**,** 288-292.
STUBBS, M., MCSHEEHY, P. M. J., GRIFFITHS, J. R. & BASHFORD, C. L. 2000. Causes and consequences of tumour acidity and implications for treatment. *Molecular Medicine Today,* 6**,** 15-19.
SUMBAYEV, V. V. & NICHOLAS, S. A. 2010. Hypoxia-inducible factor 1 as one of the "signaling drivers" of Toll-like receptor-dependent and allergic inflammation. *Arch Immunol Ther Exp (Warsz),* 58**,** 287-94.
SUNDERLAND, N., THOMPSON, J., OGLE, R., THOMSON, S. & HENNESSY, A. 2009. Tumour necrosis factor alpha induces placental antiangiogenic factors in pregnant baboons *(papio hamadryas). HBPRCA Abstract Dec 2009. in prep for publication*.
SUNDERLAND, N. S., THOMSON, S. E., HEFFERNAN, S. J., LIM, S., THOMPSON, J., OGLE, R., MCKENZIE, P., KIRWAN, P. J., MAKRIS, A. & HENNESSY, A. 2011. Tumor necrosis factor α induces a model of preeclampsia in pregnant baboons (Papio hamadryas). *Cytokine,* 56**,** 192-199.
SURMON, L., BOBEK, G., CHIU, C. L., YOUNG, S., MAKRIS, A., LIND, J. M. & HENNESSY, A. 2014. The expression of placental soluble fms-like tyrosine kinase 1 in mouse placenta varies significantly across different litters from normal pregnant mice. *Hypertens Pregnancy*.
SUZUKI, H., OHKUCHI, A., MATSUBARA, S., TAKEI, Y., MURAKAMI, M., SHIBUYA, M., SUZUKI, M. & SATO, Y. 2009. Effect of recombinant placental growth factor 2 on hypertension induced by full-length mouse soluble fms-like tyrosine kinase 1 adenoviral vector in pregnant mice. *Hypertension,* 54**,** 1129-1135.
TAILLIEU, F., SALOMON, L. J., SIAUVE, N., CLEMENT, O., FAYE, N., BALVAY, D., VAYSSETTES, C., FRIJA, G., VILLE, Y. & CUENOD, C. A. 2006. Placental perfusion and permeability: simultaneous assessment with dual-echo contrast-enhanced MR imaging in mice. *Radiology,* 241**,** 737-45.
TAKIMOTO, E., ISHIDA, J., SUGIYAMA, F., HORIGUCHI, H., MURAKAMI, K. & FUKAMIZU, A. 1996. Hypertension induced in pregnant mice by placental renin and maternal angiotensinogen. *Science,* 274**,** 995-998.
TAL, R. 2012. The role of hypoxia and hypoxia-inducible factor-1Alpha in preeclampsia pathogenesis. *Biol Reprod,* 87**,** 134.
TAL, R., SHAISH, A., BARSHACK, I., POLAK-CHARCON, S., AFEK, A., VOLKOV, A., FELDMAN, B., AVIVI, C. & HARATS, D. 2010. Effects of hypoxia-inducible factor-1Î± overexpression in pregnant mice: Possible implications for preeclampsia and intrauterine growth restriction. *American Journal of Pathology,* 177**,** 2950-2962.
TANNAHILL, G. M., CURTIS, A. M., ADAMIK, J., PALSSON-MCDERMOTT, E. M., MCGETTRICK, A. F., GOEL, G., FREZZA, C., BERNARD, N. J., KELLY, B., FOLEY, N. H., ZHENG, L.,

GARDET, A., TONG, Z., JANY, S. S., CORR, S. C., HANEKLAUS, M., CAFFREY, B. E., PIERCE, K., WALMSLEY, S., BEASLEY, F. C., CUMMINS, E., NIZET, V., WHYTE, M., TAYLOR, C. T., LIN, H., MASTERS, S. L., GOTTLIEB, E., KELLY, V. P., CLISH, C., AURON, P. E., XAVIER, R. J. & O'NEILL, L. A. J. 2013. Succinate is an inflammatory signal that induces IL-1β through HIF-1α. *Nature,* 496**,** 238-242.

TANNAHILL, G. M. & O'NEILL, L. A. J. 2011. The emerging role of metabolic regulation in the functioning of Toll-like receptors and the NOD-like receptor Nlrp3. *FEBS Letters,* 585**,** 1568-1572.

TEASDALE, F. 1985. Histomorphometry of the human placenta in maternal preeclampsia. *Am J Obstet Gynecol,* 152**,** 25-31.

THOMPSON, J. A. & WEBB, R. C. 2013. Potential role of toll-like receptors in programming of vascular dysfunction. *Clinical Science,* 125**,** 19-25.

THULBORN, K. R., WATERTON, J. C., MATTHEWS, P. M. & RADDA, G. K. 1982. Oxygenation dependence of the transverse relaxation time of water protons in whole blood at high field. *Biochim Biophys Acta,* 714**,** 265-70.

TIMMERS, L., SLUIJTER, J. P., VAN KEULEN, J. K., HOEFER, I. E., NEDERHOFF, M. G., GOUMANS, M. J., DOEVENDANS, P. A., VAN ECHTELD, C. J., JOLES, J. A., QUAX, P. H., PIEK, J. J., PASTERKAMP, G. & DE KLEIJN, D. P. 2008. Toll-like receptor 4 mediates maladaptive left ventricular remodeling and impairs cardiac function after myocardial infarction. *Circ Res,* 102**,** 257-64.

TINSLEY, J. H., CHIASSON, V. L., MAHAJAN, A., YOUNG, K. J. & MITCHELL, B. M. 2009. Toll-like receptor 3 activation during pregnancy elicits preeclampsia-like symptoms in rats. *American Journal of Hypertension,* 22**,** 1314-1319.

TJOA, M. L., LEVINE, R. J. & KARUMANCHI, S. A. 2007. Angiogenic factors and preeclampsia. *Front Biosci,* 12**,** 2395-402.

TOMLINSON, T. M., GARBOW, J. R., ANDERSON, J. R., ENGELBACH, J. A., NELSON, D. M. & SADOVSKY, Y. 2010. Magnetic resonance imaging of hypoxic injury to the murine placenta. *American Journal of Physiology - Regulatory Integrative and Comparative Physiology,* 298.

TRANQUILLI, A. L., DEKKER, G., MAGEE, L., ROBERTS, J., SIBAI, B. M., STEYN, W., ZEEMAN, G. G. & BROWN, M. A. 2014. The classification, diagnosis and management of the hypertensive disorders of pregnancy: A revised statement from the ISSHP. *Pregnancy Hypertension,* 4**,** 97-104.

TRANQUILLI, A. L. & LANDI, B. 2010. The origin of pre-eclampsia: From decidual " hyperoxia" to late hypoxia. *Medical Hypotheses,* 75**,** 38-46.

TSAPOURNIOTI, S., MYLONIS, I., HATZIEFTHIMIOU, A., IOANNOU, M. G., STAMATIOU, R., KOUKOULIS, G. K., SIMOS, G., MOLYVDAS, P. A. & PARASKEVA, E. 2013. TNFalpha induces expression of HIF-1alpha mRNA and protein but inhibits hypoxic stimulation of HIF-1 transcriptional activity in airway smooth muscle cells. *J Cell Physiol,* 228**,** 1745-53.

UNTERGASSER, A., NIJVEEN, H., RAO, X., BISSELING, T., GEURTS, R. & LEUNISSEN, J. A. 2007. Primer3Plus, an enhanced web interface to Primer3. *Nucleic Acids Res,* 35**,** W71-4.

VAN EMPEL, V. P., DE WINDT, L. J. & DA COSTA MARTINS, P. A. 2012. Circulating miRNAs: reflecting or affecting cardiovascular disease? *Curr Hypertens Rep,* 14**,** 498-509.

VAN HINSBERGH, V. W., ENGELSE, M. A. & QUAX, P. H. 2006. Pericellular proteases in angiogenesis and vasculogenesis. *Arterioscler Thromb Vasc Biol,* 26**,** 716-28.

VAN HINSBERGH, V. W. M. & KOOLWIJK, P. 2008. Endothelial sprouting and angiogenesis: Matrix metalloproteinases in the lead. *Cardiovascular Research,* 78**,** 203-212.

VAN MOURIK, M. S. M., MACKLON, N. S. & HEIJNEN, C. J. 2009. Embryonic implantation: Cytokines, adhesion molecules, and immune cells in establishing an implantation environment. *Journal of Leukocyte Biology,* 85**,** 4-19.

VAN VLIET, B. N., MCGUIRE, J., CHAFE, L., LEONARD, A., JOSHI, A. & MONTANI, J. P. 2006. Phenotyping the level of blood pressure by telemetry in mice. *Clinical and Experimental Pharmacology and Physiology,* 33**,** 1007-1015.

VAUGHAN-JONES, R. D., SPITZER, K. W. & SWIETACH, P. 2009. Intracellular pH regulation in heart. *Journal of Molecular and Cellular Cardiology,* 46**,** 318-331.

WALLUKAT, G., HOMUTH, V., FISCHER, T., LINDSCHAU, C., HORSTKAMP, B., JÃ¼PNER, A., BAUR, E., NISSEN, E., VETTER, K., NEICHEL, D., DUDENHAUSEN, J. W., HALLER, H. & LUFT, F. C. 1999. Patients with preeclampsia develop agonistic autoantibodies against the angiotensin AT1 receptor. *Journal of Clinical Investigation,* 103**,** 945-952.

WANG, Y. & WALSH, S. W. 1996. TNF alpha concentrations and mRNA expression are increased in preeclamptic placentas. *J Reprod Immunol,* 32**,** 157-69.

WATSON, E. D. & CROSS, J. C. 2005. Development of structures and transport functions in the mouse placenta. *Physiology (Bethesda),* 20**,** 180-93.

WENGER, R. H., KVIETIKOVA, I., ROLFS, A., GASSMANN, M. & MARTI, H. H. 1997. Hypoxia-inducible factor-1 alpha is regulated at the post-mRNA level. *Kidney Int,* 51**,** 560-3.

WHITEHEAD, C., PALMER, K., NILSSON, U., GAO, Y., SAGLAM, B., LAPPAS, M. & TONG, S. 2011. Placental expression of a novel primate-specific splice variant of sFlt-1 is upregulated in pregnancies complicated by severe early onset pre-eclampsia. *BJOG: An International Journal of Obstetrics and Gynaecology*.

WIENER, C. M., BOOTH, G. & SEMENZA, G. L. 1996. In vivo expression of mRNAs encoding hypoxia-inducible factor 1. *Biochem Biophys Res Commun,* 225**,** 485-8.

WILLERS, I. M. & CUEZVA, J. M. 2011. Post-transcriptional regulation of the mitochondrial H+-ATP synthase: A key regulator of the metabolic phenotype in cancer. *Biochimica et Biophysica Acta (BBA) - Bioenergetics,* 1807**,** 543-551.

WRIGHT, C., MORRIS, D. M., BAKER, P. N., CROCKER, I. P., GOWLAND, P. A., PARKER, G. J. & SIBLEY, C. P. 2011. Magnetic resonance imaging relaxation time measurements of the placenta at 1.5T. *Placenta,* 32**,** 1010-5.

WRIGHT, E. P., PARTRIDGE, M. A., PADULA, M. P., GAUCI, V. J., MALLADI, C. S. & COORSSEN, J. R. 2014. Top-down proteomics: Enhancing 2D gel electrophoresis from tissue processing to high-sensitivity protein detection. *Proteomics,* 14**,** 872-889.

XIA, Y. & KELLEMS, R. E. 2013. Angiotensin receptor agonistic autoantibodies and hypertension : Preeclampsia and beyond. *Circulation Research,* 113**,** 78-87.

XIA, Y., WEN, H. Y. & KELLEMS, R. E. 2002. Angiotensin II inhibits human trophoblast invasion through AT1 receptor activation. *Journal of Biological Chemistry,* 277**,** 24601-24608.

XU, B., CHARLTON, F., MAKRIS, A. & HENNESSY, A. 2014a. Nitric oxide (NO) reversed TNF-alpha inhibition of trophoblast interaction with endothelial cellular networks. *Placenta,* 35**,** 417-21.

XU, B., NAKHLA, S., MAKRIS, A. & HENNESSY, A. 2011. TNF-α inhibits trophoblast integration into endothelial cellular networks. *Placenta,* 32**,** 241-246.

XU, P., ZHAO, Y., LIU, M., WANG, Y., WANG, H., LI, Y. X., ZHU, X., YAO, Y., WANG, H., QIAO, J., JI, L. & WANG, Y. L. 2014b. Variations of micrornas in human placentas and plasma from preeclamptic pregnancy. *Hypertension*.

YAGEL, S. 2011. Angiogenesis in gestational vascular complications. *Thrombosis Research,* 127**,** S64-S66.

YANAGIDA, M., MIURA, Y., YAGASAKI, K., TAOKA, M., ISOBE, T. & TAKAHASHI, N. 2000. Matrix assisted laser desorption/ionization-time of flight-mass spectrometry analysis of proteins detected by anti-phosphotyrosine antibody on two-dimensional-gels of fibrolast cell lysates after tumor necrosis factor-alpha stimulation. *Electrophoresis,* 21**,** 1890-8.

YOUNG, K. C., HUSSEIN, S. M., DADIZ, R., DEMELLO, D., DEVIA, C., HEHRE, D. & SUGUIHARA, C. 2010. Toll-like receptor 4-deficient mice are resistant to chronic hypoxia-induced pulmonary hypertension. *Exp Lung Res,* 36**,** 111-9.

ZAMPETAKI, A., WILLEIT, P., DROZDOV, I., KIECHL, S. & MAYR, M. 2012. Profiling of circulating microRNAs: From single biomarkers to re-wired networks. *Cardiovascular Research,* 93**,** 555-562.

ZAMUDIO, S., KOVALENKO, O., ECHALAR, L., TORRICOS, T., AL-KHAN, A., ALVAREZ, M. & ILLSLEY, N. P. 2013. Evidence for extraplacental sources of circulating angiogenic growth effectors in human pregnancy. *Placenta,* 34**,** 1170-1176.

ZENCLUSSEN, A. C., FEST, S., JOACHIM, R., KLAPP, B. F. & ARCK, P. C. 2004. Introduction a mouse model for pre-eclampsia: Adoptive transfer of activated Th1 cells leads to pre-eclampsia-like symptoms exclusively in pregnant mice. *European Journal of Immunology,* 34**,** 377-387.

ZHANG, J., WEI, H., WU, D. & TIAN, Z. 2007. Toll-like receptor 3 agonist induces impairment of uterine vascular remodeling and fetal losses in CBA x DBA/2 mice. *J Reprod Immunol,* 74**,** 61-7.

ZHANG, Y., HUA, Z., ZHANG, K., MENG, K. & HU, Y. 2009. Therapeutic Effects of Anticoagulant Agents on Preeclampsia in a Murine Model Induced by Phosphatidylserine/Phosphatidylcholine Microvesicles. *Placenta,* 30**,** 1065-1070.

ZHENG, M., REYNOLDS, C., JO, S. H., WERSTO, R., HAN, Q. & XIAO, R. P. 2005. Intracellular acidosis-activated p38 MAPK signaling and its essential role in cardiomyocyte hypoxic injury. *FASEB Journal,* 19**,** 109-111.

ZHOU, C. C., AHMAD, S., MI, T., XIA, L., ABBASI, S., HEWETT, P. W., SUN, C., AHMED, A., KELLEMS, R. E. & XIA, Y. 2007. Angiotensin II induces soluble fms-Like tyrosine kinase-1 release via calcineurin signaling pathway in pregnancy. *Circ Res,* 100**,** 88-95.

ZHOU, C. C., ZHANG, Y., IRANI, R. A., ZHANG, H., MI, T., POPEK, E. J., HICKS, M. J., RAMIN, S. M., KELLEMS, R. E. & XIA, Y. 2008. Angiotensin receptor agonistic autoantibodies induce pre-eclampsia in pregnant mice. *Nature Medicine,* 14**,** 855-862.

ZHOU, J., CALLAPINA, M., GOODALL, G. J. & BRUNE, B. 2004. Functional integrity of nuclear factor kappaB, phosphatidylinositol 3'-kinase, and mitogen-activated protein kinase signaling allows tumor necrosis factor alpha-evoked Bcl-2 expression to provoke internal ribosome entry site-dependent translation of hypoxia-inducible factor 1alpha. *Cancer Res,* 64**,** 9041-8.

ZHOU, Y., DAMSKY, C. H. & FISHER, S. J. 1997. Preeclampsia is associated with failure of human cytotrophoblasts to mimic a vascular adhesion phenotype. One cause of defective endovascular invasion in this syndrome? *J Clin Invest,* 99**,** 2152-64.

ZUCKERBROD, M. & GRAEF, I. 1950. Clinical evaluation of disodium succinate, including a report on its ineffectiveness in two cases of severe barbiturate poisoning and some toxicologic notes on other succinate salts. *Ann Intern Med,* 32**,** 905-16.